Uranyl Sensing and Extracting Using Salen-base Quinoxalinol Ligands

by

Maya M. West

A dissertation submitted to the Graduate Faculty of
Auburn University
in partial fulfillment of the
requirements for the Degree of
Doctor of Philosophy in Chemistry

Auburn, Alabama
May 5, 2019

Keywords: uranyl, sensing, chemosensor, extracting, cellulose

Approved by

Anne Gorden, Chair, Associate Professor of Chemistry and Biochemistry
German Mills, Professor of Chemistry and Biochemistry
David Stanbury, J. Milton Harris Professor of Chemistry and Biochemistry
Wei Zhan, Associate Professor of Chemistry and Biochemistry

Abstract

In spite of infamous nuclear accidents, the increasing need for low cost, reliable energy with low greenhouse emission makes the use of nuclear power an attractive option. Unfortunately, the nuclear fuel cycle produces a plethora of radioactive metal enriched wastes. This waste consists of not only environmentally unfriendly toxins, but also recyclable radioactive metals, that could be reused. One of the main issues associated with current methods of detection is that the concentrations of contaminants found at sites are relatively low, and are difficult to detect due to having a low or weak signal. Research has shown that the signal of the low concentrated contaminants can be enhanced using a matrix or chelate. In regards to implementing a chelate to enhance the signal a 2-quinoxalinol salen ligand synthesized by the Gorden research group has shown binding capabilities of 2^{+} metal ions. Coupling this ligand with a solid support has the ability to enhance the probability of using this metal-scavenging ligand as an aid for the extraction of metals from the environment. Reported herein, is the study on how varying electronic groups of Schiff-base ligands effects the metal chelation, development of a solid-support system for uranyl extraction, and applications using the developed systems.

Acknowledgments

First and foremost, I would like to thank God for his strength and blessings over my time here at Auburn. I would also like to think my wonderful parents for their love, patience, and support, and for allowing me to pursue my PhD. I would also like to thank my family for helping me and supporting me whenever I needed them.

I would like to thank Dr. Gorden and my committee members; Dr. Mills, Dr. Peresin, Dr. Stanbury, and Dr. Zhan for their patience and guidance throughout this process. I would also like to thank Dr. Ortiz and Dr. Mulligan-Guy for their mentorship and being people, I could confide in.

I would like to extend a thank you to all the members of the Gorden lab, past and present and would like to wish the remaining few the best of luck! I would also like to thank the three undergraduates that I had the privilege to mentor: Will Scott, Kate Valentine, and Ryan Yates.

Last but not least, I would like to thank all the wonderful people I had the pleasure to meet during my time here at Auburn; Charmaine Tutson, Emily Hardy, Jessica Crumbly, Ana Dmytrejchuk, Hector Corzo, Manuel Diaz, Nick Klann, Selam Manghisteab, Radini Dissanayaka, Sam Bond, Jamonica Moore, Andrius Burton, Rachal Wills, Julie Niklas, Chasity Ward, and Joxuany Santiago, along with countless others.

Table of Contents

List of Tables

List of Figures

List of Schemes

List of Abbreviations

ACS	American Chemical Society
AEC	Atomic Energy Commission
AuNCs	gold nanoclusters
BSA-AuNCs	bovine serum albumin-stabilized gold nanoclusters
BTP	bis-1,2,4-triazide-3-yl-oligopyridine
° C	degrees Celsius
Cald	Calculated
cm	centimeter
CMC	Carboxymethyl Cellulose
CMPO	(N,N'-diisobutylcarbamoylmethyl)-octylphenylphosphine oxide
D. I.	Deionized
DIAMAX	Diamide Extraction
DIPEA	N, N-diisopropylethylamine
DMF	N, N-dimethylformamide
DMSO	Dimethyl Sulfoxide
DTBP	6,6'-bis(5,6-dialkyl[1,2,4]triazine-3-yl)[2,2']bipyridine
EBR-1	Experimental Breeder Reactor-1
ε	Extinction Coefficient (M^{-1} cm^{-1})
h	hour
HCl	Hydrogen Chloride

HEC	2-Hydroxyethyl Cellulose
HL	Heterogeneous Ligand
HMTA	Hexamethylenetetramine
HPLC	High Performance Liquid Chromatography
HOPO	Hydroxypyridonates
HRMS	High-Resolution Mass Spectrometry
ICP-OES	Inductively Coupled Plasma- Optical Emission Spectroscopy
λ_{max}	lambda max
MCC	Microcrystalline Cellulose
min	minute(s)
mL	milliliter
mm	millimeter
mmol	millimole
MOF	Metal-Organic Framework
mPVA	magnetic Polyvinyl Alcohol
N	Normality
NaOH	Sodium Hydroxide
NMR	Nuclear Magnetic Resonance
NRC	Nuclear Regulatory Commission
π	Pi
ppb	parts per billion
ppm	parts per million
PUREX	Plutonium Uranium Recovery by Extraction

RC	Regenerated Cellulose
RFU	Relative Fluorescence Units
Rpm	Revolutions per minute
SANEX	Selective Actinide Extraction process
σ	Sigma
TALSPEAK	Trivalent Actinide-Lanthanide Separation by Phosphorous reagent Extraction from Aqueous Komplexes
TAM	2,3-dihydroxy terephthalamide
TATAB	4,4′,4’-(1,3,5-triazine-2,4,6-triyltriimino)tris-benzoic acid
TBP	tri-n-butyl phosphate
TFA	Trifluoroacetic acid
THF	Tetrahydrofuran
TLC	Thin-layer Chromatography
TMB	3,3′ ,5,5′ -tetramethylbenzidine
TRUEX	Transuranium Extraction Process
v/v	volume/volume
λ	Wavelength (nm)
Wt %	weight percent
w/v	weight/volume

Chapter 1

Introduction

1.1 Uranium

Uranium, named after the planet Uranus, was discovered in 1789 by the German chemist Martin Heinrich Klaproth.[1] Though Klaproth claimed to have extracted the pure element from the yellow oxide that was precipitated from pitchblende and nitric acid, it was not until 1841 when the French chemist Eugene Peligot debunked Klaproth claims.[1-3] In a 2:1 ratio the green crystals of the uranium chloride, UCl_4, was reduced with potassium metal in a platinum crucible with gentle heat.[4] Once cooled, the products rinsed with water to dissolve the potassium salt, KCl, and yield uranium metal in the form of black powder.[4] Peligot at that time determined the atomic weight of uranium was approximately 120 amu, which was supported by other experimentalists at that time.[1] In 1869, when the Russian scientist Dimitri Mendelev was arranging all know elements into a table based on their atomic mass, he discovered Peligot's reported mass was incorrect.[1, 5] Mendelev believed that the atomic mass of uranium was only "half-correct" and that the actual mass was approximately 240, about 2 Daltons off from the accepted value used today.[1, 5]

The radioactivity of uranium would not be discovered until 1896 by the French scientist Henri Becquerel.[6-8] Continuing his father's research on the phosphorescence of uranium using photographic plates, Becquerel believed that light rays could be transferred into deeply penetrating radiations via the transformation of cathode rays into X-rays that took place in the Crookes tubes.[7] To test his theory, Becquerel wrapped a photographic plate in paper to protect it from light, on the plate he placed a uranium ore,

which would fluoresce upon the exposure of light.[6, 7] After the system was exposed to sunlight, it was disassembled, and the plate was developed revealing fluorescence where the uranium was placed, thus supporting his theory.[6, 7] He then decided to repeat the experiment using uranium sulfate crystals; however since the sun did not shine for several days, the system was stored in a drawer on a wrapped package of photographic plates.[6, 7] After development of the plates, the plates were found to have streaks like the preceding experiments in which the sun's rays caused the material to fluoresce, leading Becquerel to believe that the uranium crystals emits "radiations which penetrate paper that is opaque to light."[6, 7] He decided to test this theory using an opaque cardboard box and glass, aluminum, and emulsion plates. Each experiment revealed the same result, fluorescence, thus leading Becquerel to the conclusion that the phenomenon was not caused by luminous radiation emitted by phosphorescence, but by an undiscovered element. He termed the phenomenon radiation, and assigned Marie Curie the task of determining what element was responsible for radioactivity for her PhD thesis.[6, 7] Curie conducted research on how to efficiently measure the radiation in uranium and soon discovered that thorium possessed the same radioactive properties; she then coined the term radioactivity to describe the phenomena.[9] Working alongside her husband Pierre Curie, they discovered two more radioactive elements, polonium and radium.[6, 9] They shared the 1903 Nobel Prize in Physics with Becquerel for their research on the radiation phenomena and in 1911 Marie Curie received the Nobel Prize in Chemistry for her discovery and research of polonium and radium.[10]

1.2 Nuclear Energy

Fossil fuels emit a great amount of harmful toxins, such as greenhouse gases,

sulfur dioxide, and mercury, when burned for energy. Because of this, the use of oil and coal for energy production is also a leading cause of acid rain, due to the sulfur dioxide reacting with water molecules in the atmosphere.[11, 12] On December 20, 1951, the first commercial nuclear power station, Experimental Breeder Reactor-1 (EBR-1), began operating, nearly six years after actinides were first exploited for their energy potential. Since then over 430 commercial nuclear power stations are operating in over 31 countries, with at least 70 under construction, evidence of an increasing demand for nuclear energy.[13, 14] These reactors are responsible for providing more than 11% of the world's electricity and 20% of the United States' civilian energy.[15] Nuclear power is a reliable base-load power that affords large amounts of useable energy with limited carbon emissions and a smaller land use footprint than current available solar methods.

The capacity factor, which is the amount of electricity a generator actually produces compared to the maximum it could produce when operating at continuous full power during the same period; has increased from 50% in the early 1970's to above 90% since the turn of the millennium, providing 800 TWh/yr of energy to the United States in 2008.[15, 16] Currently, there are over 15 pending license applications under review by the U.S. Nuclear Regulatory Commission (NRC) for new nuclear reactors based on the third-generation once-through fuel cycle designs.[16] With new nuclear power plants on the rise, the challenge of managing, safely storing, and limiting the potential environmental or injurious effects is persistently increasing.

Uranium is a key component for nuclear energy because of the presence of several fissile isotopes.[17] Consisting of six isotopes, half of which are long-lived U-238 (99.2745%), U-235 (0.720%), and U-234 (0.0055%), is one of the main reasons uranium

is able to undergo nuclear fission for the production energy used in nuclear power.[18] The isotope U-235 has the ability to undergo induced nuclear fission, a rare phenomenon where a heavy nucleus is capture a neutron and split into two lighter ones releasing a large amount of energy; for this reason U-235, is critical in the production of nuclear power.[14, 19] The nuclear fuel cycle (**Figure 1.1**) begins with mining uranium from various deposits, followed by milling to separate the uranium from other material found in the ore.[18-22] After this, an increase of the concentration of the fissile isotope uranium-235 is achieved making low-enriched uranium fuel.[11] Uranium dioxide is then pressed into fuel pellets and stacked into long thin rods, which are then bundled together in a fuel assembly.[13] The fuel rods are removed from the reactor after some of the U-235 and Pu-239 have undergone fission. The material is then referred to as spent, irradiated, or used fuel. The spent fuel is then placed in water to allow it to cool; once cooled, the fuel may remain stored in the pool for years or moved to a dry storage cask.[23] The fuel is then placed in cooling pools and later stored onsite in dry casks. Ideally the nuclear plants would like to use recycled or reprocessed the spent fuel, however, in the United States energy program, there is not currently a cost-effective way to reprocess this fuel.[24]

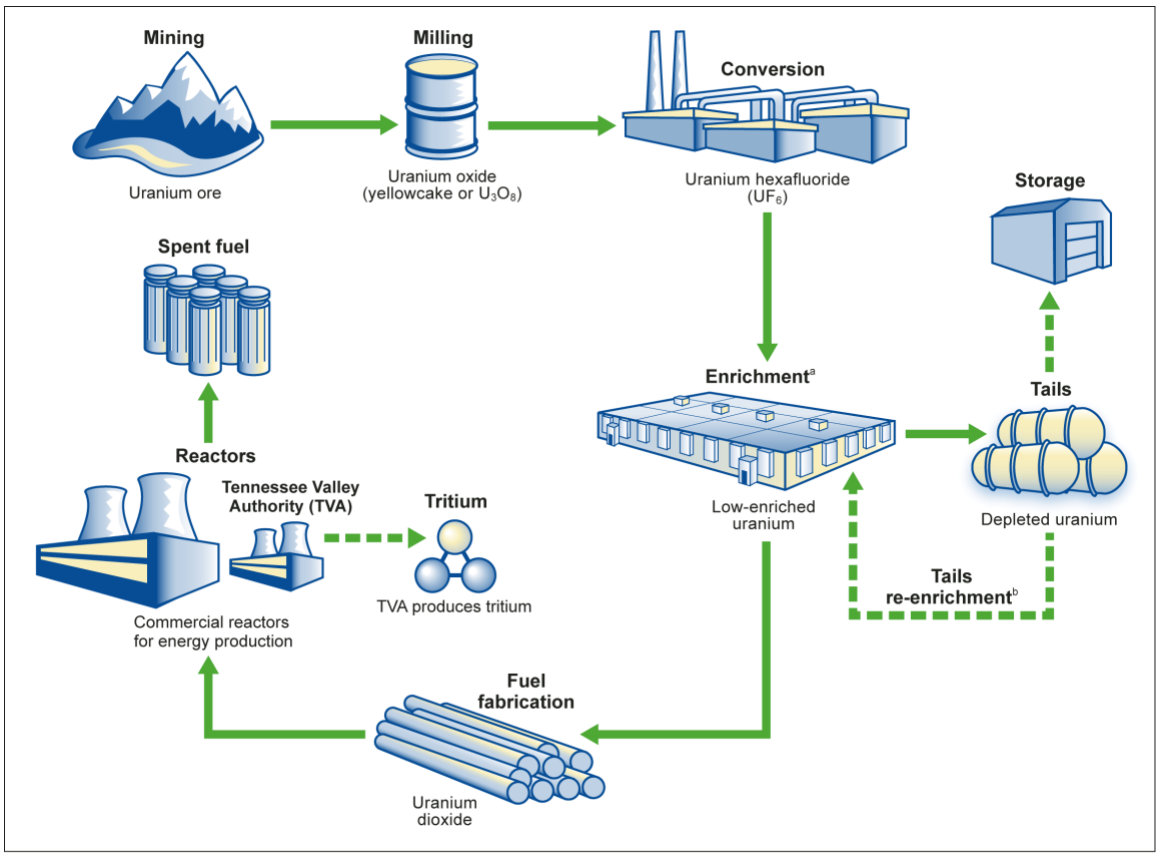

Figure 1.1 The nuclear fuel cycle[22]

James B. Conant, a former president of Harvard University, predicted that the world would turn away from the use of nuclear energy due to problems with proper waste disposal just four years after Eisenhower launched commercial generation of energy via nuclear fission.[13] During the early nuclear energy development, waste was the least of the manufacturers' concerns due to low level of understanding. Initially, the ocean was considered to be the perfect place to dump low-level radioactive waste because it was big enough to dilute the waste without causing any problems.[13] From 1946-1970, the U.S. dumped about 87,000 steel packed drums into the ocean under license by the Atomic Energy Commission (AEC); however disposal at sea did not always run smoothly. It was

determined that microorganisms can ingest toxic material and pass up toxins via the food chain to humans, thus leading to the end of ocean dumping.[25]

The U.S. turned to land disposal, which was considered a less expensive option. By 1962, 95% of radioactive waste was buried on land; in 1986 the U.S. began to develop a plan to store the waste for long-term in dry cask drums in Yucca Mountain, NV.[25-28] By 2009, there were over 1000 dry casks, each containing 100 tons or more radioactive waste scattered over 44 sites in 31 states.[29] The dry casks were originally manufactured to only last for 20 years, but were later extended to 120 years; however, the manufacturer later released a statement stating, "Leaving spent fuel on-site for extended periods of time was never intended and is not responsible."[30]

The year 2011 brought attention to the spent fuel that remained stored in pools, where the U.S. still had three quarters of their spent fuel submerged, due in large part to the nuclear crisis at the Fukushima nuclear plant in Japan. This disaster, paired with the previous September 11th terrorist attack in 2001, prompted the Department of Homeland Security and Nuclear Regulatory Commission (NRC) to investigate the possibility of a terrorist accessing the spent fuel stored in pools and releasing radioactive waste into the environment.[31] Most of the U.S. spent fuel pools were either full or had up to four times the amount they were designed to hold.[13] It was determined that the danger posed by these pools could be prevented; therefore the NRC mandated further safeguards at all operating reactor sites and a more secure storage route for dry casks, all of which are still in use today.[32-33] To date, none of the dry casks have been shipped to Yucca Mountain for storage.[15]

1.3 Current Processes for Actinides and Lanthanides Remediation

Current processes used to remediate uranium and lanthanides from spent fuel include; PUREX, DIAMEX, TRUEX, Cyanex, TALSPEAK, and SANEX. The Plutonium Uranium by Extraction (PUREX) process is the most widely used process for recycling uranium and plutonium from fuel rods as implemented in other countries, such as France.[34, 35] The PUREX process utilizes a phosphate-based ligand called tri-n-butyl phosphate (TBP) (**Figure 1.2**) to extract the uranyl from dodecane or kerosene.[36, 37] Over 99% of U(VI) and Pu(IV) ions are removed within the first few cycles of liquid-liquid extraction, and then the U(IV) and Pu(IV) are further separated.[37] Pu(IV) is reduced to Pu(III) and can be precipitated out of the solution, the U(IV) containing waste is treated with diluted acid until it precipitates out of solution.[37, 38] In the United States, issues implementing or using this method arise because of the potential for nuclear weapons proliferation with the isolation of pure plutonium.[39]

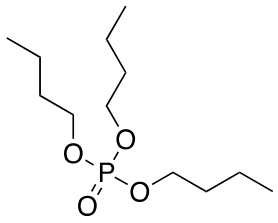

Figure 1.2 PUREX Ligand: tri-n-butylphosphate (THP)

The Diamide Extraction (DIAMAX) acts as a follow up to the PUREX process, it focuses on separating the lanthanides from the actinides.[40] It utilizes the diamide ligand, N,N'-dimethyl-N,N'-dibutyltetradecylmalonamide (**Figure 1.3**), as the extracting agent.[41] The diamide, N,N'-dimethyl-N,N'dioctylhexylethoxymalonamide (**Figure 1.3**), has been recently synthesized and used to increase the efficiency of extracting minor actinides in

the presences of lanthnides.[41]

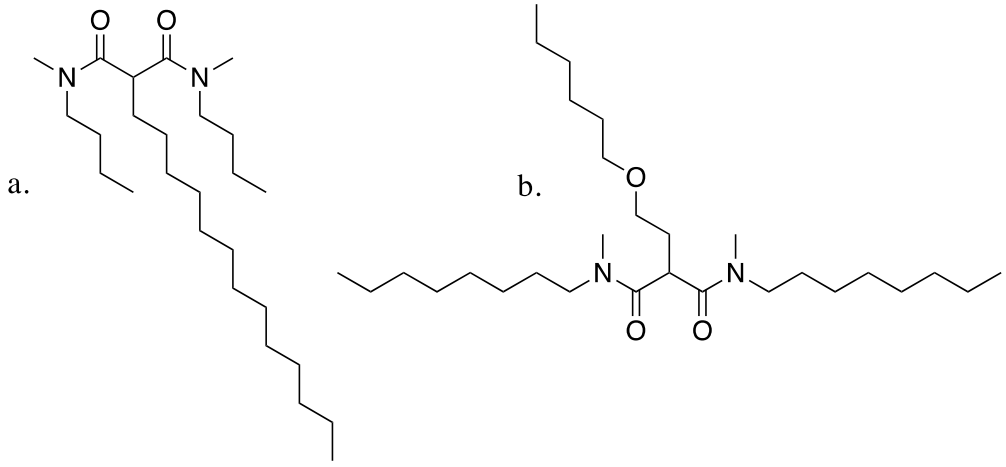

Figure 1.3 DIAMAX Ligands: (a) N,N'-dimethyl-N,N'-dibutyltetradecylmalonamide and (b) N,N'-dimethyl-N,N'dioctylhexylethoxymalonamide

The Transuranium Extraction Process, TRUEX, focuses on extracting actinides beyond uranium.[42] It utilizes the phosphine-based ligand, (N,N'-diisobutylcarbamoylmethyl)-octylphenylphosphine oxide (**Figure 1.4**), CMPO.[43] The CMPO ligand is able to successfully extract transuranium elements, however it is not considered a "stand alone" process due to its inability to differentiate between 4f and 5f elements.[43] Therefore, it has been used in conjunction with the PUREX process,[37, 44, 45] and attached to macrocycles such as calixarenes[43, 46-48] and resorcinarenes.[49, 50]

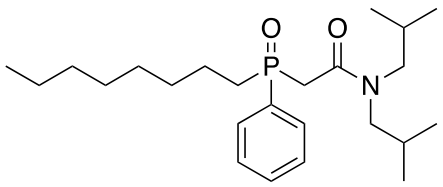

Figure 1.4 TRUEX Ligand (N,N'-diisobutylcarbamoylmethyl)-octylphenylphosphine oxide

The Cyanex process utilizes the thio-containing ligand, Cyanex 301 (**Figure 1.5**), to extract actinides over lanthanides in acidic media.[51-53] The ligand can only differentiate Am^{3+} from lanthanides, but the ligand decomposes at pH levels below 3.[54-57]

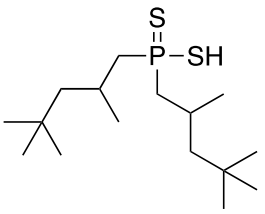

Figure 1.5 Cyanex 301[53]

The Trivalent Actinide-Lanthanide Separation by Phosphorous reagent Extraction from Aqueous Komplexes (TALSPEAK) process employs the ligand di(2-ethylhexyl)phosphoric acid (**Figure 1.6**) to extract lanthanides over actinides in aqueous media.[58] In reverse TALSPEAK the actinides are selectively removed for reprocessing.[58]

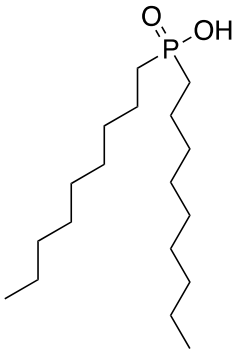

Figure 1.6 TALSPEAK ligand di(2-ethylhexyl)phosphoric acid

The Selective Actinide Extraction (SANEX) process uses N-donor ligands to selectively extract trivalent actinides in the presence of trivalent lanthanides.[59] This

process initially started with bis-1,2,4-triazide-3-yl-oligopyridine (BTP) base ligands (**Figure 1.7**) but has since move towards 6,6'-bis(5,6-dialkyl[1,2,4]triazine-3-yl)[2,2']bipyridine (DTBP) based ligands (**Figure 1.7**) to overcome the radiolytic degradation problem the BTP ligands endured in nitric acid.[60-63] The DTBP ligand not only maintained its structural integrity in acidic media, it also exhibited a high separation factor for actinides over lanthanides.[64, 65]

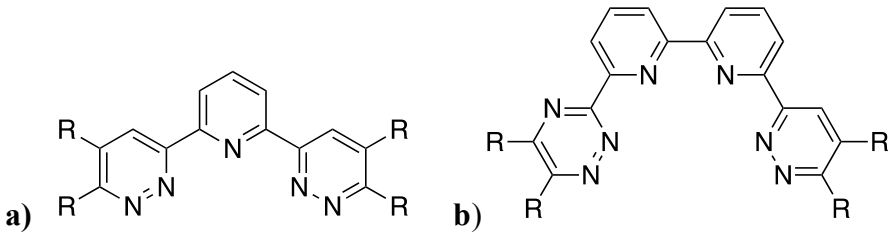

Figure 1.7 SANEX (a) bis-1,2,4-triazin-3-yloligopyridine base ligand (b) 6,6'-bis(5,6-dialkyl[1,2,4]triazine-3-yl)[2,2']bipyridine base ligand

1.4 Uranyl sensing and chemosensors

The mass accumulations of nuclear waste contain environmentally unfriendly toxins and radioactive contaminants.[15] The waste also contains recyclable radioactive metals, which could be reused if scavenged. Uranium, a major component of aqueous nuclear waste, is most commonly found in the form of the uranyl ion (UO_2^{2+}).[66] The uranyl ion is thermodynamically stable; however, uranium can also exist in various different oxidation states.[67] The reactions of uranyl ions are critical in the extraction of uranium ore, processing of nuclear fuel, precipitate processes, and in uranium distribution in the environment.[68] Unlike most transition metal oxides, the uranyl ion is linear and is more likely to create complexes with ligands in the equatorial plane, to maintain the linear U(VI) units where the two oxygen atoms ("yl"−oxygen atoms) are in the axial

positions.[18, 69] These yl-oxygen atoms were believed to be chemically inert until Clark and coworkers reported in 1999 that they are rapidly exchangeable at high pH.[70] Arnold et al. later succeeded in preparing a complex featuring covalent bond formation at one of the "yl"−oxygen atoms after uranium(VI) was reduced to uranium(V).[71-72] It is important to note, detection of some lanthanide and actinide ions based on ionic bonding is difficult in spent fuel due to similarities in ionic radii; however covalent bonds created amongst the actinides are much stronger than those created by the lanthanides, due in large to the greater radial extent of the 5f orbitals versus that of the 4f orbitals of the lanthanides.[73] Usage of detection based on covalent bond formation is useful in separation of the actinides from the lanthanides, however concentrations of actinides in contaminants are relatively low, thus giving off a very weak signal, making them hard to detect. Other issues associated with current methods of managing the nuclear contamination include; mobility, cost, sample preparation, and detection. Current methods used for actinide detection in waste include but are not limited to alpha spectroscopy and UV-Vis spectroscopy.

Alpha spectroscopy is a low-cost and robust radio-analytical method commonly used in routine analysis for the determination of isotopic ratios of alpha-radionuclides in natural samples. However, before alpha-radiometric analysis can be performed, pre-concentration and separation of the radionuclide from the matrix is required.[74] Sample preparation is vital because of the miniscule radionuclide concentration present in the sample of interest and the possibility of interference of other impurities with the emitter of alpha particles. Interferences from other impurities causes lower spectral resolution and higher detection limits. Pre-concentration and separation procedures require

additional techniques such as; extraction, co-precipitation, and ion-exchange. These additional techniques are not only time-consuming, but are costly as well.[75]

UV-Vis spectroscopy allows moderate to high sensitivity and selectivity, fair accuracy, and real-time field analysis.[75, 76] Unlike alpha spectroscopy, UV-Vis is often portable and doesn't require extensive sample preparation. Due to the low concentration of actinides in spent fuel, coupling UV-Vis with a chemosensor is ideal for the development of a real-time on-site actinide sensor. Chemosensors, such as porphyrins or salen ligands, are molecules that bind an analyte and cause a detectable change, via color change detectable by UV-Vis or an increase or decrease in fluorescence emission spectroscopy and can aid in nuclear remediation.[77] Typically, a chemosensor works by chelating a metal ion into the binding pocket. Once the metal is chelated inside the pocket, if there is a visible color change it is termed a colorimetric chemosensor, if there is a change in fluorescence it is simply referred to as a chemosensor.[76] In colorimetric chemosensors, a molecule may experience a spectral band shift from a shorter wavelength to a longer wavelength (lower frequency), which is known as a bathochromic shift, or vice versa, a hypsochromic shift. These shifts are dependent on an increase or decrease in electron densities on the chromophore moiety, which is more effectively observed for charged analytes, such as cations or anions.[78] The binding may cause a change in fluorescence; however, since metals often exist in different oxidation states a sensor must be able to efficiently detect and yield different signals for each state.[79] For example, when uranium is exposed to air it commonly forms the aforementioned uranyl (UO_2^{2+}) cation, while other actinides such as plutonium exist in the IV, V or VI oxidation state in air and aqueous solution. Therefore an efficient sensor must be able to distinguish

between these various cations.[80]

Actinides have the ability to form hydrolyzed acidic metal ions, where when placed in aqueous media, water molecules act as ligands and coordinate to the actinide ion via the oxygen donor atoms. These ions also have the ability to form strong complexes with common chelating agents, such as salen ligands.[81] These hard ions prefer to interact with hard acid donors like oxygen or carboxylate, alkoxide, and fluoride anions, but tend to exhibit covalent-like interactions with softer donor atoms, such as chloride, nitrogen, and sulfur.[79] Common methods for separation of actinides from reactor fuels tend to take advantage of their unique differences in redox chemistry.[72, 80] The large size and flexible coordination geometry of the actinide ions provides insight into the design of actinide-specific chelating agents.[82] Design specifications include using ligands that structurally control the coordination environment; therefore, an important key in designing a metal scavenging ligand is high affinity for a target metal while maintaining a low affinity for other metal ions.[83]

Salen ligands have been of interest due to their ability to form stable metal complexes.[84] They are formed from reacting a salicylaldehyde compound and an ethylene diamine compound, giving it the name "salen".[85, 86] First introduced in the 1990s, by Jacobsen and Katsuki as highly enantioselective catalysts for the asymmetric epoxidation of functionalized olefins, salen ligands have since been used in various applications.[87-89] They have been utilized as catalytic scavengers of hydrogen peroxide and cytoprotective agents, in the catalytic oxidation of secondary amines, or as catalysts for ring-opening metathesis.[88, 90] Salen-metal complexes have been utilized in medical chemistry as antitumor agents and have been shown to exhibit catalytic behavior.[91] Salen ligands can

play an important role in solid-phase extraction technologies, where they are used to scavenge toxic metals from the environment.[69, 72]

Research conducted by the Cheng research group studied chemosensors based on transmetalation of salen-based complexes.[92] In this work they determined that in order to achieve high selectivity, the ligand must have the strongest binding affinity to the metal of interest, which is nearly impossible to achieve since the ligand affinities for different metal ions cannot be anticipated in a straightforward manner.[92] In their experiment, three types of salen ligands; N,N'-bis(salicylidene)-1,2-phenylenediamine (**L1**), N,N'-bis(4-diethylamino-2hydroxybenzylidene)-1,2-dicyano-1,2-ethenediamine (**L2**) and N,N'-bis(3-chloro-5-sulfonatosalicylidene)-4,5-dimethyl-1,2-phenylenediamine disodium salt (**L3**) (**Scheme 1.1**) were studied. They were able to conclude that Cu(**L1**) exhibited the most sensitive fluorescence probes for detecting Al^{3+} giving it the ability to be used as a highly selective Al^{3+} optical chemosensor, while Pt(**L1**) complexes are phosphorescent and could be used as phosphorescent probes. Phosphorescent probes offer several advantages compared to that of fluorescence probes including: longer lifetimes of emission, larger Strokes shifts and richer excited states.[75] Unfortunately, no transmetalation reactions were observed when various metal ions were added to the solution of Pt(**L1**). The **L2** ligand, Cu(**L2**) exhibited strong capabilities for Al^{3+} selectivity, while the **L3**, which contained sulfonate groups to ensure stability and solubility in water without affecting their excited-state properties, also demonstrated great selectivity for Al^{3+} in aqueous media. This study demonstrates promising results of selective transmetalation and water-soluble sulfonated salen ligands.[92]

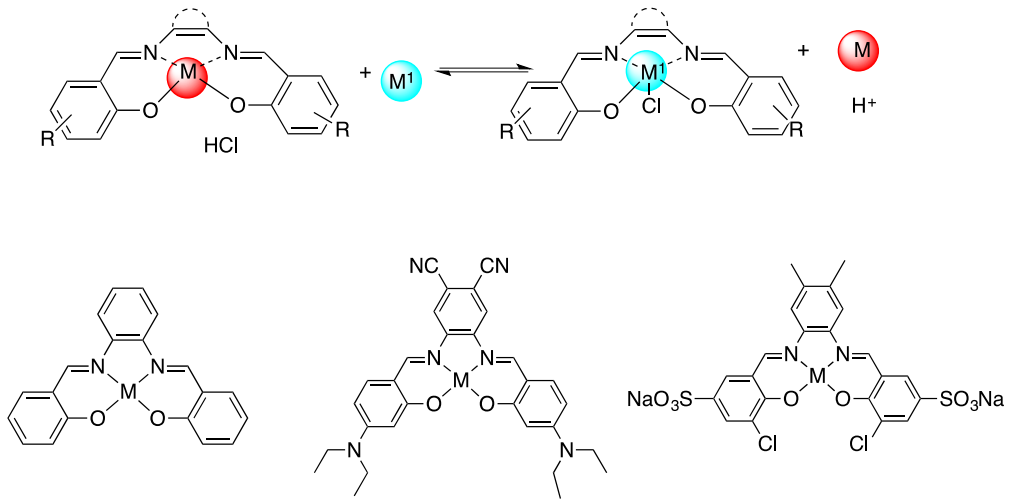

Scheme 1.1: Generic salen-based ligand detecting Al^{3+} via transmetalation and chemical structures of the actual salen complexes used in metal transmetalation.[92]

Through the use of cyclic voltammetry of the ligands depicted in **Scheme 1.2** and **1.3**, fluorescence properties of Zn pyrazolone based salen ligands shown in **Scheme 1.4**, and the reversible binding and changes in fluorescence of a binuclear Zn complex, N,N'bis(2-hydroxybenzilidene)-2,4,6-trimethylbenzene-1,3-diamine (**Scheme 1.5**) with various metals all constitutes as numerous examples of salen ligands containing Schiff base donors atoms utilized as chemosensors.[93-95] The Schley research group discovered that for the 3,5-di-tert-butyl-salicylaldehyde (bsal) based ligands (**Figure 1.8**) heterobimetallic, consisting of two different metal, complex (**1.8a**) the redox potential is 50 mV higher than that of the monometallic (**1.8b**) equivalent indicating a small electron-withdrawing effect caused by the late transition metal nickel.[93] These findings show that differences in the metal binding can cause differences in the electrochemistry of the bound metals, which could be a great way to evaluate the electrochemical behavior of actinides.[93-95]

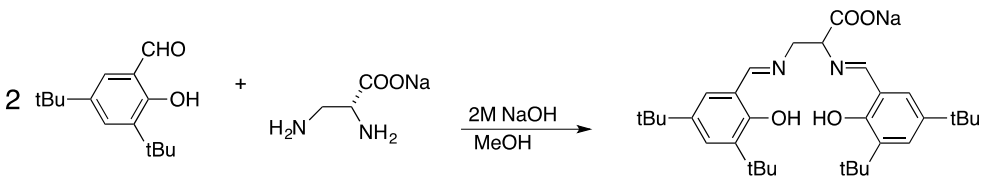

Scheme 1.2: Synthesis of salen ligand Na(H_2bsalcen) (**L4**)

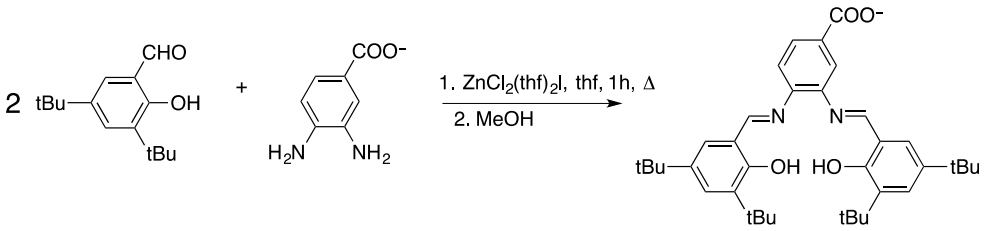

Scheme 1.3: Synthesis of salen ligand H_3bsal4cpn (**L5**) with [$ZnCl_2(THF)_2$]

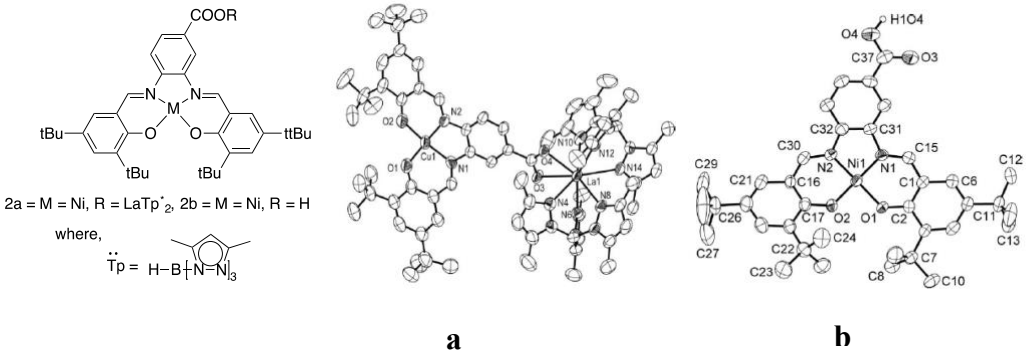

Figure 1.8: General structure of salen ligands, and crystal structures of (**a)** heterometallic complex and **(b)** monometallic complex

Song's research group studied pyrazolone-based salen ligands; they have synthesized and characterized two 4-acyl pyrazolone derivatives: N,N'-ethylamine bis[1-(4-methoxy-phenyl)-3-methyl-4-benzoylimino-2-pyrazoline-5-ol] (**L6**) and N,N'-ethylamine bis[1-(4-methoxy-phenyl)-3-methyl-4-benzoylimino-2-pyrazoline-5-ol] (**L7**) (**Scheme 1.4**).[94] Based on the ^{1}H NMR and FT-IR spectra collected, they concluded that the two Zn(II) metal complexes (**L6** and **L7**) exist as dinegative tetradentate ligands with a conjugated chelate ring in the enolized form. Upon coordinating to Zn(II), a prominent fluorescence enhancement is observed in **L6** with a significant hypsochromic shift from

544 to 459 nm denoting a CHEF (chelating-enhanced fluorescence) due to intraligand transitions.[75, 94] In contrast, coordination of **L7** with the Zn^{2+} ion, did not yield a CHEF, which may be caused by the weaker bonding forces of the Zn^{2+} ion first coordinating shell of the $(\mathbf{L7})^{2-}$ anion compared to that of the $(\mathbf{L6})^{2-}$ anion. The hypsochromic shift observed in **L6** is an important characteristic for chemosensor applications.

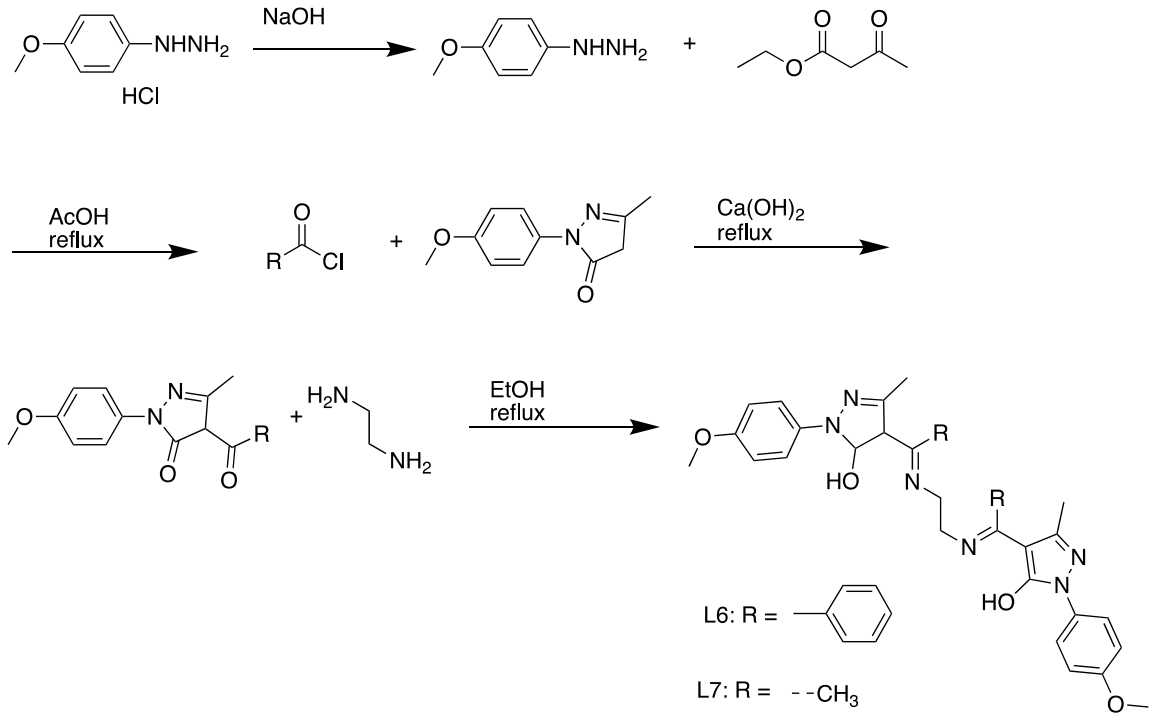

Scheme 1.4: Synthetic route of the ligands **L6** and **L7**[94]

To date, there have been only a few systems devised with the ability to selectively and reversibly recognize heavy and transition metals (HTM) ions by the emission of distinct signals; however, the Pandey research group has been able to synthesize a Schiff base ligand, N,N'bis(2-hydroxybenzilidene)-2,4,6-trimethylbenzene-1,3-diamine (**L8**), exhibiting on-off switch capabilities towards Cu^{2+} and Ag^{+} ions.[95] The binuclear Zn complex of the ligand exhibited (**Scheme 1.5**) stability in the pH range of 6-12 with

optimal stability in the range of 7.0-7.4. The maximum or minimum fluorogenic output of the ligand is attributed to the weak interactions of [M-π (-CH=N-)] between the ligand and metal ions.[95-97] The Cu^{2+} and Ag^{+} ions do not displace Zn^{2+}, instead they interact weakly with the –CH=N- unit of the ligand by metal-to-ligand-charge transfer for Cu^{2+} and ligand-to-metal-charge transfer for Ag^{+} (**Figure 1.9**). With the ability to act as a molecular keypad lock system, which follows correct chemical orders due to reversible on-off behavior, this ligand has the ability to yield a new class of chemosensors.[95] The aforementioned study once again provides a salen ligand in an application of a chemosensor that can selectively detect specific metal ions.

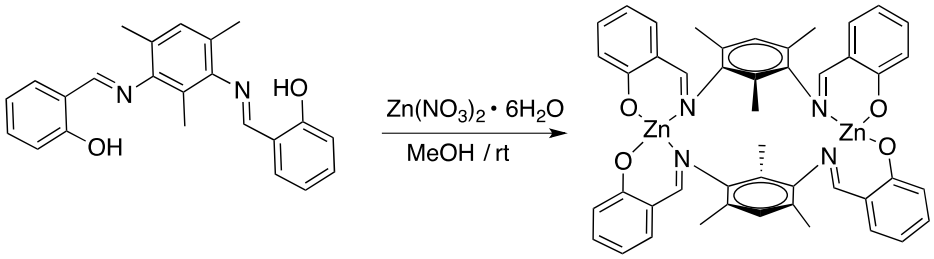

Scheme 1.5: Synthesis of **L8**-metal complex[95]

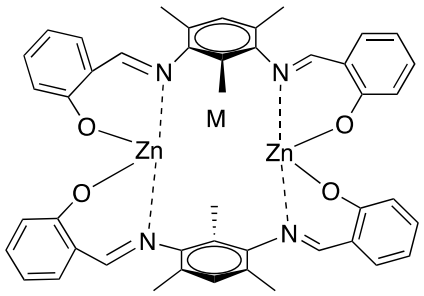

M = Ag or Cu

Figure 1.9: M = Ag^{+}/ Cu^{2+} metal ions interacting weakly with the –CH=N- unit of **L8**.[95]

Raymond and co-workers have studied actinide-specific chelators for both environmental decontamination and chelation therapy applications. This "HOPO"

(hydroxypyridonates) class of ligands offer a biomimetic, synthetic approach with the ability to mimic that of a biological process approach with promising potential as biological decorporation, the therapeutic process in which radioactive material is removed from the body, agents due to their high affinity and selectivity towards actinides.[98] They have synthesized a siderophore inspired [TAM(HOPO)^2] class of ligands (**L9**) (**Figure 1.10**) featuring a 2,3-dihydroxy terephthalamide (TAM) backbone with ethyl or phenyl linkers on either end terminating in hydroxypyridonates groups (either Me-3,2-HOPO or 1,2-HOPO).[99] Uranyl(VI) adducts of this ligand, [UO_2(**L9**)$^{2-}$] were found to exhibit saturated chelation of the uranyl ion with the oxygen atoms of the ligand. The coordinate saturation, the ligand's ability to form σ and π bond via donation and π bonds by accepting electron density from the metal to achieve complete saturation of coordinating sites, of the metal-ligand complex offers promising results for the incorporation of the uranyl ion into a salen pocket.[74, 98, 100]

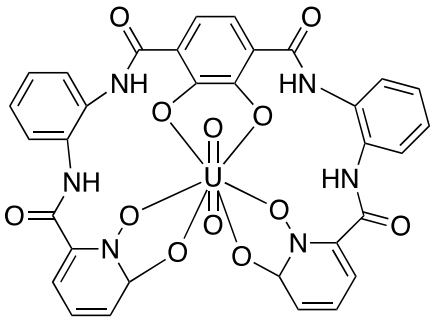

Figure 1.10: [UO_2(**L9**)$^{2-}$] ligand-metal complex with phenylene linker and 1,2-HOPO terminal groups[98]

Work conducted by Cametti and co-workers focused on the ion-recognition attributes of uranyl complexes with salen/salophen-type ligands.[99] They successfully

synthesized a salen ligand functionalized with a phenyl methoxy "side-arm" forming the $[UO_2(salen)]\cdot CsF\cdot CHCl_3$ complex, a dimeric 2:2 complex mediated by coordination of two cesium cations to two uranyl receptor molecules (**Figure 1.11**).[101] They later showed that uranyl−salophen complexes could co-crystallize tetramethylammonium halide salts revealing, that anion recognition is obtained via equatorial binding to the uranyl cation, while cation recognition is achieved through cation- π /CH- π interactions of the quaternary ions with the aromatic side arms of the ligand.[102]

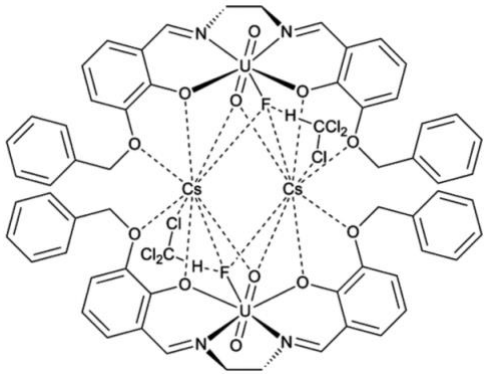

Figure 1.11: Salen ligand uranyl complex:[101] $[UO_2(salen)]\cdot CsF\cdot CHCl_3$

Research conducted by the Khashab research lab utilized bovine serum albumin-stabilized gold nanoclusters (BSA-AuNCs) to create a simple, reliable, and selective colorimetric sensor for uranyl ions in seawater.[103] As depicted in **Scheme 1.6** BSA-AuNCs strong peroxidase activity, which is mostly attributed to the transitions of free electrons of gold nanoclusters (AuNCs), the detection mechanism is based on the ability of TMB (3,3′,5,5'-tetramethylbenzidine) to oxidize in the presence of hydrogen peroxide and BSA-AuNCs and rapidly transform into a blue charge-transfer complex (chromogen).[103-105] However in the presence of uranyl, the peroxidase-like activity of BSA-AuNCs is inhibited.[103] Under optimized conditions the detection limit of uranyl is

1.86 μM with a signal-to-noise ratio of 3.[103] The selectivity of the system was then tested against other ions including; Li^+, Na^+, Al^{3+}, S^{2-}, K^+, Ca^{2+}, Fe^{3+}, Co^{2+}, Cu^{2+}, Zn^{2+}, Ag^+, I^-, Hg^{2+}, and Pb^{2+}. There were no observable changes for all the metal ions, excluding Hg^{2+} and Ag^+; however, a solution of potassium iodide was used to form a stable masking reagent with those ions, thus "muting" their assay responses and creating a selective colormetric uranyl sensor.[103]

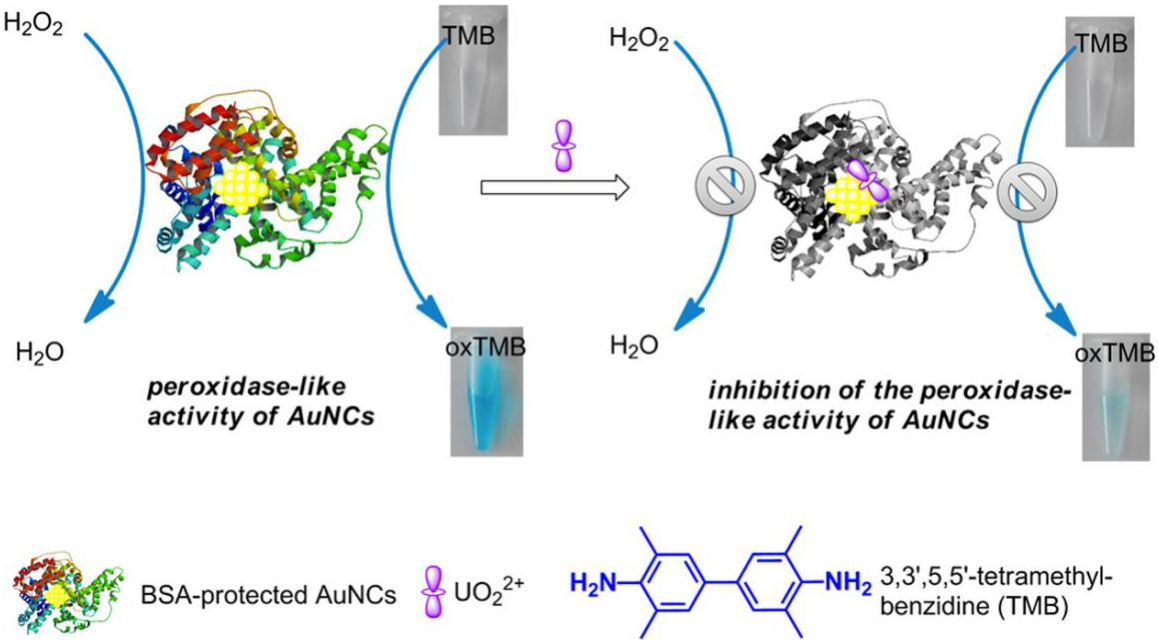

Scheme 1.6: Sensing of uranyl ion sensor via the inhibition of BSA-AuNCs peroxidase activity.[103]

Wang, and researchers have also studied the detection of uranyl in natural water systems. Their research is centered on using luminescent mesoporous terbium(III)-based Metal-Organic Framework (MOF) systems equipped with exposed Lewis base sites capable of quenching the luminescence of the system in the presence of uranyl.[106] As depicted in **Scheme 1.7**, the MOF contains a 3-D framework with a series of 1-D rhombic channels with dimensions of 27 x 23 $Å^2$ capable of accommodating uranyl

cations.[106] The channels are equipped with substantial amounts of readily available coordination amine (6 mol per mole of MOF) and triazine groups (6 mol per mole of MOF) facing inward to chelate uranyl ions.[106] In samples of 5 mg/L and 50 mg/L, the MOF was able to remove 80% and 60% of uranyl respectively from the samples in as little as 10 minutes. The detection limit of the system was determined to be 0.9 µg/L, which is lower than the maximum contamination standard (30 µg/L) in drinking water as defined by the United States Environmental Protection Agency.[106-108] To determine the selectivity of the system, the MOF was submerged in several aqueous metal nitrate solutions including, Th^{4+}, Eu^{3+}, Sr^{2+} , Al^{3+} , Ca^{2+} , Cs^{+} , K^{+}. There were negligible influences on the emission intensity of the MOF from the metal cations tested, excluding Eu^{3+} which yielded notable quenching of the luminescence but not nearly as much as uranyl.[106] When uranyl was added to the aforementioned metal solutions, the luminescence was completely quenched. Wang attributed this uranyl selective quenching to the electronic structure of the uranyl ion, which has the capability of a more efficient resonance energy transfer that can be amplified by the soft nitrogen donor ligand, which in return enables selective enrichment of the uranyl ion in the presence of competing cations.[106]

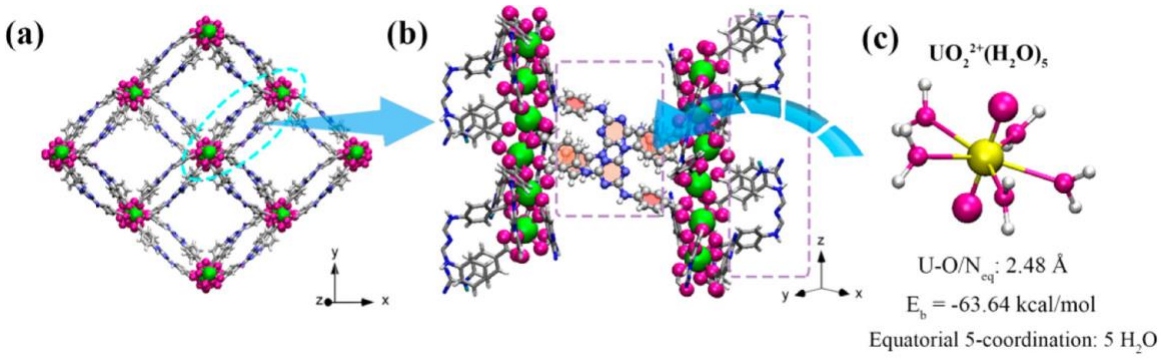

Scheme 1.7: (a) Crystal structure of compound MOF along Z axis. (b) Fragment of compound MOF. (c) Structure of uranyl hydrate.[106]

1.5 Conclusion

Since its discovery in 1789, uranium has flourished from an insignificant element commonly used to color glassware and in pottery glaze to the leading non-petroleum fuel source for nuclear energy. Nuclear power is a low cost, reliable energy source with a low carbon footprint. Unfortunately, the nuclear fuel cycle produces an abundance of recyclable radioactive metal enriched wastes. Current methods used to extract these radioactive metals include PUREX, SANEX, TALSPEAK, Cynex, DIAMAX, and, TRUEX. However, these processes are time-consuming and performed under extremely acidic conditions or require environmental-unfriendly hydrocarbons, such as kerosene and dodecane. Chemosensors are molecules that bind an analyte and cause a detectable change, via color change or fluorescence detectable by UV-Vis spectroscopy and can aid in nuclear remediation. The aforementioned research performed by Cametti, Wang, and Khashab, are all examples of promising uranyl chemosensors; however, there is still a need for a real-time, highly selective uranyl sensor with capabilities of detecting uranyl in various media.

1.6 References:

1. Wilhelm, H. A., Development of Uranium Metal Production in America. *J. Chem. Educ.* **1960,** *37* (2), 56-68.

2. Rossi, A., Eugene Melchlior Peligot. *J. Am. Chem. Soc.* **1890,** *12* (5), 128-130.

3. Weeks, M. E., The Discovery of the Elements V. Chromium. Molybdenium, Tungsten, and Uranium. *J. Chem. Educ.* **1932,** *9* (3), 459-473.

4. Regnault et al., Recherches sur l'uranium. *Annales de Chimie et de Physique* **1842**. 5-5-512

5. Zimmermann, V. C., Untersuchungen uber das uran. *Justus Liebig's Annalen der Chemie* **1882,** *213*, 285-329.

6. Madden, E., *Source books in the History of the Sciences: A Source Book in Physics*. Harvard University Press: 1963. General Ed.

7. Garrett, A., Radioactivity- Henri Becquerel. *J. Chem. Educ.* **1962,** *39* (10), 533-534.

8. Emsley, J., *Nature's Building Blocks*. Oxford University Press: Oxford, NY, 2011.

9. Wolke, R., Marie Curie's Doctoral Thesis- Prelude to a Nobel Prize. *J. Chem. Educ.* **1988,** *65* (7), 561-573

10. Waclawek, W.; Waclawek, M., Marie Sklodowska-Curie and her Contributions to Chemistry, Radiochemistry and Radiotherapy. *Anal. Bioanal. Chem.* **2011,** *400* (6), 1567-75.

11. Ferguson, C. D., *Nuclear Energy: What Everyone Needs to Know*. Oxford University Press: New York, NY, 2011

12. Chestnut, L. G.; Mills, D. M., A Fresh Look at the Benefits and Costs of the US Acid Rain Program. *J. Environ. Manage.* **2005,** *77* (3), 252-66.

13. Alley, W. M. Alley, R., *Too Hot to Touch: The Problem of High-Level Nuclear Waste*. Cambridge University Press: New York, NY, 2013

14. Hala, J.; Navratil, J. D., *Radioactivity, Ionizing Radiation, and Nuclear Energy*. Konvoj, spol. s.r.o. (Ltd): Brno, Czech Republic, 2003.

15. Pravalie, R.; Bandoc, G., Nuclear Energy: Between Global Electricity Demand, Worldwide Decarbonisation Imperativeness, and Planetary Environmental Implications. *J. Environ. Manage.* **2018,** *209*, 81-92.

16. Kharecha, P. A.; Kutscher, C. F.; Hansen, J. E.; Mazria, E., Options for Near-Term Phaseout of CO_2 Emissions from Coal use in the United States. *Environ. Sci. Technol.* **2010,** *44* (11), 4050-62

17. Committee of Nuclear and Alternative Energy Systems National ResearchCouncil., *Problems of U. S. Uranium Resources and Supply to the Year 2010: Supporting Paper 1*. National Academy of Sciences: Washington, D. C., 1978

18. Maher, K.; Bargar, J. R.; Brown, G. E., Jr., Environmental Speciation of Actinides. *Inorg. Chem.* **2013,** *52* (7), 3510-32.

19. Jovanovic, S. V.; Pan, P.; Wong, L., Bioaccessibility of Uranium in Soil Samples from Port Hope, Ontario, Canada. *Environ. Sci. Technol.* **2012,** *46* (16), 9012-8.

20. Choppin, G.; Liljenzin, J.-O.; Rydberg, J., *Radiochemistry and Nuclear Chemistry*. 3rd ed.; Butterworth-Heinemann: Woburn, MA, 2002.

21. Spiro, T. G.; Stigliani, W. M., *Chemistry of the Environment*. 2nd ed.; Prentice-Hall Inc.: Upper Saddle River, NJ, 2003.

22. Markey, E.; Burgess, M., Interagency Review Needed to Update U.S. Position on Enriched Uranium That Can Be Used for Tritium Production. Department of Energy. United States Government Accountability Office: 2014.

23. Buck, A., *The Atomic Energy Commission*. U.S. Department of Energy: Washington, D.C, 1983. https://www.energy.gov/sites/prod/files/AEC%20History.pdf (accessed April 13, 2019)

24. The Uranium Insitute., *Uranium and Nuclear Energy: 1988*. A E Thompson Publishing: London, 1989.

25. Vosniakos, F. K., *Radioactivity Transfer in the Environment and in Food*. Springer: New York, 2012.

26. Cohen, J. J.; Lewis, A. E.; Braun, R. L., Use of a Deep Nuclear Chimney for the In-situ Incorporation of Nuclear Fuel-Reprocessing Waste in Molten Silicate Rock. *Nuclear Tech.* **1972,** *13*, 76-88.

27. Hanks, T. C.; Winograd, I. J.; Anderson, R. E.; Reilly, T. E.; Weeks, E. P., *Yucca Mountain as a Radioactive-Waste Repository*. U.S. Geological Survey: Menlo Park, CA, 1998.

28. Ringholz, R. C., *Uranium Frenzy: Saga of the Nuclear West*. Revised and Expanded Ed.; Utah State University Press: Logan, UT, 2002.

29. Sullivan, J., Environment: Nuclear Plants face Storing Toxic Waste. *The New York Times* 2001.

30. United States Nuclear Waste Technical Review Board. *Summer Board Meeting*; Las vegas, NV, 2009. https://www.nwtrb.gov/docs/default-source/meetings/2009/june/09june11a7989148abad67069638ff00003d5b4b.pdf?sfvrsn=6. (accessed April 13, 2019)

31. Committee of Safety and Security of Commerical Spent Nuclear Fuel Storage Board of Radioactive Waste Management. *Safety and Security of Commericial Spent Fuel Storage: Public Report* The National Academy of Sciences: Washington, D. C., 2006.

32. Rules and Regulations. Federal Register: Washington, D. C., 2008; Vol. 73, pp 59479-60094.

33. Issuance of Order to Modify Licenses with Regard to Requirements for Mitigation Strategies for Beyond-Design Basis External Events. U. S. A. Nuclear Regulatory Commission. In *EA-12-049*, Commission, United States of America Regulatory Commission. Washington, D. C., 2012.

34. Joshi, J. M.; Pathak, P. N.; Manchanda, V. K., Selective Removal of Uranium from High‐Level Waste Solution Employing Tri‐n‐Butyl Phosphate as the Extractant. *Solvent Extr. Ion Exc.* **2005,** *23* (5), 663-675.

35. May, I.; Taylor, R. J.; Wallwork, A. L.; Hastings, J. J.; Fedorov, Y. S.; Zilberman, B. Y.; Mishin, E. N.; Arkhipov, S. A.; Blazheva, I. V.; Poverkova, L. Y.; Livens, F. R.; Charnock, J. M., The Influence of Dibutylphosphate on Actinide Extraction by 30% Tributylphosphate. *Radiochim. Acta* **2000,** *88* (5).

36. International Atomic Energy Agency. Spent Fuel Reprocessing Options. Agency, **2008**. IAEA-TECDOC-1587

37. Paiva, A. P.; Malik, P., Recent Advances on the Chemistry of Solvent Extraction Applied to the Reprocessing of Spent Nuclear Fuels and Radioactive Wastes. *J. Radioanal. Nucl. Chem.* **2004,** *261* (2), 485-496.

38. Mckibben, J. M., Chemistry of the Purex Process. *Radiochim. Acta* **1984,** *36*.

39. Galperin, A.; Reichert, P.; Radkowsky, A., Thorium Fuel for Light Water Reactors—Reducing Proliferation Potential of Nuclear Power Fuel Cycle. *Science & Global Security* **1997,** *6* (3), 265-290.

40. Modolo, G.; Vijgen, H.; Serrano‐Purroy, D.; Christiansen, B.; Malmbeck, R.; Sorel, C.; Baron, P., DIAMEX Counter‐Current Extraction Process for Recovery of Trivalent Actinides from Simulated High Active Concentrate. *Sep. Sci. Technol.* **2007,** *42* (3), 439-452.

41. Serrano-Purroy, D.; Baron, P.; Christiansen, B.; Malmbeck, R.; Sorel, C.; Glatz, J. P., Recovery of Minor Actinides From HLLW Using the DIAMEX Process. *Radiochim. Acta* **2005,** *93*, 351-355.

42. Horwitz, E. P.; Kalina, D. G.; Diamond, H.; Vandegrift, G. F.; Schulz, W. W., The Truex Process- A Process for the Extraction of the Transuranic Elements From Nitric Acid Wastes Utilizing Modified Purex Solvent. *Sol. Extr. Ion Exc.* **1985,** *3* (1 & 2), 75-109.

43. Schwing-Weill et al. Calix[4]Arenes with CMPO Functions at the Narrow Rim. Synthesis and Extraction Properties. *J. Chem. Soc. Perkin Trans. 2* **1999**, 719-723.

44. Chitnis, R. R.; Wattal, P. K.; Ramanujam, A.; Dhami, P. S.; Gopalakrishnan, V.; Bauri, A. K.; Banerji, A., Recovery of Actinides Extracted by Truex Solvent From High Level Waste Using Complexing Agents A. Counter-Current Studies. *J. Radioanal. Nucl. Chem.* **1999,** *240* (3), 727-730.

45. Peters, M. W.; Werner, E. J.; Scott, M. J., Enhanced Selectivity for Actinides over Lanthanides with CMPO Ligands Secured to a C3-Symmetric Triphenoxymethane Platform. *Inorg. Chem.* **2002,** *41* (1707-1716).

46. Motornaya, A.; Vatsouro, I.; Shokova, E.; Hubscher-Bruder, V.; Alyapyshev, M.; Babain, V.; Karavan, M.; Arnaud-Neu, F.; Böhmer, V.; Kovalev, V., Adamantylcalixarenes with CMPO Groups at the Wide Rim: Synthesis and Extraction of Lanthanides and Actinides. *Tetrahedron* **2007,** *63* (22), 4748-4755.

47. Arduini, A. B. h., V.; Delmau, L.; Desreux, J. F.; Dozol, J. F.; Carrera, M. A. G. L., B.; Musigmann, C.; Pochini, A.; Shivanyuk, A. U., F., Rigidified Calixarenes Bearing Four Carbamoylmethylphosphineoxide or Carbamoylmethylphosphoryl Functions at the Wide Rim. *Chem. Eur. J.* **2000,** *6*, 2135-2144.

48. Schmidt, C. S., M.; Bo¨hmer, V.; Host, V.; Spirlet, M. R.; Desreux, J. F. B., F.; Arnaud-Neu, F.; Dozol, J. F., Modification of Calix[4]Arenes with CMPO-Functions at the Wide Rim. Synthesis, Solution Behavior, and Separation of Actinides From Lanthanides. *Org. Biomol. Chem.* **2003,** *1*, 4089-4096.

49. Boerrigter, H.; Verboom, W.; Jong, F.; Reinhoudt, D., Europium(III) Extraction with New Resorcinarene Cavitand CMP(O) Ligands- Solvent Extraction and Mechanistic Study. *Radiochim. Acta* **1998,** *81*, 39-45.

50. Boerrigter, H.; Verboom, W.; Reinhoudt, D., Novel Resorcinarene Cavitand-Based CMP(O) Cation Ligands- Synthesis and Extraction Properties. *J. Org. Chem.* **1997,** *62* (21), 7148-7155.

51. Sole, K. C.; Hiskey, J. B., Solvent Extraction of Copper by Cyanex 272, Cyanex 302 and Cyanex 301. *Hydrometallurgy* **1995,** *37*, 129-147.

52. Bhattacharyya, A.; Mohapatra, P. K.; Manchanda, V. K., Separation of Trivalent Actinides and Lanthanides Using a Flat Sheet Supported Liquid Membrane Containing Cyanex-301 as the Carrier. *Sep. and Purif. Technol.* **2006,** *50* (2), 278-281.

53. Hill, C.; Madic, C.; Baron, P.; Ozawa, M.; Tanaka, Y., Trivalent Minor Actinides: Lanthanides Separation, Using Organophosphinic Acids. *J. Alloys Compd.* **1998,** *271*, 159-162.

54. Modolo, G.; Odoj, R., Influence of the Purity And Irradiation Stability of Cyanex 301 on the Separation of Trivalent Actinides From Lanthanides By Solvent Extraction. *J. Radioanal. Nucl. Chem.* **1998,** *228* (1-2), 83-88.

55. Modolo, G.; Odoj, R., The Separation of Trivalent Actinides From Lanthanides By Dithiophosphinic Acids From HNO_3 Acid Medium. *J. Alloys Compd.* **1998,** *271-273*, 248-251.

56. Scott et al. CMPO-Functionalized C3-Symmetric Tripodal Ligands in Liquid/Liquid Extractions: Efficient, Selective Recognition of Pu(IV) with Low Affinity for 3+ Metal Ions. *Inorg. Chem.* **2007,** *46*, 10549-10563.

57. Klaehn, J. R.; Peterman, D. R.; Harrup, M. K.; Tillotson, R. D.; Luther, T. A.; Law, J. D.; Daniels, L. M., Synthesis of Symmetric Dithiophosphinic Acids for "Minor Actinide" Extraction. *Inorg. Chim. Acta* **2008,** *361* (8), 2522-2532.

58. Nilsson, M.; Nash, K. L., Review Article: A Review of the Development and Operational Characteristics of the TALSPEAK Process. *Solvent Extr. Ion Exch.* **2007,** *25* (6), 665-701.

59. Hudson, M. J.; Boucher, C. E.; Braekers, D.; Desreux, J. F.; Drew, M. G. B.; Foreman, M. R. S. J.; Harwood, L. M.; Hill, C. M.; Madic, C.; Marken, F.; Youngs, T. G. A., New Bis(Triazinyl) Pyridines for Selective Extraction of Americium(III). *New J. Chem.* **2006,** *30* (8), 1171.

60. Kolarik, Z.; Müllich, U.; Gassner, F., Selective Extraction Of Am(III) Over Eu(III) By 2,6-Ditriazolyl- and 2,6-Ditriazinylpyridines. *Solvent Extr. Ion Exch.* **1999,** *17* (1), 23-32.

61. Kolarik, Z.; Mullich, U.; Gassner, F., Extraction of Am(Ill) and Eu(Ill) Nitrates By 2-6-Di-(5,6-Dipropyl-1,2,4-Triazin-3-yl)Pyridines. *Solvent Extr. Ion Exch* **2010,** *17* (5), 1155-1170.

62. Drew, M. G. B.; Foreman, M. R. S. J.; Geist, A.; Hudson, M. J.; Marken, F.; Norman, V.; Weigl, M., Synthesis, Structure, And Redox States of Homoleptic D-Block Metal Complexes with Bis-1,2,4-Triazin-3-yl-Pyridine And 1,2,4-Triazin-3-yl-Bipyridine Extractants. *Polyhedron* **2006,** *25* (4), 888-900.

63. Geist, A.; Hill, C.; Modolo, G.; Foreman, M. R. S. J.; Weigl, M.; Gompper, K.; Hudson, M. J., 6,6' - Bis(5,5,8,8 - tetramethyl - 5,6,7,8 - tetrahydro - benzo[1,2,4]triazin - 3 - yl) [2,2']bipyridine, an Effective Extracting Agent for the Separation of Americium(III) and Curium(III) from the Lanthanides. *Solvent Extr. Ion Exch* **2006,** *24* (4), 463-483.

64. Magnusson, D.; Christiansen, B.; Malmbeck, R.; Glatz, J.-P., Investigation of the Radiolytic Stability of a Cyme4-BTBP Based SANEX Solvent. *Radiochim. Acta* **2009,** *97* (9).

65. Magnusson, D.; Christiansen, B.; Glatz, J. P.; Malmbeck, R.; Modolo, G.; Serrano-Purroy, D.; Sorel, C., Towards an Optimized Flow-Sheet for a SANEX Demonstration Process Using Centrifugal Contactors. *Radiochim. Acta* **2009,** *97* (3).

66. Bots, P.; Morris, K.; Hibberd, R.; Law, G. T.; Mosselmans, J. F.; Brown, A. P.; Doutch, J.; Smith, A. J.; Shaw, S., Formation of Stable Uranium(VI) Colloidal Nanoparticles in Conditions Relevant to Radioactive Waste Disposal. *Languir* **2014,** *30* (48), 14396-405.

67. Zielinski, R. A.; Chafin, D. T.; Banta, E. R.; Szabo, B. J., Use of 234U and 238U Isotopes to Evaluate Contamination of Near-Surface Groundwater with Uranium-Mill Effluent: A Case Study in South-Central Colorado, U.S.A. *Environ. Geol.* **1997,** *32* (2), 124-136.

68. Peled, Y.; Krent, E.; Tal, N.; Tobias, H.; Mandler, D., Electrochemical Determination of Low Levels of Uranyl by a Vibrating Gold Microelectrode. *Anal. Chem.* **2015,** *87* (1), 768-76.

69. Moll, H.; Rossberg, A.; Steudtner, R.; Drobot, B.; Muller, K.; Tsushima, S., Uranium(VI) Chemistry in Strong Alkaline Solution: Speciation and Oxygen Exchange Mechanism. *Inorg. Chem.* **2014,** *53* (3), 1585-93.

70. Clark, D. L.; Conradson, S. D.; Donohoe, R. J.; Keogh, D. W.; Morris, D. E.; Palmer, P. D.; Rogers, R. D.; Tait, C. D., Chemical Speciation of the Uranyl Ion Under Highly Alkaline Conditions. Synthesis,Structures, and Oxo Ligand Exchange Dynamics. *Inorg. Chem.* **1999,** *38* (7), 1456-1466.

71. Arnold, P. L.; Pecharman, A. F.; Love, J. B., Oxo Group Protonation and Silylation of Pentavalent Uranyl Pacman cCmplexes. *Angew. Chem. Int. Ed. Engl.* **2011,** *50* (40), 9456-8.

72. Arnold, P. L.; Hollis, E.; White, F. J.; Magnani, N.; Caciuffo, R.; Love, J. B., Single-Electron Uranyl Reduction by a Rare-Earth Cation. *Angew. Chem. Int. Ed. Engl.* **2011,** *50* (4), 887-90.

73. Lukens, W. W.; Edelstein, N. M.; Magnani, N.; Hayton, T. W.; Fortier, S.; Seaman, L. A., Quantifying The Sigma And Pi Interactions Between U(V) F Orbitals And Halide, Alkyl, Alkoxide, Amide and Ketimide Ligands. *J. Am. Chem. Soc.* **2013,** *135* (29), 10742-54.

74. Pashalidis, I.; Tsertos, H., Radiometric Determination of Uranium in Natural Waters After Enrichment and Separation by Cation-Exchange and Liquid-Liquid Extraction. *J. Radioanal.Nucl. Chem.* **2004,** *260* (3), 439-442.

75. Skoog, D. A.; Hollar, F. J.; Crouch, S. R., *Instrumental Analysis*. International Student Ed.; Cengage Learning: 2007.

76. Sessler, J. L.; Melfi, P. J.; Seidel, D.; Gorden, A. E. V.; Ford, D. K.; Palmer, P. D.; Tait, C. D., Hexaphyrin(1.0.1.0.0.0). A New Colorimetric Actinide Sensor. *Tetrahedron* **2004,** *60* (49), 11089-11097.

77. Shamov, G. A., Oxidative Nucleophilic Substitution of Hydrogen in the Sapphyrin Dioxouranium(VI) Complex: A Relativistic DFT Study. *J. Am. Chem. Soc.* **2011,** *133* (12), 4316-29.

78. Kaur, N.; Kumar, S., Colorimetric Metal Ion Sensors. *Tetrahedron* **2011,** *67* (48), 9233-9264.

79. Choppin, G. R., Solution Chemistry of the Actinides. *Radiochim. Acta* **1982,** *32* (1), 43-53.

80. Morss, L. R, Edelstein, N. Fuger, J., Katz, J. J. *The Chemistry of the Actinides and Transactinides Elements*. 3rd ed.; Springer: Dordrecht, The Netherlands, 2006; Vol. 1.

81. Clark, D. L.; Hobart, D. E.; Neu, M. P., Actinide Carbonate Complexes and Their Importance in Actinide Environmental Chemistry. *Chem Rev* **1995,** *95* (1), 25-48.

82. Gorden, A. E. V.; Xu, J.; Raymond, K. N.; Durbin, P., Rational Design of Sequestering Agents for Plutonium and Other Actinides. *Chem. Rev.* **2003,** *103* (11), 4207-4282.

83. Xu, J.; Radkov, E.; Ziegler, M.; Raymond, K. N., Plutonium(IV) Sequestration: Structural and Thermodynamic Evaluation of the Extraordinarily Stable Cerium(IV) Hydroxypyridinonate Complexes1. *Inorg. Chem.* **2000,** *39* (18), 4156-4164.

84. Bregman, H.; Williams, D. S.; Atilla, G. E.; Carroll, P. J.; Meggers, E., An Organometallic Inhibitor for Glycogen Synthase Kinase 3. *J. Am. Chem. Soc.* **2004,** *126* (42), 13594-5.

85. Gorden, A. E. V.; Wu, X. 2-Quinoxalinol Salen Compounds and Uses Thereof. U. S. Patent 0286968, November 19, 2009.

86. Wu, X.; Bharara, M. S.; Bray, T. H.; Tate, B. K.; Gorden, A. E. V., Synthesis and Characterization of 2-Quinoxalinol Schiff-Base Metal Complexes. *Inorg. Chim. Acta* **2009,** *362* (6), 1847-1854.

87. Irie, R.; Noda, K.; Ito, Y.; Matsumoto, N.; Katsuki, T., Catalytic Asymmetric Expoxidation of Unfunctionalized Olefins. *Tetrahedron Lett.***1990,** *31* (50), 7345-7348.

88. Zhang, W.; Loebach, J. L.; Wilson, S. R.; Jacobsen, E. N., Enantioselective Epoxidation of Unfunctionalized Olefins Catalyzed by Salen Manganese Complexes. *J. Am. Chem. Soc.* **1990,** *112* (7), 2801-2803.

89. Naik, A. D.; Fontaine, G.; Bellayer, S.; Bourbigot, S., Crossing the Traditional Boundaries: Salen-Based Schiff Bases for Thermal Protective Applications. *ACS Appl. Mater. Interfaces* **2015,** *7* (38), 21208-17.

90. Holbach, M.; Weck, M., Modular Approach for the Development of Supported, Monofunctionalized, Salen Catalyst. *J. Org. Chem* **2006,** *71* (5), 1825-1836.

91. Marzano, C.; Pellei, M.; Colavito, D.; Alidori, S.; Lobbia, G. G.; Gandin, V.; Tisato, F.; Santini, C., Synthesis, Characterization, and in Vitro Antitumor Properties of Tris(hydroxymethyl)phosphine Copper(I) Complexes Containing the New Bis(1,2,4-triazol-1-yl)acetate Ligand. *J. Medi. Chem.* **2006,** *49* (25), 7317-7324.

92. Cheng, J.; Ma, X.; Zhang, Y.; Liu, J.; Zhou, X.; Xiang, H., Optical Chemosensors Based on Transmetalation of Salen-Based Schiff Base Complexes. *Inorg. Chem.* **2014,** *53* (6), 3210-9.

93. Schley, M.; Fritzsche, S.; Lonnecke, P.; Hey-Hawkins, E., Soluble Monometallic Salen Complexes Derived From O-Functionalised Diamines as

Metalloligands for the Synthesis of Heterobimetallic Complexes. *Dalton Trans* **2010,** *39* (17), 4090-106.

94. Song, X.-Q.; Peng, Y.-Q.; Cheng, G.-Q.; Wang, X.-R.; Liu, P.-P.; Xu, W.-Y., Substituted Group-Directed Assembly of Zn(II) Coordination Complexes Based on Two New Structural Related Pyrazolone Based Salen Ligands: Syntheses, Structures and Fluorescence Properties. *Inorg. Chim. Acta* **2015,** *427*, 13-21.

95. Pandey, R.; Kumar, P.; Singh, A. K.; Shahid, M.; Li, P. Z.; Singh, S. K.; Xu, Q.; Misra, A.; Pandey, D. S., Fluorescent Zinc(II) Complex Exhibiting "On-Off-On" Switching Toward Cu^{2+} and Ag^{+} Ions. *Inorg. Chem.* **2011,** *50* (8), 3189-97.

96. Buncic, G.; Donnelly, P. S.; Paterson, B. M.; White, J. M.; Zimmermann, M.; Xiao, Z.; Wedd, A. G., A Water-Soluble Bis(Thiosemicarbazone) Ligand. A Sensitive Probe and Metal Buffer For Zinc. *Inorg. Chem.* **2010,** *49* (7), 3071-3.

97. Khatua, S.; Choi, S. H.; Lee, J.; Huh, J. O.; Do, Y.; Churchill, D. G., Highly Selective Fluorescence Detection of Cu^{2+} in Water by Chiral Dimeric Zn^{2+} Complexes through Direct Displacement. *Inorg. Chem.* **2009,** *48* (5), 1799-1801.

98. Szigethy, G.; Raymond, K. N., Designing The Ideal Uranyl Ligand: A Sterically Induced Speciation Change in Complexes with Thiophene-Bridged Bis(3-Hydroxy-N-Methylpyridin-2-One). *Inorg. Chem.* **2009,** *48* (24), 11489-91.

99. Jones, M. B.; Gaunt, A. J., Recent Developments in Synthesis and Structural Chemistry of Nonaqueous Actinide Complexes. *Chem. Rev.* **2013,** *113* (2), 1137-98.

100. Taube, H., New Coordination Chemistry of Saturated Ligands. *Coord. Chem. Rev.* **1978,** *26*, 33-45.

101. Cametti, M.; Nissinen, M.; Cort, A. D.; Rissanen, K.; Mandolini, L., Crystal Structure of a CsF-Uranyl-Salen Complex. An Unusual Cesium-Chlorine Coordination. *Inorg. Chem.* **2006,** *45* (16), 6099-6101.

102. Cametti, M.; Ilander, L.; Valkonen, A.; Nieger, M.; Nissinen, M.; Nauha, E.; Rissanen, K., Non-Centrosymmetric Tetrameric Assemblies of Tetramethylammonium Halides with Uranyl Salophen Complexes in the Solid State. *Inorg. Chem.* **2010,** *49* (24), 11473-84.

103. Zhang, D.; Chen, Z.; Omar, H.; Deng, L.; Khashab, N. M., Colorimetric Peroxidase Mimetic Assay for Uranyl Detection in Sea Water. *ACS Appl. Mater. Interfaces* **2015,** *7* (8), 4589-94.

104. Guo, Y.; Deng, L.; Li, J.; Guo, S.; Wang, E.; Dong, S., Hemin-Graphene Hybrid Nanosheets with Intrinsic Peroxidase-like Activity for Label-free Colorimetric Detection of Single-Nucleotide Polymorphism. *ACS Nano* **2011,** *5* (2), 1282-1290.

105. Zheng, J.; Nicovich, P. R.; Dickson, R. M., Highly Fluorescent Noble-Metal Quantum Dots. *Ann. Rev. Phys. Chem.* **2007,** *58* (1), 409-431.

106. Liu, W.; Dai, X.; Bai, Z.; Wang, Y.; Yang, Z.; Zhang, L.; Xu, L.; Chen, L.; Li, Y.; Gui, D.; Diwu, J.; Wang, J.; Zhou, R.; Chai, Z.; Wang, S., Highly Sensitive and Selective Uranium Detection in Natural Water Systems Using a Luminescent Mesoporous Metal-Organic Framework Equipped with Abundant Lewis Basic Sites: A Combined Batch, X-ray Absorption Spectroscopy, and First Principles Simulation Investigation. *Environ. Sci. Technol.* **2017,** *51* (7), 3911-3921.

107. Brindha, K.; Elango, L.; Nair, R. N., Spatial and Temporal Variation of Uranium in a Shallow Weathered Rock Aquifer in Southern India. *J. Earth Syst. Sci.* **2011,** *120* (5), 911-920.

108. National Primary Drinking Water Regulations | Ground Water and Drinking Water | US EPA. https://www.epa.gov/ground-water-and-drinking-water/national-primary-drinking-water-regulations#Radionuclides (accessed Feburary 3, 2019).

Chapter 2

Ligand Design: Electronic Effects on Metal Chelation of Schiff-based Salen Ligands

2.1 Introduction

Electronic effects are those that influence the structure, reactivity, or properties of a molecule; they are responsible for the ionization and hybridization state of the molecule. The most common types of electronic effects are: induction, resonance (formally known as mesomerism), resonance effect of a substituent, and hyperconjugation.[1, 2] Induction is defined as the phenomenon of withdrawing electrons via sigma (σ) bonds to the more electronegative atom or group in a molecule.[1] The resonance effect is the donation or withdrawal of electrons via orbital overlap with neighboring pi (π) bonds.[2] Resonance effects of a substituent is the term used to incorporate two obsolete effects: mesomeric and electromeric effects.[3] The mesomeric effect is caused by a substituent due to overlap of its π orbitals with the π orbital of the rest of the molecule, resulting in induced or extended delocalization caused by the electronic flow to or from the substituent.[1] The electromeric effect is an intermolecular electron displacement caused by the complete shift of the bonding π electrons in a double or triple bond to an atom within the same atomic octet.[3] Hyperconjugation is the interaction resulting from the overlap of a vacant π orbital on one atom with a neighboring sigma σ bond.[2] The aforementioned effects and phenomena, along with a few others, all give rise to the electronic effects of a molecule/system.

Electronic effects have been used in catalysis to explain the enantioselectivity of certain Rh(I) catalysts[4] as well as to explain the effects on late transition metal olefin polymerization catalysis.[5] It has been used in biochemistry to study the effects on metal-flavin ligation[6] and on the analogs of 4-hydroxy-3-(hydroxymethyl) phenyl ester interactions with the protein kinase C1 domain.[7] Electronic effects have been used to study their influence on metal-ligand chelation.[8-12] It has also been used to study the effects on metal-mediated enediyne cyclization,[13] the photophysical properties of triarylboranes,[14] as well as studying the π complexation between cyano-olefins and π bases.[15]

Research in the Gorden lab has focused on the synthesis of Schiff-base salen ligands for metal chelation and uranyl sensing.[16-28] The ligands consist of a 2-quinoxalinol backbone, which is subjected to an acid-catalyzed condensation reaction with salicylaldehydes bearing various R-groups to yield a quinoxalinol salen-based ligand bearing a tetradentate (O-N-N-O) pocket (**Scheme 2.1**).

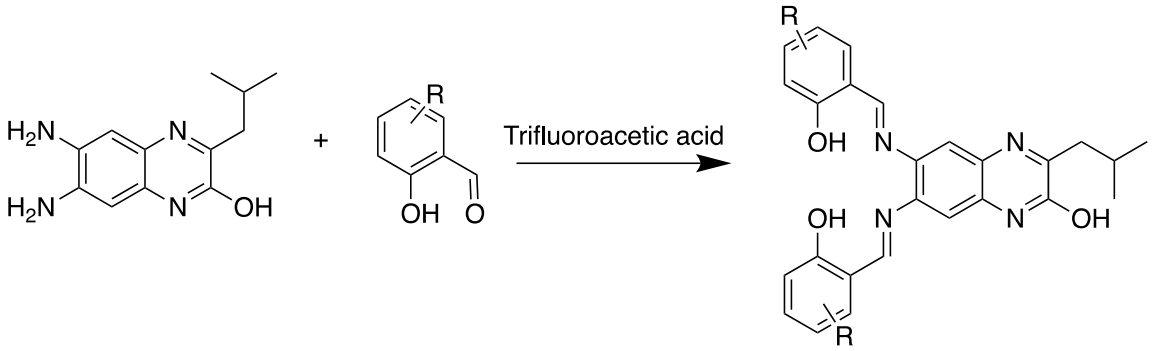

Scheme 2.1: General synthesis of 2-quinoxalinol salen-base ligand

These ligands have also been used for the catalytic oxidation of propargylic alcohols[29-32] and as solid-support heterogeneous ligands for copper extraction in aqueous media.[23] Reported herein, is the study of how electronic effects influence the chelation of various di-, tri-, and tetravalent metal ions with 2-quinoxalinol Schiff-base salen ligands.

2.2 Results:

Synthesis

The 2-quinoxalinol salen-based ligands were synthesized via an acid-catalyzed condensation reaction between the 6,7-diamino-3-isobutyl-2-quinoxalinol backbone and the salicylaldehyde of interest as depicted in the synthetic shown route in **Scheme 2.1.** The synthesis of the 3-formyl-4-hydroxybenzoic acid was completed via saponification of the methyl ester or via the Duff reaction.[7, 33]

UV-Vis Absorption Studies:

With the six salen ligands, **L1**, **L2**, **L3**, **L4**, **L5**, and **L6** synthesized (**Figure 2.1**), determination of the ligands' ability to chelate assorted di-, tri-, and tetravalent metal ions were studied. Each ligand contained either an electron donating or accepting group in the 5-position, while **L4** containing a hydrogen atom in the 5-position was used as a reference compound.

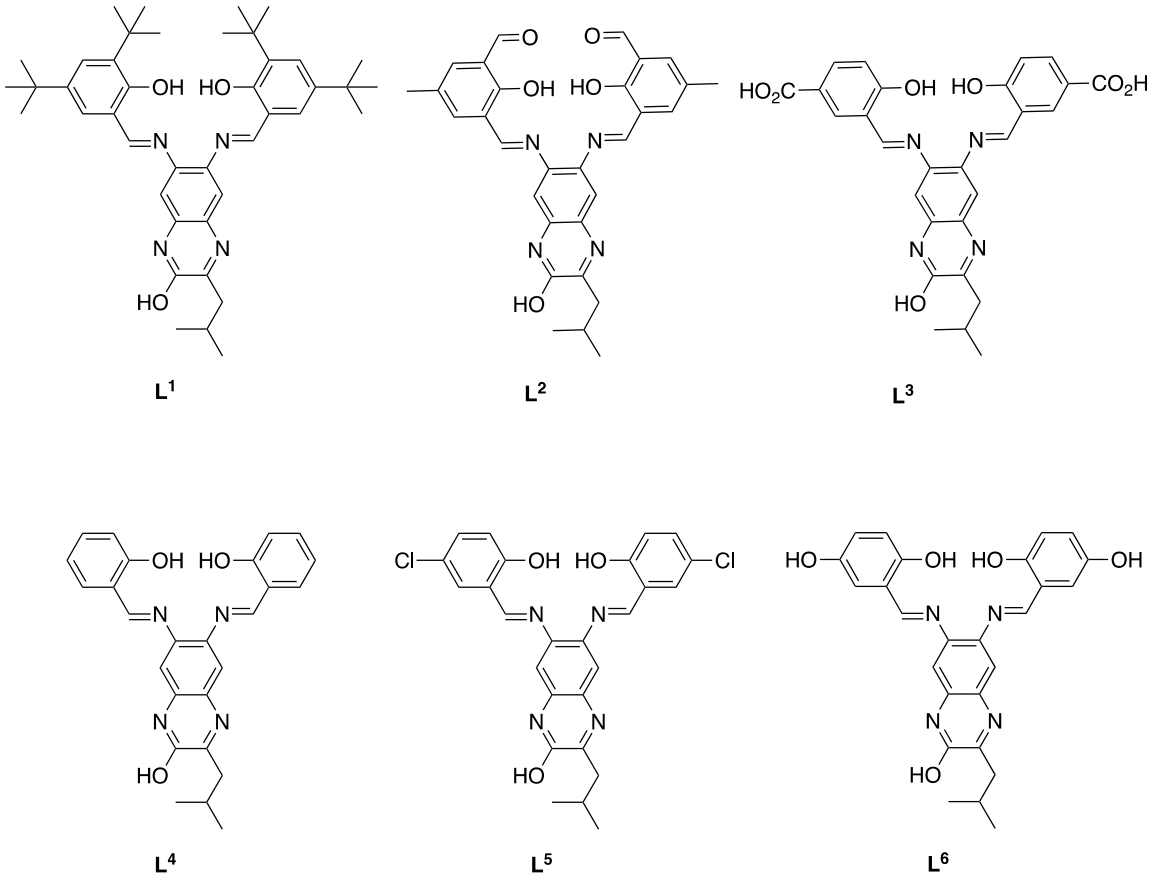

Figure 2.1: Structures of salen ligands employed

A Cary 50 spectrophotometer was used for all Ultraviolet-visible spectra data. The ligand solutions prepared were 20 ppm (parts per million) in concentration in N'N-dimethylformamide. The 20 ppm metal solutions were made by dissolving 0.5 mg of metal salt in methanol into a 25 mL volumetric flask. Serial titrations were completed by the addition of the metal salt solution in 20 μL aliquots to minimize the amount of solvent in the cuvette. Each serial titration was performed over a 20 min period, to determine their ability to be used as a real-time detector. Metal to ligand molar ratios ranged from 0.09-2.3: 1 to ensure the completion of metal chelation. Note: for simplicity only, the metal to

ligand ratio of 2.3:1 is displayed in each UV-Vis spectrum; the complete spectra of individual titrations can be found in the Appendix.

The **L1** ligand features a *t*-butyl group, a weakly activating and electron donating group, in the 5-position. The UV-Vis spectra of the ligand exhibited two major peaks at 310 nm and 383 nm. Upon the addition of the vanadyl solution (**Figure 2.2)** a hypsochromic shift from 310 nm to 280 nm accompanied by a small shift from 383 nm to 386 nm of the second peak was observed. As the copper(II) chloride solution was added to the free base, the formation of a shoulder at 287 nm was observed accompanied by a bathochromic shift from 310 nm to 330 nm and the formation of a possible charge transfer band at 452 nm. When the zinc solution was added to the free base, a new peak was observed at 478 nm accompanied small bathochromic shifts from 310 nm to 315 and 383 nm to 389 nm. Upon the addition of the cobalt solution, a small hypsochromic shift was observed from 310 nm to 300 nm along with a minor bathochromic shift from 383 nm to 385 nm. Similar results were observed when uranyl (310 nm to 305 nm and 383 nm to 382 nm) and thorium (310 nm to 305 nm and 383 nm to 385 nm) metal solutions were added to the free base. There were no significant spectroscopic changes for the other metals titrated. The summary of these titrations can be found in **Table 2.1**. The ligand (20 ppm) exhibited a fluorescence intensity of 151 relative fluorescence units (RFU), which was nearly completely quenched with the addition of the transition metals, excluding vanadyl, and experienced significant quenching with the addition of the actinides.

Table 2.1: UV-Vis data for serial titration of **L1** with various metal ions (data shown at 2.2:1 metal to ligand molar ratios) Ligand concentration: 20 ppm.

	λ (nm)	**Absorbance**
L1	310, 383	0.84, 0.84
VO^{2+} + [L1]	280, 386	0.91, 0.60
Cr^{3+} + [L1]	310, 330	0.69, 0.61
Mn^{2+} + [L1	312, 374	0.57, 0.61
Fe^{2+} + [L1]	307, 383	0.65, 0.64
Co^{2+} + [L1]	300, 385	0.63, 0.61
Ni^{2+} + [L1]	303, 385	0.68, 0.68
Cu^{2+} + [L1]	287, 330	0.66, 0.64
Zn^{2+} + [L1]	315, 389	0.68, 0.60
Dy^{3+} + [L1]	308, 385	0.60, 0.60
Yb^{3+} + [L1]	295, 382	0.83, 0.60
Th^{4+} + [L1]	305, 385	0.65, 0.63
UO_2^{2+} + [L1]	305, 382	0.63, 0.61

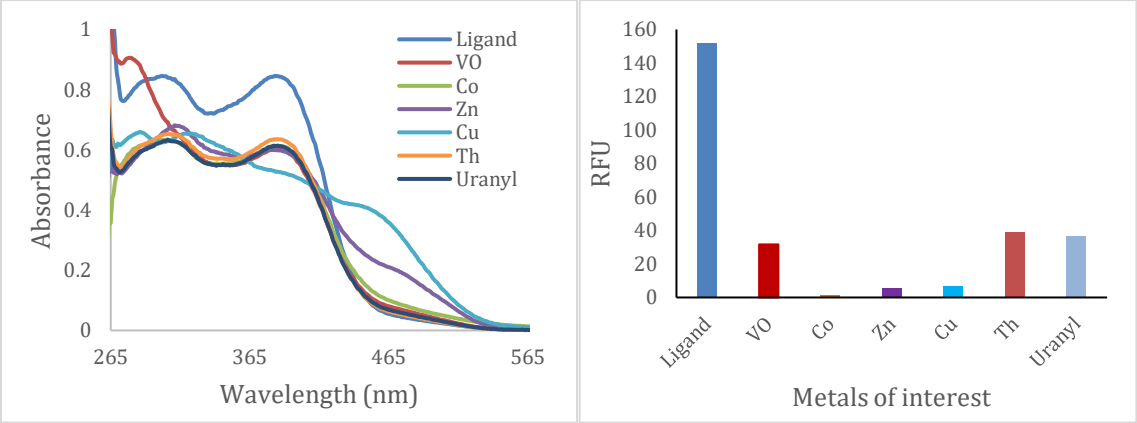

Figure 2.2: Spectra of results of serial titration of **L1** with metals of interest at 2.3: 1 metal to ligand ratio: UV-Vis highlighting spectral shifts (L) and fluorescence data depicting quenching upon the addition of metals (excitation at 383 nm) (R). Ligand concentration: 20 ppm.

The **L2** ligand consisted of an electron donating and weakly activating methyl group in the 5-position. It exhibited four peaks; 360 nm, 385 nm, 404 nm, and 486 nm (**Figure 2.3**). Upon the addition of cobalt solution, a small hypsochromic shift from 360 nm to 354 nm was observed as well as the formation of a small shoulder at 424 nm. Similarly, with the addition of zinc solution induced a small hypsochromic shift from 360

nm to 356 nm and a small shoulder was observed at 435 nm. Notable spectroscopic changes were observed upon the addition of copper, a hypsochromic shift from 360 nm to 353 nm and the formation of a possible large charge transfer band at 420 nm. There were no significant spectroscopic changes for the other metals titrated. The full summary of the metal titrations with the **L2** can be found in **Table 2.2**. The ligand (20 ppm) exhibited a fluorescence intensity of 150 RFU, which was nearly completely quenched with the addition of the other metals (transition, lanthanides, and actinides).

Table 2.2: UV-Vis data for serial titration of **L2** with various metal ions (data shown at 2.2:1 metal to ligand molar ratios) Ligand concentration: 20 ppm.

	λ_{max}	**Absorbance**
L2	360, 385, 404, 486	0.99, 0.75, 0.64, 0.35
VO^{2+} + [L2]	356, 397	0.82, 0.52
Cr^{3+} + [L2]	358, 378, 399, 439	0.82, 0.65, 0.53, 0.23
Mn^{2+} + [L2]	358, 382, 401, 424	0.75, 0.61, 0.58, 0.40
Fe^{2+} + [L2]	354, 399	0.87, 0.53
Co^{2+} + [L2]	354, 402, 424	0.76, 0.50, 0.40
Ni^{2+} + [L2]	354, 402, 430	0.75, 0.45, 0.40
Cu^{2+} + [L2]	353, 420	0.79, 0.50
Zn^{2+} + [L2]	356, 401, 435	0.79, 0.50, 0.33
Dy^{3+} + [L2]	358, 383, 402, 437	0.79, 0.64, 0.56, 0.29
Yb^{3+} + [L2]	358, 385, 402, 445	0.81, 0.60, 0.51, 0.20
Th^{4+} + [L2]	360, 383, 402	0.88, 0.67, 0.55
UO_2^{2+} + [L2]	356, 383, 402, 441	0.87, 0.63, 0.52, 0.18

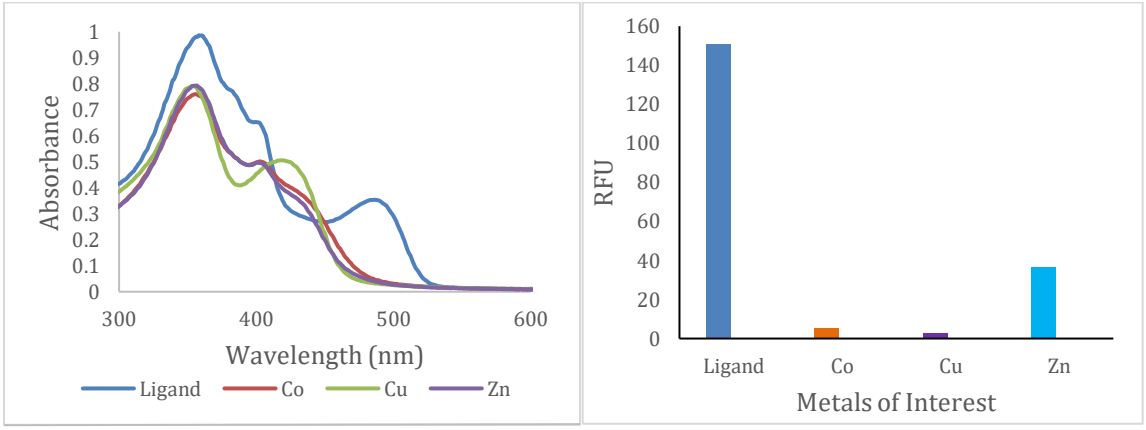

Figure 2.3: Spectra of results of serial titration of **L2** with metals of interest at 2.3: 1 metal to ligand ratio: UV-Vis highlighting spectral shifts (L) and Fluorescence data depicting quenching upon the addition of metals (excitation at 383 nm) (R). Ligand concentration: 20 ppm.

The **L3** ligand consisted of a carboxylic acid group in the 5-position, which is a mildly deactivating and electron withdrawing group. The ligand exhibited three peaks; 308 nm, 381 nm, and 399 nm (**Figure 2.4**). As the chromium solution was added a bathochromic shift from 308 nm to 331 nm was observed. While the addition of the cobalt and nickel solutions resulted in the formation of a new peak around 398 nm, the two ligand peaks (381 nm and 399 nm) diminished. Upon the addition of copper an 11 nm bathochromic shift from 399 nm to 411 nm and a small shoulder at 390 nm were observed. In contrast, the addition of zinc solution resulted in a hypsochromic shift from 399 nm to 394 nm with a small shoulder at 326 nm. Addition of the uranyl solution resulted in a small hypsochromic shift from 381 nm 379 nm and 399 nm to 392 nm, accompanied by a small shoulder at 364 nm. There were no significant spectroscopic changes for the other metals titrated, the observations are summarized in **Table 2.3**.

Table 2.3: UV-Vis data for serial titration of **L3** with various metal ions (data shown at 2.2:1 metal to ligand molar ratios. Ligand concentration: 20 ppm.

	λ_{max}	**Absorbance**
L3	308, 381, 399	0.67, 0.68, 0.69
VO^{2+} + [L3]	324, 381, 400	0.44, 0.54, 0.51
Cr^{3+} + [L3]	331, 381, 400	0.56, 0.54, 0.50
Mn^{2+} + [L3]	381, 400	0.54, 0.52
Fe^{2+} + [L3]	324, 381, 400	0.44, 0.54, 0.55
Co^{2+} + [L3]	298, 397	0.63, 0.51
Ni^{2+} + [L3]	298, 398	0.63, 0.53
Cu^{2+} + [L3]	296, 411	0.96, 0.70
Zn^{2+} + [L3]	296, 326, 394	0.40, 0.37, 0.54
Dy^{3+} + [L3]	300, 324, 381, 396	0.38, 0.40, 0.51, 0.51
Yb^{3+} + [L3]	300, 324, 381, 396	0.38, 0.40, 0.53, 0.51
Th^{4+} + [L3]	324, 379, 394	0.39, 51, 0.48
UO_2^{2+} + [L3]	300, 324, 364, 379, 392	10.49, 0.51, 0.60, 0.68, 0.61

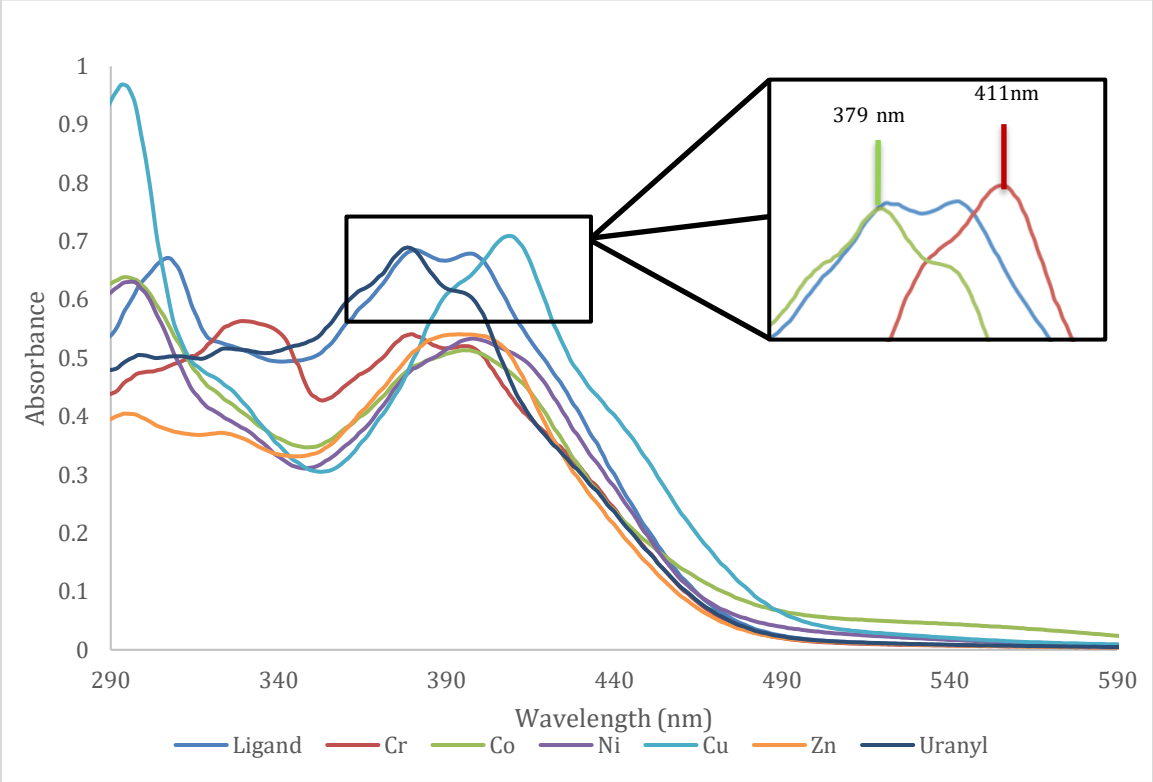

Figure 2.4: Spectra of results of serial titration of **L3** with metals of interest at 2.3: 1 metal to ligand ratio: UV-Vis highlighting spectral shifts. Inset expand view of the spectroscopic differentiation observed between uranyl and copper. Ligand concentration: 20 ppm.

It is important to note that distinct spectral shifts occurred only for the uranyl and copper species. The shifts are presented in **Figure 2.4** for the **L3** ligand (blue, λ=381 nm and 400 nm) with uranyl (green λ=379 nm) and copper (red, λ=411 nm) indicating blue and red shifts, respectively. This differentiation is important because it demonstrates a spectral method to differentiate binding of copper, a common false-positive, from that of the metal of interest, uranyl.

Fluorescence Studies:

Due to its capability to differentiate between Cu^{2+} and uranyl ions, the photophyisical properties of the **L3** were studied via fluorescence spectroscopy. The **L3**

ligand (20 ppm) exhibits a maximum intensity at 500 nm, which exhibited a bathochromic shift for copper and uranyl of 456 nm ($\Delta\lambda = 44$ nm) and 467 nm ($\Delta\lambda = 23$ nm) respectively. To study the sensitivity of the ligand, serial titrations with the metal ions were performed.

As the uranyl solution was added, the ligand fluorescence was quenched and reached complete saturation after the introduction of 1.5 equivalent of uranyl **(Figure 2.5).**

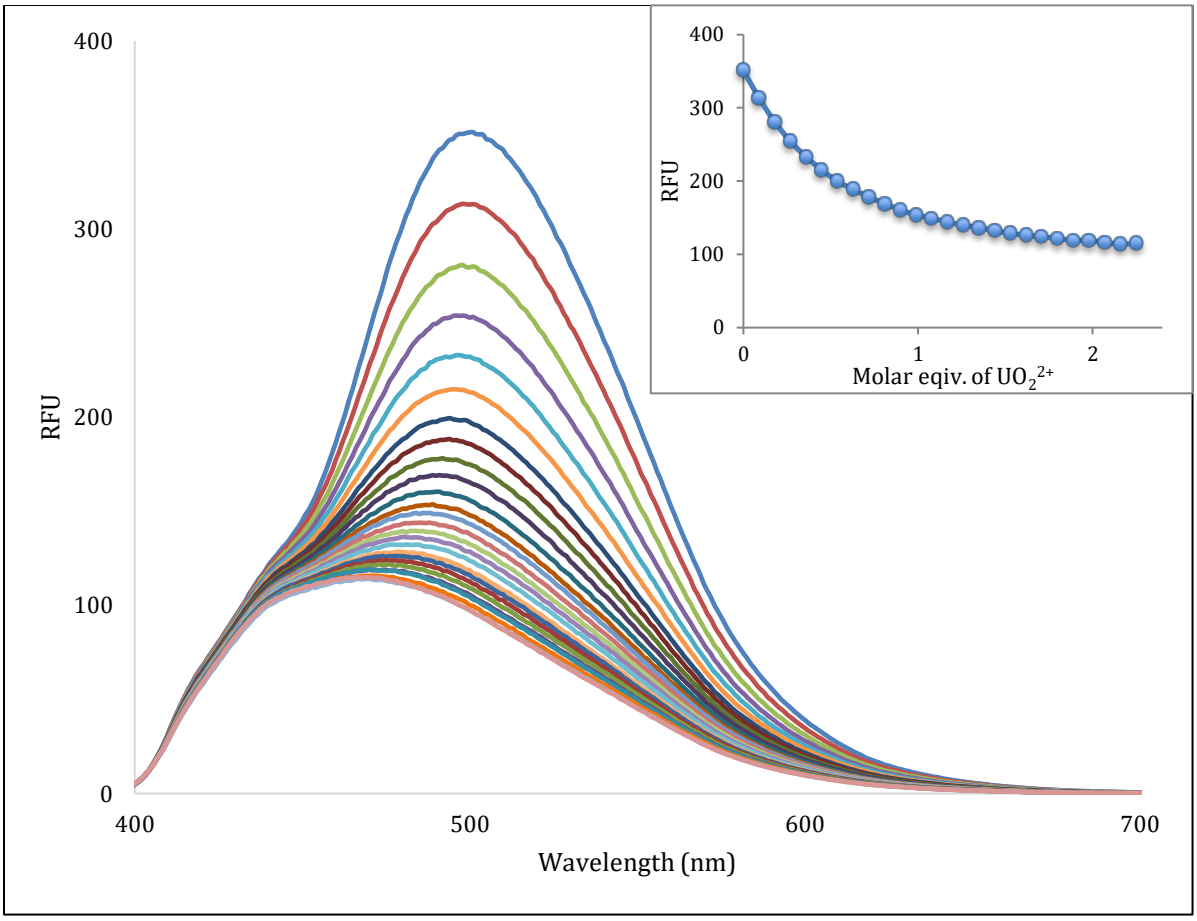

Figure 2.5. Quenching of emission spectra of serial titration of **L3** with 0.09 molar equivalent of uranyl per addition (excitation at 381 nm). The inset is the fluorescence intensity upon addition of uranyl ions up to 2.2 equiv. (emission: 501 nm)

In contrast, as the copper solution was added complete quenching of the ligand peak was observed (**Figure 2.6**) due the copper ions' ability to attain a square planar geometry in the pocket of the ligand and the ease of reduction of Cu(II) to Cu(I) and oxidation to

Cu(II). Saturation of the ligand with the copper ions occurred after 1.7 molar equivalents was added.

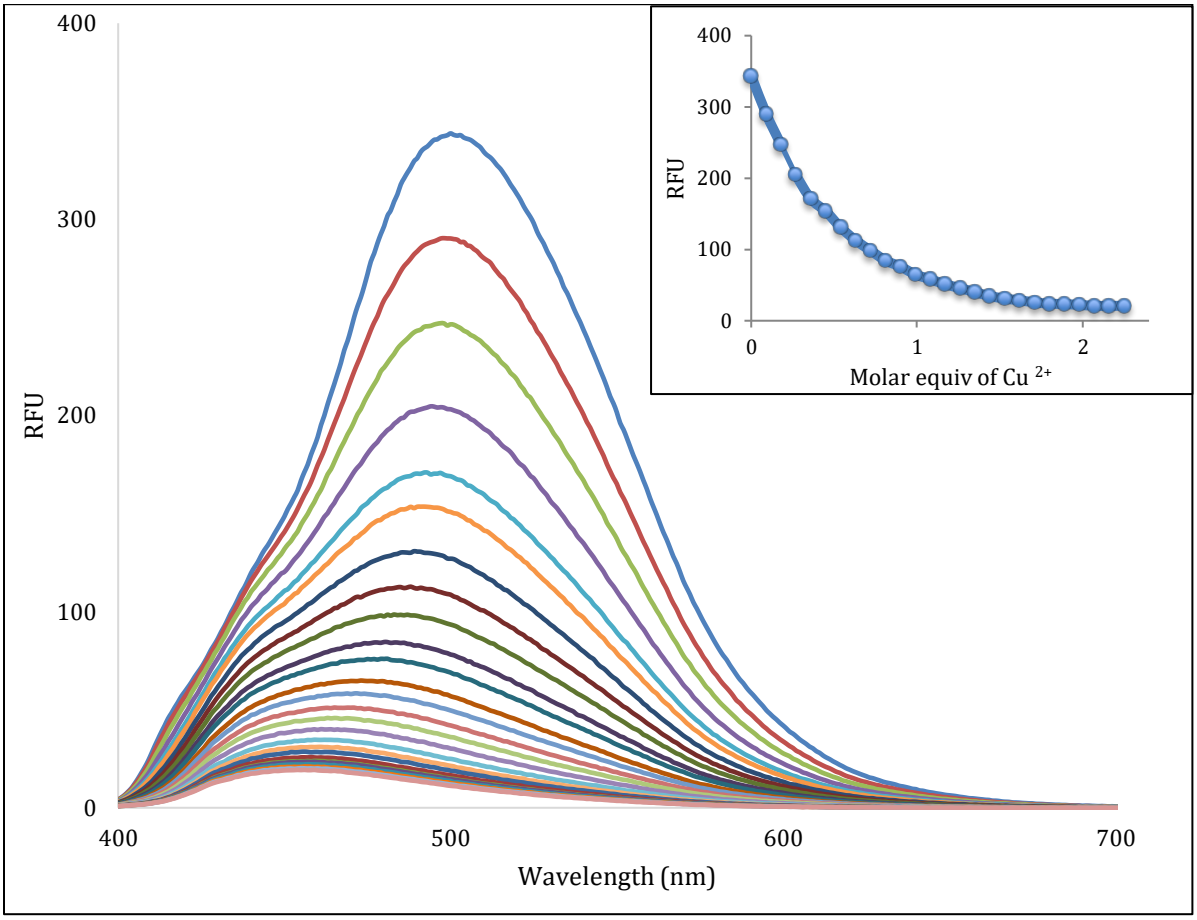

Figure 2.6: Quenching of emission spectra of serial titration of **L3** with 0.09 molar equivalent of copper per addition (excitation at 381 nm). The inset is the fluorescence intensity upon addition of copper ions up to 2.2 equiv. (emission: 501 nm)

The **L4** is considered control ligand, possessing a hydrogen atom in the 5-position. This ligand exhibited three major absorptions; 362 nm, 377 nm, and 396 nm (**Figure 2.7**). Due to the lack of electronic groups in the 5-position of the ligand, which influence the chelation of metal ions, very subtle changes (1-2 nm shifts) were observed with the addition of cobalt, nickel, and zinc. However, upon the addition of copper a significant spectral changed occurred. As the copper solution was added a 13 nm bathochromic shift from 396 nm to 409 nm occurred. There were no significant spectroscopic changes for the other

metals titrated which is summarized in **Table 2.4**. The ligand exhibited a fluorescence intensity of 112 RFU, which was significantly quenched with the addition of copper, however little to no decrease in fluorescence occurred with the other transition metals.

Table 2.4: UV-Vis data for serial titration of **L4** with various metal ions (data shown at 2.2:1 metal to ligand molar ratios) Ligand concentration: 20 ppm.

	λ (nm)	**Absorbance**
L4	362, 377, 396	0.66, 0.75, 0.50
VO^{2+} + [L4]	362, 377, 396	0.55, 0.61, 0.40
Cr^{3+} + [L4]	362, 377, 396	0.55, 0.61, 0.40
Mn^{2+} + [L4]	362, 377, 396	0.53, 0.60, 0.41
Fe^{2+} + [L4]	362, 377, 396	0.60, 0.65, 0.43
Co^{2+} + [L4]	364, 377, 396	0.47, 0.52, 0.42
Ni^{2+} + [L4]	361, 377, 396	0.50, 0.58, 0.42
Cu^{2+} + [L4]	392, 409	0.61, 0.58
Zn^{2+} + [L4]	361, 377, 396	0.50, 0.59, 0.43
Dy^{3+} + [L4]	362, 377, 396	0.54, 0.60, 0.39
Yb^{3+} + [L4]	362, 377, 396	0.54, 0.60, 0.39
Th^{4+} + [L4]	362, 377, 396	0.54, 0.60, 0.39
UO_2^{2+} + [L4]	362, 377, 396	0.53, 0.60, 0.39

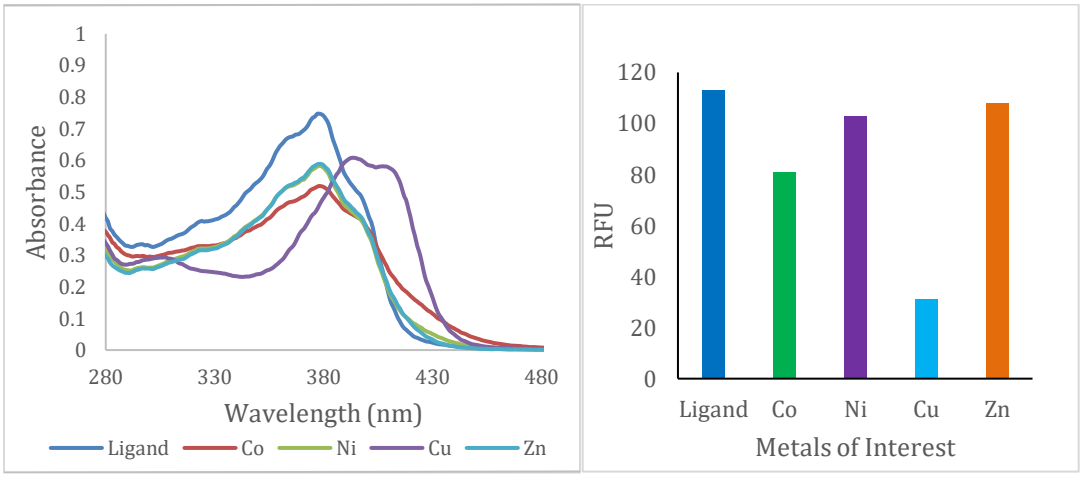

Figure 2.7: Spectra of results of serial titration of **L4** with metals of interest at 2.3: 1 metal to ligand ratio: UV-Vis highlighting spectral shifts (L) and Fluorescence data depicting quenching upon the addition of metals (excitation at 383 nm) (R). Ligand concentration: 20 ppm.

The **L5** ligand consists of a weakly deactivating and electron withdrawing chlorine atom in the 5-position. The least amount of spectrophotometric shifts, resulting from the introduction of metal ions, occurred with this ligand due to the electron withdrawing chlorine pulling electron density away from the tetradentate pocket of the ligand. The **L5** ligand exhibits 2 peaks at 341 nm and 381as depicted in **Figure 2.8**. Upon the addition of copper, a small band grew in at 417 nm, suggesting a charge-transfer, accompanied by a small shoulder at 392 nm. The full summary of the metal titrations with the **L5** could be found in **Table 2.5**. The ligand exhibited a fluorescence intensity of 427 RFU, which was slightly quenched with the addition of copper.

Table 2.5: UV-Vis data for serial titration of **L5** with various metal ions (data shown at 2.2:1 metal to ligand molar ratios) Ligand concentration: 20 ppm.

	λ (nm)	**Absorbance**
L5	341, 381	0.81, 0.80
VO^{2+} + [L5]	341, 381	0.69, 0.65
Cr^{3+} + [L5]	341, 381	0.72, 0.65
Mn^{2+} + [L5	341, 381	0.65, 0.64
Fe^{2+} + [L5]	341, 381	0.77, 0.70
Co^{2+} + [L5]	341, 381	0.66, 0.56
Ni^{2+} + [L5]	341, 381	0.65, 0.58
Cu^{2+} + [L5]	339, 396, 419	0.57, 0.60, 0.61
Zn^{2+} + [L5]	341, 381	0.65, 0.60
Dy^{3+} + [L5]	341, 381	0.69, 0.65
Yb^{3+} + [L5]	341, 381	0.68, 0.66
Th^{4+} + [L5]	341, 381	0.68, 0.65
UO_2^{2+} + [L5]	341, 381	0.67, 0.65

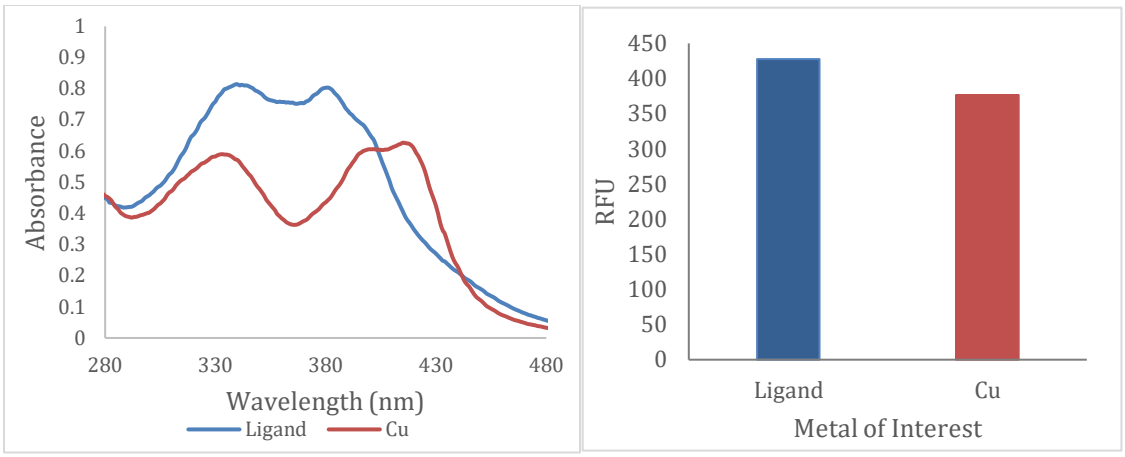

Figure 2.8: Spectra of results of serial titration of **L5** with metals of interest at 2.3: 1 metal to ligand ratio: UV-Vis highlighting spectral shifts (L) and Fluorescence data depicting quenching upon the addition of metals (excitation at 383 nm) (R). Ligand concentration: 20 ppm.

The **L6** ligand includes an electron donating strongly activating hydroxyl group in the 5-position. It exhibited two peaks; 307 nm and 391 nm (**Figure 2.9**). Upon the addition of the vanadium solution, a small hypsochromic shift occurs from 307 nm to 281 nm. The addition of manganese to the free base resulted in bathochromic shift from 307 nm 383 nm accompanied by a small shoulder at 342 nm. As the concentration of cobalt increased, a bathochromic shift from 307 nm to 327 nm was observed, accompanied by a small shoulder at 374 nm, and a charge transfer band at 449 nm. With increasing in nickel concentration, a small bathochromic shift from 307 nm to 315 nm, a hyposchromic shift from 391 nm to 383 nm, and two small charge transfer peaks at 446 nm and 523 nm were observed. Very distinguishable spectroscopic changes were observed upon the addition of copper and zinc. With the addition of copper, a bathochromic shift from 307 nm to 327 nm was observed and was supplemented by a large charge transfer band at 473 nm. Similarly, as the zinc concentration increased a small bathochromic shift from 307 nm to 317 nm was observed, accompanied by a large charge transfer band at 462 nm There were no significant

spectroscopic changes for the other metals studied. The full summary of the metal titrations with the **L6** could be found in **Table 2.6**. The ligand (20 ppm) exhibited a fluorescence intensity of 634 RFU, which was significantly quenched with the addition of the transition metals.

Table 2.6: UV-Vis data for serial titration of **L6** with various metal ions (data shown at 2.2:1 metal to ligand molar ratios) Ligand concentration: 20 ppm.

	λ (nm)	**Absorbance**
L6	307, 391	0.54, 0.49
VO^{2+} + [L6]	281, 391	0.47, 0.40
Cr^{3+} + [L6]	307, 391	0.42, 0.42
Mn^{2+} + [L6]	278, 342, 383	0.23, 0.36, 0.41
Fe^{2+} + [L6]	310, 391	0.45, 0.42
Co^{2+} + [L6]	273, 327, 374, 449	0.50, 0.43, 0.36, 0.29
Ni^{2+} + [L6]	273. 315, 383, 446, 523	0.37, 0.43, 0.38, 0.27, 0.13
Cu^{2+} + [L6]	276, 327, 473	0.28, 0.41, 0.42
Zn^{2+} + [L6]	317, 462	0.45, 0.43
Dy^{3+} + [L6]	305, 391	0.39, 0.40
Yb^{3+} + [L6]	307, 391	0.39, 0.42
Th^{4+} + [L6]	313, 383	0.33, 0.36
UO_2^{2+} + [L6]	312, 391	0.37, 0.39

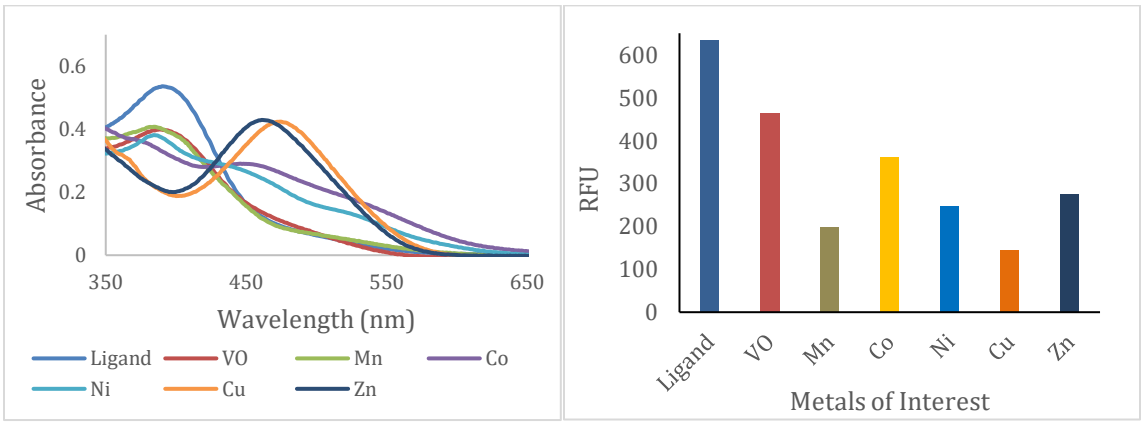

Figure 2.9: Spectra of results of serial titration of **L6** with metals of interest at 2.3: 1 metal to ligand ratio: UV-Vis highlighting spectral shifts (L) and Fluorescence data depicting quenching upon the addition of metals (excitation at 383 nm) (R). Ligand concentration: 20 ppm.

2.3 Conclusion:

Six Schiff-base salen ligands were synthesized, each containing a different electronic group, to determine the effect such groups exert on the ligand's chelation ability for various metal ions. Although possible anion coordination effects may have played a role in the kinetics of the metal chelation for salts like vanadyl acetylacetonate and chromium(III) acetylacetonate, this study just focuses on the effects caused by varying the electronic groups. Using **L4** (H in 5-position) as a reference ligand, it was determined that the ligands containing electron withdrawing groups, such as a halogen (**L5**) greatly affected the chelating properties of the ligand causing it to only coordinate with the copper ions. In contrast, the ligands containing electron withdrawing carbonyl groups, **L2** and **L3**, were able to chelate several metal ions due to resonance stabilization. The ligands containing electron donating groups, **L1** and **L6,** were able to chelate a wide range of metal ions, including both transition metals and actinides, due to their ability to donate electron density to the tetradentate pocket of the ligand. Previous research in the Gorden lab showed that **L1** can differentiate between copper, a common false positive, and uranyl, but only after allowing the ligand (**LI**) and metal solution to react for 2-3 h prior to conducting spectral analysis.[18] Though the electron donating ligands were more successful at chelating metal ions, only **L3** was able to differentiate between copper and uranyl within a reasonable time frame of twenty minutes. This supports the goal for a real time, on-site sensor, therefore it was further probed as a uranyl chemosensor.

2.4 Experimental:

Caution! The uranium metal salt – $UO_2(NO_3)_2 \cdot 6H_2O$ – used in this study contained depleted uranium. Standard precautions for handling radioactive materials or heavy metals, such as uranyl nitrate and lead sulfate, were followed.

Reagents:

The reagents THF (Macron), ethyl acetate (Macron), ethanol (200 proof, PharmCo-Aaper), methanol (HPLC grade, EMD Millipore), N, N-dimethyl formamide (Fisher Scientific) and hexanes (ACS grade, EMD Millipore), L-Leucine methylester · HCl (98 % TCI Chemicals), N,N-diisopropylethylamine (99 % Alfa Aesar), palladium on carbon (dry, 5 %, Alfa Aesar), trifluoroacetic acid (TFA) (99 %, Alfa Aesar), Celite hyflo super-cel (Alfa Aesar), 2,5-dihydroxybenzaldehyde (98+ %, Alfa Aesar), 5-chlorosalicyaldehyde (98%, Alfa Aeser), ammonium hydroxide (28-30 %, BDH), silica gel (60-200 um, BDH), ammonium formate (97 %, Sigma-Aldrich), methyl 3-formyl-4-hydroxybenzoate (Sigma-Aldrich), regenerated cellulose film (0.021 mm thickness, Sigma-Aldrich), *p*-hydroxybenzoic acid (99+ %, Aldrich), and 1,3-difluoro-4,6-dinitrobenzene (97 %, Matrix Scientific), salicyaldehyde (99 %, Acros Organic), hexamethylenetetramine (EMD Millipore Corporation) were purchased and used as received without any further purification. Uranyl nitrate hexahydrate was purchased from Fischer Scientific, recrystallized in 6 M nitric acid, and stored under hexanes until used to prevent moisture. Deuterated DMSO and chloroform were purchased from Cambridge Isotope and kept in a desiccator when not in use. The following metal salts were used; copper(II) chloride

dihydrate, manganese(II) chloride, chromium(III) acetylacetonate, vanadyl acetylacetonate, cobalt(II) chloride, nickel(II) chloride octahydrate, zinc(II) chloride, dysprosium(III) acetate, ytterbium(III) acetate, and thorium(IV) nitrate.

Instrumentation

The 1H NMR analysis was conducted on Bruker AC 250 or 400 spectrometer with shift values given as δ values (ppm). DMSO-d6 was the solvent used to analyze all samples. Mass spectrometry analysis was conducted using a Micromass Q-TOF mass spectrometer from the Waters Corp (Miliford, MA). UV-Vis spectra were collected on a VARIAN Cary 50 WinUV Spectrometer and the fluorescence data collected on a Shimadzu RF-5301 PF fluorospectrophotometer.

Synthesis of the 6,7-diamino-2-quinoxalinol backbone:

In a 250-mL round-bottom flask equipped with a magnetic stirrer; 1,5-difluoro-2,4-dinitrobenzene (2.00 mmol), isoleucine methyl ester (2.00 mmol), N,N-diisopropylethylamine, DIPEA (2:1 equivalent), tetrahydrofuran, THF and ethanol were added and allowed to stir for 22 h, the reaction was monitored by TLC. Ammonium hydroxide (6.00 mmol) was added to the flask, and the flask was then sealed with Parafilm and allowed to stir for 23 h. Wet palladium on carbon (5 %), ammonium formate (0.04 mmol) and ethanol were then added to the flask and stirred for 4.5 h at 65 °C. The reaction was then cooled and filtered over Cellite. The solution was concentrated via rotary evaporation, then purified by column chromatography to afford 6,7-diamino-2-quinoxalinol as a bright yellow solid; yield: 65 %.

^{1}H NMR (400 MHz, DMSO-d_6): δ 0.88 (d, J.6.8 Hz, 6H), 2.13 (m, 1H), 2.52 (d, 2H), 4.60 (br s, 2H) 5.37 (br s, 2H), 6.34 (s, 1H), 6.78 (s, 1H), 11.74 (s, 1H). HRMS m/z: calcd 233.1402, found 233.14.

Synthesis of 3-formyl-4-hydroxybenzoic acid (both synthetic methods were used):

5-Methyl 3-formyl-4-hydroxybenzoate (2.5 mmol) was dissolved in methanol (1 mL) and was charged in a 50-mL round-bottom flask containing a 10 % aqueous solution of NaOH (25 mL). The solution was brought to a boil and stirred vigorously for 2 h. The solution was then cooled and concentrated via rotoary evaporation. The solution was then acidified via the drop-wise addition of 1 M HCl until precipitation occurred. The precipitate was filtered and washed with cold ethanol, then dried under vacuum to afford the product as a pale-yellow solid; yield 93 %

Duff Reaction[7, 33]

HMTA (2 mol) dissolved in TFA was added drop-wise to a solution of *p*-hydroxybenzoic acid dissolved in TFA over a period of 20 min. The reaction was heated to 90 °C and was allowed to react for 16 h. Upon cooling, the reaction was quenched with copious amounts of deionized water (~ 200 mL) and then acidified with a 4 N HCl solution. With acidification, the reaction was stirred at room temperature to facilitate precipitation of the pale-yellow product. The solid was filtered off and recrystallized from ethanol to yield the desired product; yield 51 %

^{1}H NMR (400 MHz DMSO-d_6): δ 7.08 (1H, d), 8.04 (1H. dd), 8.23 (1H, s), 10.29 (1H, s),

11.47 (1H, bs), 12.86 (1H, bs). HRMS: found (167.2163), calcd (166.03).

3.5-ditertbutyl-2-quinoxalinol Salen Ligand (L1):

2-Quinoxalinol (1 mmol) was charged in a 100-mL round-bottom flask containing 2.2 molar equivalent of 3,5-di-tert-butyl-2-hydroxybenzaldehyde, and a drop of trifluoroacetic acid in ethanol (40 mL). The reaction mixture was stirred at reflux temperature for 16 h. Then the reaction mixture was allowed to cool and was filtered. The precipitate was washed with cold ethanol. The solid collected was dried under vacuum to afford the 3-5-ditertbutyl-2-quinoxalinol salen ligand; yield: 69 %.

^{1}H NMR (250 MHz DMSO-*d6*): δ 0.82 (d, 6H), 1.10 (s, 9H), 1.11 (s, 9H), 1.19 (s, 9H), 1.22 (s, 9H), 2.13 (m, 1H), 2.57 (d, 2H), 7.1 (d, 2H), 6.88 (s, 1H), 7.04- 7.06 (dd, 2H), 7.21 (d, 2H), 7.23 (d, 2H), 7.47 (s, 1H), 8.47 (s, 1H), 8.58 (s, 1H), 12.08 (bs, 1H), 13.15 (bs, 1H), 13.25 (bs, 1H). HRMS: found (666.4431), calcd (665.44).

5-methyl-3-formyl-2-quinoxalinol Salen Ligand (L2)

2-Quinoxalinol (1 mmol) was charged in a 100-mL round-bottom flask containing 2.2 molar equivalent of 2,6-diformyl-4-methyl phenol and a drop of trifluoroacetic acid in ethanol (40 mL). The reaction mixture was stirred at reflux temperature for 16 h. The solution was cooled and concentrated via rotary evaporation then purified by column chromatography. The solid collected was dried under vacuum to afford the corresponding symmetric salen ligands; yield: 76 %.

^{1}H NMR (400 MHz DMSO-*d6*): δ 0.98 (d, 6H), 2.24-2.30 (m, 4H), 2.37 (s, 3H), 2.87 (d, 2H), 7.54 (d, 1H), 7.60 (d, 1H), 7.66 (d, 1H), 7.82 (d, 1H), 8.41 (d, 1H), 8.98 (s, 1H), 9.09 (s, 1H), 10.9 (d, 2H), 11.91 (bs, 1H), 12.80 (bs, 1H), 12.91 (bs, 1H). HRMS: found 525.2191, cald 524.21

5-carboxylic acid-2-quinoxalinol Salen Ligand (L3)

2-Quinoxalinol (1 mmol) was charged in a 100-mL round-bottom flask containing 2.2 molar equivalent of 3-formyl-4-hydroxybenzoic acid in ethanol (40 mL). The reaction mixture was stirred at reflux temperature for 16 h under nitrogen then was cooled and filtered. The precipitate was washed with cold ethanol. The solid collected was dried under vacuum to afford the 5-carboxylic acid-2-quinoxalinol salen ligands; yield: 83 %.

^{1}H NMR (400 MHz DMSO-*d6*): δ 0.93 (d, 6H), 2.28 (m, 1H), 2.82 (d, 2H), 7.18-7.20 (dd, 2H), 7.82 (dd, 1H) 8.39 (d, 1H), 8.52 (d, 1H), 8.58 (dd, 1H), 8.64 (dd, 1H), 8.84 (dd, 1H), 8.98 (s, 1H), 9.31 (s, 1H) 12.21 (s, 2H) 13.8 (s, 2H). HRMS: found (529.2401), calcd (528.16).

Salicyl-2-quinoxalinol Salen Ligand (L4)

2-Quinoxalinol (1 mmol) was charged in a 100-mL round-bottom flask containing 2.2 molar equivalent of salicylaldehyde and a drop of trifluoroacetic acid in ethanol (40 mL). The reaction mixture was stirred at reflux temperature for 16 h. The solution was cooled and concentrated via rotary evaporation then purified by column chromatography. The

solid collected was dried under vacuum to afford the corresponding symmetric salen ligand; yield: 81 %.

^{1}H NMR (400 MHz DMSO-*d*$_6$): δ 0.90 (d, 6H), 2.27 (m, 1H), 2.81 (d, 2H), 6.99-7.05 (d, 2H), 7.17 (t, 1H), 7.35 (m , 1H), 7.50-7.67 (m, 2H), 7.81 (d, 1H), 7.98 (d, 1H), 8.35 (s, 1H), 8.90 (s, 1H), 8.97 (s, 1H), 12.21 (bs, 1H). HRMS: found 441.1941, cald 440.18

5-chloro-2-quinoxalinol Salen Ligand (L5)

2-Quinoxalinol (1 mmol) was charged in a 100-mL round-bottom flask containing 2.2 molar equivalent of 5-chlorosalicylaldehyde and a drop of trifluoroacetic acid in ethanol (40 mL). The reaction mixture was stirred at reflux temperature for 16 h. The solution was cooled and concentrated via rotary evaporation then purified by column chromatography. The solid collected was dried under vacuum to afford the corresponding symmetric salen ligands; yield: 60 %.

^{1}H NMR (400 MHz DMSO-*d6*): δ 0.96 (d, 6H), 2.35 (m, 1H), 2.88 (d, 2H), 6.99-7.07 (dd, 2H), 7.02 (dd, 2H), 7.34 (dd, 1H), 7.51 (dd, 1H), 7.95 (dd, 1H), 8.07 (dd, 1H), 8.39 (d, 1H), 8.49 (d, 1H), 8.95 (s, 1H), 9.02 (s 1H)), 11.89 (bs, 1H), 12.78 (bs, 1H), 12.83 (bs, 1H). HRMS: found 509.118, cald 508.11

3,5-dihydroxy-2-quinoxalinol Salen Ligand (L6)

80 mL of methanol was purged under argon for 30 minutes. Using a 3-neck round bottom, 15 molar equivalents of 2,5-dihydroxybenzaldehyde dissolved in 20 mL of the purged

methanol was allowed to slowly drip into the round bottom containing 40 mL solution of the 2-quinoxalinol (1mmol) in the purged methanol. The reaction mixture was stirred at room temperature for 16 h under a constant flow of argon. The precipitate was washed with cold ethanol and dichloromethane. The solid was dried under vacuum to afford the corresponding symmetric salen ligand; yield: 72%

^{1}H NMR (400 MHz DMSO-*d6*): δ 0.98 (d, 6H), 2.27-2.31 (m, 1H), 2.71 (d, 2H), 6.77-6.91 (m, 4H), 7.06 (s, 2H), 7.14 (s, 1H), 7.92 (s, 1H), 8.77 (s, 1H), 9.01 (s, 1H), 9.12 (bs, 1H), 9.15 (bs, 1H), 11.49 (bs, 1H), 12.36 (bs, 1H), 12.45 (bs, 1H). HRMS: found 473.1832, cald (472.18).

Metal Serial Titrations:

Spectra were collected on a VARIAN Cary 50 WinUV Spectrometer. The ligand solutions prepared were 20 (parts per million) ppm in concentration in N'N-dimethylformamide. The 20 ppm metal solutions were made by dissolving 0.5 mg of metal salt in methanol into a 25 mL volumetric flask. Serial titrations were completed by the addition of the metal salt solution in 20 μL aliquots to minimize the amount of solvent in the cuvette. The solutions were shaken for 5 seconds and replaced in the spectrometer and the absorbance spectrum was collected. Metal to ligand ratios ranged from 0.09-2.3: 1 to ensure the completion of metal chelation. This process was repeated, and data collected on a Shimadzu RF-5301 PF fluorospectrophotometer.

2.5 References:

1. Anslyn, E. V.; Dougherty, D. A., *Modern Physical Organic Chemistry*. University Science Books: 2006.

2. McMurry, J., *Organic Chemistry*. Brooks/Cole, Cengage Learning Belmont, CA, 2008.

3. Jaffé, H. H., On the Separation of Inductive and Mesomeric Effects by Molecular Orbital Theory. *J. Am. Chem. Soc.* **1955,** *77* (2), 274-280.

4. Wu, H.-C.; Hamid, S. A.; Yu, J.-Q.; Spencer, J. B., Possible Origin of Electronic Effects in Rh(I)-Catalyzed Enantioselective Hydrogenation. *J. Am. Chem. Soc.* **2009,** *131*, 9604-9605.

5. Popeney, C.; Guan, Z., Ligand Electronic Effects on Late Transition Metal Polymerization Catalysts. *Organometallics* **2005,** *24*, 1145-1155.

6. Clarke, M. J.; Dowling, M. G.; Garafalo, A. R.; Brennan, T. F., Structural and Electronic Effects Resulting from Metal-Flavin Ligation. *J. Biol. Chem.* **1980,** *255* (8), 3472-3481.

7. Talukdar, D.; Panda, S.; Borah, R.; Manna, D., Membrane Interaction and Protein Kinase C-C1 Domain Binding Properties of 4-Hydroxy-3-(hydroxymethyl) Phenyl Ester Analogues. *J. Phys. Chem. B* **2014,** *118* (27), 7541-7553.

8. Khusnutdinova, J. R.; Luo, J.; Rath, N. P.; Mirica, L. M., Late First-Row Transition Metal Complexes of a Tetradentate Pyridinophane Ligand: Electronic Properties and Reactivity Implications. *Inorg. Chem.* **2013,** *52* (7), 3920-32.

9. DuPoint, J. A.; Yap, G. P. A.; Rlordan, C. G., Influence of Ligand Electronic Effects on the Structure of Monovalent Cobalt Complexes. *Inorg. Chem.* **2008,** (47), 10700-107007.

10. Berchmans, S.; Thomas, P. J.; Rao, C. N. R., Novel Effects of Metal Ion Chelation on the Properties of Lipoic Acid-Capped Ag and Au Nanoparticles. *J. Phys. Chem. B* **2002,** *106*, 4647-4651.

11. Cazacu, M.; Shova, S.; Soroceanu, A.; Machata, P.; Bucinsky, L.; Breza, M.; Rapta, P.; Telser, J.; Krzystek, J.; Arion, V. B., Charge and Spin States in Schiff Base Metal Complexes with a Disiloxane Unit Exhibiting a Strong Noninnocent Ligand Character: Synthesis, Structure, Spectroelectrochemistry, and Theoretical Calculations. *Inorg. Chem.* **2015,** *54* (12), 5691-706.

12. Canac, Y.; Lepetit, C., Classification of the Electronic Properties of Chelating Ligands in cis-[LL'Rh(CO)2] Complexes. *Inorg. Chem.* **2017,** *56* (1), 667-675.

13. Clark, A. E.; Bhattacharryya, S.; Zaleski, J. M., Density Functional Analysis of Ancillary Ligand Electronic Contributions to Metal-Mediated Enediyne Cyclization. *Inorg. Chem.* **2009,** *48*, 3926-3933.

14. Hudson, Z. M.; Wang, S., Impact of Donor-Acceptor Geometry and Metal Chelation on Photophysical Properties and Applications of Triarylboranes. *Acc. Chem. Res.* **2009,** *42* (10), 1584-1596.

15. Sheppard, W. A.; Henderson, R. M., Electronic Effects of Cyanocarbon Groups. *J. Am. Chem. Soc.* **1967,** *89* (17), 4446-4450.

16. Bharara, M. S.; Strawbridge, K.; Vilseck, J. A.; Brey, T. H.; Gorden, A. E., Novel Dinuclear Uranyl Complexes with Asymmetric Schiff Base Ligands- Synthesis, Structural Characterization, Reactivity, and Extraction Studies. *Inorg. Chem.* **2007,** *46*, 8309-8315.

17. Bharara, M. S.; Tonks, S. A.; Gorden, A. E., Uranyl Stabilized Schiff Base Complex. *Chem. Commun.* **2007,** (39), 4006-8.

18. DeVore, M. A.; Kerns, S. A.; Gorden, A. E. V., Characterization of Quinoxolinol Salen Ligands as Selective Ligands for Chemosensors for Uranium. *Eur. J. Inorg. Chem.* **2015,** *2015* (34), 5708-5714.

19. Gorden, A. E.; DeVore, M. A., 2nd; Maynard, B. A., Coordination Chemistry With F-Element Complexes for an Improved Understanding of Factors That Contribute to Extraction Selectivity. *Inorg. Chem.* **2013,** *52* (7), 3445-58.

20. Gorden, A. E. V.; Wu, X. 2-Quinoxalinol Salen Compounds and Uses Thereof. 2009. U. S. Patent 0286968, November 19, 2009.

21. Hardy, E. E.; Eddy, M. A.; Maynard, B. A.; Gorden, A. E., Solid State Pi-Pi Stacking and Higher Order Dimensional Crystal Packing, Reactivity, and Electrochemical Behaviour of Salphenazine Actinide and Transition Metal Complexes. *Dalton Trans.* **2016,** *45* (36), 14243-51.

22. Wu, X.; Bharara, M. S.; Bray, T. H.; Tate, B. K.; Gorden, A. E. V., Synthesis and Characterization of 2-Quinoxalinol Schiff-Base Metal Complexes. *Inorg. Chim. Acta* **2009,** *362* (6), 1847-1854.

23. Wu, X.; Gorden, A. E. V., 2-Quinoxalinol Salen Ligands Incorporated into Functionalized Resins for Selective Solid-Phase Extraction of Copper(II). *Tetrahedron Lett.* **2008,** *49* (35), 5200-5203.

24. Wu, X.; Gorden, A. E. V., An Efficient Method for Solution-Phase Parallel Synthesis of 2-Quinoxalinol Salen Schiff-Base Ligands. *J. Comb. Chem.* **2007,** *9* (4), 601-608.

25. Wu, X.; Gorden, A. E. V.; Tonks, S. A.; Vilseck, J. A., Regioselective Synthesis of Asymmetrically Substituted 2-Qu Salen Ligand. *J. Org. Chem.* **2007,** *72*, 8691-8699.

26. Wu, X.; Hubbard, H. K.; Tate, B. K.; Gorden, A. E. V., One-Pot Metal Templated Synthesis For The Preparation of 2-Quinoxalinol Salen Metal Complexes. *Polyhedron* **2009,** *28* (2), 360-362.

27. Hardy, E. E.; Wyss, K. M.; Keller, R. J.; Gorden, J. D.; Gorden, A. E. V., Tunable Ligand Emission of Napthylsalophen Triple-Decker Dinuclear Lanthanide(III) sandwich complexes. *Dalton Trans.* **2018,** *47* (4), 1337-1346.

28. Hardy, E. E.; Wyss, K. M.; Gorden, J. D.; Ariyarathna, I. R.; Miliordos, E.; Gorden, A. E. V., Th(IV) and Ce(IV) Napthylsalophen Sandwich Complexes: Characterization of Unusual Thorium Fluorescence in Solution and Solid-State. *Chem. Commun.* **2017,** *53* (88), 11984-11987.

29. Black, C. C.; Gorden, A. E. V., Propargylic C-H Activation Using A Cu(II) 2-Quinoxalinol Salen Catalyst and tert -Butyl Hydroperoxide. *Tetrahedron Lett.* **2018,** *59* (9), 803-806.

30. Li, Y.; Lee, T.; Weerasiri, K.; Wang, T.; Buss, E. E.; McKee, M. L.; Gorden, A. E., 2-Quinoxalinol Diamine Cu(II) Complex: Facilitating Catalytic Oxidation Through Dual Mechanisms. *Dalton Trans.* **2014,** *43* (36), 13578-83.

31. Weerasiri, K. C.; Gorden, A. E. V., Oxidation of Propargylic Alcohols with a 2-Quinoxalinol Salen Copper(II) Complex and tert-Butyl Hydroperoxide. *Eur. J. Org. Chem.* **2013,** *2013* (8), 1546-1550.

32. Weerasiri, K. C.; Gorden, A. E. V., Cu(II) 2-Quinoxalinol Salen Catalyzed Oxidation of Propargylic, Benzylic, and Allylic Alcohols Using Tert-Butyl Hydroperoxide in Aqueous Solutions. *Tetrahedron* **2014,** *70* (43), 7962-7968.

33. Bereau, V.; Jubera, V.; Arnaud, P.; Kaiba, A.; Guionneau, P.; Sutter, J. P., Modulation of the Luminescence Quantum Efficiency for Blue Luminophor $\{Al(salophen)\}^+$ by Ester-Substituents. *Dalton Trans.* **2010,** *39* (8), 2070-7.

Chapter 3

Incorporation of a Schiff-Base Salen Ligand into Cellulose Films for Uranyl Extraction

3.1 Introduction

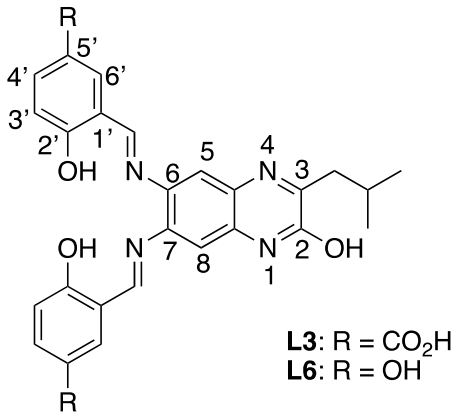

Figure 3.1: Structure of **L3/6** Ligands

Previously in the Gorden lab, the Schiff-base ligand **L6** was used in conjunction with a solid support for metal extraction.[1-3] Reported in 2008, the **L6** ligand was covalently linked via the 5' hydroxyl group on the ligand (**Figure 3.1**) to a functionalized polystyrene aminomethyl resin *via* a modified Steglich esterification reaction. The heterogeneous ligand (HL) was able to extract 100 % of the Cu^{2+} ions from a DCM/MeOH bi-phase system in as little as 30 min at a metal to HL ratio of 1:12.[1] Using the same process, the **L6** ligand was later incorporated onto functionalized magnetic polyvinyl alcohol (mPVA) beads and used to extract uranyl ions from aqueous media.[2] This HL was able to successfully remove 95.4 % of the uranyl ions in as little as 5 min at a metal to HL ratio of 1:1, due to its ability to absorb the large uranyl ions onto the surface of the mPVA

resin.[3] Here, because of the ability to spectroscopically differentiate between copper (as Cu^{2+}) and uranyl (UO_2^{2+}) ions achieved with the **L3** ligand, **L3** is paired with cellulose as a solid-support, and further investigated for usage as a uranyl extractor.

Cellulose is the most profuse, natural, eco-friendly and inexhaustible biopolymer available in nature.[4, 5] It is considered to be an important alternative resource in replacing petrochemicals for obtaining biofuels, chemicals, and materials.[6] The recent demands for products made from renewable and sustainable resources that are not only biodegradable, carbon neutral, non-petroleum based, with low environmental, animal/human health and safety risks on the rise by the consumers, industry, and the government, is resulting in an increased interest in cellulose research. Cellulose research includes using the polymer to aid in drug delivery,[7-9] imaging and therapeutic agents for cancer research,[10] heavy metal extraction and/or adsorption,[11-22] antimicrobial and microbial biomedical research,[23,24] sensors,[25,26] and catalysis.[27] Reported herein is the synthetic route for creating and perfecting cellulose film for the incorporation of a Schiff-based salen ligand for the extraction of uranyl ions in aqueous media.

3.2 Results:

3. 2. 1. Absorption of Schiff-base Ligands onto Cellulose Films

All metals concentrations were analyzed using Inductively Coupled Plasma with Optical Emission Spectroscopy (Perkin Elmer Optima 7100 DV).

Metal extractions were performed in aqueous media using the 3 ligands of interest (**L1**, **L2**, and **L3**). The study was conducted to determine the ligands' ability to extract metal ions from aqueous media and study the effectiveness of using cellulose film as a

solid-support. As depicted in **Figure 3.2**, the cellulose film coated with salen ligand as well as the bare cellulose film removed the most uranyl ions in comparison to the rest of the metal ions examined. The preference for the uranyl ions could be caused by the ability of the large uranyl ions absorbing onto the surface of the film as well as chelating into the ligand's pocket. The **L3** was able to extract the most uranyl ions from the aqueous media in comparison to the other ligands within 5 minutes; it extracted 36 % of the uranyl ions compared to 28 % for both the **L1** and **L2** ligands and 31 % for the cellulose film.

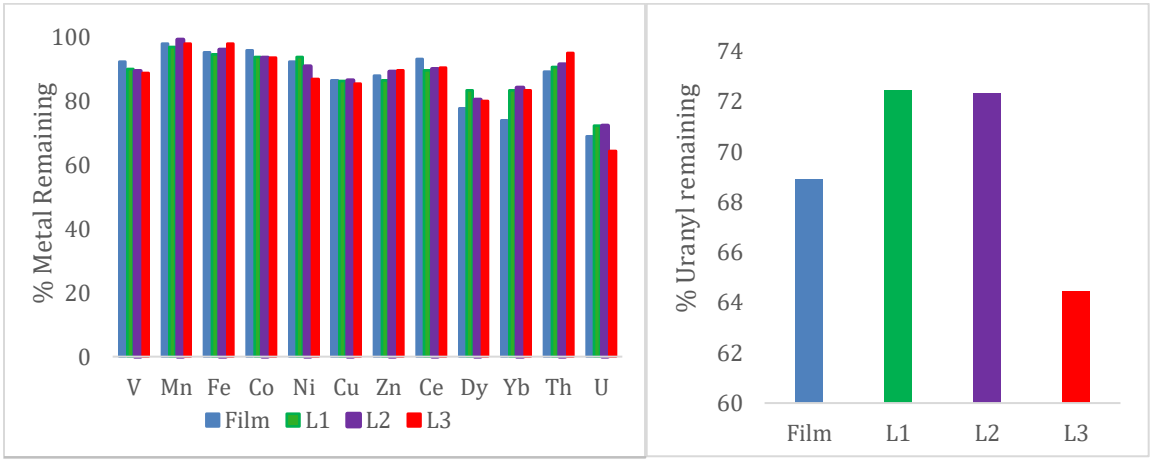

Figure 3.2: The percent of metal ions remaining in solution after 5min extracting period. (left) The results of extraction using the salen coated films showing results for the metal of interest, uranyl. (right)

Unfortunately, leaching of the ligand from the film into the solution was observed after only 15 minutes at the following pH: 5, 7, 8, and 12. (**Figure 3.3**) The leaching continued to increase after 30 minutes, with a great increase at the pH of 14, thus proving to be not only an inefficient metal extracting method over a wide pH range, but also over a long period of time.

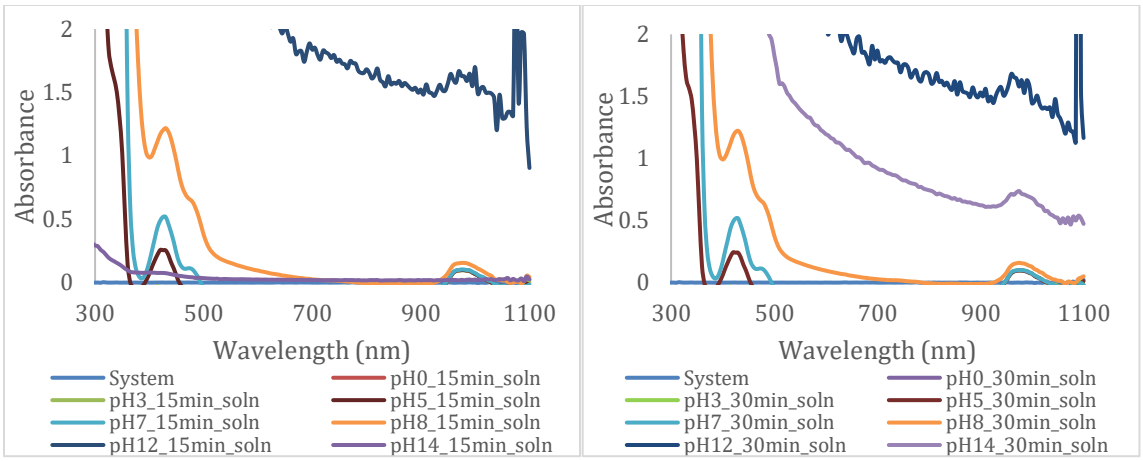

Figure 3.3: Absorbance spectra of salen coated films indicating leaching over varying pH range (0-14)

3. 2. 2. Toward the Synthesis of regenerated cellulose (RC) film from Microcrystalline Cellulose (MCC)

(Methodology adopted from Bansal 2012 publication.[5]) A sample of 5 g of micro-crystalline cellulose (**Figure 3.4**) was added to a 100 mL solution containing 7 % NaOH and 12 % urea in water. Urea dramatically increases the solubility of cellulose in aqueous alkali media.[28] The solution was stirred at room temperature for 30 minutes then kept static for 16 h at -20 °C. Upon thawing the cellulose was regenerated by adding 10 times v/v of deionized water to prepare a regenerated cellulose (RC). The regenerated cellulose (RC), was precipitated and separated *via* centrifugation at 5000 revolutions per minute (rpm). The resulting precipitate was washed several times with deionized water to remove any remnants of NaOH and urea. The RC was preserved at 4 °C as a 2 % slurry (in deionized water) until use. From the stock of RC, stock solutions containing various concentrations of cellulose was prepared in deionized water. The solution was then ultrasonicated for 2 min using a 2 mm probe at 75 % amplitude. The pH of the solution was measured before and after sonication to ensure that the value remained very close to 8; if not, a small aliquot

(1-1.5 mL) solution of 1 M NaOH or HCl was used to adjust it.

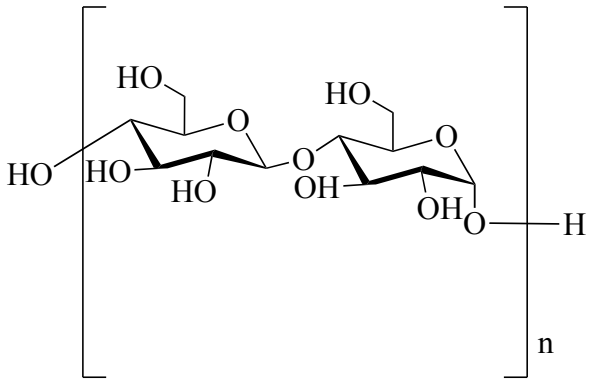

Figure 3.4: Structure of MCC Monomer Unit

Freestanding films of RC were prepared by pouring the dispersed RC (10 mL) in a glass Petri dish (~ 100 mm diameter), the solvent was allowed to evaporate slowly at room temperature, and then dried in an oven at 70 °C for 2 h. Upon drying, the film was peeled from the Petri dish using forceps; however, the film obtained was very fragile during the removal process, resulting in only small (~ 1 cm) pieces being attained. The film was transparent, flexible, and insoluble in water, due to the significant loss of crystallinity and hydrogen bonding of the original MCC.[5]

Ligand in-trapped films of RC was prepared using the aforementioned procedure; however, 5 mL of 1000 ppm **L3** in DMF was added to the dispersed cellulose prior to solvent evaporation. Unlike the freestanding film, the solution for the ligand in-trapped film never formed a film upon solvent evaporation, due to the ligand precipitating out of solution upon dilution, thus resulting in the disruption and clumping of the regenerated cellulose. In order to create cellulose film, cellulose and all solutes must be fully dissolved or completely dispersed in the solvent of choice, otherwise no film will be obtained.[5] This

method proved to be a practical method for making cellulose film, without chemically modifying cellulose to disrupt the strong intra and intermolecular hydrogen bonds; however, it was not found to be practical for the making of ligand chemisorbed films due to some precipitation of the ligand.

3. 2. 3. Toward the Synthesis of Sodium Carboxymethyl cellulose film.

(Methodology adopted from Rhim's 2015 publication.[29]) Using a 250 mL round-bottom flask, 3 g of CMC (**Figure 3.5**) and 0.9 g of glycerol (plasticizer), was added into 150 mL of distilled water with stirring, and was heated at 90 °C for 20 min or until the CMC was fully dissolved. Plasticizers are low molecular weight chemicals that are often added to polymers to increase flexibility and/or plasticity while reducing brittleness.[30] They work by introducing a hydrogen donor, which reduces the amount of hydrogen bonding amongst the constituent molecules.[30] The solution was then poured into a glass mold and allowed to dry at room temperature. Once the solvent was evaporated, the film was dried in an oven for 2 h at 40 °C. The film obtained was transparent and flexible, however it was water-soluble due to the numerous polar carboxyl groups that decorate the surface of the film, thus resulting in an impractical solid-support for uranyl extraction in aqueous media.

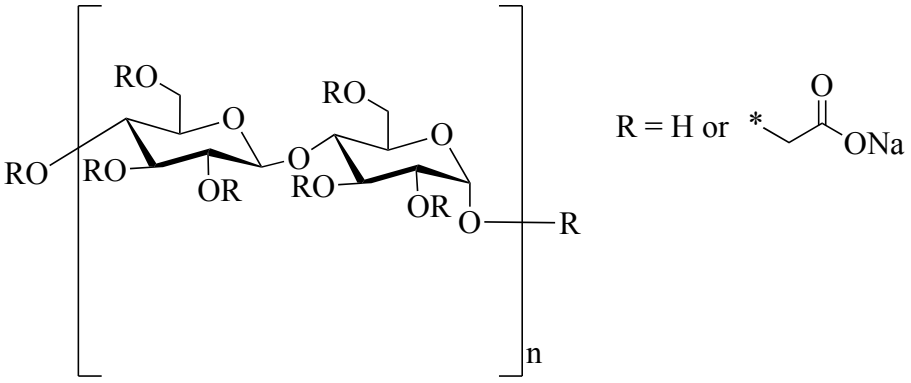

Figure 3.5: Structure of Sodium Carboxymethyl Cellulose Monomer Unit

Ligand incorporating films of CMC film were prepared using the aforementioned procedure; however, 5 mL of 1000 ppm **L3** in DMF was added to the dissolved CMC and glycerol solution prior to solvent evaporation. The film obtained was a pale yellow transparent and flexible film. Resembling the characteristics of the free-standing film, this ligand in-trapped film was also soluble in water, thus making it not useful as a uranyl extractor in aqueous media.

3. 2. 4. Toward the Synthesis Cellulose Film using epichlorohydrin as Cross-linker (Cell-1)

A modified procedure was adopted from a Yan 2013 published method.[31] For 5% ligand loading of the cellulose film, 0.56 g of 2-hydroxyethyl cellulose (HEC) (**Figure 3.6**) with an average molecular weight of 1.30 x 10^6 g/mol was placed in 100 mL of water and heated at 40 °C until the cellulose was fully dissolved. The solution was then allowed to cool to room temperature. Next 0.1 mL of epichlorohydrin (3 wt %) was added to the solution under stirring to obtain a homogeneous (20-45 min). After the solution had become homogeneous, 10 mL solution of the **L3** ligand (1000 ppm) was added and stirred

vigorously (~1000 rpms) for about 5 mins. The mixture was then poured into a Petri dish where the solvent was allowed to evaporate (~3-5 days). Once dried, the film was washed with 5% acetic acid and deionized water, then dried in an oven at 40 °C for 2 h.

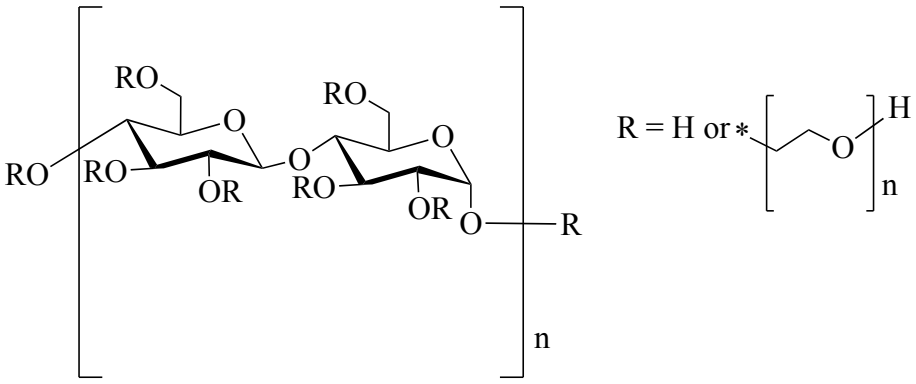

Figure 3.6: Structure of 2-Hydroxyethyl Cellulose Monomer Unit

3. 2. 5. Toward the Synthesis Cellulose Film using glutaraldehyde as Cross-linker (Cell-2 and Cell-3)

Methodologies were adopted from Mills 2006 publication.[32] For 5 % ligand loading of the cellulose film, 0.081 HEC (MW= 90,000 g/mol) was dissolved in water (12 mL for Cell-2 and 100 mL for Cell-3) and heated at 40 °C, the solution was then allowed to cool to room temperature, then a solution of 1 % glutaraldehyde (0.75mL for Cell-2 and 9 mL for Cell-3) was added and stirred for 5 min, followed by the addition of a 0.5 M HCl solution. The reaction was allowed to stir for 30 s followed by the addition (10 mL) of the 1000 ppm **L3** (in DMF) solution. The solution was then vigorously stirred (~ 900 -1000 rpms) for 5 min, then poured into a glass mold, where it was allowed to air dry for 2-3 days. For standard films, the process was repeated using an equivalent amount DMF in place of the ligand solution. For Cell-3 film, the aforementioned procedure

proceeded as written using HEC with a molecular weight of 1,300,000 g/mol in place of the original HEC (MW = 90,000 g/mol). Successful crosslinking was confirmed via FT-IR (see Appendix for spectra).

3. 2.6. Toward the Synthesis Cellulose Film using citric acid as a Cross-linker (Cell-4 and Cell 5)

Methodologies were adopted from Mills 2006 publication.[32] For 5 % ligand loading of the cellulose film, 0.81 g of HEC (MW = 1,300,000 g/mol) was dissolved in water (100 mL for Cell-4 and 12 mL for Cell-5) and heated at 40 °C, the solution was then allowed to cool to room temperature, then a solution of 1 % citric acid (9 mL for Cell-4 and 0.75mL for Cell-5) was added and stirred for 5 min, followed by the addition of a 0.5 M HCl solution. The reaction was allowed to stir for 30 s followed by the addition of the 1000 ppm **L3** (in DMF) solution (10 mL). The solution was then vigorously stirred (~ 900 -1000 rpms) for 5 min, then poured into a Petri dish, where it was allowed to air dry for 2-3 days. For standard films, the process was repeated using an equivalent amount DMF in place of the ligand solution. For Cell-5 film, the aforementioned procedure proceeded as stated using HEC with a molecular weight of 90,000 g/mol in place of the original HEC (MW = 1,300,000 g/mol). Successful crosslinking was confirmed via FT-IR (see Appendix for spectra).

3. 2. 7. Uranyl extraction using ligand-trapped Cellulose films

With five functionalized ligand-trapped cellulose films in hand, Cell-1, -2, -3, -4, -5, determining their ability to extract uranyl from aqueous media was studied. The amount

of uranyl (in ppm) remaining was determined spectroscopically using the Arsenazo III method.[33, 34] Arsenazo III (**Figure 3.7**) is a bis-azo chromogenic reagent known for its high sensitivity, low selectivity, and its ability to form stable metal complexes (**Figure 3.7**) with actinides and lanthanides over a wide pH range.[35, 36]

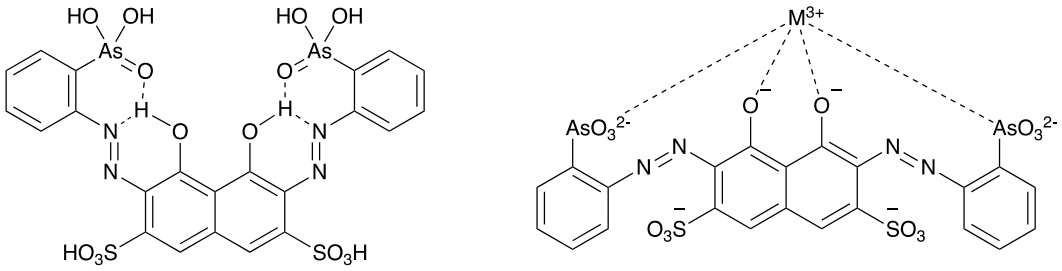

A B

Figure 3.7: Structure of Arsenazo III (A) un-complexed and (B) complexed

The 1:1 Arsenazo III-uranyl complex exhibits signals at 610 nm and 651 nm.[33, 37] Using standard uranyl solutions, a linear correlation (**Figure 3.8**) between the concentration of uranyl (ppm) and the absorbance at 651 nm was plotted and used to determine the percent uranyl removed after the extraction periods (10 min, 30 min, 1 h, 5 h, 10 h, 24 h and 72 h).

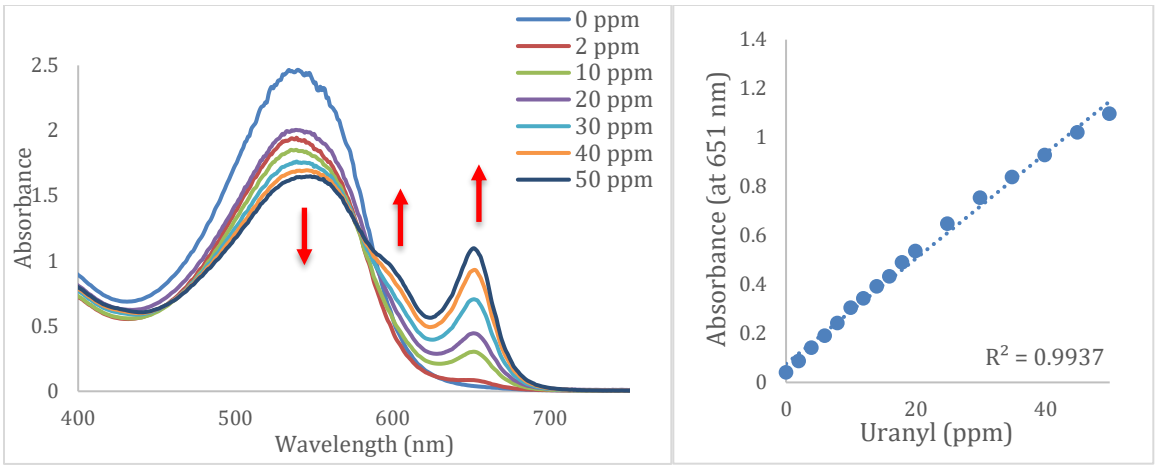

Figure 3.8: (L) Absorbance spectra of Arsenazo dye titrated with uranyl showing increase in 1:1 metal to ligand complex at 651 nm. (R) Arsenazo III Standard Curve showing increase in 1:1 metal complex at 651 nm.

Each film was cut into 2.5 cm x 5 cm rectangular strips, one strip was then placed in a Petri dish containing 10 mL of 10 ppm aqueous uranium solution. The solution was then agitated, after the extraction period the film was removed, and a 0.25 mL sample of the uranyl solution was tested. The sample was mixed with 2.0 mL of the Arsenazo III dye and analyzed via UV-Vis spectroscopy, where the uranyl complex absorbance peak at 651 nm was used to determine the amount of uranyl remaining in the solution. The fluorescence of the film was then analyzed via excitation at 380 nm. The film was then placed back into the uranyl solution and agitated until the next extraction analysis. It is important to note that no direct comparison within the series of films was possible because the amount of crosslinker used in each film was determined based on percent weight, instead of molar ratio.

3. 2. 7. 1. Uranyl extraction using ligand-trapped Cellulose films: Cell 1

Aqueous uranyl extractions studies began with Cell-1, the cellulose film in which epichlorohydrin was utilized as the crosslinker (**Scheme 3.1**), resulting in the addition of free hydroxyl groups, which aid in the swelling properties of the film. Swelling of the film

allows for the uranyl ions to bind in the unexposed pockets of the salen ligands (**L6**) that are trapped within the film.

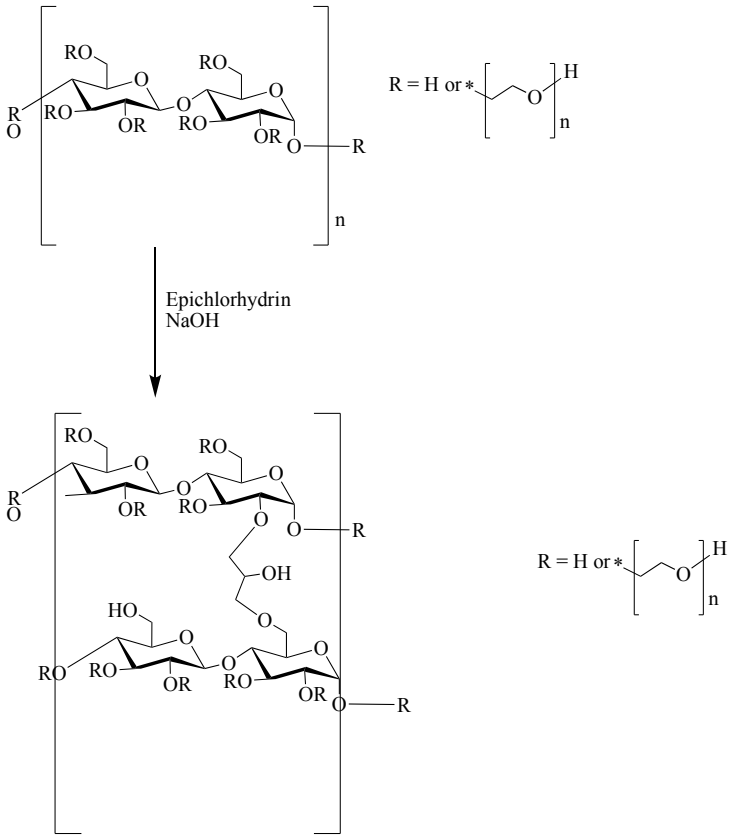

Scheme 3. 1: Reaction of 2-HEC with epichlorohydrin

Cell-1 film exhibits very promising uranyl extracting properties (**Figure 3.9**); in as little as 10 minutes it extracted over 40 % of the uranyl in the sample. Within an hour it removed over 55 %, unfortunately around this time the integrity film was becoming compromised. After an hour the film began to swell excessively into a jelly-like substance, due to too little crosslinking. The film was then remade several times, increasing the cross-linking from 3 wt % up to 25 wt %. With the increase in crosslinking the ability of the film to swell decreased significantly, thus limiting the amount of uranyl ions that can flow into

the film. Unfortunately, the films continued to decompose after about an 2-3 hours in aqueous media, thus rendering the epichlorohydrin film an ineffective solid support for uranyl extraction in aqueous media.

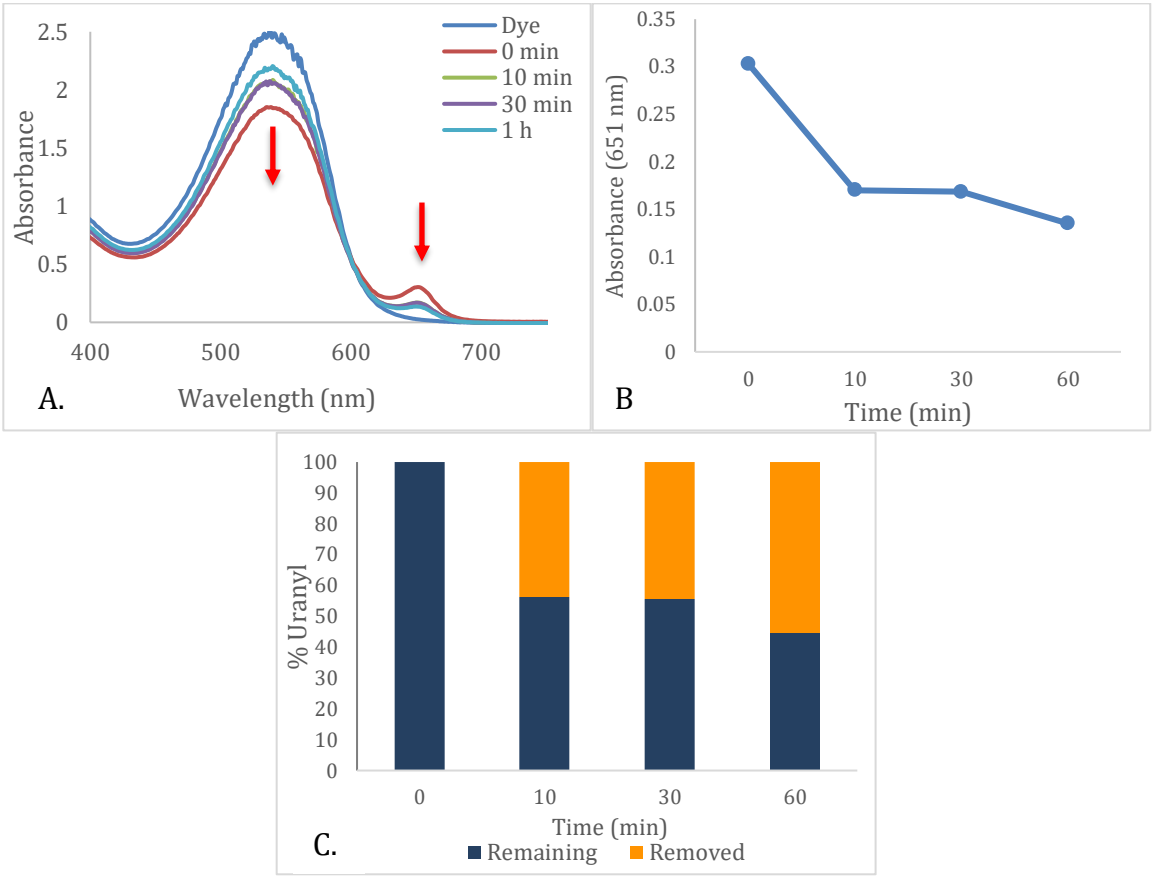

Figure 3.9: Uranyl extraction analysis of Cell-1 (A) showing a decrease in 1:1 metal to ligand complex at 651 nm UV-Vis spectrum (B) decrease of metal complexation at 651 nm (C) Percent uranyl extracted and remaining after 1 hour of extraction using Cell-1.

3. 2. 7. 2. Uranyl extraction using ligand-trapped Cellulose films: Cell 2 and Cell 3

Aqueous uranyl extraction studies also used Cell-2 and 3, where the hydroxyl groups on the cellulose monomers undergo a nucleophilic substitution with glutaraldehyde as the crosslinker (**Scheme 3.2**). This doubled the amount of free hydroxyl groups and an elongated carbon chain between the monomers.

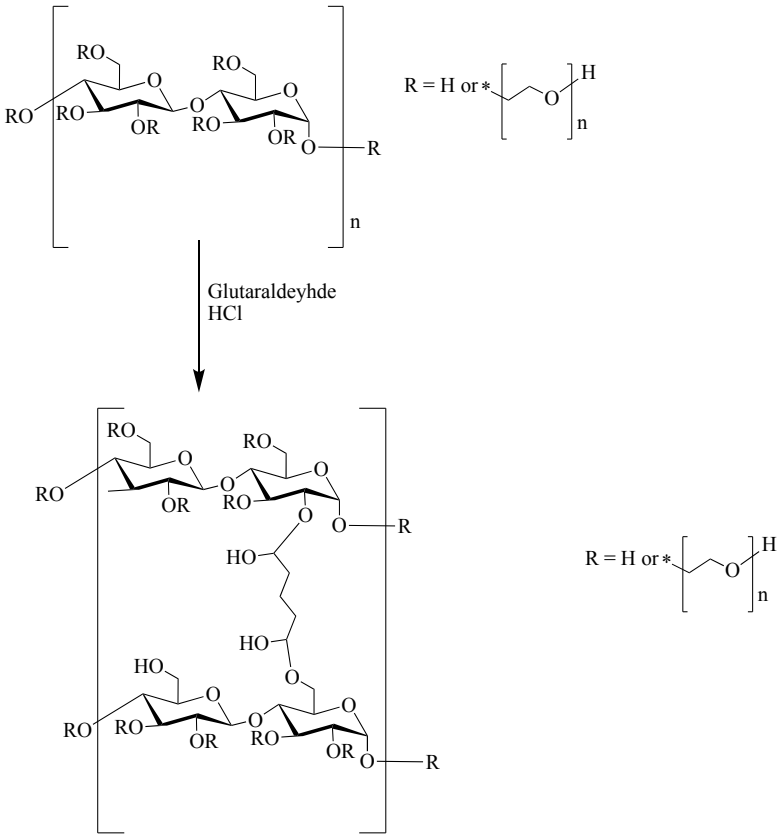

Scheme 3. 2: Reaction of 2-HEC with glutaraldehyde

Cell-2 film was then explored for its ability to extract uranyl from aqueous media over a period of 3 days. As depicted in **Figure 3.10a and 3.10b**, over the duration of the extraction a decrease in the absorbance peak at 651 nm was observed indicating a decrease in uranyl concentration. In as little as 10 minutes it extracted about 15 % of the uranyl in the sample (**Figure 3.10c**), which is significantly less than Cell-1, however the Cell-2 film retained its structural integrity. Within an hour it removed about 40-45 % of the uranyl in the solution and began to level off there for several hours, then after 72-h. The removal fraction increased to about 65 %. The standard film, without the ligand present only removed 11 % of the uranyl over the 72-h period. This indicates that the salen ligand

present plays a critical role in removing the uranyl ions via chelation in the tetradentate pocket. Fluorescence data of the Cell-2 film, with an excitation at 381 nm, correlates with the aforementioned (Chapter 2) data observed for the salen ligand (**L3**) in solution phase, where the chelation of uranyl inside the pocket of the ligand quenches its fluorescence (**Figure 3.10d**).

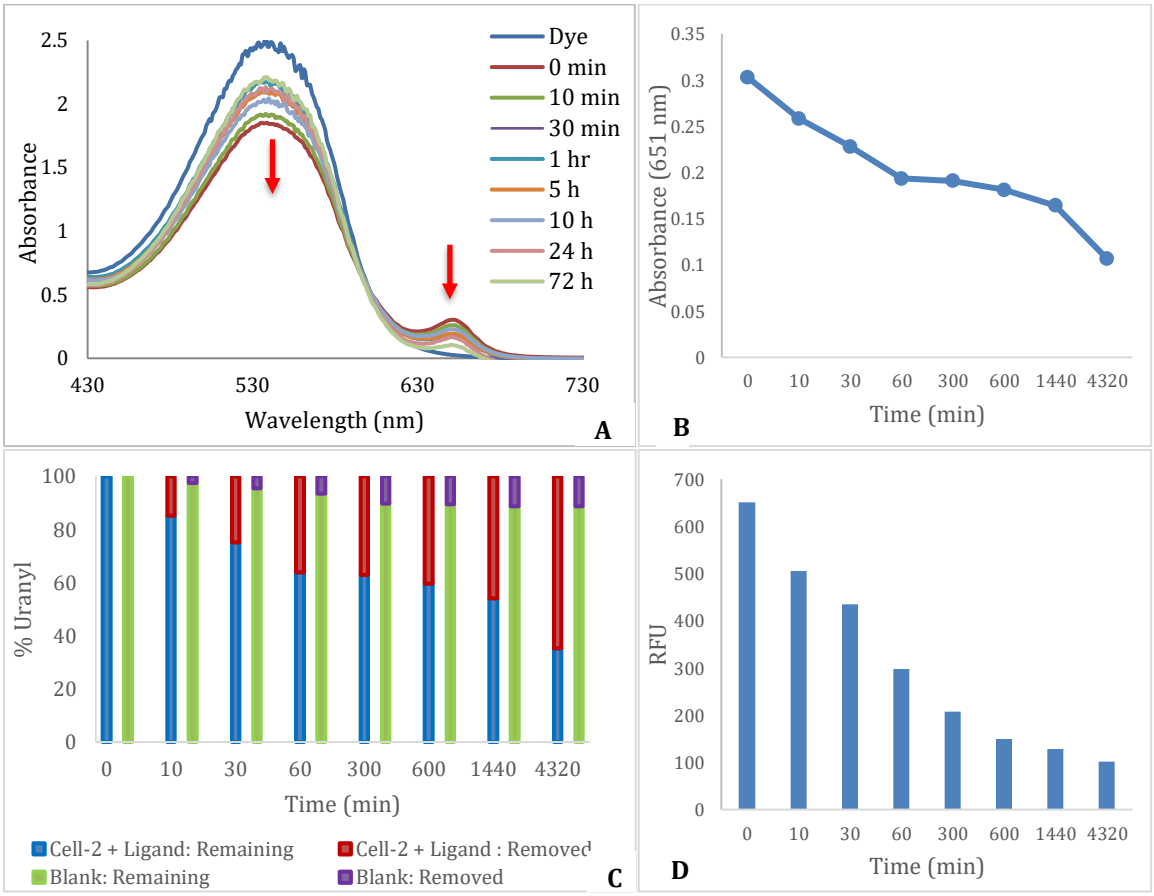

Figure 3.10: Uranyl extraction analysis of Cell-2 (A) showing a decrease in 1:1 metal to ligand complex at 651 nm UV-Vis spectrum (B) decrease of metal complexation at 651 nm (C) Percent uranyl extracted and remaining after 1 hour of extraction using Cell-2 (D) Fluorescence of Cell-2 film over extraction period showing a decrease in intensity.

Cell-3 film was then explored for its ability to extract uranyl from aqueous media over a period of 3 days. As depicted in **Figure 3.11a and 3.11b**, over the duration of the extraction a decrease in the absorbance peak at 651 nm was observed indicating a decrease

in uranyl concentration of the solution. In as little as 10 minutes it extracted about 25 % of the uranyl in the sample (**Figure 3.11c**), within an hour it removed about 30 % of the uranyl in the solution. After about 5 hours it increased about 56 % then began to level off after several hours at around 66-70 %. The standard film, the film without the ligand present only removed 46 % of the uranyl over the 72-h period. These results indicated that the salen ligand present enhances the films' ability to remove the uranyl ions via chelation in with the Schiff base. Fluorescence data of the Cell-2 film, with an excitation at 381 nm, correlates with the aforementioned (Chapter 2) data observed for the salen ligand (**L3**) in solution phase, where the chelation of uranyl inside the pocket of the ligand quenches its fluorescence (**Figure 3.11d**).

Along with the ligand's chelation ability, the molecular weight of the cellulose units utilized affects the amount of uranyl extracted. With the increasing molecular weight of the cellulose the films becomes more permeable extensively swelling in aqueous media, thus allowing more uranyl ions to flow into and become trapped within the film's matrix. With this permeability, comes the potential for the ligand to leach out of the film, which could be responsible for the rapid decrease in fluoresence of the film over time.

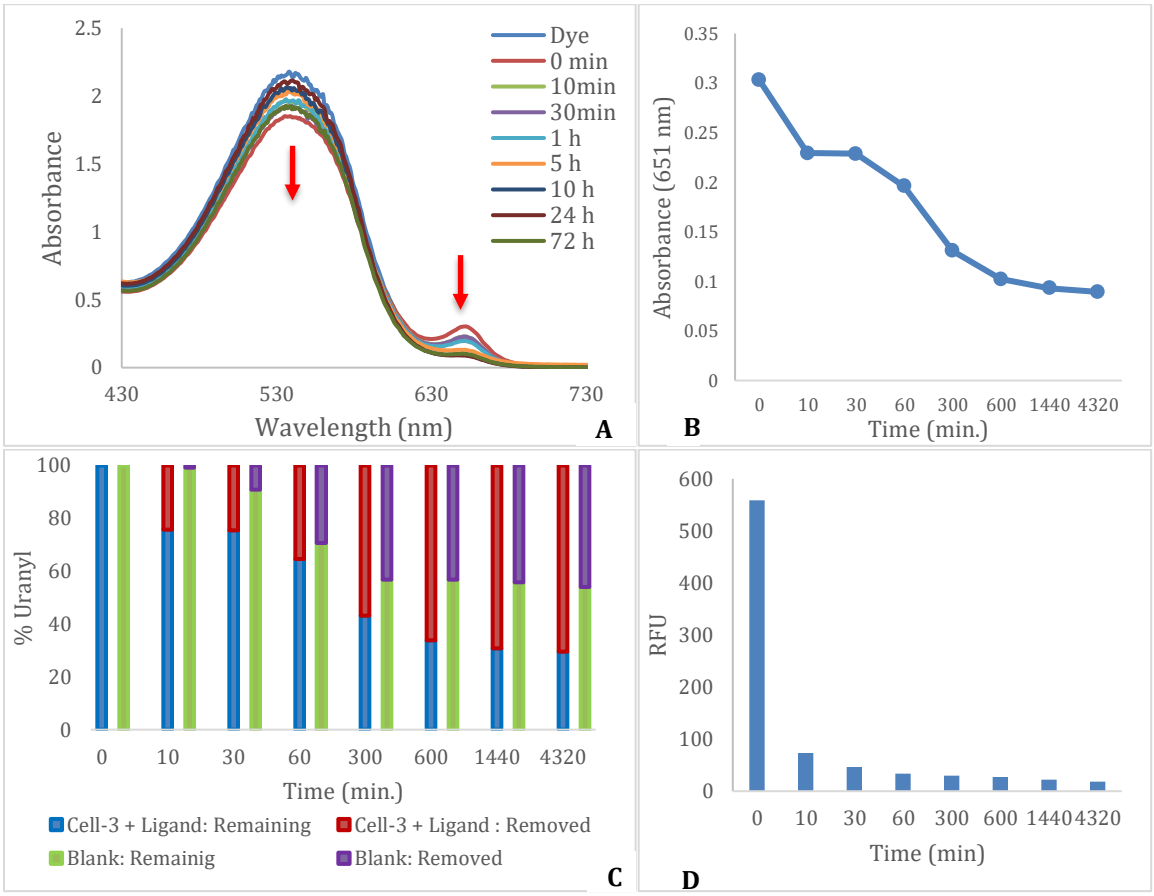

Figure 3.11: Uranyl extraction analysis of Cell-3 (A) showing a decrease in 1:1 metal to ligand complex at 651 nm UV-Vis spectrum (B) decrease of metal complexation at 651 nm (C) Percent uranyl extracted and remaining after 1 hour of extraction using Cell-3 (D) Fluorescence of Cell-3 film over extraction period showing a decrease in intensity.

3. 2. 7. 3. Uranyl extraction using ligand-trapped Cellulose films: Cell-4 and Cell-5

The free hydroxyl groups of Cell-4 and Cell-5 were subjected to an acid catalyzed esterification reaction with citric acid (**Scheme 3.3**). The esterification resulted in 2 new carbonyls, a carboxylic acid, and a hydroxyl group, crosslinking the monomers, each consisting of electron donating oxygens capable of chelating free uranyl ions.

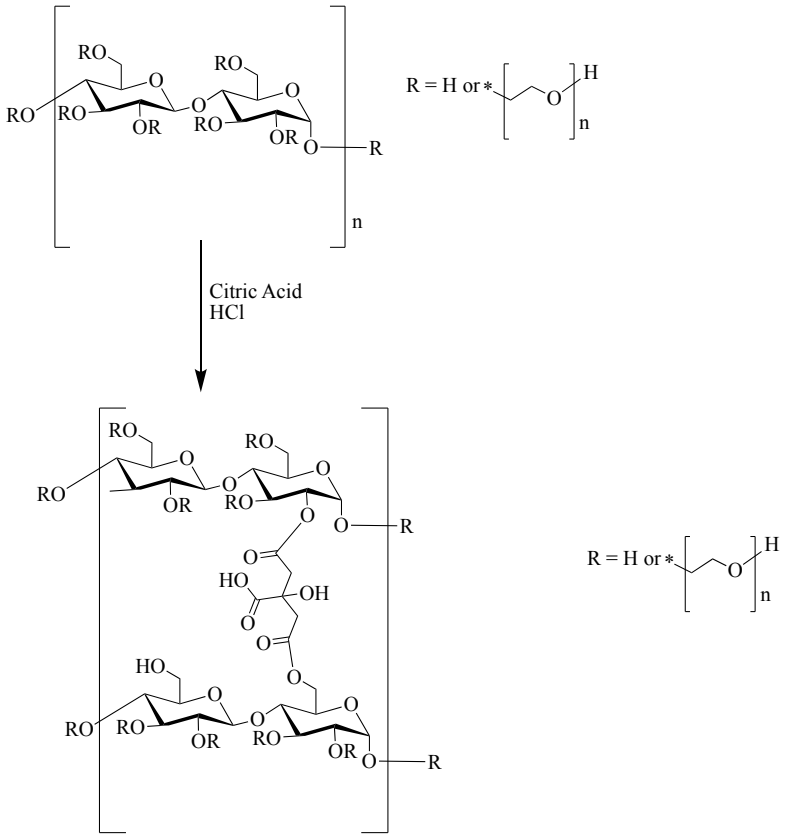

Scheme 3. 3: Reaction of 2-HEC with citric acid

Cell-4 film was then explored for its ability to extract uranyl from aqueous media over a period of 3 days. As depicted in **Figure 3.12a and 3.12b**, over the duration of the extraction a decrease in the absorbance peak at 651 nm was observed indicating a decrease in uranyl concentration of the solution. Within 30 minutes it extracted about 8 % of the uranyl in the sample (**Figure 3.12c**). After an hour it removed about 10-15 % of the uranyl in the solution and began to level off there for several hours, then after 72 h it increased to about 35 %. In comparison the film without the ligand present only removed 15 % of the uranyl over the 72-h period. This indicates that the salen ligand present is playing a role in removing the uranyl ions via chelation in the tetradentate pocket. However, the dramatic decrease in uranyl being removed with Cell-4 in comparison to that of Cell-2 and Cell-3

indicates that the molecular weight of the cellulose polymer chain may be affecting the extraction.

Fluorescence data of the Cell-4 film, with an excitation at 381 nm, correlates with the aforementioned (Chapter 2) data observed for the salen ligand (**L3**) in solution phase, where the chelation of uranyl inside the pocket of the ligand quenches its fluorescence (**Figure 3.12d**). However, the fluorescence results does not correlate with the absorbances data very well suggesting that there is another cause for the decrease in ligand fluorescence that's not caused by chelation of the metal.

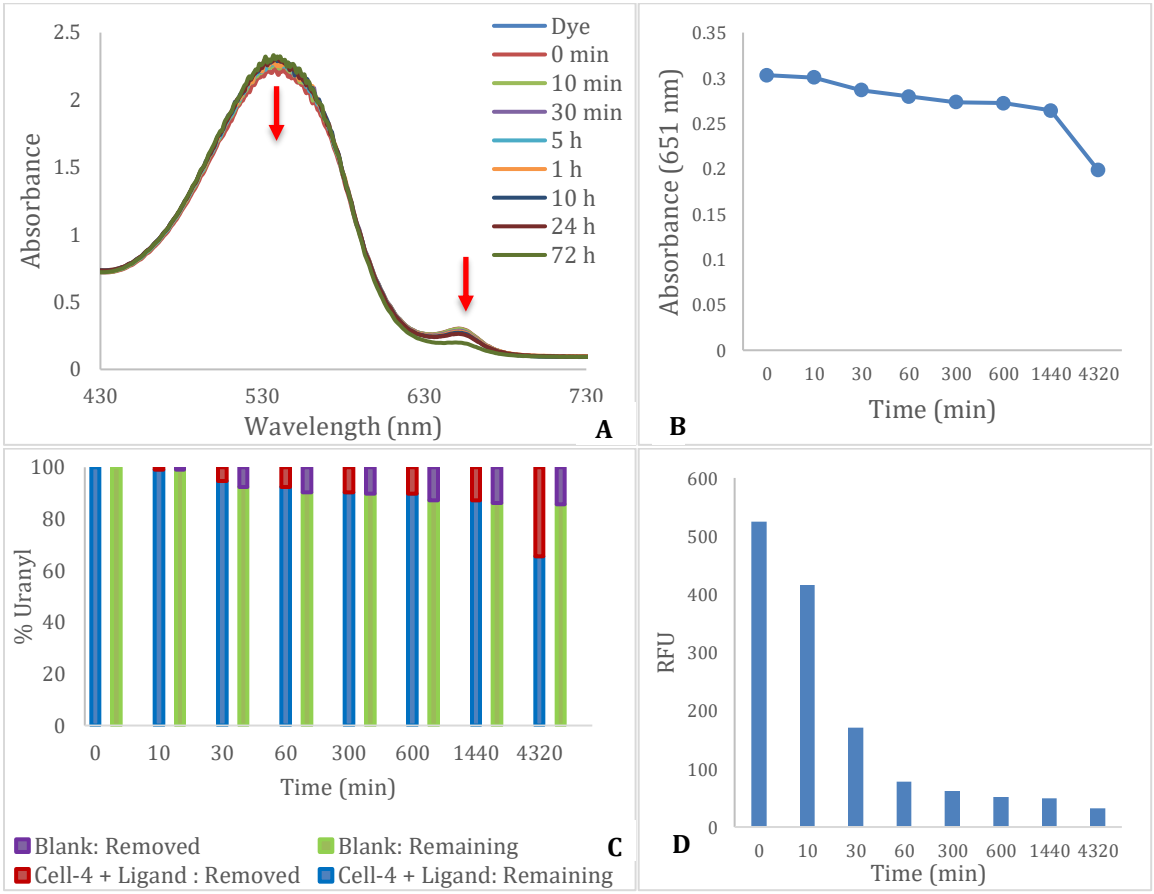

Figure 3.12: Uranyl extraction analysis of Cell-4 (A) showing a decrease in 1:1 metal to ligand complex at 651 nm UV-Vis spectrum (B) decrease of metal complexation at 651 nm (C) Percent uranyl extracted and remaining after 1 hour of extraction using Cell-4 (D) Fluorescence of Cell-4 film over extraction period showing a decrease in intensity

Cell-5 film was then explored for its ability to extract uranyl from aqueous media over a period of 3 days. As depicted in **Figure 3.13a and 3.13b**, over the duration of the extraction a decrease in the absorbance peak at 651 nm was observed indicating a decrease in the solution uranyl concentration. Within 10 minutes the film extracted about 10 % of the uranyl in the sample (**Figure 3.13c**), and about 20 % after 1 hour. The amount of uranyl extracted began to level out around 40 % after 5 hours, and maximized at 41 % after 72 h. In comparison, the film without the ligand present, extracted only 26 % of the uranyl over the 72-h period. Fluorescence data of the Cell-5 film, with an excitation at 381 nm, correlates with the aforementioned (Chapter 2) data observed for the salen ligand (**L3**) in solution phase, where the chelation of uranyl inside the pocket of the ligand quenches its fluorescence (**Figure 3.13d**).

It's important to note the differences between Cell-4 and Cell-5 extraction capabilities. Cell-4 was only able to extract an overall ~ 34% while Cell-5 extracted ~ 41 %. These differences could be attributed to the molecular weight of the cellulose used to make the films. The most notable difference about the two films is their ability to swell in aqueous media. Cell-4 swelled extensively when placed in water which in turn caused the ligands trapped in the film to leach into the solution, thus resulting in less uranyl being extracted by the film and a decrease in the fluorescence intensity.

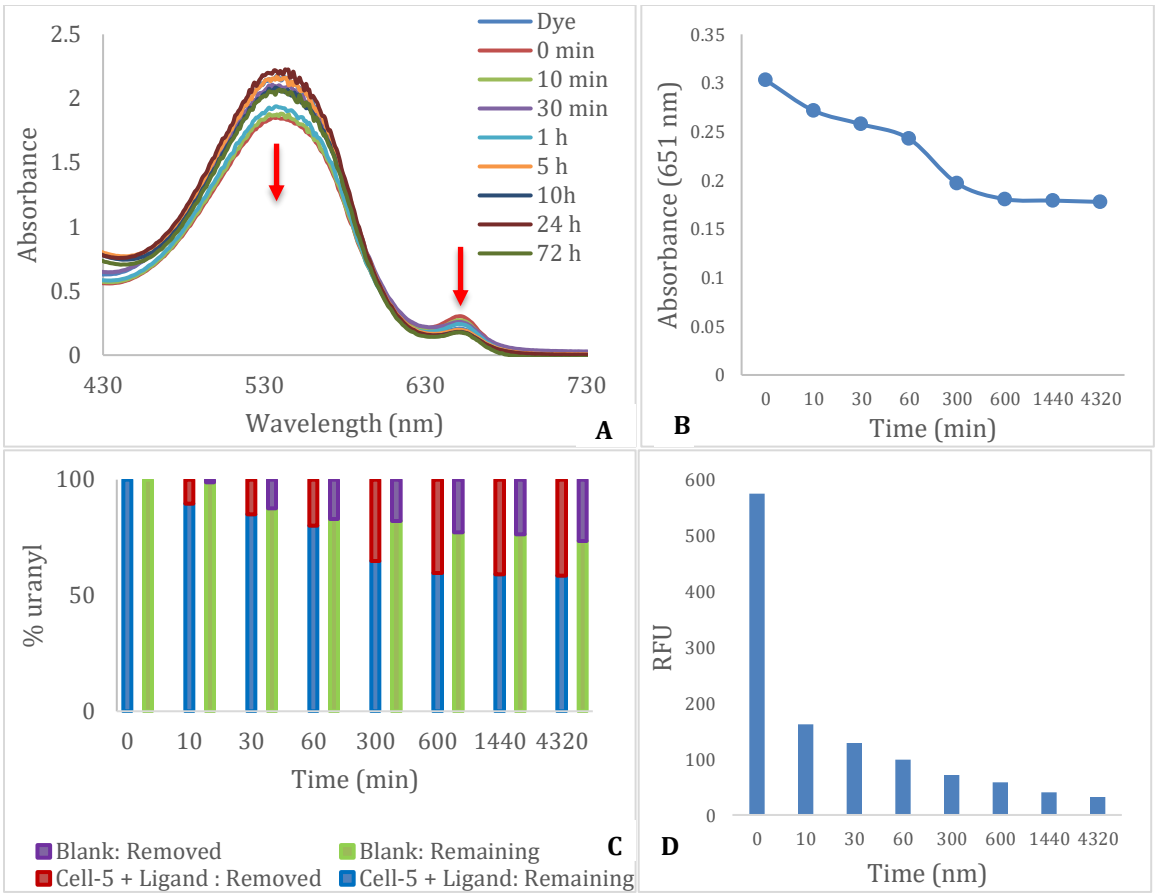

Figure 3.13: Uranyl extraction analysis of Cell-5 (A) showing a decrease in 1:1 metal to ligand complex at 651 nm UV-Vis spectrum (B) decrease of metal complexation at 651 nm (C) Percent uranyl extracted and remaining after 1 hour of extraction using Cell-5 (D) Fluorescence of Cell-5 film over extraction period showing a decrease in intensity.

3. 2. 8 Leaching Test

Utilization of the films as a solid-phase extractor exhibits the possibility of leaching of the ligand into the solution or structural degradation of the system. This can occur immediately or over time; to monitor such processes a leaching study was performed to ensure that the ligand remains incorporated into the film and that the film retains its integrity over a 1-week period in basic, neutral, and acidic media. Unfortunately, leaching occurred within 30 minutes due to ligands that weren't completely trapped in the film. Ligand leaching took place upon the film swelling in solution, thus explaining the rapid decrease in fluorescence

of the film. Basic environments yielded the most leaching, followed by the acidic media, thus making neutral solutions the optimal conditions (see Appendix for UV-Vis spectra for each film).

3. 2. 9 Towards the Synthesis of Covalently Linked Cellulose Films

A modified Steglich esterification on ligand **L7** (**Scheme 3.4**) was used to covalently link the free hydroxy groups of the cellulose film with the 5 and/or 5' carboxylic acids of the ligand (**Scheme 3.4**) in an attempt to prevent leaching of the ligand from the film.[1]

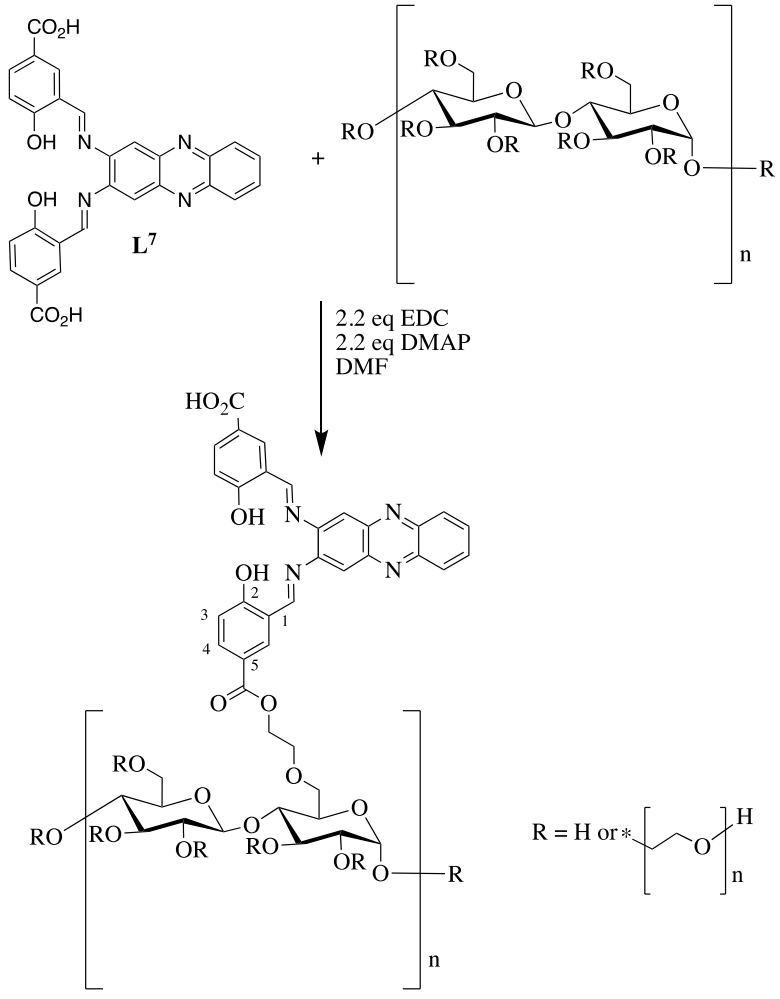

Scheme 3.4: Steglich esterification of **L7** and 2-HEC

The **L7** ligand was chosen to replace **L3** for 2 reasons; 1. The extended conjugation of the backbone and 2. Elimination of the possible tautomer between the cyclic imine and hydroxyl group of the 2-quinoxalinol backbone. This elimination is important because it allows esterification to only take place in a more uniform matter, only at the 5 and 5' positions of the ligands with free hydroxyl groups of the cellulose. Resembling the **L3** ligand**, L7** exhibited spectral differentiation between uranyl and copper (**Figure 3.14**). The **L7** ligand exhibited 2 peaks at 411 nm and 431 nm with a small shoulder at 519 nm. Upon the addition of copper, a hypsochromic shift to 448 nm was observed, while a small bathochromic shift to 405 nm was observed with the addition of uranyl. Similar to **L3, L7** exhibits quenching of fluorescence upon the addition of the copper solution. However, unlike **L3**, **L7** exhibits an increase in fluorescence as the uranyl salt was titrated with the free base. This increase in fluorescence is possibly due to the formation of aggregates within the solution.

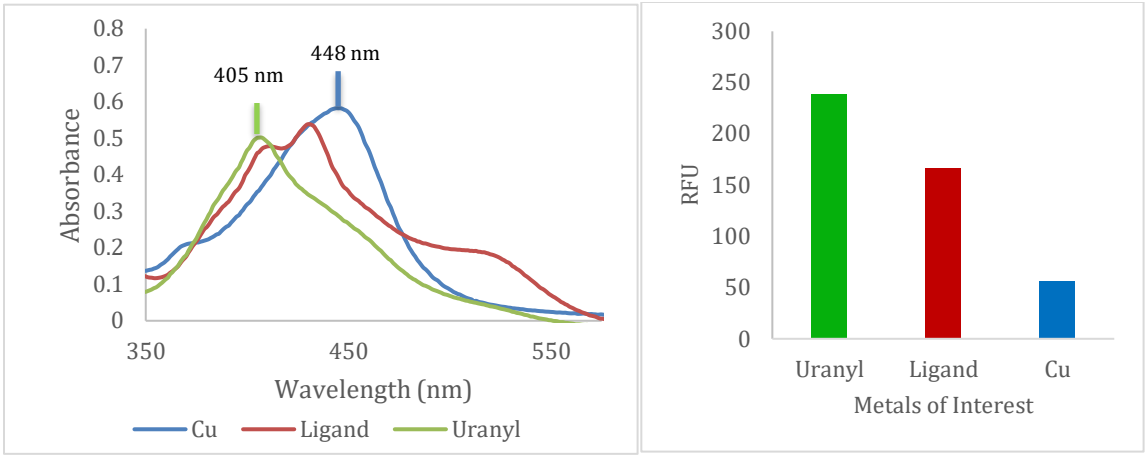

Figure 3.14: The Absorbance spectra of **L7** with copper and uranyl (shown at 2.3: 1 metal to ligand ratio) showing red and blue shifts, respectively as the result of serial titration, (left) and fluorescence intensity of serial titration indicating an increase in intensity in the presence of uranyl and a quenching occurring in the presence of copper. (right)

With the covalently linked cellulose-**L7** unit in hand, the films were made using the aforementioned method utilizing citric acid and glutaraldehyde as cross-linkers.

The Cell-6 film (cellulose MW = 90,000 g/mol and crosslinker = glutaraldehyde) exhibited great potential as a uranyl extractor over the period of 3 days. As depicted in **Figure 3.15a and 3.15b**, over the duration of the extraction a decrease in the absorbance peak at 651 nm was observed indicating a decrease in uranyl solution concentration. Within 10 minutes the ligand extracted about 10 % of the uranyl in the sample (**Figure 3.15c**), and within an hour it removed about 25 % of the uranyl in the solution. After about 5 hours the extraction increased to about 50 % and slowly increasing to 60 % after 10 hours. The extraction began to level off to around 65-70 % over the final hours. In comparison, the film without the ligand only removed 11 % of the uranyl over the 72-h period, reaffirming the importance of the presence of the ligand. Fluorescence data of the Cell-6 film, with an excitation at 411 nm, correlates with the data observed for the salen ligand (**L3**) in solution phase, where the chelation of uranyl inside the pocket of the ligand

quenches the fluorescence (**Figure 3.15d**) but not with the **L7** ligand where an increase in intensity is observed upon the chelation of uranyl within the pocket, which suggest possible leaching of the ligand from the film.

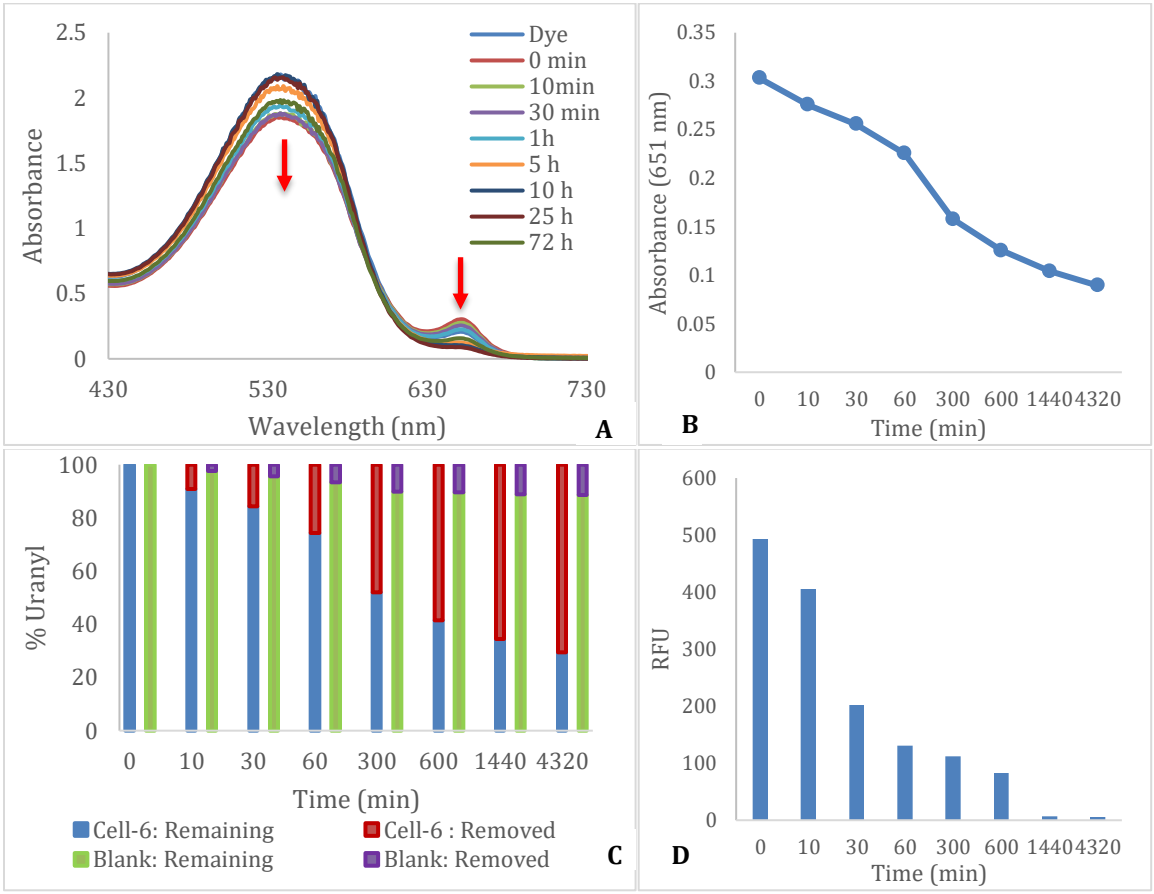

Figure 3.15: Uranyl extraction analysis of Cell-6 (A) showing a decrease in 1:1 metal to ligand complex at 651 nm UV-Vis spectrum (B) decrease of metal complexation at 651 nm (C) Percent uranyl extracted and remaining after 1 hour of extraction using Cell-6 (D) Fluorescence of Cell-6 film over extraction period showing a decrease in intensity.

Similar to previous films tested, Cell-7 film (cellulose MW = 1,300,000 g/mol and crosslinker = glutaraldehyde) exhibited potential as a uranyl extractor over the period of 3 days. As depicted in **Figure 3.16a and 3.16b**, decreasing in the absorbance peak at 651 nm was observed correlating to a decrease in uranyl solution concentration. Extraction of

uranyl started off very slowly, extracting barely 1 % in 10 minutes and about 10 % in 30 minutes (**Figure 3.16c**). After about 5 hours it increased about 30 % and slowly increased to 36 % after 10 hours then began to level off afterwards to around 41-43 % over the final hours. For the film without the ligand present, 46 % of the uranyl was removed over the 72-h period. Similar to the fluorescence data of the Cell-6 film, the fluorescence data of Cell-7 suggest possible leaching of the ligand from the film (**Figure 3.16d**).

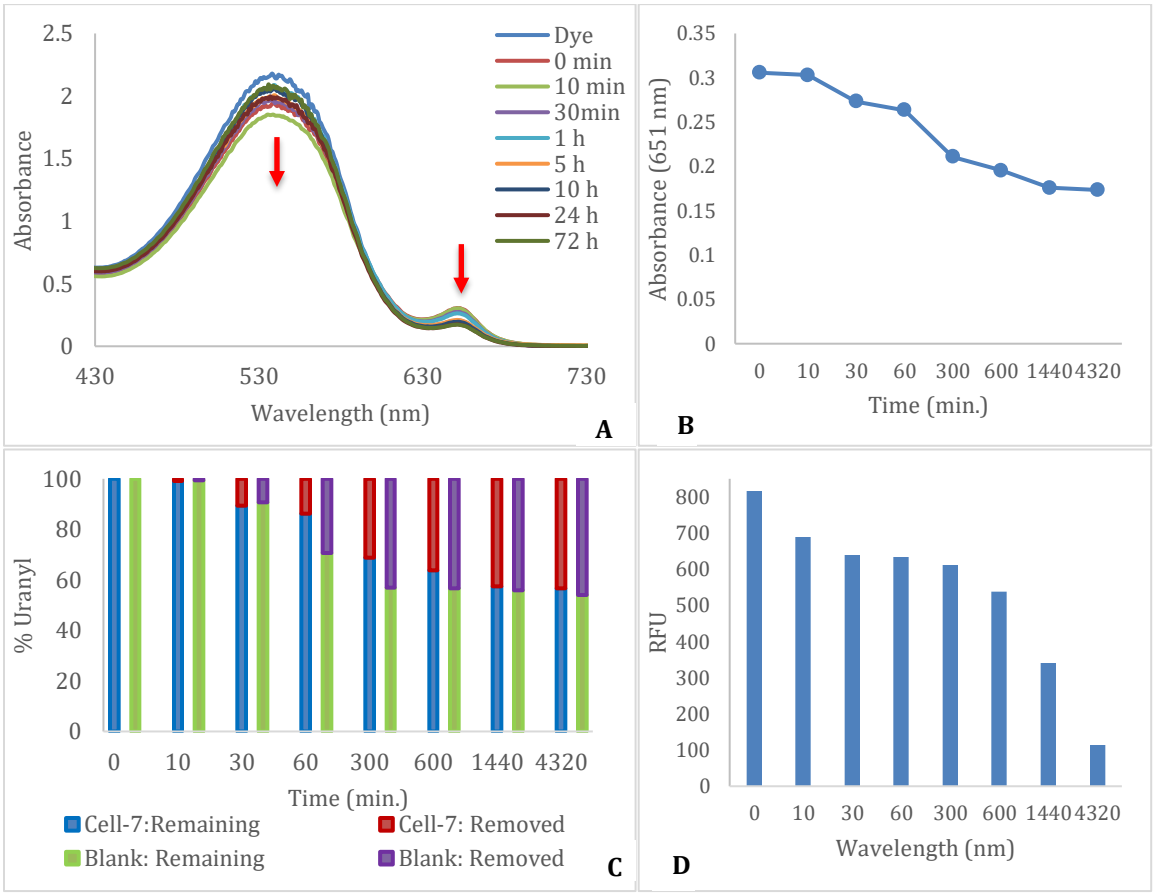

Figure 3.16: Uranyl extraction analysis of Cell-7 (A) showing a decrease in 1:1 metal to ligand complex at 651 nm UV-Vis spectrum (B) decrease of metal complexation at 651 nm (C) Percent uranyl extracted and remaining after 1 hour of extraction using Cell-7 (D) Fluorescence of Cell-7 film over extraction period showing a decrease in intensity.

As previously stated, the ligand's chelation ability, as well as the molecular weight

of the cellulose units utilized influences the amount of uranyl extracted, which is evident in the extraction abilities of Cell-6 and Cell-7. Cell-6 extracted an overall ~ 65 % while Cell-7 extracted ~ 42 %. These differences could be attributed to the molecular weight of the cellulose used to make the films as well as the chelation ability of the ligand.

Cell-8 film (cellulose MW = 90,000 g/mol and crosslinker = citric acid) was then explored for its ability to extract uranyl from aqueous media over a period of 3 days. As depicted in **Figure 3.17a and 3.17b**, over the duration of the extraction a decrease in the absorbance peak at 651 nm was observed, corresponding to a decrease in the uranyl solution concentration. After the 10 minutes of extraction only 8 % of the uranyl in the sample was removed (**Figure 3.17c**), within an hour the amount of uranyl extracted barely increased (9 %). After about 5 hours the amount extracted continued to linger around 9 % and then slowly increased to an overall removal of 40 % over the duration of the extraction period. The film without the ligand present only removed 26 % of the uranyl over the 72-h period, indicating that the salen ligand present enhances the films' ability to remove the uranyl ions via chelation in with the Schiff base. This data was in accordance with the previous fluorescence data observed for the salen ligand (**L3**) in solution phase, where the chelation of uranyl inside the pocket of the ligand quenches the fluorescence (**Figure 3.17d**) but not with the **L7** ligand which experience an increase in intensity, suggesting leaching of the ligand from the film.

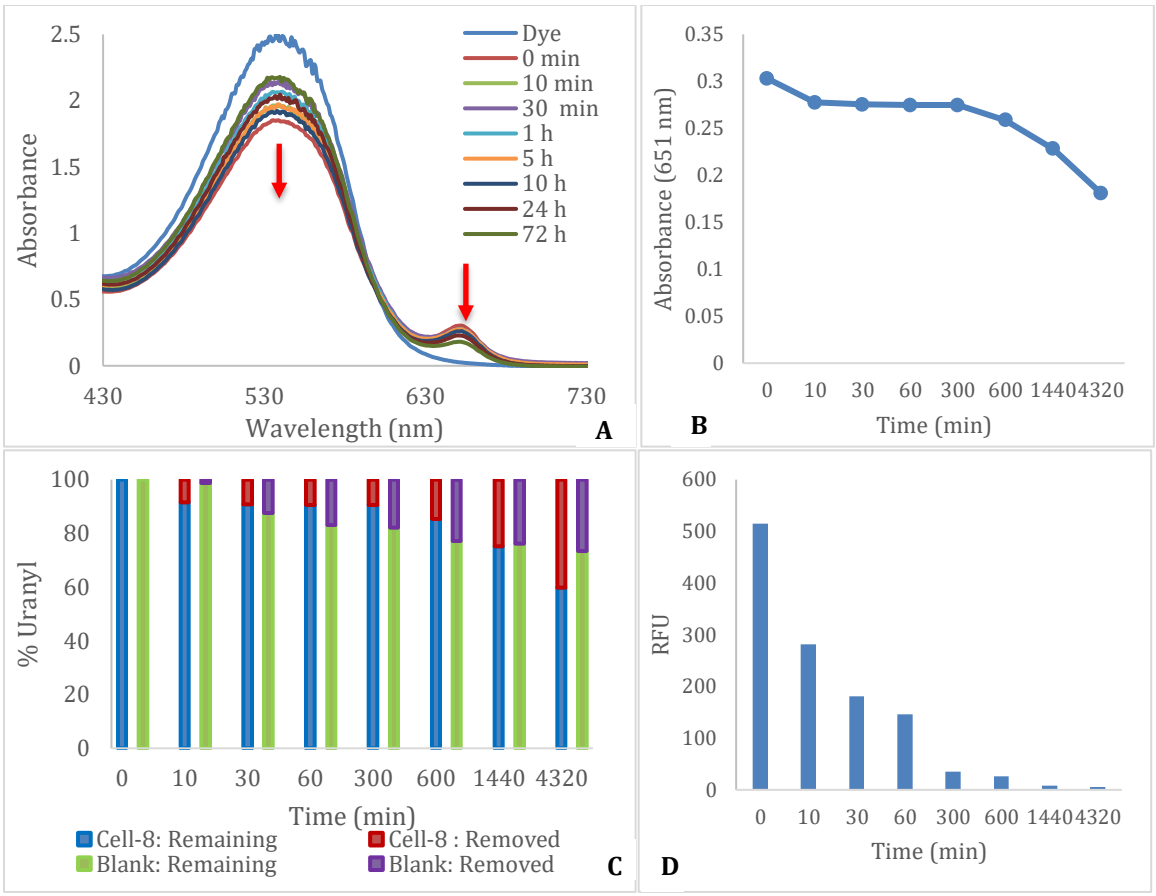

Figure 3.17: Uranyl extraction analysis of Cell-8 (A) showing a decrease in 1:1 metal to ligand complex at 651 nm UV-Vis spectrum (B) decrease of metal complexation at 651 nm (C) Percent uranyl extracted and remaining after 1 hour of extraction using Cell-8 (D) Fluorescence of Cell-8 film over extraction period showing a decrease in intensity

Cell-9 film (cellulose MW = 1,300,000 g/mol and crosslinker = citric acid) was then investigated for its ability to extract uranyl from aqueous media over 3 days. As illustrated in **Figure 3.18a and 3.18b**, a decrease in the uranyl complexation peak at 651 nm was observed consistently as the uranyl concentration decreased. Similar to Cell-8, extraction began at a very slow pace, extracting only 1-2 % after 30 minutes (**Figure 3.18c**) with a slow increase to 5-7 % within 5 hours, followed by a gradual increase to an overall removal of 27 % over the duration of the extraction period. The film without the ligand present only removed 14 % of the uranyl over the 72-h period, indicating that the salen

ligand present enhances the films' ability to remove the uranyl ions via chelation inside the tetradentate pocket. As with the previous films, Cell-9 fluorescence data, exhibited quenching of the ligand upon chelation, indicating the possibility of leaching. (**Figure 3.18d**).

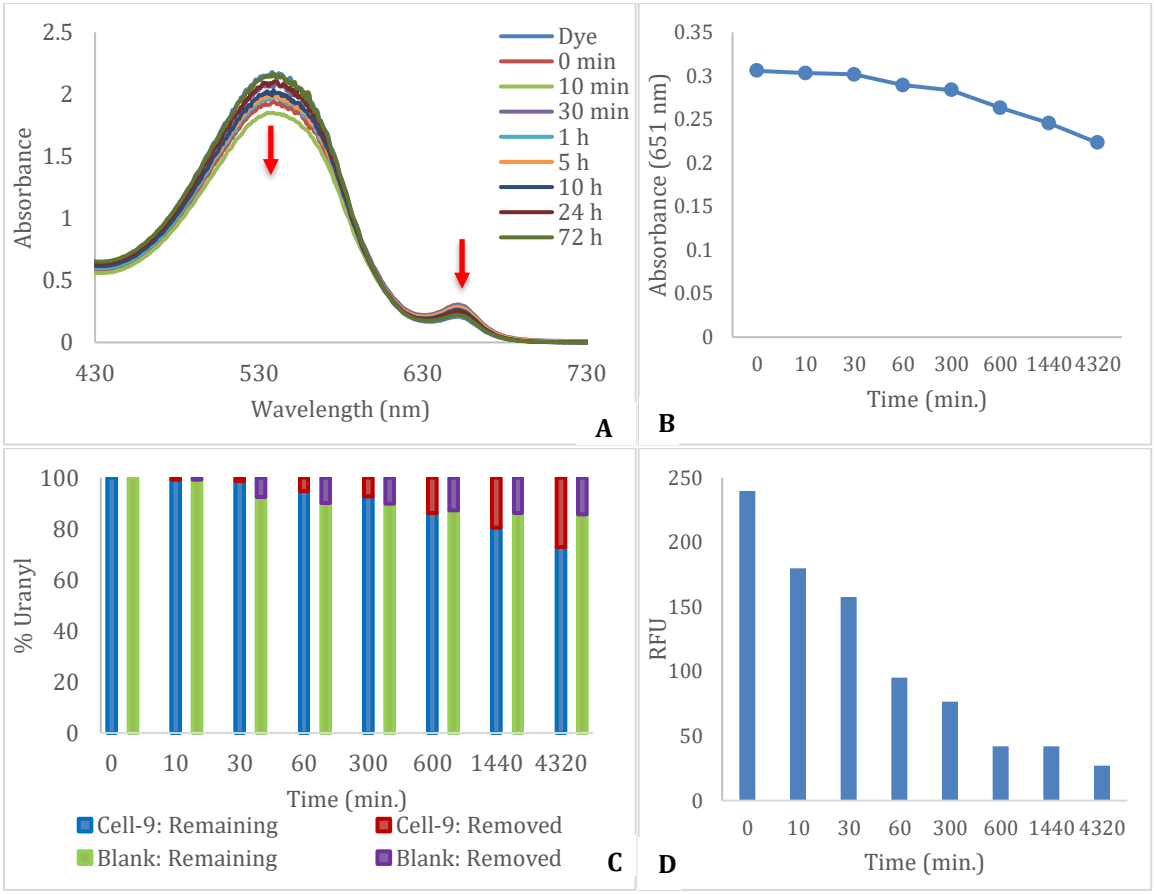

Figure 3.18: Uranyl extraction analysis of Cell-9 (A) showing a decrease in 1:1 metal to ligand complex at 651 nm UV-Vis spectrum (B) decrease of metal complexation at 651 nm (C) Percent uranyl extracted and remaining after 1 hour of extraction using Cell-9 (D) Fluorescence of Cell-9 film over extraction period showing a decrease in intensity.

The most notable difference about the two films (Cell-8 and Cell-9), is their ability to swell in aqueous media. Cell-9 swelled extensively when placed in water which in turn compromised the integrity of the film but also allowed less uranyl ions to become

efficiently trapped in the pocket of the salen ligand.

3. 2. 10 Leaching Test

Similar to the ligand-trapped films, Cell-2 through Cell-5, the covalently linked films are subject to leaching, therefore they were examined for possible leaching over a 1-week period in basic, neutral, and acidic media. Unfortunately, these films too, were plagued by leaching as well though with a significantly less amount of leaching taking place, compared to the ligand-trapped films. Similar to the ligand-trapped films, a neutral environment was the optimal condition for the films while the basic environment was the most detrimental. (see Appendix for UV-Vis spectra for each film)

3.3 Conclusions:

In conclusion, cellulose serves as a green, efficient, and viable solid support for the extraction of uranyl from aqueous media. Absorption of the salen ligand onto the surface of the cellulose film resulted in the extraction of more than 36 % uranyl in as little as 5 minutes using the **L3** ligand; unfortunately, this method resulted in rapid leaching of the salen ligand into the aqueous media, thus consequentially yielding an inefficient method for uranyl extraction.

To overcome the leaching, Cell-2 through Cell-5 were synthesized. Like the aforementioned Salen-absorped films, these films also utilized **L3** as the ligand for chelation due to its ability to distinguish between the false positive, copper ion, as well as the exhibition of selectivity towards the uranyl ions. The Cell-2 through 5 films, though slower were able to extract 27-70 % uranyl over the 72-h extraction period, with Cell-3

extracting the most, 70 %, uranyl. However, these films too were plagued with leaching, due to some of the ligands not efficiently being trapped within the film's matrix.

The covalently linked films, though initially slower at extracting the uranyl ion, exhibited promising characteristics as uranyl extractants. The films successfully extracted 27-65 % uranyl over the 72-h extraction period, with Cell-6 extracting the most, 65 %, uranyl. Similar to some of the in-trapped films, these films maintained their structural integrity over the 3-day extraction period as well as withstood the basic (pH = 10.62) and acid (pH = 4.17) environments.

It is important to note the effects the crosslinkers played on the extracting properties of the film; overall the films utilizing glutaraldehyde as the cross-linker outperformed those prepared using citric acid as a cross-linker. When the films with citric acid, as the cross-linker were placed in aqueous media they swelled nearly 3x in size, in comparison to the glutaraldehyde films, it was initially believed that the swelling to promote the intake of uranyl ions. Unfortunately, instead it facilitated the leaching of the ligand out of the film, which in return caused less uranyl to be extracted from the samples.

3.4 Experimental:

Caution! The uranium metal salts – $UO_2(NO_3)_2 \cdot 6H_2O$ – used in this study contained depleted uranium, standard precautions for handling radioactive materials, such as uranyl nitrate, were followed.

Reagents

The reagents THF (Macron), ethyl acetate (Macron), ethanol (200 proof, PharmCo-Aaper),

methanol (HPLC grade, EMD Millipore) and hexanes (ACS grade, EMD Millipore), N'N'-dimethyl formamide (Fisher Scientific) NaOH (EMD Millipore), MCC (Alfa Aesar), glycerol (99 %, Pure synthetic, Alfa Aesar) urea (98 %, Aldrich), 2-hydroxyethyl cellulose (MW = 1,300,000 g/mol, and 90,000 g/mol, Sigma-Aldrich) and regenerated cellulose film (0.021 mm thickness, Sigma-Aldrich), epichlorohydrin (Fluka), glutaraldehyde (Fluka), hydrochloric acid (Fisher Scientific), citric acid (Acros Organics), uranium nitrate hexahydrate (Fisher Scientific), 1-ethyl-3-(3-dimethylaminopropyl) carbodiimide (Thermo Scientific), 4-dimethylaminopyridine (Acros Organics)

Metal Adsorption Method

The cellulose film was cut into four 2 x 3 cm rectangles, which were each coated with 2.0 mL of ligand solution 75 ppm in ethanol. The solvent was allowed to evaporate at room temperature then cured in an oven at 110 °C for 2 h. The 12 di-, tri-, and tetravalent metals of interest; copper(II) chloride dihydrate, manganese(II) chloride, vanadyl acetacetonate, cobalt(II) chloride, nickel(II) chloride octahydrate, zinc(II) chloride, cerium(III) chloride heptahydrate, dysprosium(III) acetate, ytterbium(III) acetate, and thorium(IV) nitrate, samples were prepared in 40-ppm solutions in water. Then 2 mL of each sample were pipetted into 12 individual test tubes. The initial concentrations of the samples were determined; then film pieces of equal size were placed into the test tubes. The test tubes were placed on a shaker and agitated for 5 min. The film was removed and then the concentration of the remaining aqueous solution was analyzed using ICP-OES to determine the concentration of metal ions was removed.

Using ICP-OES to analyze metal concentration

All metals concentrations were analyzed using Inductively Coupled Plasma with Optical Emission Spectroscopy (Perkin Elmer Optima 7100 DV). A standard solution consisting of the 12 metals of interest (copper(II) chloride dihydrate, manganese(II) chloride, vanadyl acetacetonate, cobalt(II) chloride, nickel(II) chloride octahydrate, zinc(II) chloride, cerium(III) chloride heptahydrate, dysprosium(III) acetate, ytterbium(III) acetate, and thorium(IV) nitrate) at a 50 ppm concentration was made in 2 % nitric acid. This standard was used to standardize the instrument for looking at the various metals. The initial and final metal concentrations per extraction were determined using ICP-OES.

Leaching Test

Samples were prepared using 1 cm x 1 cm square pieces of film and 10 ppm uranyl aqueous solutions at the following pHs: neutral (pH = 7), basic (pH = 8, 12, and 14), and acidic (pH = 0, 3, and 5). To increase the pH a 50 % NaOH solution was used while 1 M nitric acid was used to reduce the pH. The UV-Vis absorbance of the samples was analyzed after 0 min, 15 min, and 30 min to determine if any leaching have occurred. After 30 min the leaching study was terminated due to leaching occurring over the short period of time.

Synthesis of NC film from MCC[5, 6, 28]

5 g of MCC was added into a 100 mL solution of 7 % NaOH and 12 % urea. The solution was stirred at room temperature for 30 min then kept static for 16 h at -20 °C. The mixture was thawed, and the cellulose was regenerated by adding 10 times v/v of deionized water. The regenerated cellulose (RC), was precipitated and separated via centrifugation at

5000 revolutions per minute (rpm), the precipitate was washed several times with deionized water to remove remnants of NaOH and urea. The RC was preserved at 4 °C as a 2 % slurry (in deionized water) until further use.

From the stock of RC, several solutions containing various concentrations of cellulose was prepared in deionized water. The solutions with the known concentrations were then ultrasonicated for 2 min using a 2 mm probe at 75 % amplitude. The pH of the solution was measured before and after sonication to ensure it was around 8 if not, a solution of 1 M NaOH or HCl was used to adjust it.

Free standing films of RC were prepared by pouring the dispersed cellulose (10 mL) in a glass Petri dish (~ 100 mm diameter), the solvent was allowed to slowly evaporate at room temperature, placed in an oven at 70 °C for 2 h, and then peeled off slowly with forceps. Ligand in-trapped films of RC was prepared using the aforementioned procedure, however 5 mL of 1000 ppm **L3** in DMF was added to the dispersed cellulose prior to solvent evaporation.

Synthesis of Sodium Carboxymethyl Cellulose (CMC) film[29, 38, 39]

3 g (2 % w/v) of CMC, 0.9 g of glycerol (or 30 % of CMC weight), and 150 mL of distilled water was heated at 90 °C for 20 min or until the CMC was fully dissolved. The solution was then poured into a glass mold and allowed to dry at room temperature. Once all the solvent was evaporated, the film was dried in an oven for 2 h at 40 °C.

Ligand-trapped films of CMC film was prepared using the aforementioned procedure, however 5 mL of 1000 ppm **L3** in DMF was added to the dissolved CMC and glycerol solution prior to solvent evaporation.

Synthesis of Cellulose Film using epichlorohydrin as a Cross-linker[31](Cell-1)

A modified procedure was adopted from Yan 2013[31] published method. Free standing film was made by dissolving 0.5625 g of 2-hydroxyethyl cellulose (HEC) (MW = 1.30 x 10^6 g/mol) in 100 mL of water and heated at 40 °C until the solution was transparent. The solution was then allowed to cool to room temperature. Next 0.50 mL of epichlorohydrin (3 wt %) was added to the solution under stirring to obtain a homogeneous solution (20-45 min). After the solution had become homogeneous, it was poured into a Petri dish where the solvent was allowed to evaporate (~3-5 days), the film was then washed with 5% acetic acid and deionized water, then dried in an oven at 40 °C for 2 h.

Synthesis of Cellulose Film using glutaraldehyde as a Cross-linker (Cell-2)

Methodologies were adopted from Mills 2006 publication.[32] 0.8102 g of HEC (MW = 90,000 g/mol) was dissolved in 12 mL of water and heated at 40 °C, the solution was then allowed to cool to room temperature, then 0.75 mL of a 1 % glutaraldehyde solution was added and stirred for 5 min, followed by the addition of 0.75 mL of a 0.5 M HCl solution and allowed to stir for 30 s. The solution was then poured into a glass mold and allowed to air dry for 2-3 days. Ligand-trapped film was prepared using the aforementioned procedure, however 10 mL of the 1000 ppm **L3** (in DMF) solution was added to the cellulose mixture and vigorously stirred (~ 900 -1000 rpms) for 5 min, before pouring into the glass mold. Once dried the film was washed with methanol and water. For **Cell 5**, the aforementioned procedure was completed as stated, however using the equivalent amount

of 1 % citric acid in place of the 1 % glutaraldehyde, as the crosslinker.

Synthesis of Cellulose Film using Citric acid as a Cross-linker (Cell 3)

Methodologies were adopted from Mills 2006 publication.[32] 0.8102 g of HEC (MW = 1,300,000 g/mol) was dissolved in 100 mL of water and heated at 55 °C, the solution was then allowed to cool to room temperature, then 9.0 mL of a 1 % glutaraldehyde solution was added and stirred for 5 min, followed by the addition of 1.5 mL of a 0.5 M HCl solution and allowed to stir for 30 s. The solution was then poured into a glass mold and allowed to air dry for 2-3 days. Ligand-trapped film was prepared using the aforementioned procedure, however 10 mL of the 1000 ppm **L3** (in DMF) solution was added to the cellulose mixture and vigorously stirred (~ 900 -1000 rpms) for 5 min, before pouring into the glass mold. Once dried the film was washed with methanol and water. For **Cell 4**, the aforementioned procedure was completed as stated, however using the equivalent amount of 1 % citric acid in place of the 1 % glutaraldehyde, as the crosslinker.

Synthesis of Covalently linked L7-cellulose Film using glutaraldehyde as a Cross-linker (Cell 6)

Modified methodologies were adapted using Wu[1] and Mills publications[32] 0. 1 g of 2-HEC (MW = 1,300,000 g/mol) was dissolved in 100 mL of DMF. 40 mg of L7 was then added followed by 2.2 molar equivalents of 4-dimethyl-aminopyridine (DMAP) and 2.2 equivalents *N*-ethyl-*N*′-(3-dimethylaminopropyl) carbodiimide (EDC). The reaction was allowed to proceed at room temperature for 3 days. Once complete the reaction was placed in a freezer at -80° C for 12 h, then placed on the lyophilizer. Once removed the

solution was stored in a -15° C freezer until ready for use. 0.8102 g of HEC (MW = 90,000) was dissolved in 100 mL of water and heated at 55 °C, the solution was then allowed to cool to room temperature, then 9.0 mL of a 1 % glutaraldehyde solution was added and stirred for 5 min, followed by the addition of 1.5 mL of a 0.5 M HCl solution and allowed to stir for 30 s followed by the addition of 10 mL of the concentrated covalently linked L7-cellulose solution (in DMF) and vigorously stirred (~ 900 -1000 rpms) for 5 min, before pouring into the glass mold. Once dried the film was washed with methanol and water. The solution was then poured into a glass mold and allowed to air dry for 2-3 days. For **Cell 8**, the aforementioned procedure was completed as stated, however using the equivalent amount of 1 % citric acid in place of the 1 % glutaraldehyde, as the crosslinker. For **Cell 7** and **Cell 9,** the aforementioned procedure was used, using the 1,300,000 g/mol 2-HEC in place of the 90, 000 g/mol and using glutaraldehyde and citric acid respectively as cross-linkers.

Determination of thickness of films

The thickness of the films was measured using an *i*GAGING® electronic micrometer. The films were cut in to 2.5 cm x 5 cm rectangles. 5 measurements were recorded using the micrometer at the locations depicted in **Figure 3.19** for an average thickness (**Table 3.1**) of the films.

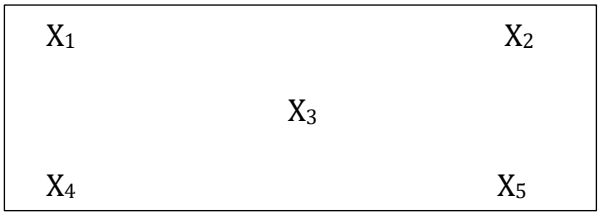

Figure 3.19 Points of measurements for determination of film thickness

Table 3.1: Measurements (in mm) and averages of thickness of films

Films	X_1 (mm)	X_2 (mm)	X_3 (mm)	X_4 (mm)	X_5 (mm)	Average ± Standard Deviation
Cell-2	0.053	0.057	0.057	0.061	0.076	0.061 ± 0.008
Cell-2 (blank)	0.047	0.056	0.061	0.056	0.056	0.055 ± 0.005
Cell-3	0.040	0.045	0.054	0.030	0.041	0.042 ± 0.009
Cell-3 (blank)	0.024	0.032	0.034	0.030	0.041	0.032 ± 0.006
Cell-4	0.043	0.075	0.072	0.041	0.070	0.060 ± 0.017
Cell-4 (blank)	0.041	0.034	0.035	0.037	0.044	0.038 ± 0.004
Cell-5	0.086	0.039	0.059	0.031	0.034	0.050 ± 0.023
Cell-5 (blank)	0.043	0.047	0.044	0.041	0.041	0.050 ± 0.023
Covalently linked Films						
Cell-6	0.052	0.049	0.051	0.067	0.049	0.054 ± 0.007
Cell-7	0.092	0.047	0.033	0.076	0.031	0.056 ±0.027
Cell-8	0.083	0.083	0.066	0.082	0.069	0.077 ± 0.009
Cell-9	0.172	0.133	0.119	0.108	0.106	0.128±0.027

Determination of uranyl using the Arsenazo III method[33, 34]

The Arsenazo III method was adapted by the Khan et al 2006 publication.[34] A standard solution of the disodium salt of the 2,7-bis (2-arsenophenylazo)-1,8-dihydroxynaphthalene-3,6-disulfonic acid (commonly referred to as Arsenazo III) was prepared by dissolving 11.66 mg of the Arsenazo III salt into a 1 L volumetric flask and diluting it with of 3 M $HClO_4$ to the 1-L marker on the flask. 1 mL of the standard uranyl stock solution, each varying in concentration (1-1000 ppm) of uranyl in D. I. water, was mixed with 4 mL of the standard Arsenazo III solution. The absorbance was measured from 600-700 nm with a Cary 50 spectrophotometer. A correlation curve between uranium concentration (ppm) and absorbance at 651 nm was plotted to determine the remaining uranium concentration of the samples after extraction with the functionalized cellulose film.

15 mL of an aqueous 10 ppm solution of uranyl was poured into a vial. The functionalized cellulose film was added to the solution and agitated for various amounts of time (10 min, 30 min, 1 h, 5 h, 10 h, and 24 h). The film was removed, and the remaining uranyl solutions were concentrated to near dryness via rotary evaporation and taken up to 1 mL using $HClO_4$. The solution was then diluted up to 10 mL with D. I. water and analyzed using the aforementioned Arsenazo III method.

Leaching Test

Samples were prepared using 1 cm x 1 cm square pieces of film and 10 ppm uranyl aqueous solutions at the following pHs: neutral (pH = 7.492), basic (pH = 10.619), and acidic (pH = 4.170). To increase the pH a 50 % NaOH solution was used while 1 M nitric acid was used to reduce the pH. The UV-Vis absorbance of the samples were measured after 30 min, 1 h, 5 h, 12 h, 24 h, 48 h, 72h, 96 h, 120 h, 144 h, and 168 h.

3.5 References:

1. Wu, X.; Gorden, A. E. V., 2-Quinoxalinol Salen Ligands Incorporated Into Functionalized Resins for Selective Solid-Phase Extraction Of Copper(II). *Tetrahedron Lett.* **2008,** *49* (35), 5200-5203.

2. West, M.; Tutson, C.; Yates, W.; Gorden, A. E., Magnetic Poly(vinyl alcohol) Beads Functionalized with a Salen Derived Ligand for the Extraction and Detection of Uranyl (UO_2^{2+}) *(In Preparation)*.

3. Tutson, C. Exploring Actinide Chemistry: Uranyl Detection and Thorium Catalysis. Auburn University, 2017.

4. Cao, X.; Sun, S.; Peng, X.; Zhong, L.; Sun, R.; Jiang, D., Rapid Synthesis of Cellulose Esters by Transesterification of Cellulose With Vinyl Esters Under the Catalysis of NaOH or KOH in DMSO. *J. Agric. Food Chem.* **2013,** *61* (10), 2489-95.

5. Adsul, M.; Soni, S. K.; Bhargava, S. K.; Bansal, V., Facile Approach for the Dispersion of Regenerated Cellulose in Aqueous System in the Form of Nanoparticles. *Biomacromolecules* **2012,** *13* (9), 2890-5.

6. Shankar, S.; Rhim, J. W., Preparation of Nanocellulose From Micro-Crystalline Cellulose: The Effect on the Performance and Properties of Agar-Based Composite Films. *Carbohydr. Polym.* **2016,** *135*, 18-26.

7. Voon, L. K.; Pang, S. C.; Chin, S. F., Porous Cellulose Beads Fabricated from Regenerated Cellulose as Potential Drug Delivery Carriers. *J. Chem.* **2017,** *2017*, 1-11.

8. Tang, J.; Sisler, J.; Grishkewich, N.; Tam, K. C., Functionalization of Cellulose Nanocrystals for Advanced Applications. *J. Colloid Interface Sci.* **2017,** *494*, 397-409.

9. Gericke, M.; Trygg, J.; Fardim, P., Functional Cellulose Beads: Preparation, Characterization, and Applications. *Chem. Rev.* **2013,** *113* (7), 4812-36.

10. Guo, M.; Her, S.; Keunen, R.; Zhang, S.; Allen, C.; Winnik, M. A., Functionalization of Cellulose Nanocrystals with PEG-Metal-Chelating Block Copolymers via Controlled Conjugation in Aqueous Media. *ACS Omega* **2016,** *1* (1), 93-107.

11. Gurgel, L. V. A.; Gil, L. F., Adsorption of Cu(II), Cd(II), and Pb(II) From Aqueous Single Metal Solutions by Succinylated Mercerized Cellulose Modified with Triethylenetetramine. *Carbohydr. Polym.* **2009,** *77* (1), 142-149.

12. Gurnani, V., Cellulose Based Macromolecular Chelator Having Pyrocatechol as an Anchored Ligand: Synthesis and Applications as Metal Extractant Prior to Their

Determination by Flame Atomic Absorption Spectrometry. *Talanta* **2003,** *61* (6), 889-903.

13. Burchard, W. et al. Cellulose Solutions in Water Containing Metal Complexes. *Macromolecules* **2000,** *33* (11), 4094-4107.

14. Dong, C.; Zhang, F.; Pang, Z.; Yang, G., Efficient and Selective Adsorption of Multi-Metal Ions Using Sulfonated Cellulose as Adsorbent. *Carbohydr. Polym.* **2016,** *151*, 230-236.

15. Abdel-Razik, H. H.; El-Asmar, A. M.; Abbo, M., Heavy Metal Absorbents Based on Chelating Amidoximated Grafted Cellulose. *J. Basic Appl. Chem. Sci. (International)* **2013,** *3* (4).

16. O'Connell, D. W.; Birkinshaw, C.; O'Dwyer, T. F., Heavy Metal Adsorbents Prepared From The Modification of Cellulose: A Review. *Bioresour. Technol.* **2008,** *99* (15), 6709-24.

17. Navarro, R. R.; Sumi, K.; Fujii, N.; Matsumura, M., Mercury Removal From Wastewater using Porous Cellulose Carrier Modified with Polyethyleneimine. *Wat. Res.* **1996,** *30* (10), 2488-2494.

18. Yu, X.; Kang, D.; Hu, Y.; Tong, S.; Ge, M.; Cao, C.; Song, W., One-pot Synthesis of Porous Magnetic Cellulose Beads for The Removal of Metal Ions. *RSC Advances* **2014,** *4* (59), 31362.

19. Guo, D.-M.; An, Q.-D.; Xiao, Z.-Y.; Zhai, S.-R.; Shi, Z., Polyethylenimine-functionalized Cellulose Aerogel Beads for Efficient Dynamic Removal of Chromium(VI) From Aqueous Solution. *RSC Advances* **2017,** *7* (85), 54039-54052.

20. Luo, X.; Lei, X.; Cai, N.; Xie, X.; Xue, Y.; Yu, F., Removal of Heavy Metal Ions from Water by Magnetic Cellulose-Based Beads with Embedded Chemically Modified Magnetite Nanoparticles and Activated Carbon. *ACS Sustainable Chemistry & Engineering* **2016,** *4* (7), 3960-3969.

21. Navarro, R. R.; Tatsumi, K.; Sumi, K.; Matsumura, M., Role of Anions on Heavy Metal Sorption of a Cellulose Modified with Poly(Glycidyl Methacrylate) and Polyethyleneimine. *Wat. Res.* **2001,** *35* (11), 2724-2730.

22. Ma, H.; Hsiao, B. S.; Chu, B., Ultrafine Cellulose Nanofibers as Efficient Adsorbents for Removal of UO_2^{2+} in Water. *ACS Macro Lett.* **2011,** *1* (1), 213-216.

23. Czaja, W. K.; Young, D. J.; Kaweck, M.; Brown, R. M., The Future Prospects of Microbial Cellulose in Biomedical Applications. *Biomacromolecules* **2007,** *8* (1).

24. Feese, E.; Sadeghifar, H.; Gracz, H. S.; Argyropoulos, D. S.; Ghiladi, R. A., Photobactericidal Porphyrin-Cellulose Nanocrystals: Synthesis, Characterization, and Antimicrobial Properties. *Biomacromolecules* **2011,** *12* (10), 3528-39.

25. Kumari, S.; Chauhan, G. S., New Cellulose-Lysine Schiff-Base-Based Sensor-Adsorbent for Mercury Ions. *ACS Appl. Mater. Interfaces* **2014,** *6* (8), 5908-17.

26. Nawaz, H.; Tian, W.; Zhang, J.; Jia, R.; Chen, Z.; Zhang, J., Cellulose-Based Sensor Containing Phenanthroline for the Highly Selective and Rapid Detection of Fe(2+) Ions with Naked Eye and Fluorescent Dual Modes. *ACS Appl. Mater. Interfaces* **2018,** *10* (2), 2114-2121.

27. Wu, X.; Shi, Z.; Fu, S.; Chen, J.; Berry, R. M.; Tam, K. C., Strategy for Synthesizing Porous Cellulose Nanocrystal Supported Metal Nanocatalysts. *ACS Sustainable Chem. Eng.* **2016,** *4* (11), 5929-5935.

28. Isobe, N.; Noguchi, K.; Nishiyama, Y.; Kimura, S.; Wada, M.; Kuga, S., Role of Urea in Alkaline Dissolution of Cellulose. *Cellulose* **2013,** *20* (1), 97-103.

29. Oun, A. A.; Rhim, J.-W., Preparation and Characterization of Sodium Carboxymethyl Cellulose/Cotton Linter Cellulose Nanofibril Composite Films. *Carbohydr. Polym.* **2015,** *127*, 101-109.

30. Sirviö, J. A.; Visanko, M.; Ukkola, J.; Liimatainen, H., Effect of Plasticizers on The Mechanical and Thermomechanical Properties of Cellulose-Based Biocomposite Films. *Ind. Crop. Prod.* **2018,** *122*, 513-521.

31. Guo, B.; Chen, W.; Yan, L., Preparation of Flexible, Highly Transparent, Cross-Linked Cellulose Thin Film with High Mechanical Strength and Low Coefficient of Thermal Expansion. *ACS Sustainable Chem. Eng.* **2013,** *1* (11), 1474-1479.

32. Korchev, A.; Bojack, M.; Slaten, B..; Mills, G., Polymer-Initiated Photogeneration of Silver Nanoparticles in SPEEK:PVA Films- Direct Metal Photopatterning. *J. Am. Chem. Soc.* **2003,** *26* (1), 10-11.

33. Jauberty, L.; Drogat, N.; Decossas, J. L.; Delpech, V.; Gloaguen, V.; Sol, V., Optimization of the arsenazo-III Method for the Determination of Uranium in Water and Plant Samples. *Talanta* **2013,** *115*, 751-4.

34. Khan, M. H.; Warwick, P.; Evans, N., Spectrophotometric Determination Of Uranium with Arsenazo-III in Perchloric Acid. *Chemosphere* **2006,** *63* (7), 1165-9.

35. Matharu, K.; Mittal, S. K.; Ashok Kumar, S. K.; Sahoo, S. K., Selectivity Enhancement of Arsenazo(III) Reagent Towards Heavier Lanthanides Using Polyaminocarboxylic Acids: A Spectrophotometric Study. *Spectrochim. Acta A Mol. Biomol. Spectrosc.* **2015,** *145*, 165-175.

36. Rohwer, H.; Collier, N.; Hosten, E., Spectrophotometric Study of Arsenazo III and its Interactions with Lanthanides. *Anal. Chim. Acta* **1995,** *314*, 219-223.

37. Serenjeh, F. N.; Hashemi, P.; Ghiasvand, A. R.; Rasolzadeh, F., A New Optical Sensor for Selective Quantitation of Uranium by the Immobilization of Arsenazo III on an Agarose Membrane. *Anal. Methods* **2016,** *8* (21), 4181-4187.

38. Rhim, J.-W., Effect of Clay Contents on Mechanical and Water Vapor Barrier Properties of Agar-Based Nanocomposite Films. *Carbohydr. Polym.* **2011,** *86* (2), 691-699.

39. Rhim, J. W.; Lee, S. B.; Hong, S. I., Preparation and Characterization of Agar/Clay Nanocomposite Films: The Effect of Clay Type. *J. Food Sci.* **2011,** *76* (3), N40-8.

Chapter 4

Application I: Using Functionalized Cellulose Films for Uranyl Extraction from Sea Water

4.1 Introduction

Nuclear power is crucial for a greener future of less greenhouse gas emission, a low carbon footprint, and renewable energy source. There is an increase in research towards the development of adsorbent materials that efficiently sequester uranium from seawater, a truly inexhaustible alternative to the traditional mining of uranium ore.[1, 2] Seawater contains almost 4.5 billion metric tons of uranium, which is significantly more than the identified and economically recoverable 4.7 million tons found in terrestrial sources.[2] Unfortunately three major challenges plague extracting uranium from the ocean, the low concentrations of uranium in the ocean (3.3 ppb), extracting uranium from the stable tris- and biscarbonato species, $[(UO_2)(CO_3)_3]^{4-}$ and $[(UO_2)(CO_3)_2]^{2-}$ respectively, and also developing an economically feasible process.[2-4]

Dating back to the 1960s, research conducted on extracting uranium from the ocean focused on using ion-exchange resins and processes similar to the PUREX process, and then later turned to sorbent materials.[5-9] In 2011, the U. S. Department of Energy established a research program to develop a cost effective and efficient method for uranium extraction from seawater, and successfully managed to increase the adsorbent material capacity for uranium from ~1.5 g to over 6 g for each kg of absorbent used.[10-12] Presently the most common functional group found on polymer sorbents are amidoximes (**Figure 4.1**), due to their high affinity and selectivity for uranyl ions.[2, 6, 8, 13]

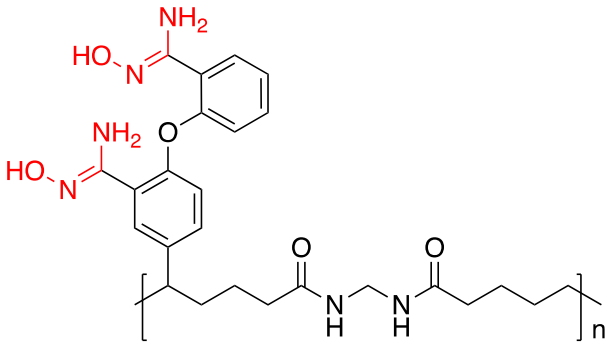

Figure 4.1 Structure of general Bis-amidoxime polymer sorbent, with amidoxime units highlighted in red.[14]

Reported herein is the use of the cellulose films that were the most effective at extracting uranyl; ligand-trapped cellulose film, Cell-3, and the covalently linked cellulose film, Cell-6, as sorbent materials to extract uranium from sea water (structural details for films are highlighted in Chapter 3).

4.2 Results

The films were cut into 2 x 3 cm rectangles and placed in 12.5 mL of spiked (~3.5 ppm) seawater from four different beaches around the States; Orange Beach, Al, Tybee Island, Ga, Clearwater Beach, Fl, and Dockweiler State Beach, Ca. Performing uranyl extraction on environmental samples typically gives an indication of how the films will perform in a non-standardized environment, in particular how the films will perform in the presence of competing metal ions within the pH range of 6.8-7.9 and with uranium concentrations of 0.025-0.032 ppm (concentrated control samples)

As reported in **Table 4.1**, Cell-3 extracted a significantly lower amount of uranyl from seawater than in the controlled environment, a maximum of 28 % versus 70 %, respectively. These

results indicate the influence of competing ions for the Schiff base, specifically competition from the common false-positive, copper. Over the 3-h extraction period, the amount of copper present in the natural sample decreased by more than 51 % in some samples and as much as 94 % in others, suggesting that the ligand is more selective for copper. Recovering the uranium from Cell-3 via partially digesting the film in a 1M nitric acid solution, allowing for hydrolyzation of the Schiff base to release the uranium extracted, resulted in a very promising green approach to harvesting the uranium removed from the sea. Unlike most sorbent material, that are digested when placed in the acidic media, Cell-3 remained intact suggesting the possibility of recycling the film. Under acidic conditions, over 80 % of uranium was successfully recovered from Cell-3 in as little as 20 minutes.

Table 4.1: Uranyl analysis of environmental samples using Cell-3 highlighting the amount of uranyl extracted over the 3 h extraction period and the amount of uranyl recovered with 20 min.

Location where water samples were collected	**pH of sample**	Uranyl extracted (%)	Uranyl Recovered (%)
Orange Beach, Al	7.90	16.29 ± 0.01	80.45
Tybee Island, Ga*	7.14	10.69 ± 0.01	99.92
Clearwater Beach, Fl	6.84	28.20 ± 0.08	81. 36
Dockweiler State Beach, Ca	7.90	18.44 ± 0.11	98.37

*Data collected after 1 h

Table 4.2 highlights the results from the extraction performed with Cell-6; similar to Cell-3 the amount of uranyl extracted was significantly lower than in the controlled environment, a maximum of 42 % versus 65 %, respectively. These results indicate the influence of competing metal ions with the Schiff base, probably competition from the common false-positive, copper. Over the 3-h extraction period, the amount of copper present in the natural sample decreased by more than 22 % in some samples and as much as 65 % in others, suggesting more selectivity

towards uranium than Cell-3 but with some competition for copper. Recovering the uranium from Cell-6 resulted in a bit of misfortune, contrary to its ability to remain intact during the leaching study and previous extracting experiments, the films' structural integrity was severely compromised with the agitation (150 rpm), thus resulting the inability to recover the uranium from the film.

Table 4.2: Uranyl analysis of environmental samples using Cell-6 highlighting the amount of uranyl extracted over the 3 h extraction period and the amount of uranyl recovered with 20 min.

Location where water samples were collected	**pH of sample**	Uranyl extracted (%)	Uranyl Recovered (%)
Orange Beach, Al	7.898	42.95 ± 0.039	-
Tybee Island, Ga	7.144	34.70 ± 0.242	-
Clearwater Beach, Fl	6.839	32.64 ± 0.036	-
Dockweiler State Beach, Ca	7.902	17.79 ± 0.047	-

4.3 Conclusion

In conclusion, Cell-3 and Cell-6 films were used to extract uranium from four different spiked environmental samples. Overall both films succeeded at extracting uranium from the environmental samples but exhibited some setbacks. Though Cell-3 remained intact and exhibited promising recycling capabilities, it was beset by the competition with other trace metals presented in the samples, resulting in significantly lower amount of uranium being extracted. In contrast, Cell-6 managed to extract more uranium from the samples than Cell-3, a maximum of 28 % versus 42 %, but did not weather the agitation well, which could possibly be overcome by decreasing the revolutions per minute.

4.4 Experimental

Caution! The uranium metal salts – $UO_2(NO_3)_2 \cdot 6H_2O$ – used in this study contained depleted uranium, standard precautions for handling radioactive materials, such as uranyl nitrate, were followed.

4. 4. 1. Determination of pH of environmental samples

Upon filtration, the pH of the environmental samples was determined using Fisher Scientific AR15 pH meter. The pH meter was calibrated using standardized buffer samples at pH of 4, 7, and 10. The pH of the samples were determined by placing the glass electrode in the solution and recording the pH value upon stabilization. The electrode was then washed with distilled water into a waste beaker and wiped dry with a Chemwipe before measuring other samples.

4. 4. 2. Uranyl Extraction of spiked environmental samples using ICP-OES

Natural water samples collected were prepared using the previously published method by Jauberty et al.[15] Each sample was subjected to vacuum filtrations to remove any stray solids like sand, seaweed, seashell pieces, etc. Once filtered, 100 mL of the sample was concentrated near dryness using a rotary evaporator and taken up to 1 mL in 1 M HNO_3. The sample was then spiked (~3.5 ppm using uranium nitrate) and further diluted up to 25 mL with distilled water. Uranium determination was performed using agitation (Barnstead Lab-Line: Max^Q 3000 at 150 rpm), which mimics that of the ocean and ICP-OES (Perkin Elmer Optima 7100 DV) over a period of 3 hour, collecting analysis after 30 min, 1 h, 2 h, and 3 h. Uranium was recovered by mildly digesting the film in a 1 M HNO_3 solution with agitations over a 20 min period. The standard/controlled solutions were prepared using the aforementioned process but were not spiked with uranium.

4. 4. 3. Determination of concentration of copper in environmental samples using ICP-OES

Natural water samples collected were prepared using the previously published method by Jauberty et al.[15] Each sample was subjected to vacuum filtrations to remove any stray solids like sand, seaweed, seashell pieces, etc. Once filtered, 100 mL of the sample was concentrated near dryness using a rotary evaporator and taken up to 1 mL in 1 M HNO_3. The sample was then spiked (~3.5 ppm using uranium nitrate) and further diluted up to 25 mL with distilled water. Copper determination was performed using agitation (Barnstead Lab-Line: Max^Q 3000 at 150 rpm), which mimics that of the ocean and ICP-OES (Perkin Elmer Optima 7100 DV) over a period of 3 hour, where the concentration of copper was measured before the extraction period and after 30 min, 1 h, 2 h, and 3 h periods of extraction.

4.5 References

1. Sun, Q.; Aguila, B.; Perman, J.; Ivanov, A. S.; Bryantsev, V. S.; Earl, L. D.; Abney, C. W.; Wojtas, L.; Ma, S., Bio-Inspired Nano-Traps for Uranium Extraction From Seawater and Recovery From Nuclear Waste. *Nat Commun* **2018,** *9* (1), 1644.

2. Kuo, L.-J.; Gill, G. A.; Tsouris, C.; Rao, L.; Pan, H.-B.; Wai, C. M.; Janke, C. J.; Strivens, J. E.; Wood, J. R.; Schlafer, N.; D'Alessandro, E. K., Temperature Dependence of Uranium and Vanadium Adsorption on Amidoxime-Based Adsorbents in Natural Seawater. *ChemistrySelect* **2018,** *3* (2), 843-848.

3. Endrizzi, F.; Rao, L., Chemical Speciation of Uranium(VI) in Marine Environments: Complexation of Calcium and Magnesium Ions with $[(UO_2)(CO_3)_3]^{4-}$ and the Effect on the Extraction of Uranium From Seawater. *Chem. Eur. J.* **2014,** *20* (44), 14499-506.

4. Lindner, H.; Schneider, E., Review of Cost Estimates For Uranium Recovery From Seawater. *Energ. Econ.* **2015,** *49*, 9-22.

5. Davies, R. V.; Kennedy, J.; McIlroy, R. W.; Spence, R.; Hill, K. M., Extraction of Uranium from Sea Water. *Nature* **1964,** *203*, 1110-1115.

6. Parker, B. F.; Zhang, Z.; Rao, L.; Arnold, J., An Overview and Recent Progress in the Chemistry of Uranium Extraction From Seawater. *Dalton Trans.* **2018,** *47* (3), 639-644.

7. Rao, L., Recent International R&D Activities in the Extraction of Uranium from Seawater. Lawrence Berkeley National Laboratory, LBNL-4034. **2011**.

8. Abney, C. W.; Mayes, R. T.; Saito, T.; Dai, S., Materials for the Recovery of Uranium from Seawater. *Chem. Rev.* **2017,** *117* (23), 13935-14013.

9. Chouyyok, W.; Pittman, J. W.; Warner, M. G.; Nell, K. M.; Clubb, D. C.; Gill, G. A.; Addleman, R. S., Surface Functionalized Nanostructured Ceramic Sorbents for the Effective Collection and Recovery of Uranium From Seawater. *Dalton Trans.* **2016,** *45* (28), 11312-25.

10. Tsouris, C., Uranium Extraction: Fuel From Seawater. *Nat. Energy* **2017,** *2* (4), 17022.

11. Gill, G. A.; Kuo, L.-J.; Janke, C. J.; Park, J.; Jeters, R. T.; Bonheyo, G. T.; Pan, H.-B.; Wai, C.; Khangaonkar, T.; Bianucci, L.; Wood, J. R.; Warner, M. G.; Peterson, S.; Abrecht, D. G.; Mayes, R. T.; Tsouris, C.; Oyola, Y.; Strivens, J. E.; Schlafer, N. J.; Addleman, R. S.; Chouyyok, W.; Das, S.; Kim, J.; Buesseler, K.; Breier, C.; D'Alessandro, E., The Uranium from Seawater Program at the Pacific Northwest National Laboratory: Overview of Marine Testing, Adsorbent Characterization, Adsorbent Durability, Adsorbent Toxicity, and Deployment Studies. *Ind. Eng. Chem. Res.* **2016,** *55* (15), 4264-4277.

12. Oyola, Y.; Janke, C. J.; Dai, S., Synthesis, Development, and Testing of High-Surface-Area Polymer-Based Adsorbents for the Selective Recovery of Uranium from Seawater. *Ind. Eng. Chem. Res* **2016,** *55* (15), 4149-4160.

13. Barber, P. S.; Kelly, S. P.; Griggs, C. S.; Wallace, S.; Rogers, R. D., Surface Modification of Ionic Liquid-Spun Chitin Fibers for the Extraction of Uranium from Seawater: Seeking the Strength of Chitin and the Chemical Functionality of Chitosan. *Green Chem.* **2014,** *16*, 1824-1836.

14. Piechowicz, M.; Abney, C. W.; Thacker, N. C.; Gilhula, J. C.; Wang, Y.; Veroneau, S. S.; Hu, A.; Lin, W., Successful Coupling of a Bis-Amidoxime Uranophile with a Hydrophilic Backbone for Selective Uranium Sequestration. *ACS Appl. Mater. Interfaces* **2017,** *9* (33), 27894-27904.

15. Jauberty, L.; Drogat, N.; Decossas, J. L.; Delpech, V.; Gloaguen, V.; Sol, V., Optimization of The Arsenazo-III Method for the Determination of Uranium in Water and Plant Samples. *Talanta* **2013,** *115*, 751-4.

Chapter 5

Application II: Arsenazo III-trapped Cellulose Film for Uranyl Sensing

5.1 Introduction

Extensive research has been conducted on the chromogenic bis-azo dye, arsenazo III (**Figure 5.1**), due to its high selectivity, high sensitivity, and its ability to form stable metal complexes over a broad pH range. Arsenazo III has demonstrated 1:1 metal complexation with lanthanides[1-4] and actinides[5-7] at a low pH range (~1-4) and both 1:1 and 2:1 dye to calcium ions[8] complexation at the physiological pH range (6.56-7.82). It is considered an octa-protic weak acid, H_8A, having pK_a values ranging from ~ -2.5-12.4, thus making it an effective metal complexing agent over a wide pH range.[9-11]

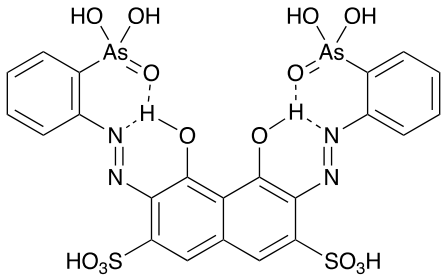

Figure 5.1: Structure of Arsenazo III

Arsenazo III has found use in a large variety of applications, including for determining the uranium concentration in water, ores, and plant samples.[12-16] It has been used as a colorimetric uranyl sensor to detect uranium on the Plexiglass, glass, and steel surfaces of buildings.[17] Arsenazo III has been paired with several solid supports including; functionalized magnetic carbon

composites (Fe_3O_4@C@ASA)[18] and scintillating resin[19] for the extraction of uranyl in aqueous media. It has also been used to remove uranyl from aqueous solutions via the complexation with the uranyl ion being accelerated by ultrasonicated-assisted adsorption onto Au-NPs supported carbon nanotubes.[20] Herein, we describe the use of Arsenazo III-chemisorbed cellulose films for sensing uranyl in aqueous media.

5.2 Results

Through the modification of the Cell-1 film, a dye-trapped porous, water-swelling cellulose film has been used to successfully sense uranyl in aqueous environments. The idea of making a real-time colorimetric uranyl sensor has been of interest for decades. However, finding a ligand with high selectivity towards actinides, in particular uranium, and pronounced chromogenic properties have been challenging. By immobilizing the Arsenazo III into the modified cellulose film, a rapid, efficient, colorimetric sensor for uranyl was created. Taking advantage of the properties of the di-azo dye, chromogenic, rapid 1:1 metal to ligand complexation (**Figure 5.2**), high metal sensitivity and low selectivity, and pairing it with the porous cellulose film allowed for the synthesis of a real-time portable colorimetric uranyl sensor.

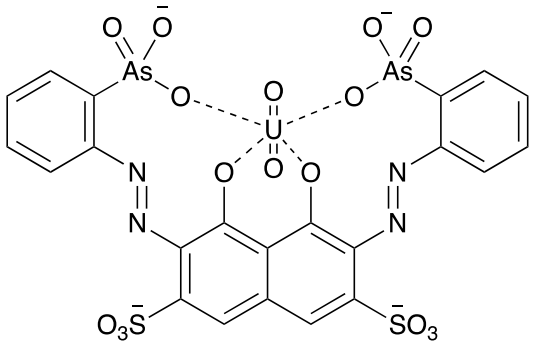

Figure 5.2: 1:1 Uranyl metal complex with the Arsenazo III dye

Increasing the amount of cellulose (400 % increase), enabled preparation of more rigid and porous films, with abilities to withstand the acidic media better than the aforementioned films, which simply decomposed into jelly-like substances upon being placed in the acidic solution of the Arsenazo-III dye (10 mL). Increasing the amount of cellulose also allowed the film to be more porous, thus causing it to swell extensively in aqueous media, which proves to be an effective method for determining the concentration of uranyl in a solution.

As depicted in **Figure 5.3** the modified Cell -1 film containing the trapped Arsenazo III dye appeared as a bright magenta colored film. The uranyl solution began to penetrate the edges of the film and then moving towards the center causing it to go from bright magenta to a turquoise blue. The complete transition was accomplished in less than one minute, due to the rapid chelation of the uranyl to the dye, thus making it a rapid and effective method for uranyl sensing. Repeating the process with varying concentrations of uranyl allowed for a colorimetric scale to be made (**Figure 5.4**) which aids in estimating the concentration of uranyl in unknown solutions.

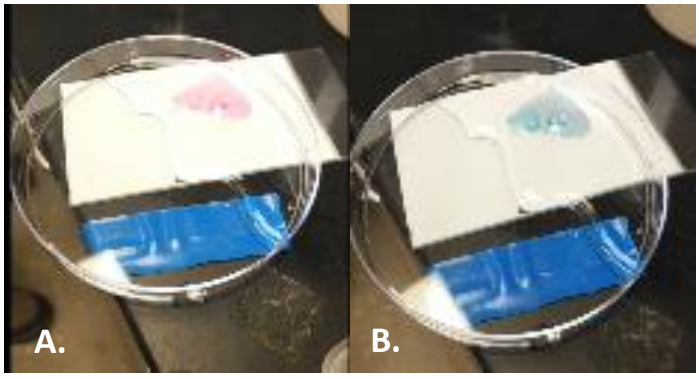

Figure 5.3: Images of the Arsenazo 3-trapped film (pink) (A) Arsenazo 3-trapped film after reacting with 1000 ppm uranyl solution (teal) (B) highlighting the colorimetric properties of dye (~45 s time-lapse between A and B)

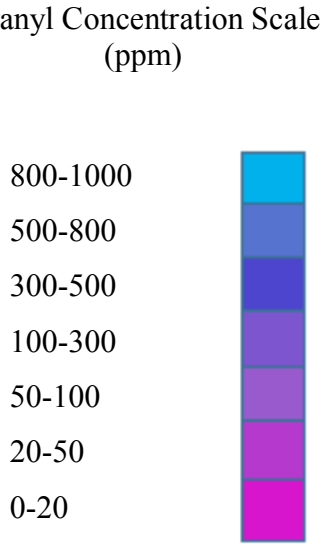

Figure 5.4: Colorimetric Uranyl Concentration Scale (in ppm)

Though the Arsenazo III-trapped film proves to be a fast and reliable method for sensing uranyl, it has several disadvantages. One drawback of this method is that the response of the di-azo dye is pH dependent for actinides, only able to sense them in acidic media (pH of 4 and below). Unfortunately, the cellulose films are acid-sensitive and begin to break down at low pH levels. Though the amount of cellulose was increased for the films in this study, they still experienced slight decomposition from being in the acid, films left in the acidic dye solution for more than 5 min. experienced significant decomposition while those left in the dye for over 10 min, completely decomposed into a jelly-like substance. Another drawback is the toxic nature of the dye,[10] since the cellulose films begin to decompose in the acidic solution, it can lead to the possibility of the dye contaminating wastewater. However, this can be reduced by simply removing and testing small samples instead of placing the film directly into the spill or wastewater of interest.

To determine the efficiency and selectivity of the of the dye, serial titrations with uranyl (UO_2^{2+}), ytterbium (Yb^{3+}), and copper (Cu^{2+}) were performed at 3 different pH conditions;

acidic (pH =0), neutral (pH = 7.483), and basic (pH =11.165). For simplicity, only the metal to ligand ratio of 1.2 :1 is displayed in each UV-Vis spectrum; the complete spectra of individual titrations can be found in the Appendix. **Figure 6.5a** depicts that in acidic media the dye selectively chelated with uranyl to form a 1:1 metal complex as evident by the new peak centered at 651 nm. At neutral pH, **Figure 6.5b** shows evidence of a small bathochromic shift from 585 nm to 577 nm in the presence of copper, but no significant spectral shifts were observed for the actinide or lanthanide. Under basic conditions, see **Figure 6.5c,** there were no major spectroscopic shifts for any of the metal ions examined. Results from these titrations indicate that the dye is only effective at chelating uranyl under acidic conditions, with and shows little to no selectivity for transition metals like copper of lanthanides like ytterbium. (See Appendix for UV-Vis spectra for each individual metal titration at the various pH)

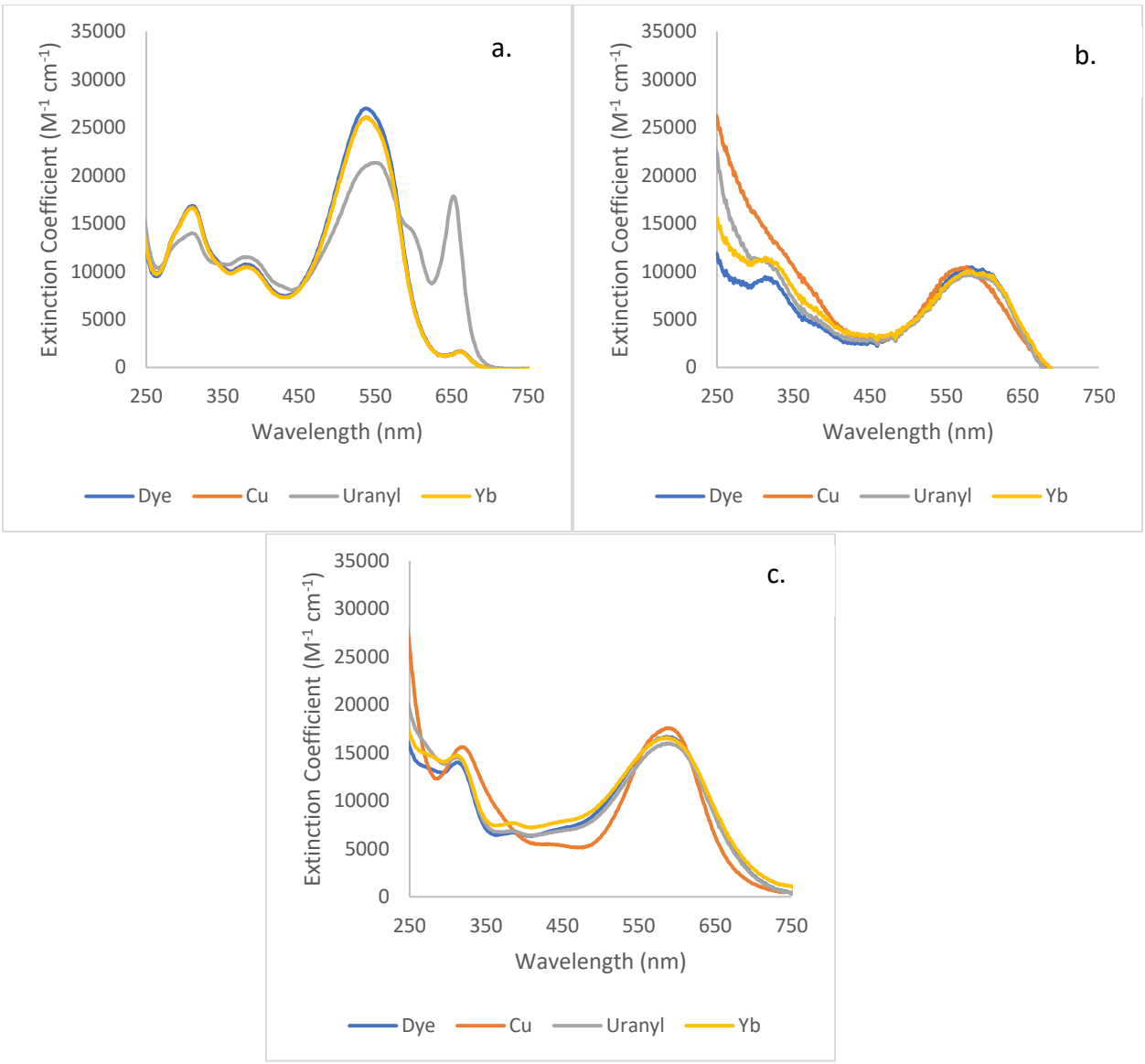

Figure 5.5: Absorbance spectra of results of serial titration of Arsenazo III dye with copper, uranyl, and ytterbium at 1.2 : 1 metal to ligand molar ratio depicting the selectivity and pH dependence of the Arsenazo III dye at (a.) pH = 0 (b.) pH = 7.483 and (c.) 11.165. (Dye concentration: 11.66 ppm)

5.3 Conclusions

In conclusion, extensive research has been performed on the chromogenic bis-azo dye to study its binding properties with calcium, actinides and lanthanides. With its pronounced and rapid colorimetric properties and high selectivity, Arsenazo III exhibits all the qualities desired for use

as a successful sensor. Without interference from the common false positive, copper, or other lanthanide at low pH levels, makes the Arsenazo III dye considered to be one of the best and most efficient way for sensing uranium. Unfortunately, most studies use the dye to perform spectrophotometric studies on the metal complex in order to quantify, thus usually requiring some form of UV-vis spectrophotometer which can range from being inexpensive to very costly. Reported here, Arsenazo III-trapped film was used to create an efficient real-time colorimetric sensor for uranyl in aqueous media. By in-trapping the chromophoric dye inside biodegradable cellulose, we are able to create a simple, eco-friendly, rapid, and portable way to detect and quantify uranyl in aqueous media. This method is efficient and cost-effective since there is not a need for instrumentation to analyze the sample.

5.4 Experimental

Caution! The uranium metal salts – $UO_2(NO_3)_2 \cdot 6H_2O$ – used in this study contained depleted uranium, standard precautions for handling radioactive materials, such as uranyl nitrate, were followed.

5. 4. 1. Towards the Synthesis of Arsenazo III-trapped Cellulose Film

Modified Cell-1 film was prepared using the procedure as described in Chapter 3 (*vide supra)*. Cell-1 film used in this experiment was prepared using the same procedure discussed in previously; however, the amount of cellulose was increased from 0.281 grams to 1.125 and the amount of epichlorohydrin was increased proportionally, resulting in a 3 wt % epichlorohydrin. Modified Cell-1 was then placed into a 5 mL solution of Arsenazo III in 3 M perchloric acid, and the solution was allowed to fully penetrate the film for 1-2 min. The film was then removed and rinsed with

methanol and de-ionized water to remove excess acid. The film was then placed in 10 mL of aqueous uranyl standard solutions with concentrations ranging from 0-1000 ppm and allowed to react for ~30 s. The film was then used to create a real-time colorimetric sensor for uranyl, by creating a color-coded scale displaying colors correlating to concentration ranges of uranyl (in ppm).

5. 4. 2. Serial Titration

A standard solution (11.66 ppm) of the disodium salt of the 2,7-bis (2-arsenophenylazo)-1,8-dihydroxynaphthalene-3,6-disulfonic acid (commonly referred to as Arsenazo III) was prepared by dissolving 11.66 mg of the Arsenazo III salt into a 1 L volumetric flask and diluting it with 3 M $HClO_4$ to the 1-L marker on the flask. Three 10-mL samples of the dye solution were adjusted to the following pH levels; acidic (pH = 0, standard), neutral (pH = 7.483), and basic (pH = 11.165). A 3 M phosphoric acid solution and 50 % NaOH solution were added dropwise (~20 μL) to adjust the pH of the neutral and basic solutions.

The metal salt solutions (200 ppm) were made from the following metal salts; copper(II) chloride dihydrate, ytterbium(III) acetate, and uranyl nitrate hexahydrate. 5 mg of each metal salt was placed into different 25 mL volumetric flask, the salts were dissolved in methanol and diluted up to the 25-mL marker on the flask.

For the serial titration, 2 mL of the dye was placed in 1 cm quartz curvetted and fifteen 10-μL (metal to ligand ratios of 0.08-1.2 : 1) aliquot additions of the metal solution was added, with 5-seconds of swirling between each measure collected.

5. 4. 3. Determination of pH of metal solutions

The pH of metal solutions was determined using a Fisher Scientific AR15 pH meter. The pH meter was calibrated using standardized buffer samples at pH of 4, 7, and 10. The pH of the samples were determined by placing the glass electrode in the solution and recording the pH value upon stabilization. The electrode was then washed with distilled water into a waste beaker and wiped dry with a Chemwipe before measuring other samples.

6.5 References

1. Rohwer, H.; Hosten, E., pH Dependence of the Reactions of Arsenazo III with the Lanthanides. *Anal. Chim. Acta* **1997,** *339*, 271-277.

2. Rohwer, H.; Collier, N.; Hosten, E., Spectrophotometric Study of Arsenazo III and its Interactions with Lanthanides. *Anal. Chim. Acta* **1995,** *314*, 219-223.

3. Hosten, E.; Rohwer, H., Interaction of Anions with Arsenazo III-Lanthanide (III) Complexes. *Anal .Chim. Acta* **1997,** *345*, 227-233.

4. Matharu, K.; Mittal, S. K.; Ashok Kumar, S. K.; Sahoo, S. K., Selectivity Enhancement of Arsenazo(III) Reagent Towards Heavier Lanthanides Using Polyaminocarboxylic Acids: A Spectrophotometric Study. *Spectrochim. Acta A Mol. Biomol. Spectrosc.* **2015,** *145*, 165-175.

5. Kuroda, R.; Kurosaki, M.; Hayashibe, Y.; Ishimaru, S., Simultaneous Determination of Uranium and Thorium with Arsenazo III by Second-Derivative Spectrophotometry. *Talanta* **1990,** *37* (6), 619-624.

6. Hosten, E.; Rohwer, H., Complexation Reactions of Uranyl with Arsenazo III. *Anal. Chim. Acta* **1997,** *355*, 95-100.

7. Rohwer, H.; Rheeder, N.; Hosten, E., Interactions of Uranium and Thorium with Arsenazo III in an Aqueous Medium. *Anal. Chim. Acta* **1997,** *341*, 263-268.

8. Ogan, K.; Simons, E. R., The Influence of pH on Arsenazo Ill. *Anal. Biochem.* **1979,** *96*, 70-76.

9. Nemcova, I.; Metal, B.; Podlaha, J., Dissociation Constants of Arsenazo III. *Talanta* **1986,** *33* (10), 841-842.

10. Alosmanov, R., Adsorption of Arsenazo (III) Due by Phosphorus-Containing Polymer Sorbent. *J. Serb. Chem. Soc.* **2016,** *81* (8), 907-921.

11. Rowatt, E.; Williams, R. J. P., The Interaction of Cations with the Dye Arsenazo III. *Biochem. J.* **1989,** *259*, 295-298.

12. Khan, M. H.; Warwick, P.; Evans, N., Spectrophotometric Determination of Uranium with Arsenazo-III in Perchloric Acid. *Chemosphere* **2006,** *63* (7), 1165-9.

13. Jauberty, L.; Drogat, N.; Decossas, J. L.; Delpech, V.; Gloaguen, V.; Sol, V., Optimization of the Arsenazo-III Method for the Determination of Uranium in Water and Plant Samples. *Talanta* **2013,** *115*, 751-4.

14. Serenjeh, F. N.; Hashemi, P.; Ghiasvand, A. R.; Rasolzadeh, F., A New Optical Sensor for Selective Quantitation of Uranium by the Immobilization of Arsenazo III on an Agarose Membrane. *Anal. Methods* **2016,** *8* (21), 4181-4187.

15. Wang, F.; Li., H.; Lui, Q.; Li, Z. ; Li, R.; Zhang, H.; Lui, L.; Emelchenko, G. A.; Wang, J. A Graphene Oxide/Amidoxime Hydrogel for Enhanced Uranium Capture. Nature Scientitific Reports. **2015.** DOI: 10.1038/srep19367.

16. Kuo, L.-J.; Gill, G. A.; Tsouris, C.; Rao, L.; Pan, H.-B.; Wai, C. M.; Janke, C. J.; Strivens, J. E.; Wood, J. R.; Schlafer, N.; D'Alessandro, E. K., Temperature Dependence of Uranium and Vanadium Adsorption on Amidoxime-Based Adsorbents in Natural Seawater. *ChemistrySelect* **2018,** *3* (2), 843-848.

17. Greene, P. A.; Copper, C. L.; Berv, D. E.; Ramsey, J. D.; Collins, G. E., Colorimetric Detection of Uranium(VI) on Building Surfaces After Enrichment by Solid Phase Extraction. *Talanta* **2005,** *66* (4), 961-6.

18. Li, P.; Wang, J.; Wang, X.; He, B.; Pan, D.; Liang, J.; Wang, F.; Fan, Q., Arsenazo-Functionalized Magnetic Carbon Composite for Uranium(VI) Removal From Aqueous Solution. *J. Mol. Liq.* **2018,** *269*, 441-449.

19. Duval, C. E.; DeVol, T. A.; Husson, S. M., Extractive Scintillating Polymer Sensors for Trace-Level Detection of Uranium in Contaminated Ground Water. *Anal Chim. Acta* **2016,** *947*, 1-8.

20. Omidi, M. H.; Azad, F. N.; Ghaedi, M.; Asfaram, A.; Azqhandi, M. H. A.; Tayebi, L., Synthesis and Characterization of Au-Nps Supported on Carbon Nanotubes: Application for the Ultrasound Assisted Removal of Radioactive UO_2^{2+} Ions Following Complexation with Arsenazo III: Spectrophotometric Detection, Optimization, Isotherm and Kinetic Study. *J. Colloid Interface Sci.* **2017,** *504*, 68-77.

Chapter 6

Conclusions and Future Work

6.1 Conclusions

In conclusion, six Schiff base salen ligands were synthesized, each containing a different electronic group, to determine the effect electronics have on the ligand's chelation ability for various metal ions. Using **L4** (H in 5-position) as a reference ligand, it was determined that the ligands containing electron withdrawing groups, such as a halogen (**L5**) greatly affected the chelating properties of the ligand, while the ligands containing carbonyl groups, **L2** and **L3**, were able to chelate several metal ions due to resonance stabilization. The ligands containing electron donating groups, **L1** and **L6,** were able to effectively chelate both transition metals and actinides, due to their ability to donate electron density to the tetradentate pocket of the ligand. Though the electron donating ligands were more successful at chelating metal ions, **L3** was the only ligand able to differentiate between copper, a common false-positive, and uranyl, thus it was further probed for use as a uranyl chemosensor.

Cellulose serves as a green, efficient, and viable solid support for the extraction of uranyl from aqueous media. Absorption of the salen ligand onto the surface of the cellulose film resulted in the extraction of more than 36 % uranyl in as little as 5 minutes but was plagued by leaching of the ligand into the solutions. To overcome this, ligand in-trapped films (Cell-2 through Cell-5) were synthesized. The Cell-2 through 5 films, though slower were able to extract 27-70 % uranyl over the 72-h extraction period, with Cell-3 extracting the most, 70 %, uranyl. However, these films too were plagued with leaching, due to the remaining ligands that weren't efficiently trapped within the film's matrix leaching out into the aqueous media. To overcome the leaching problem, covalently-linked ligand-films (Cell-6 through Cell 9) were synthesized. They extracted 27-65 %

uranyl over 72-h, with Cell-6 extracting the most, 65 %, uranyl. Similar to some of the in-trapped films, these films maintained their structural integrity over the 3-day extraction period and were able to withstand the basic (pH = 10.62) and acidic (pH = 4.17) environments with minimum leaching in neutral conditions. It is important to note the effects the crosslinkers have on the extracting ability of the films: generally, the films utilizing glutaraldehyde as the cross-linker outperformed the films cross-linked with citric acid. This is influenced by the number of oxygens presented in each linkage, 5 for citric acid versus 2 for glutaraldehyde.

The cellulose films used in this research were then used in two applications; for the extraction of uranyl from spiked sea water and the colorimetric sensing of Arsenazo III dye in-trapped cellulose film. Cell-3 and Cell-6 films were used to extract uranium from four different spiked environmental samples, where they succeeded at extracting uranium from the samples, extracting a maximum of 28 % and 42 %, respectively, in the presence of competitive trace metals. Taking advantage of the rapid chromogenic properties of the Arsenzo III and eco-friendly cellulose film yielded the development of a real-time colorimetric scale for uranyl sensing.

6.2 Future Work

6. 2. 1. Ligand Design

Since the early 60's extensive research on uranyl chelation with amidoxime ligands had been conducted.[1, 2] Amidoxime ligands consist of an enamine bidentate chelating pocket (**Figure 6.1**), which has a shown strong affinity towards uranyl.[3, 4] Beginning in the early 80's these ligands were incorporated into resins and used for the extraction of the tri-carbonate uranyl complexes found in seawater.[5, 6] Since then they have become the focus of research at many national labs,[7-11]

including Oak Ridge National Laboratory and Pacific Northwest National Laboratory, as well as around the world[12-15] for the extraction of uranium from seawater.

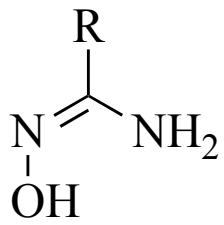

Figure 6.1 General structure of amidoxime

As depicted in **Figure 6.2** the cyclic and open chain ligands exhibit several binding motifs for uranyl binding including; monodentate via the oxime, bidentate, tridentate (cyclic imide dioximes)[15]

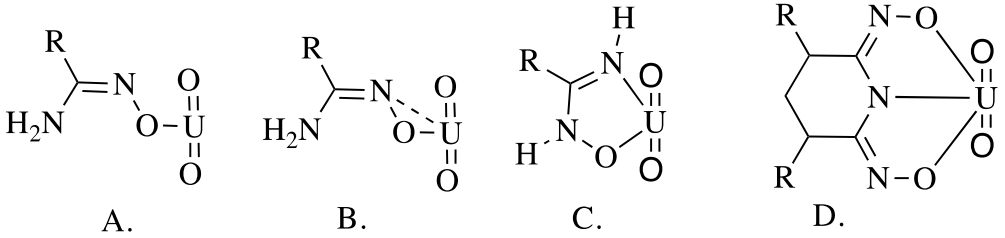

Figure 6.2 Binding motifs of uranyl with amidoxime ligands

Incorporating the amidoxime binding pocket and a highly conjugated backbone, similar to that of 2-quinoxalinol, would yield a highly selective uranyl ligand. Incorporation of aromatic rings not only enhances the stability of the amidoxime ligands under strongly acidic media, but would allow for high signal to noise ratios, high extinction coefficients, and pronounced spectroscopic shifts.

Starting with the commercially available 1,3-dichloroisoquinone, a bis-amidoxime ligand could be synthesized in four simple steps, exhibiting a high affinity for uranyl (**Scheme 6.1**).[11, 16, 17]

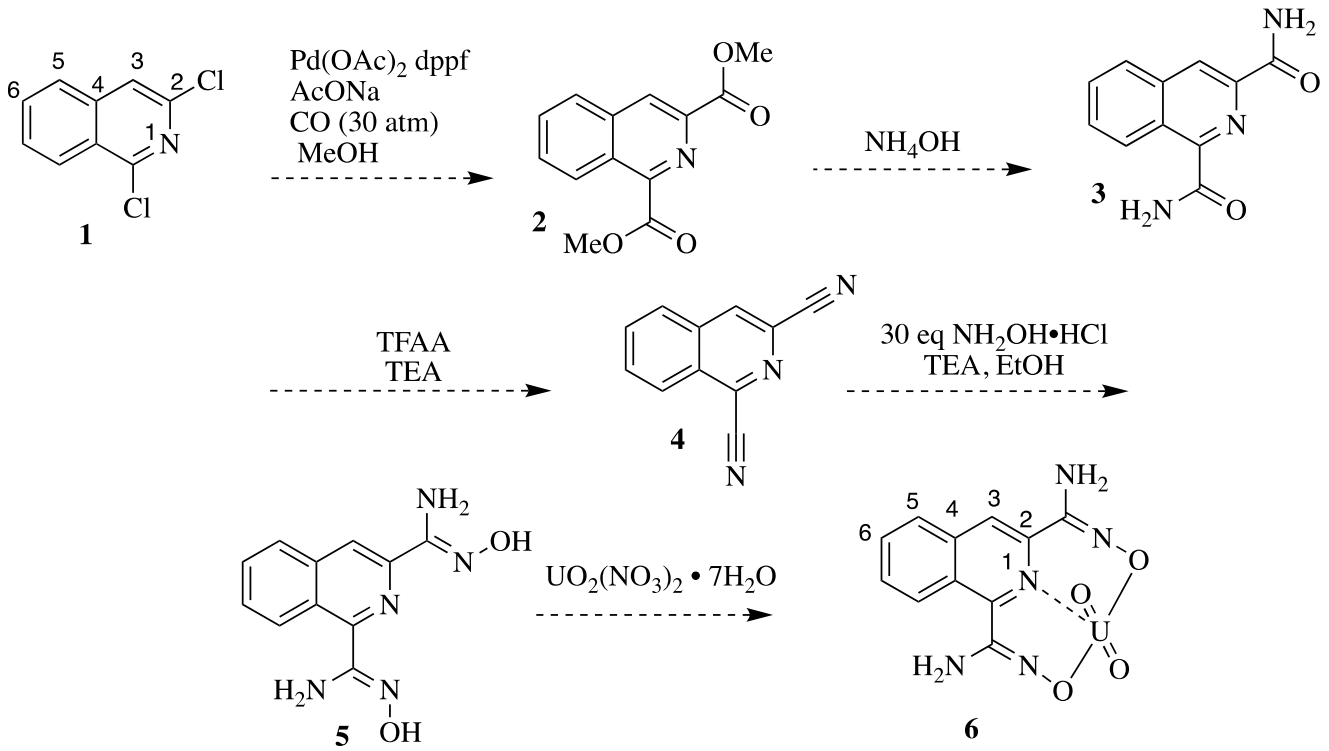

Scheme 6.1 Proposed synthesis of bis-amidoxime ligand

The electronic effects on the ligand's selectivity could be studied by adding different electron donating or withdrawing groups to the 6-position.

6. 2. 2. Solid-supports

Hydrogels are a class of materials that are composed of three-dimensional hydrophilic polymer networks, high water content, and excellent water retention.[18,19] The networks are generally composed of either synthetic or natural polymers that are cross-linked physically or chemically and exhibit chemical interactions such as covalent bonds, hydrogen bonds, ionic bonds and van

der Waals forces to prevent dissolution into the aqueous phase.[18,19] Hydrogels' popularity has increased due to their wide applicability in fields including; drug delivery, tissue engineering, artificial organs, sorbents, (bio)sensors, contact lenses, and purification.[1, 20-32] As depicted in **Figure 6.3**, hydrogels have the ability to swell extensively in aqueous media, thus making them viable options for uranyl extraction in aqueous media.[28-32]

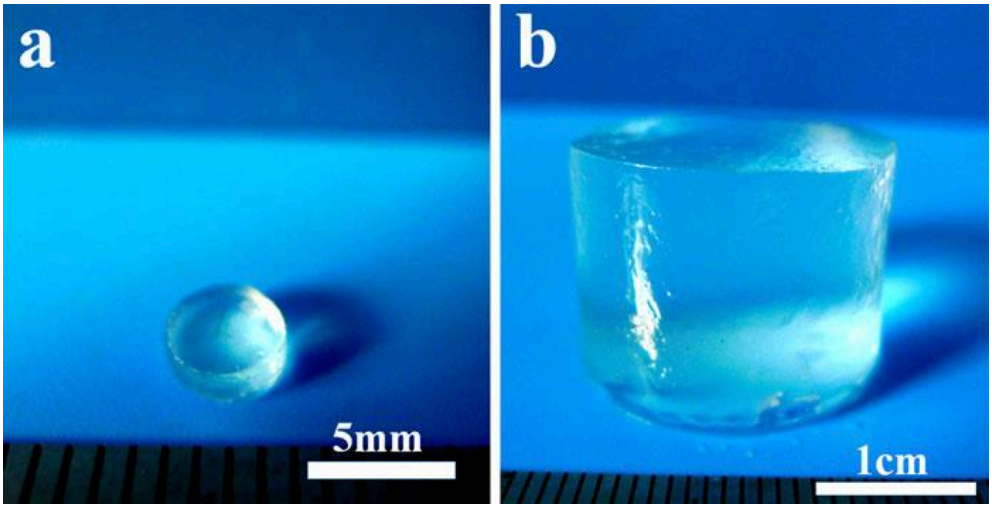

Figure 6.3: Images of (a) freshly prepared hydrogel (4 wt % cellulose and 5% ECH) and (b) swollen hydrogel[22]

By incorporating the highly fluorescencent 2-quinoxalinol salen ligands or highly selective amidoxime ligands into hydrogels via crosslinking could make for efficient, convenient, and possibly luminescent uranyl sensors (**Figure 6.4**).

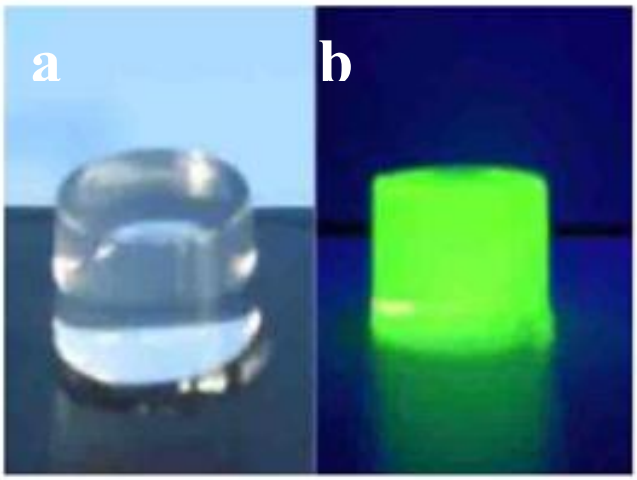

Figure 6.4 Images of cellulose-quantum dots hydrogel (a) under visible light and (b) under UV lamp (302 nm)[24]

6.3 References

1. Abney, C. W.; Mayes, R. T.; Saito, T.; Dai, S., Materials for the Recovery of Uranium from Seawater. *Chem. Rev.* **2017,** *117* (23), 13935-14013.

2. Eloy, F.; Lenaers, R., The Chemistry of Amidoximes and Related Compounds. *Chem. Rev.* **1962,** *62* (2), 155-183.

3. Barros, C.; Frieitas, J.; Oliviera, R.; Filho, J., Synthesis of Amidoximes Using an Efficient and Rapid Ultrasound Method. *J. Chil. Chem. Soc.* **2011,** *56* (2), 721-722.

4. Bell, C. L.; Nambury, C. N. V.; Bauer, L., The Structure of Amidoximes. *J. Org. Chem.* **1964,** *29* (10), 2873-2877.

5. Saito, K.; Hori, T.; Furusaki, S.; Sugo, T.; Okamoto, J., Porous Amidoxime-Group-Containing Membrane for the Recovery of Uranium from Seawater. *Ind. Eng. Chem. Res.* **1987,** *26* (10), 1977-1981.

6. Vernon, F.; Shah, T., The Extraction of Uranium from Seawater by Poly(hydroxamic acid) Resins and Fibre *Reactive Polymers* **1983,** *1*, 301-308.

7. Ladshaw, A.; Kuo, L.-J.; Strivens, J.; Wood, J.; Schlafer, N.; Yiacoumi, S.; Tsouris, C.; Gill, G., Influence of Current Velocity on Uranium Adsorption from Seawater Using an Amidoxime-Based Polymer Fiber Adsorbent. *Ind. Eng. Chem. Res.* **2017,** *56* (8), 2205-2211.

8. Ladshaw, A. P.; Das, S.; Liao, W. P.; Yiacoumi, S.; Janke, C. J.; Mayes, R. T.; Dai, S.; Tsouris, C., Experiments and Modeling of Uranium Uptake by Amidoxime-Based Adsorbent in the Presence of Other Ions in Simulated Seawater. *Ind. Eng. Chem. Res.* **2015,** *55* (15), 4241-4248.

9. Pan, H.-B.; Kuo, L.-J.; Wai, C. M.; Miyamoto, N.; Joshi, R.; Wood, J. R.; Strivens, J. E.; Janke, C. J.; Oyola, Y.; Das, S.; Mayes, R. T.; Gill, G. A., Elution of Uranium and Transition Metals from Amidoxime-Based Polymer Adsorbents for Sequestering Uranium from Seawater. *Ind. Eng. Chem. Res.* **2015,** *55* (15), 4313-4320.

10. Kuo, L.-J.; Janke, C. J.; Wood, J. R.; Strivens, J. E.; Das, S.; Oyola, Y.; Mayes, R. T.; Gill, G. A., Characterization and Testing of Amidoxime-Based Adsorbent Materials to Extract Uranium from Natural Seawater. *Ind. Eng. Chem. Res.* **2015,** *55* (15), 4285-4293.

11. Piechowicz, M.; Abney, C. W.; Thacker, N. C.; Gilhula, J. C.; Wang, Y.; Veroneau, S. S.; Hu, A.; Lin, W., Successful Coupling of a Bis-Amidoxime Uranophile with a Hydrophilic Backbone for Selective Uranium Sequestration. *ACS Appl. Mater. Interfaces* **2017,** *9* (33), 27894-27904.

12. Yin, Z.; Xiong, J.; Chen, M.; Hu, S.; Cheng, H., Recovery of Uranium(VI) from Aqueous Solution by Amidoxime Functionalized Wool Fibers. *J. Radioanal. Nucl. Chem.* **2015,** *307* (2), 1471-1479.

13. Xiong, J.; Hu, S.; Liu, Y.; Yu, J.; Yu, H.; Xie, L.; Wen, J.; Wang, X., Polypropylene Modified with Amidoxime/Carboxyl Groups in Separating Uranium(VI) from Thorium(IV) in Aqueous Solutions. *ACS Sustainable Chem. Eng.* **2017,** *5*, 1924-1930.

14. Zhang, H.; Zhang, L.; Han, X.; Kuang, L.; Hua, D., Guanidine and Amidoxime Cofunctionalized Polypropylene Nonwoven Fabric for Potential Uranium Seawater Extraction with Antifouling Property. *Ind. Eng. Chem. Res.* **2018,** *57* (5), 1662-1670.

15. Qin, Z.; Shi, S.; Yang, C.; Wen, J.; Jia, J.; Zhang, X.; Yu, H.; Wang, X., The Coordination of Amidoxime Ligands With Uranyl in the Gas Phase: A Mass Spectrometry and DFT Study. *Dalton Trans.* **2016,** *45* (41), 16413-16421.

16. Yamamoto, H.; Takagi, Y.; Oshiro, T.; Mitsuyama, T.; Sasaki, I.; Yamasaki, N.; Yamada, A.; Kenmoku, H.; Matsuo, Y.; Kasai, Y.; Imagawa, H., Total synthesis of (-)-Thallusin: Utilization of Enzymatic Hydrolysis Resolution. *J. Org. Chem.* **2014,** *79* (18), 8850-5.

17. Hardy, E. E.; Wyss, K. M.; Eddy, M. A.; Gorden, A. E. V., An Example of Unusual Pyridine Donor Schiff Base Uranyl (UO_2^{2+}) Complexes. *Chem. Commun.* **2017,** *53* (42), 5718-5720.

18. Dong, H.; Snyder, J. F.; Williams, K. S.; Andzelm, J. W., Cation-induced Hydrogels of Cellulose Nanofibrils with Tunable Moduli. *Biomacromolecules* **2013,** *14* (9), 3338-45.

19. Bannerman, D.; Li, X.; Wan, W., A 'degradable' Poly(vinyl alcohol) Iron Oxide Nanoparticle Hydrogel. *Acta Biomater.* **2017**, *58*, 376-385.

20. Rao, L., Recent International R&D Activities in the Extraction of Uranium from Seawater. Lawrence Berkeley National Laboratory, LBNL-4034. **2011**.

21. Denizli, A.; Arpa, C.; Bektas, S.; Genc, O., Adsorption of Mercury(II) Ions on Procion Blue MX-3G-attached Magnetic Poly(vinyl alcohol) Gel Beads. *Adsorpt. Sci. Technol.* **2002,** *20*, 91-106.

22. Qin, X.; Lu, A.; Zhang, L., Gelation Behavior of Cellulose in NaOH-Urea Aqueous System via Cross-Linking. *Cellulose* **2013,** *20*, 1669-1677.

23. Hoare, T. R.; Kohane., D. S., Hydrogels in Drug Delivery- Progress and Challenges. *Polymer* **2008,** *49*, 1993-2007.

24. Chang, C., and Zhang, L., Cellulose-Based Hydrogels- Present Status and Application Prospects. *Carbohydr. Polym.* **2011,** *84*, 40-53.

25. Deligkaris, K.; Tadele, T.; Olthius, W.; Van der Berg, A., Hydrogel-based Devices for Biomedical Applications. *Sens. Actuators B: Chemical* **2010,** *147*, 765-774.

26. Sannino, A.; Demitri, C.; Madaghiele, M., Biodegradable Cellulose-based Hydrogels-Design and Applications. *Materials* **2009,** *2*, 353-373.

27. Hoffman, A. S., Hydrogels for Biomedical Applications. *Adv. Drug Delivery Rev.* **2012,** *64*, 18-23.

28. Wang, X.; Liu., Q.; Liu, J.; Chen, R.; Zhang, H.; Li, R.; Li, Z.;Wang, J., 3-D Self-Assembly Polyethyleneimine Modified Graphene Oxide Hydrogel for the Extraction of Uranium From Aqueous Solution. *Appl. Surf. Sci.* **2017,** *426*, 1063-1074.

29. Wang, F.; Li., H.; Lui, Q.; Li, Z. ; Li, R.; Zhang, H.; Lui, L.; Emelchenko, G. A.; Wang, J. A Graphene Oxide/Amidoxime Hydrogel for Enhanced Uranium Capture. Nature Scientitific Reports. **2015.** DOI: 10.1038/srep19367.

30. Kou, S.; Yang, Z.; Sun, F., Protein Hydrogel Microbeads for Selective Uranium Mining from Seawater. *ACS Appl. Mater. Interfaces* **2017,** *9* (3), 2035-2039.

31. Liu, Y.; Cao, X.; Hua, R.; Wang, Y.; Lui, Y., Pang, C.; Wang, Y., Selective Adsorption of Uranyl Ion on Ion-Imprinted Chitosan/PVA Cross-Linked Hydrogel. *Hydrometallurgy* **2010,** *104*, 150-155.

32. Ulusoy, H. I.; Simsek, S., Removal of Uranyl Ions in Aquatic Mediums by Using a New Material: Gallocyanine Grafted Hydrogel. *J. Hazard. Mater.* **2013,** *254-255*, 397-405.

Appendix

A.1 Chapter 2: Ligand Design: Electronic Effects on Metal Chelation of Schiff-based Salen Ligands

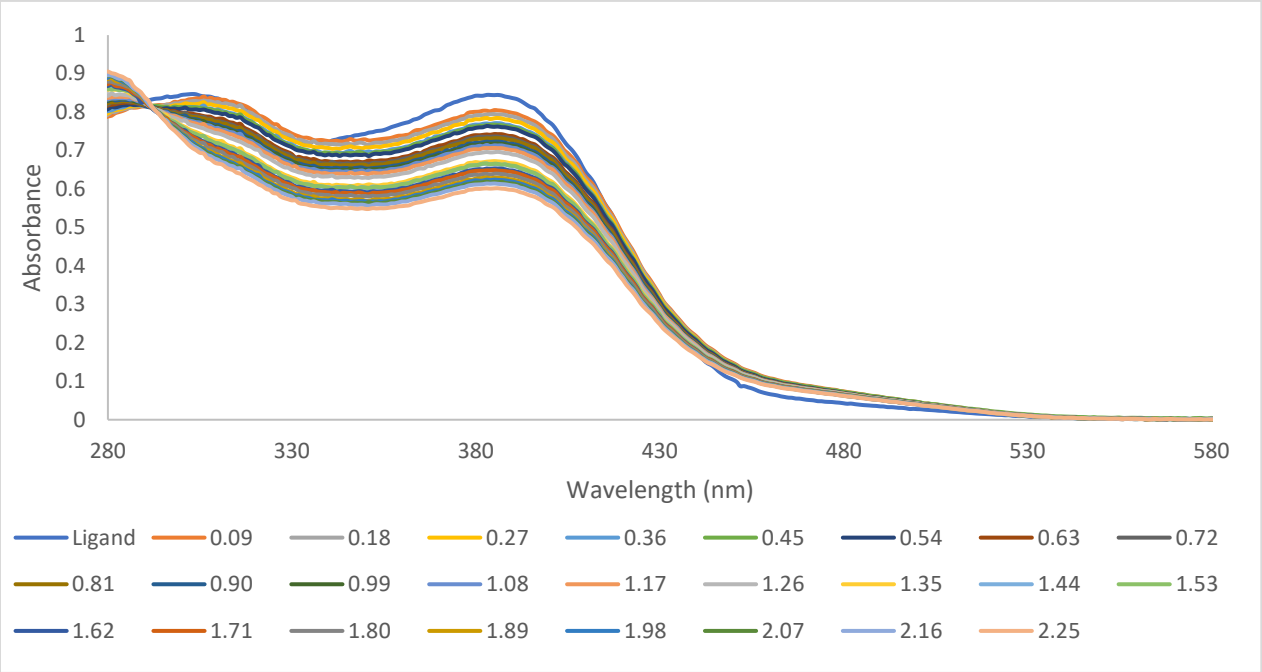

A.2.1 L1 (DMF) titration with Vanadyl (MeOH) (Shown at metal to ligand molar ratios of 0.09-2.25: 1)

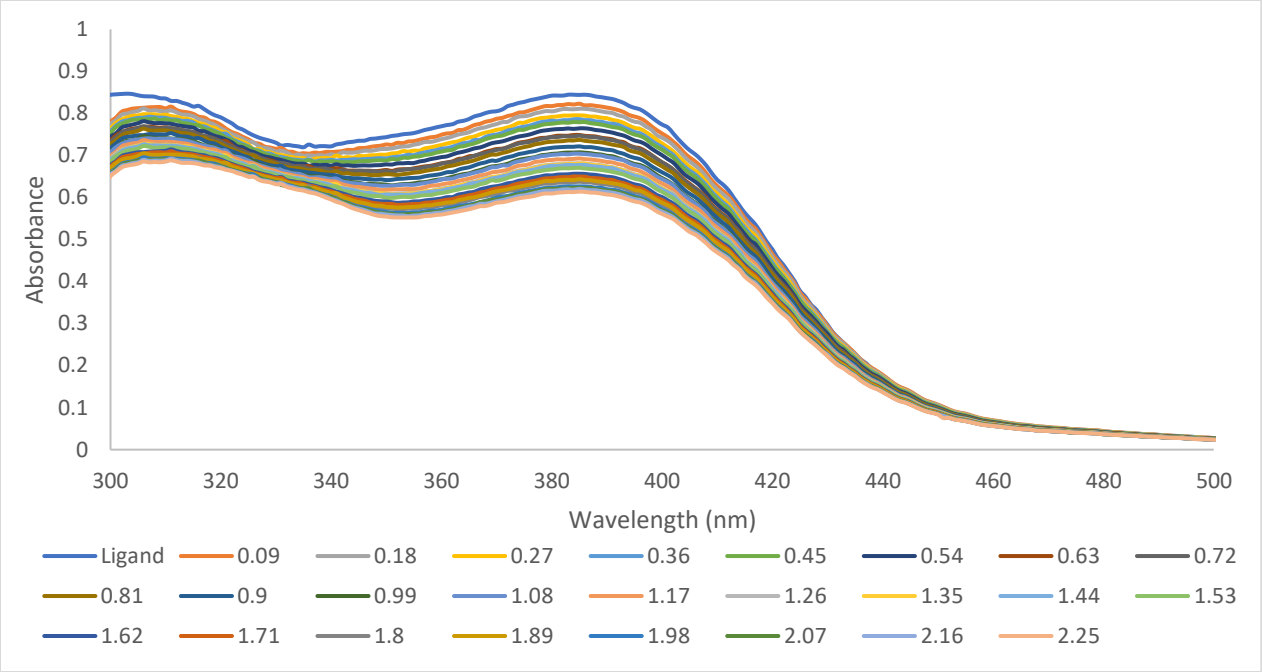

A.2.2 L1 (DMF) titration with Chromium (MeOH) (Shown at metal to ligand molar ratios of 0.09-2.25: 1)

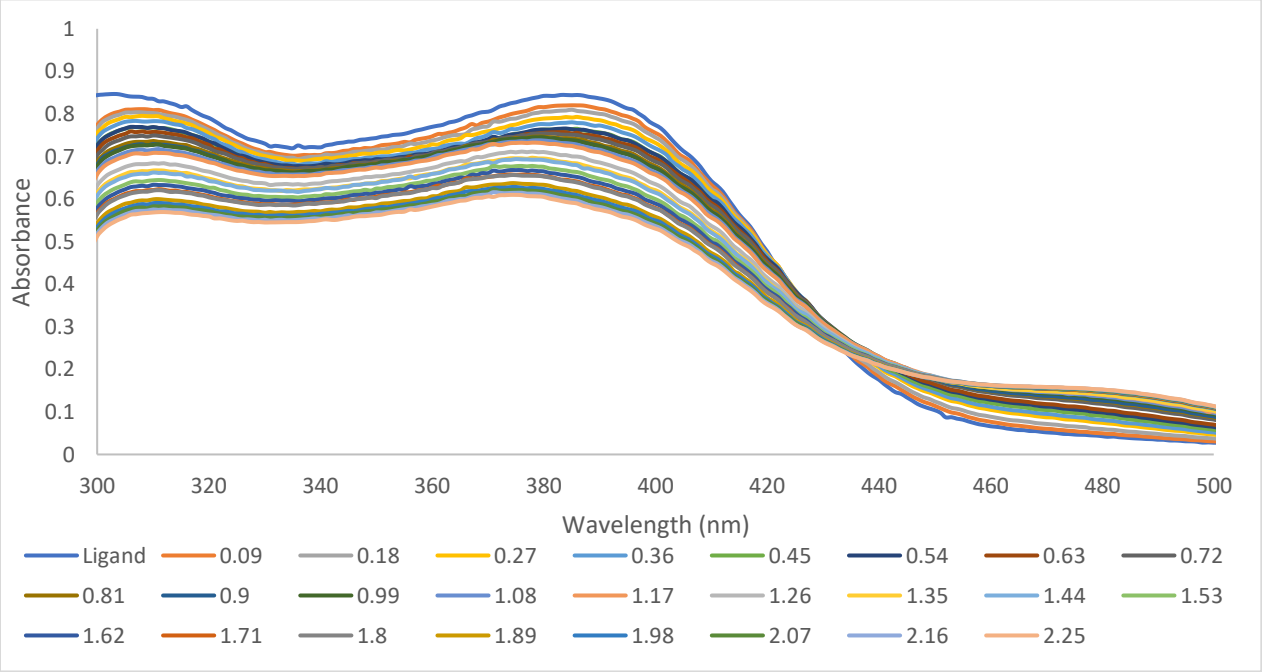

A.2.3 L1 (DMF) titration with Manganese (MeOH) (Shown at metal to ligand molar ratios of 0.09-2.25: 1)

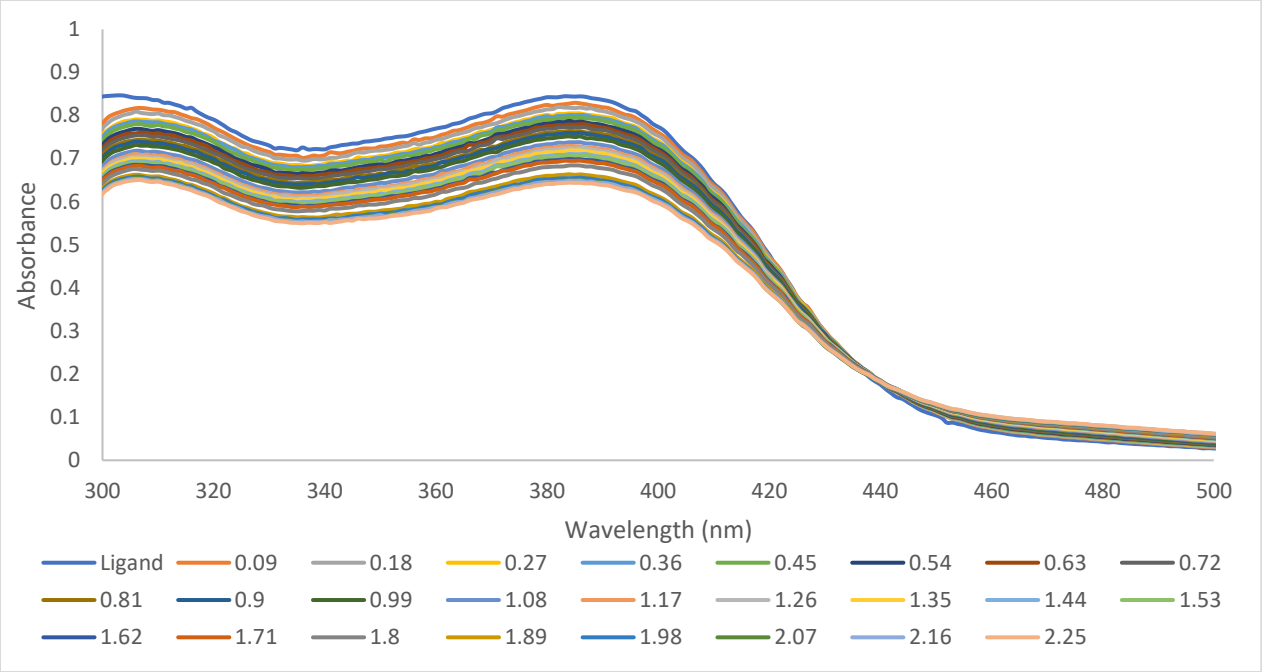

A.2.4 L1 (DMF) titration with Iron (MeOH) (Shown at metal to ligand molar ratios of 0.09-2.25: 1)

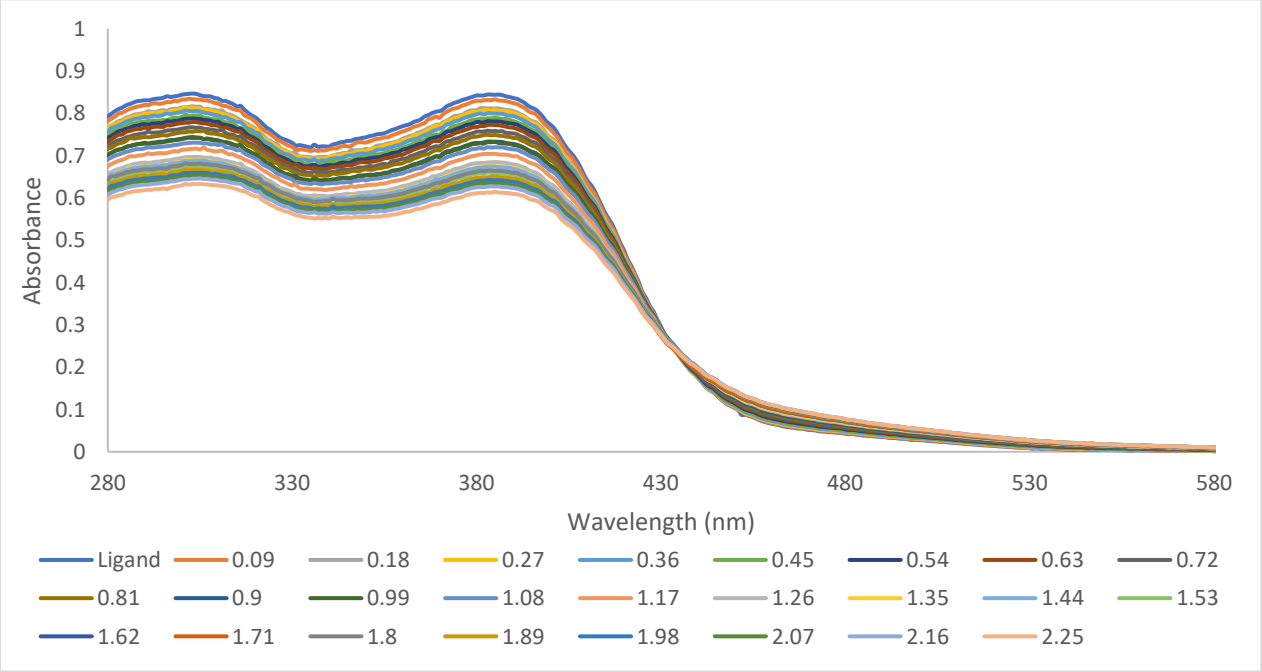

A.2.5 L1 (DMF) titration with Cobalt (MeOH) (Shown at metal to ligand molar ratios of 0.09-2.25: 1)

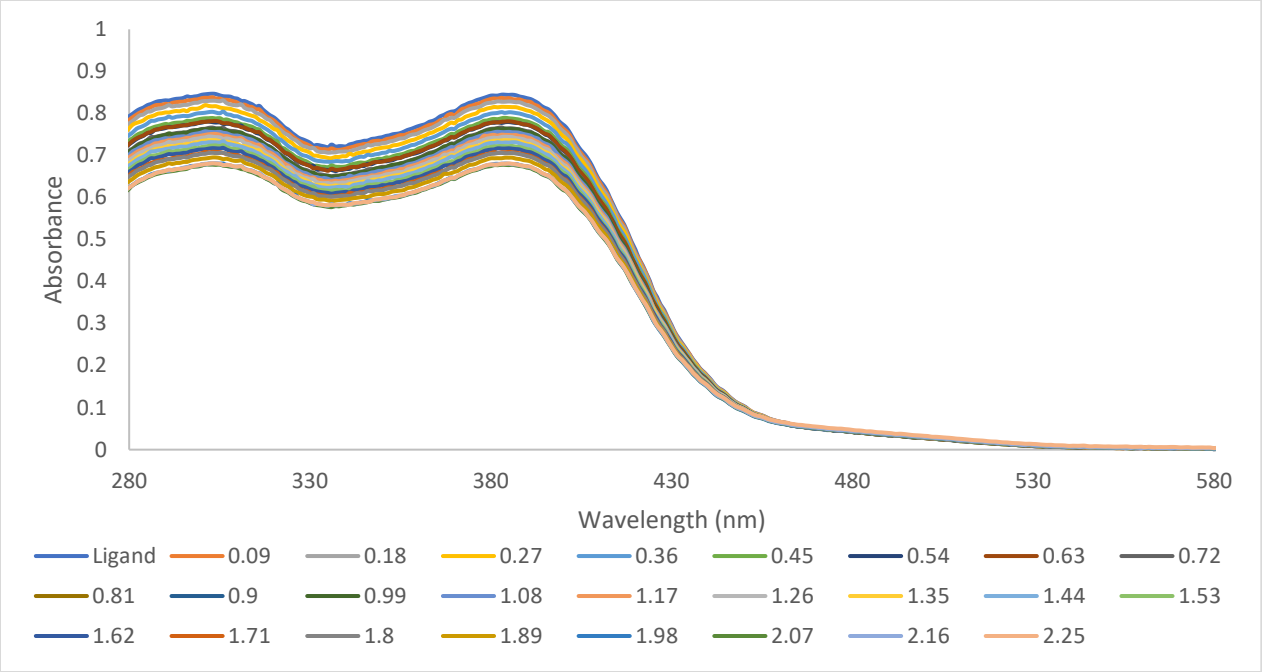

A.2.6 L1 (DMF) titration with Nickel (MeOH) (Shown at metal to ligand molar ratios of 0.09-2.25: 1)

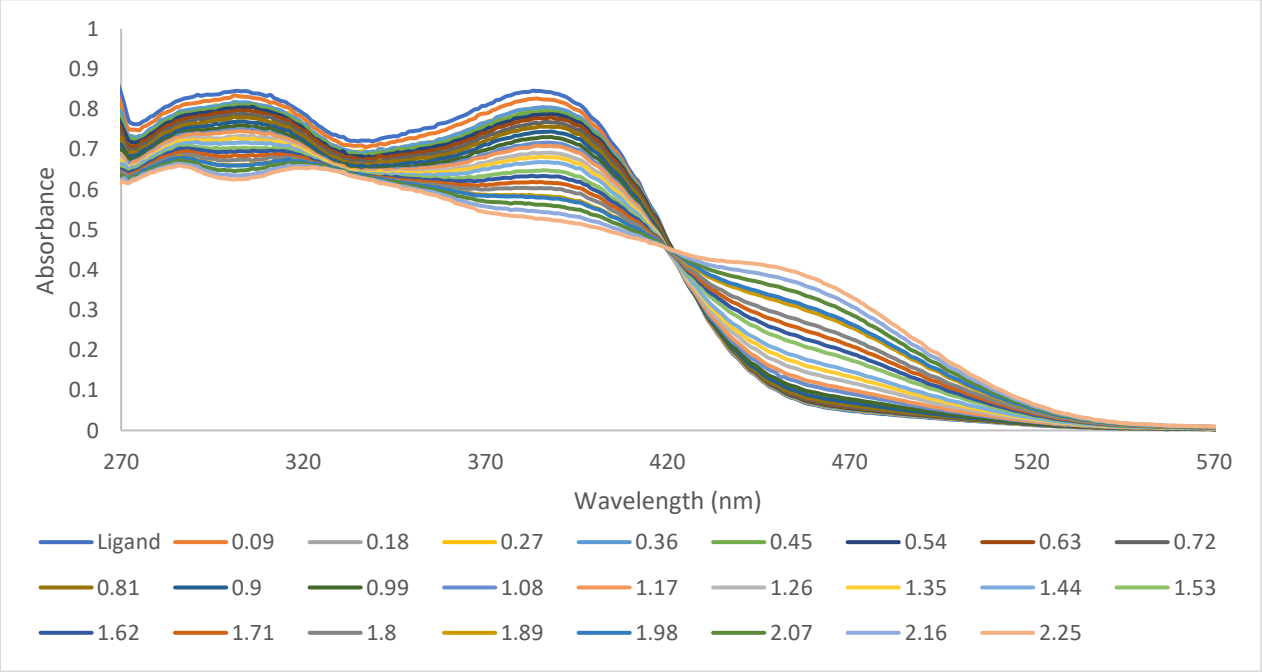

A.2.7 L1 (DMF) titration with Copper (MeOH) (Shown at metal to ligand molar ratios of 0.09-2.25: 1)

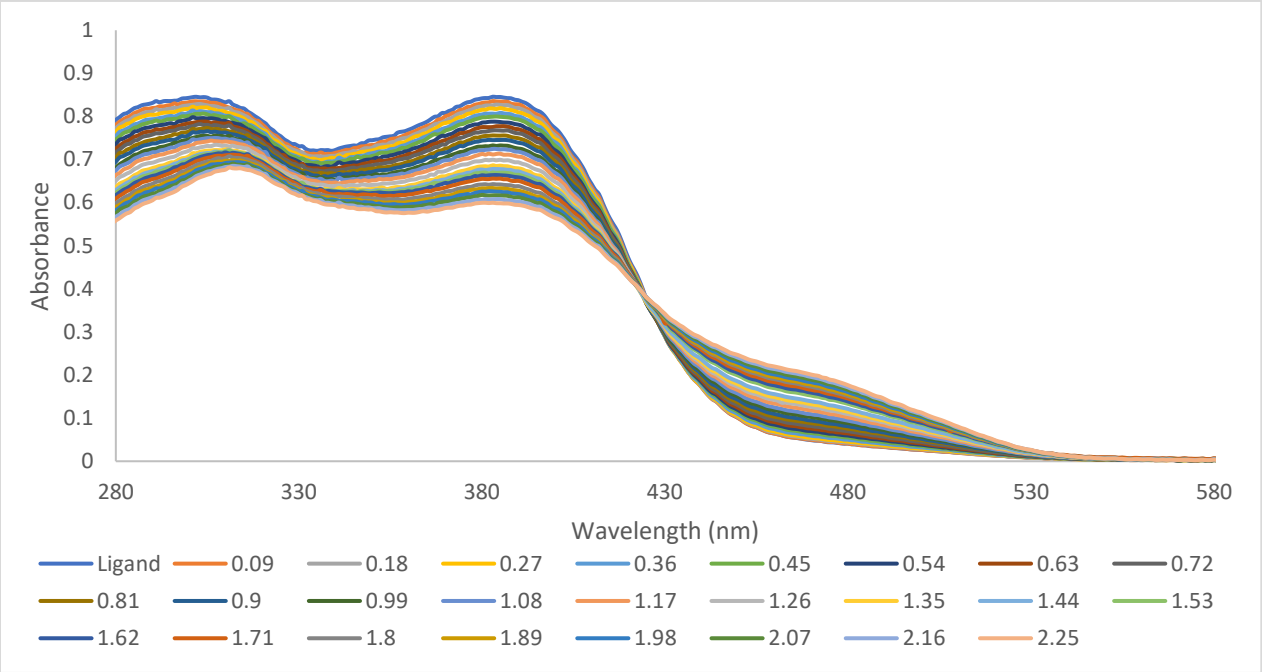

A.2.8 L1 (DMF) titration with Zinc (MeOH) (Shown at metal to ligand molar ratios of 0.09-2.25: 1)

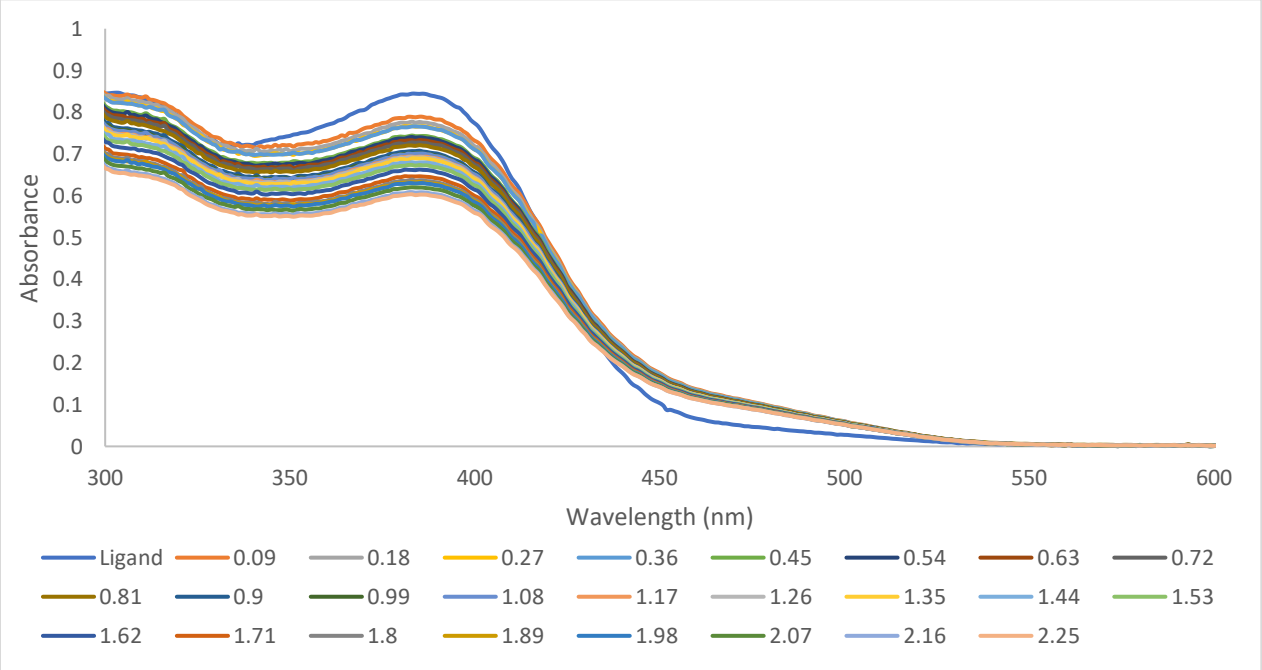

A.2.9 L1 (DMF) titration with Ytterbium (MeOH) (Shown at metal to ligand molar ratios of 0.09-2.25: 1)

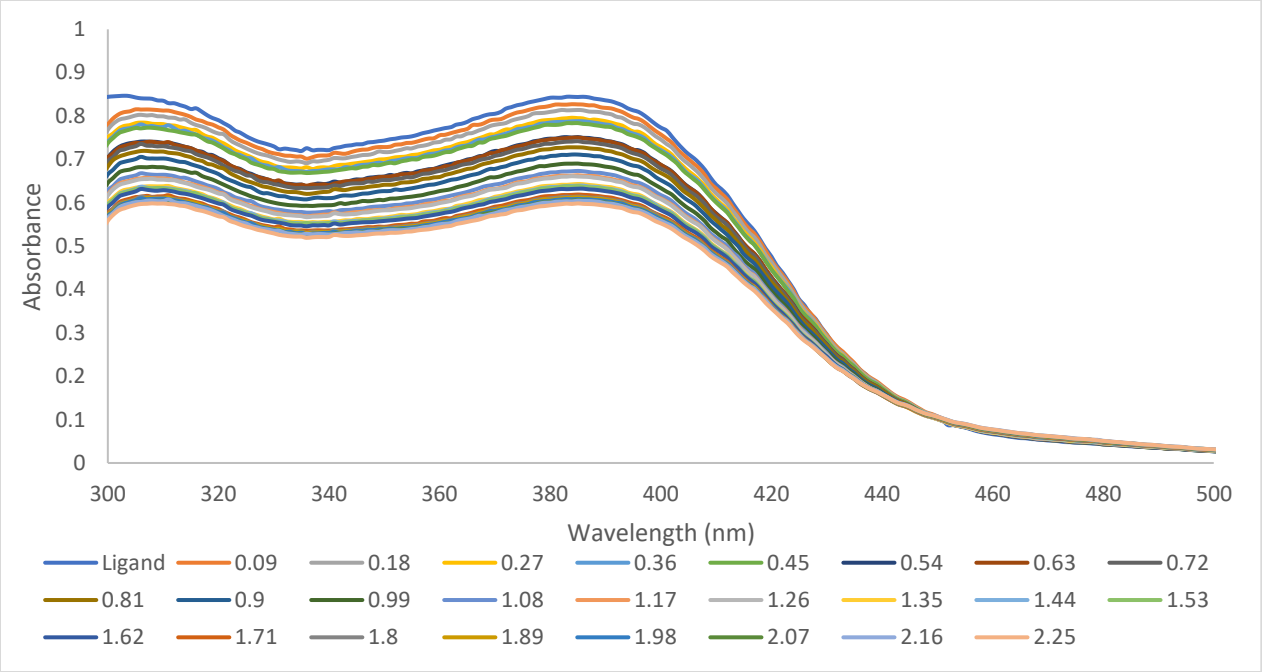

A.2.10 L1 (DMF) titration with Dysprosium (MeOH) (Shown at metal to ligand molar ratios of 0.09-2.25: 1)

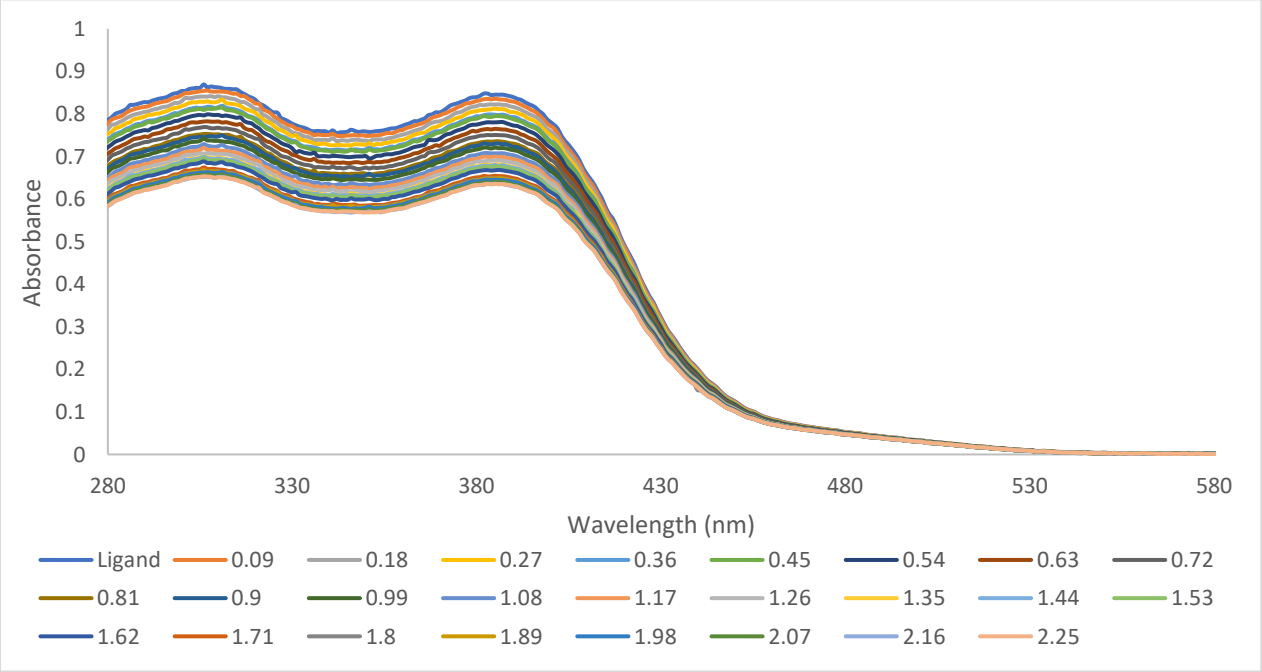

A.2.11 L1 (DMF) titration with Thorium (MeOH) (Shown at metal to ligand molar ratios of 0.09-2.25: 1)

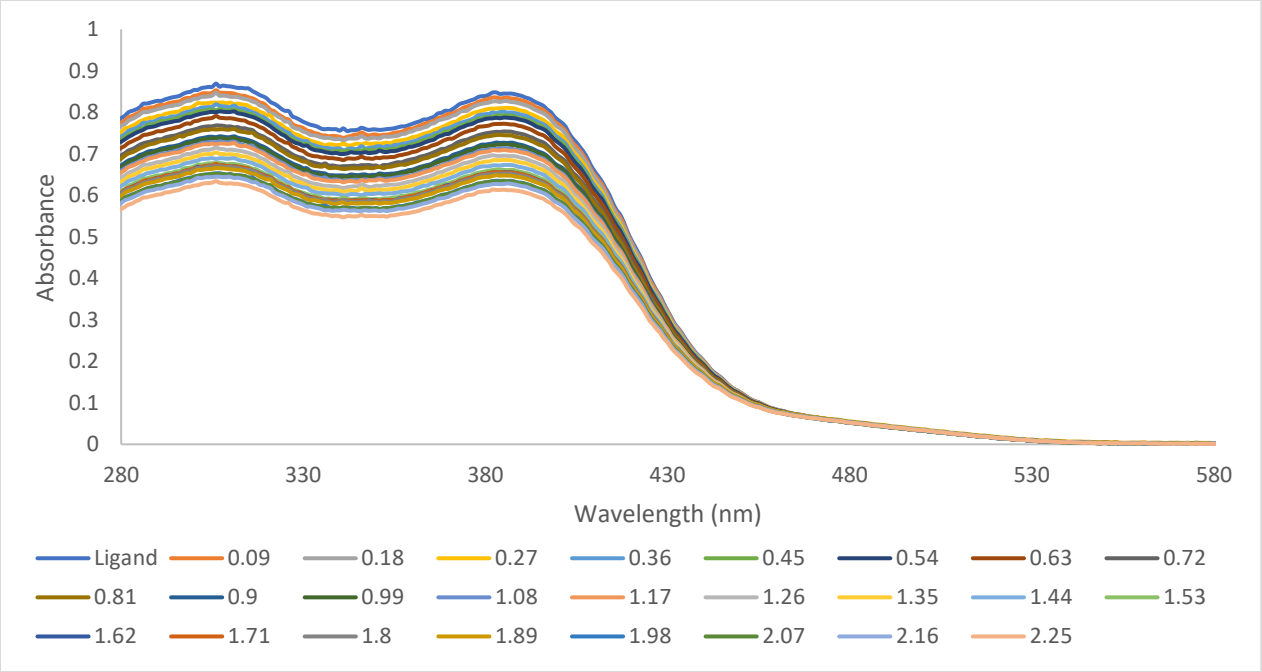

A.2.12 L1 (DMF) titration with Uranyl (MeOH) (Shown at metal to ligand molar ratios of 0.09-2.25: 1)

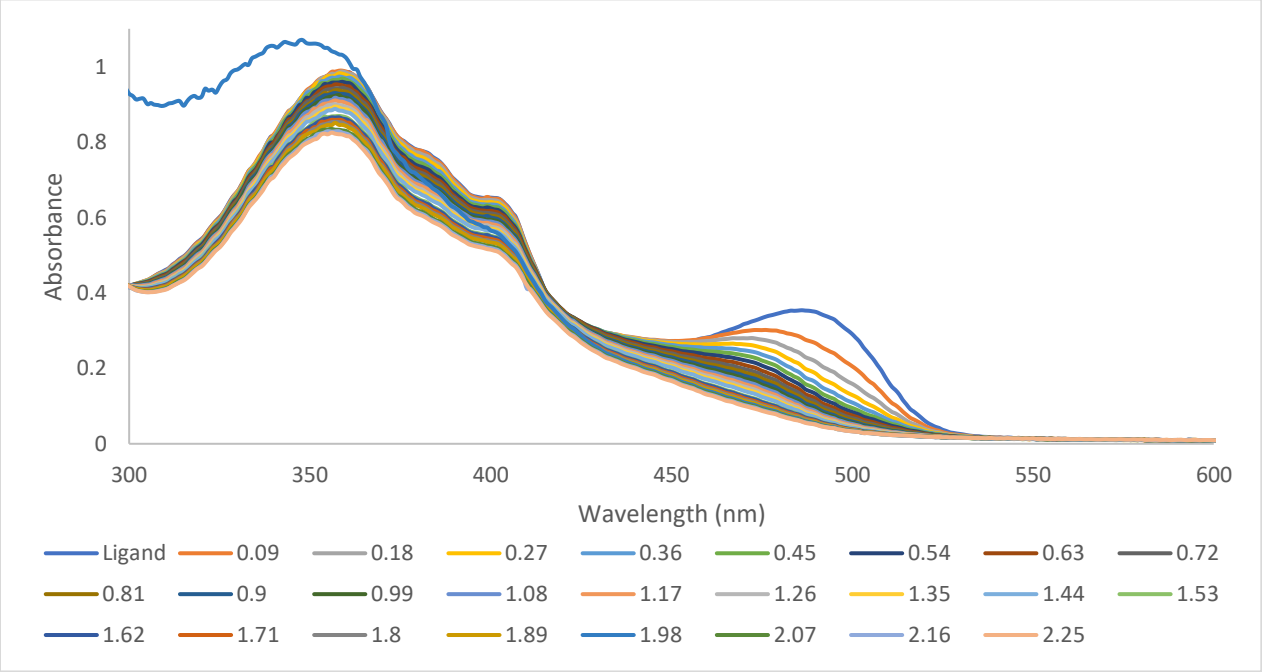

A.2.13 L2 (DMF) titration with Vanadyl (MeOH) (Shown at metal to ligand molar ratios of 0.09-2.25: 1)

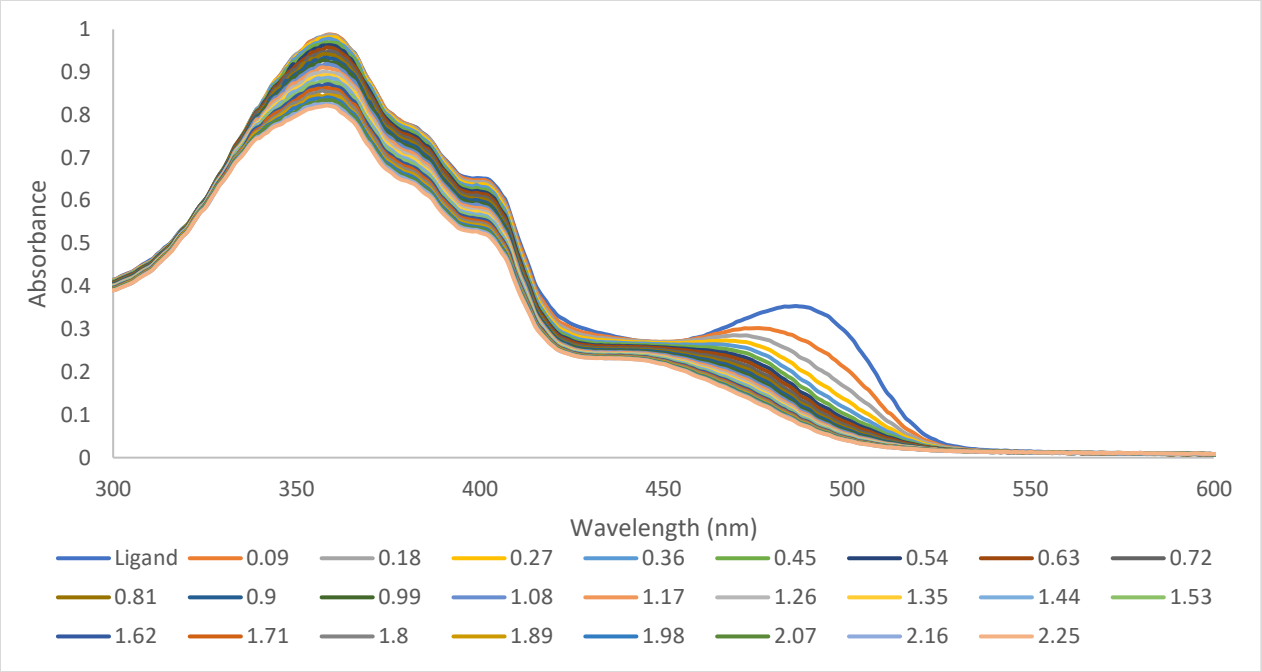

A.2.14 L2 (DMF) titration with Chromium (MeOH) (Shown at metal to ligand molar ratios of 0.09-2.25: 1)

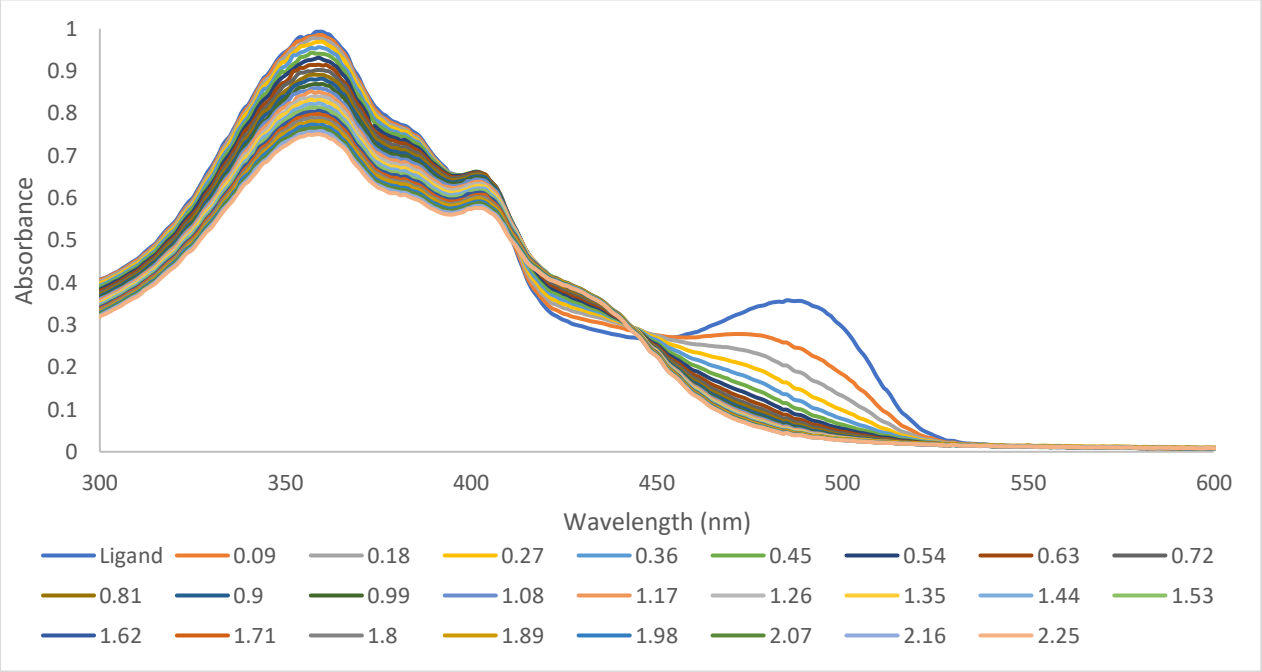

A.2.15 L2 (DMF) titration with Manganese (MeOH) (Shown at metal to ligand molar ratios of 0.09-2.25: 1)

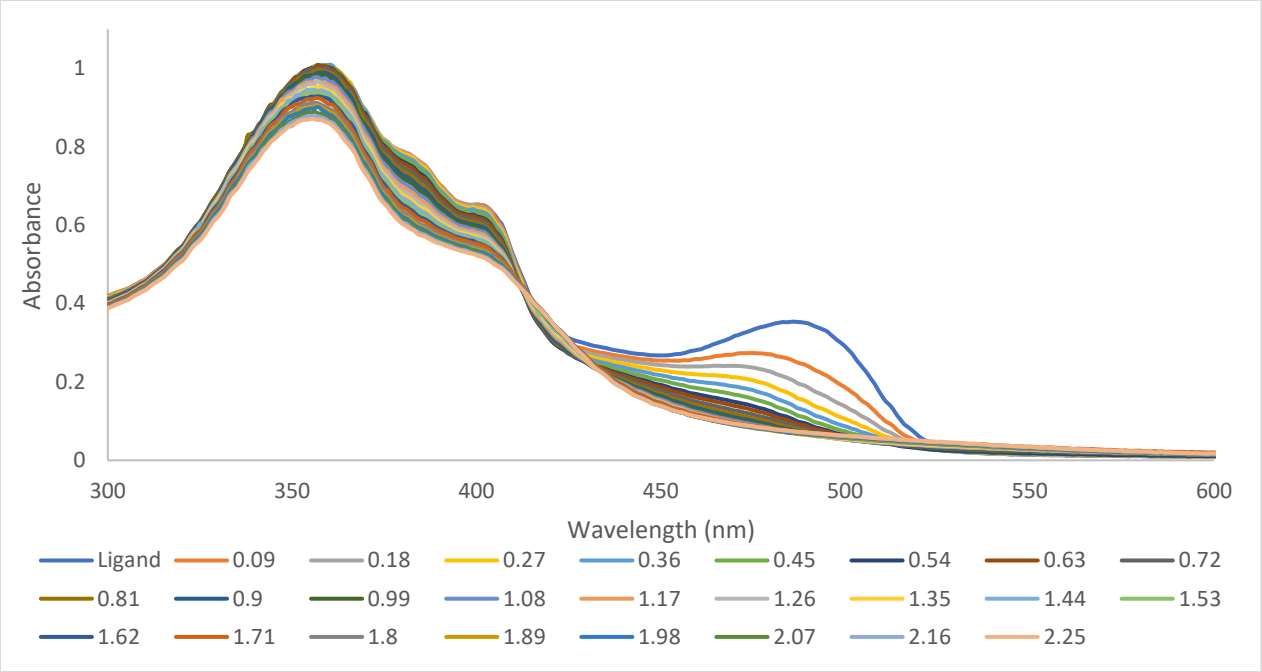

A.2.16 L2 (DMF) titration with Iron (MeOH) (Shown at metal to ligand molar ratios of 0.09-2.25: 1)

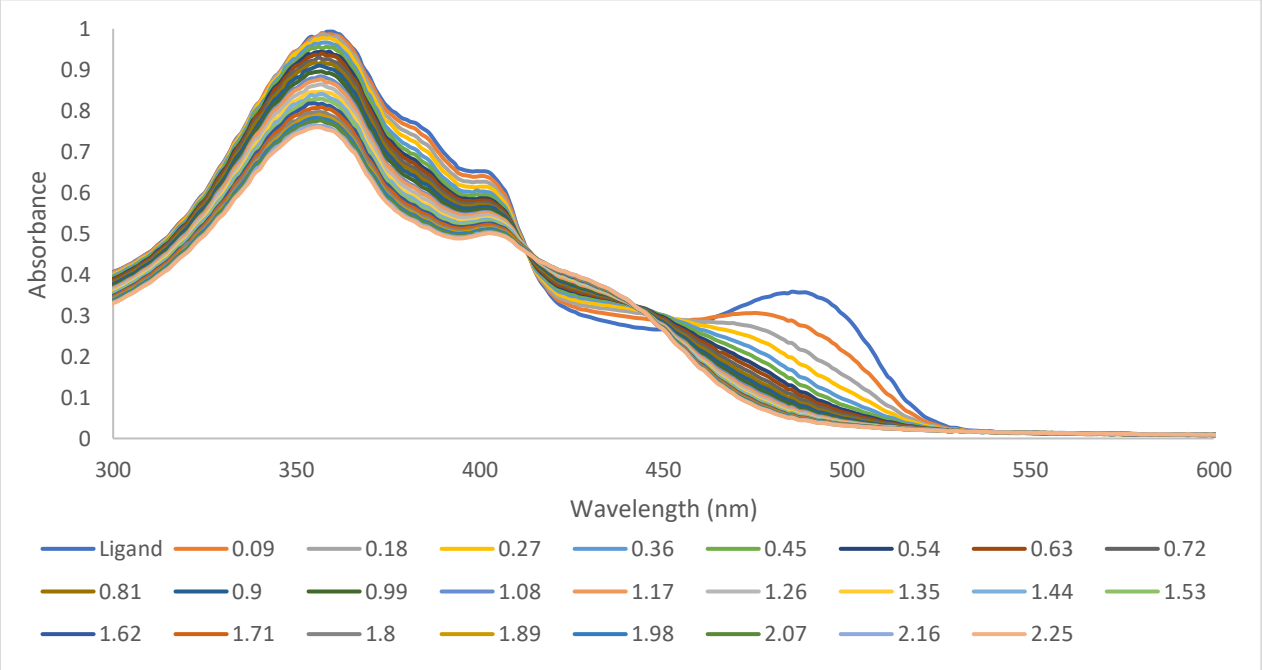

A.2.17 L2 (DMF) titration with Cobalt (MeOH) (Shown at metal to ligand molar ratios of 0.09-2.25: 1)

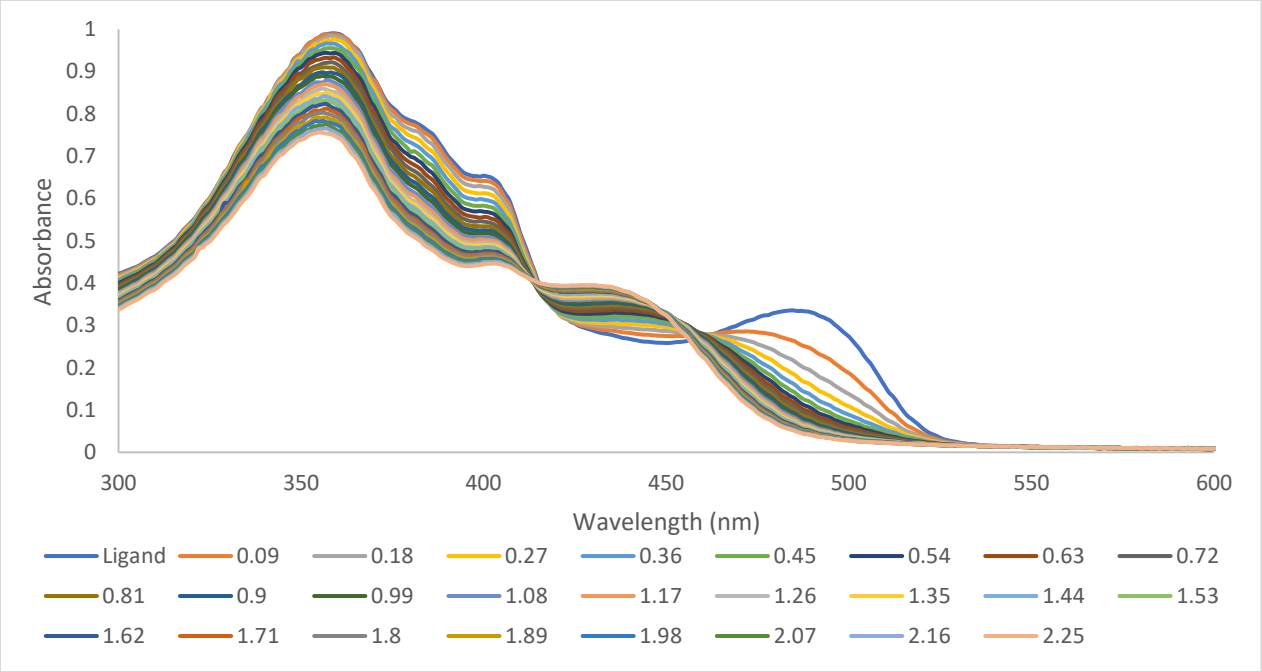

A.2.18 L2 (DMF) titration with Nickel (MeOH) (Shown at metal to ligand molar ratios of 0.09-2.25: 1)

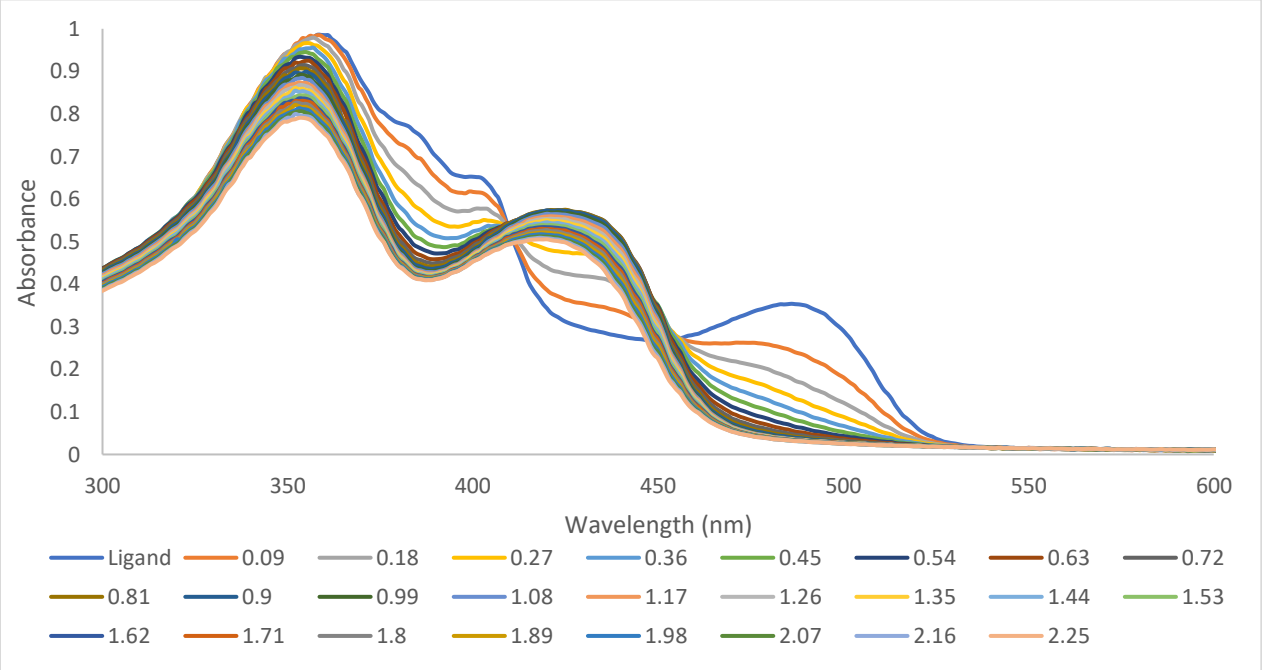

A.2.19 L2 (DMF) titration with Copper (MeOH) (Shown at metal to ligand molar ratios of 0.09-2.25: 1)

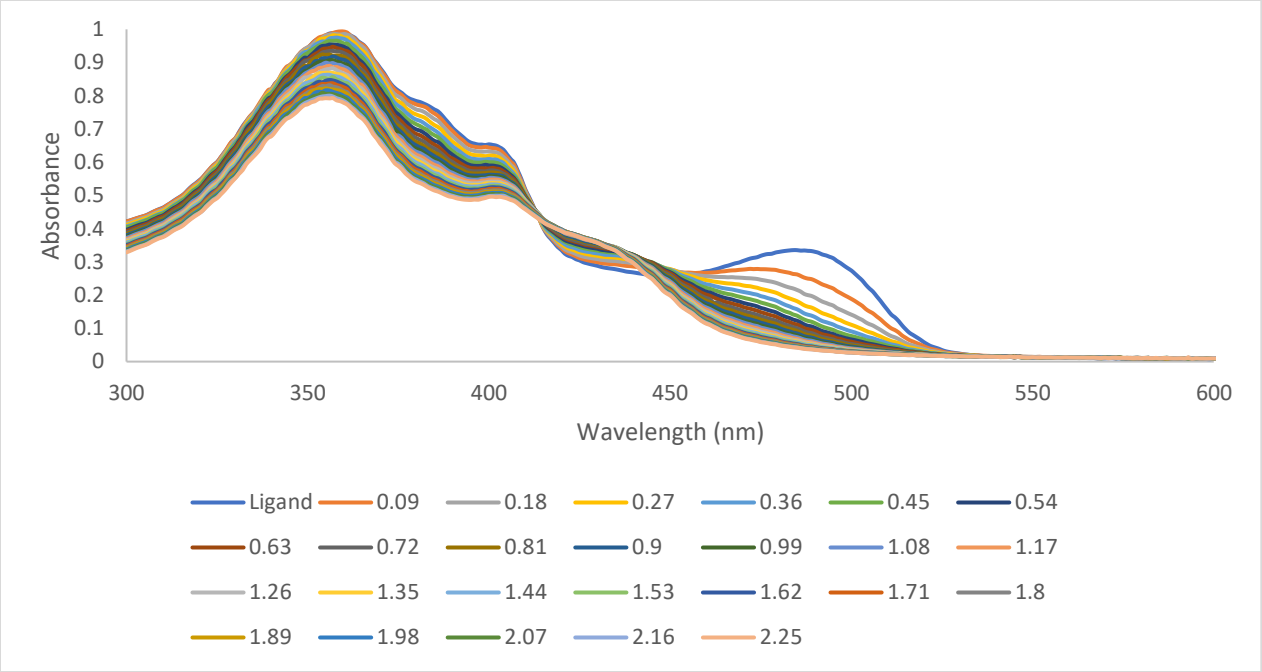

A.2.20 L2 (DMF) titration with Zinc (MeOH) (Shown at metal to ligand molar ratios of 0.09-2.25: 1)

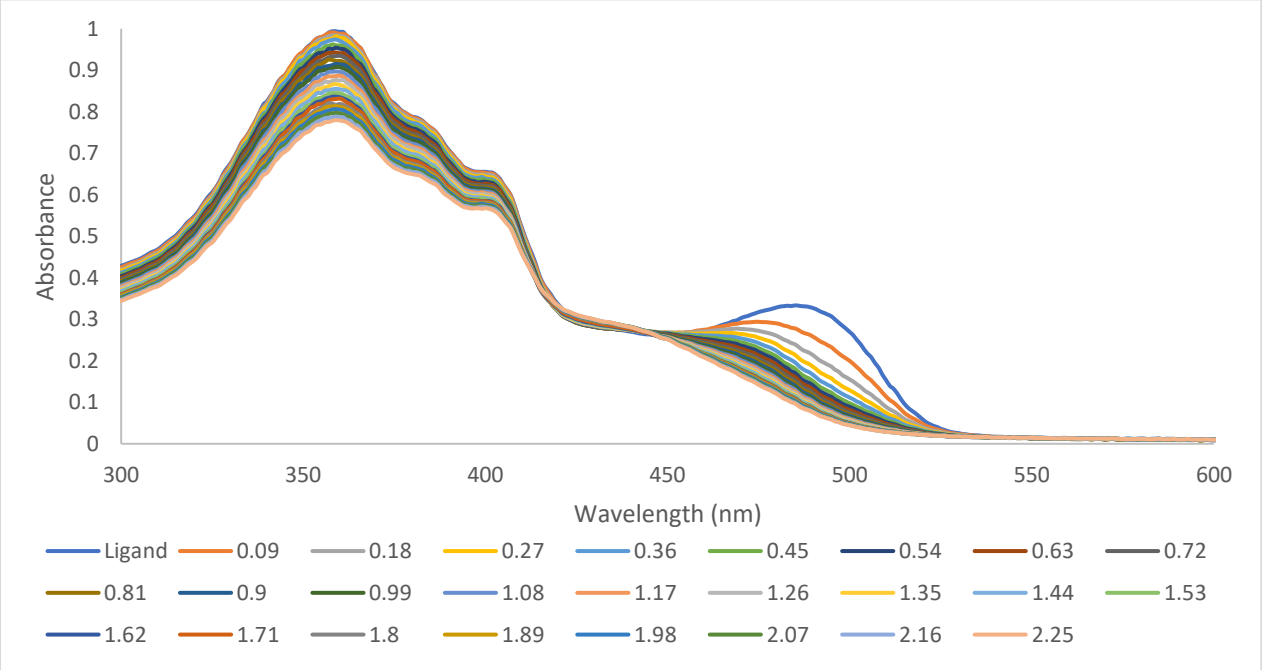

A.2.21 L2 (DMF) titration with Dysprosium (MeOH) (Shown at metal to ligand molar ratios of 0.09-2.25: 1)

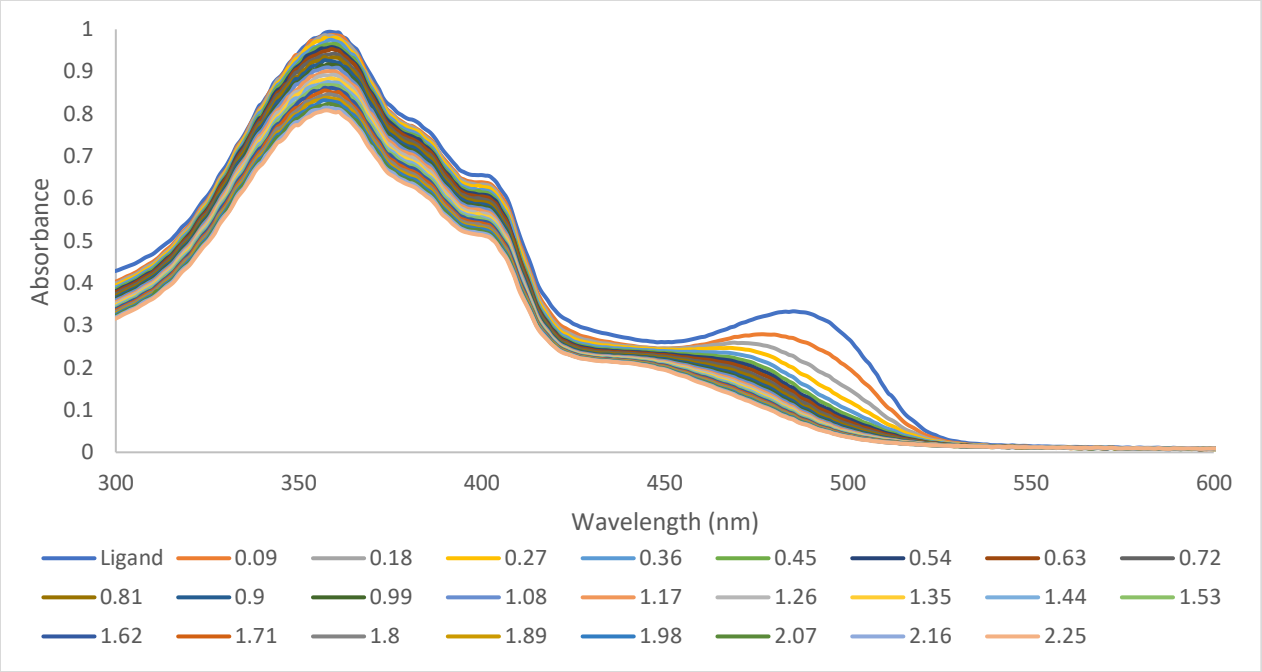

A.2.22 L2 (DMF) titration with Ytterbium (MeOH) (Shown at metal to ligand molar ratios of 0.09-2.25: 1)

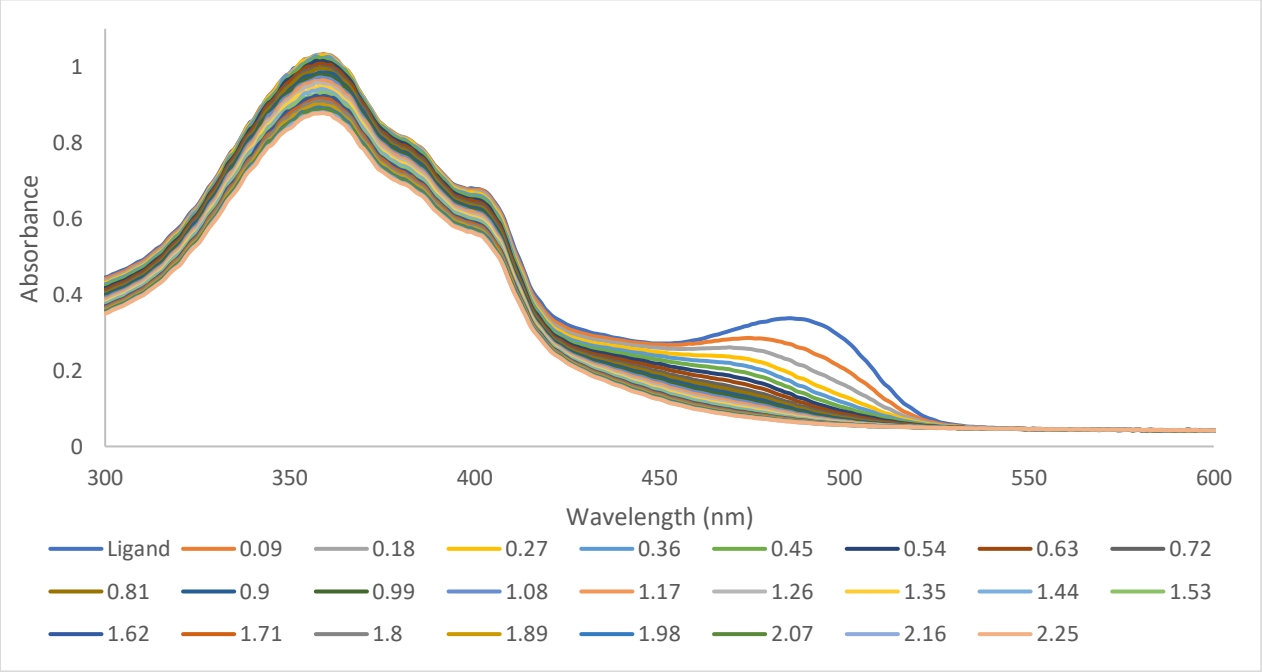

A.2.23 L2 (DMF) titration with Thorium (MeOH) (Shown at metal to ligand molar ratios of 0.09-2.25: 1)

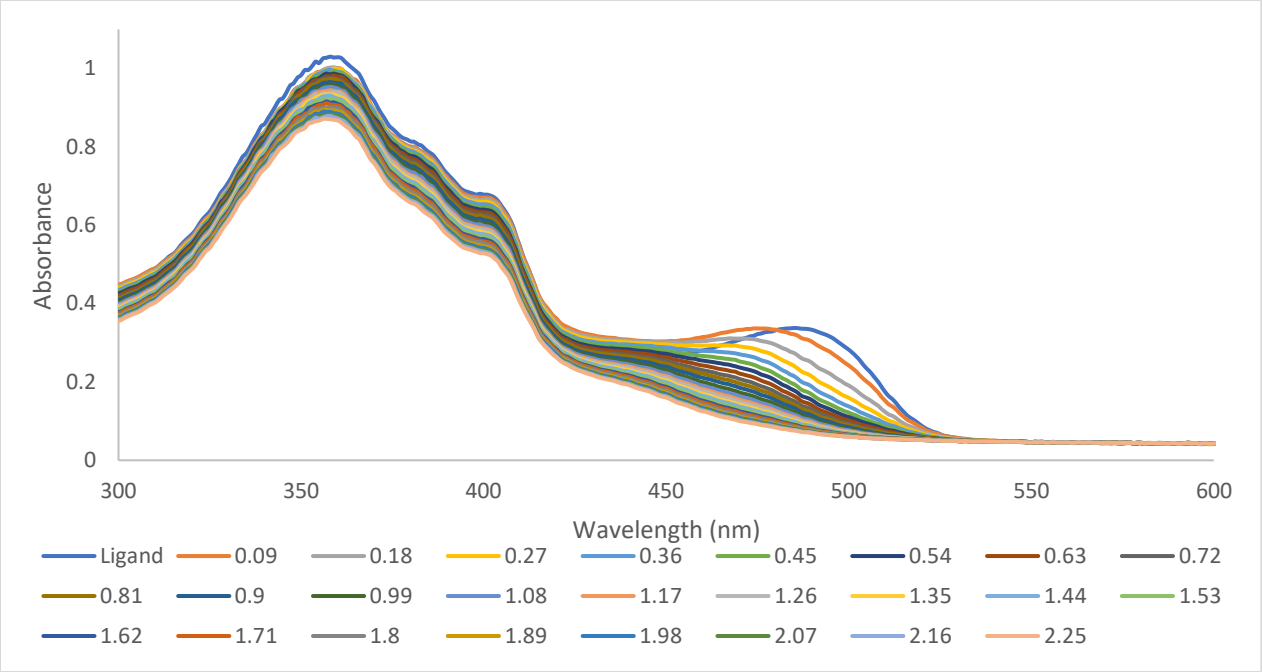

A.2.24 L2 (DMF) titration with Uranyl (MeOH) (Shown at metal to ligand molar ratios of 0.09-2.25: 1)

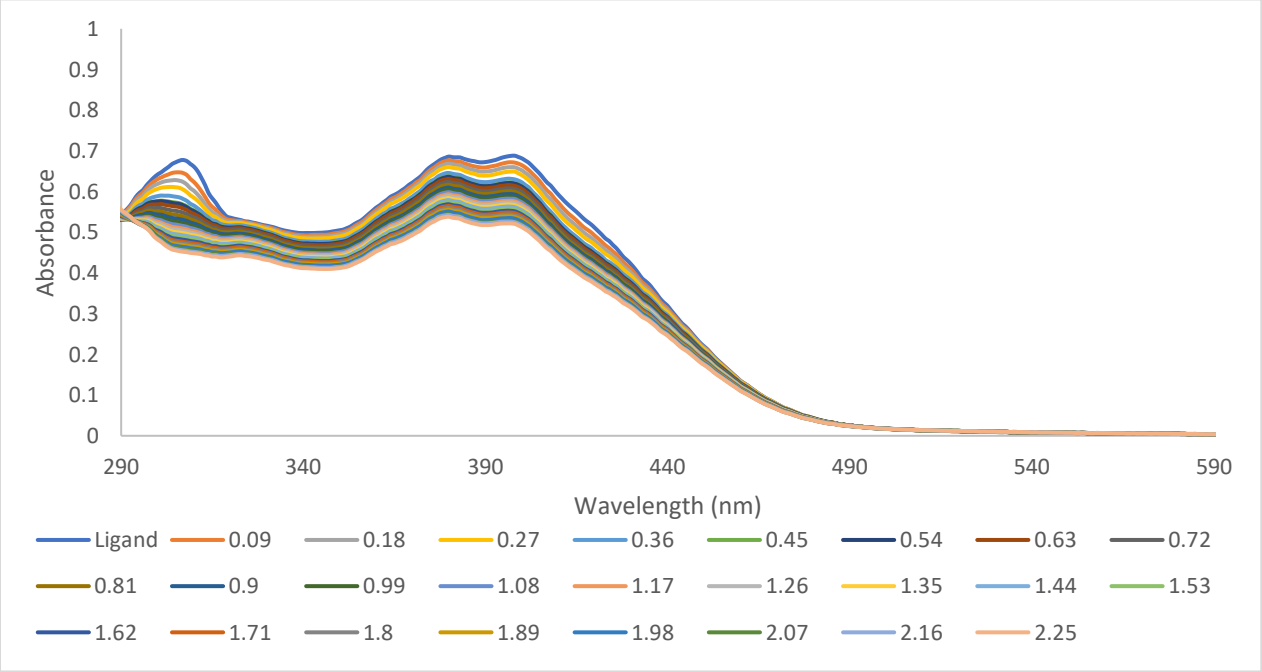

A.2.25 L3 (DMF) titration with Vanadyl (MeOH) (Shown at metal to ligand molar ratios of 0.09-2.25: 1)

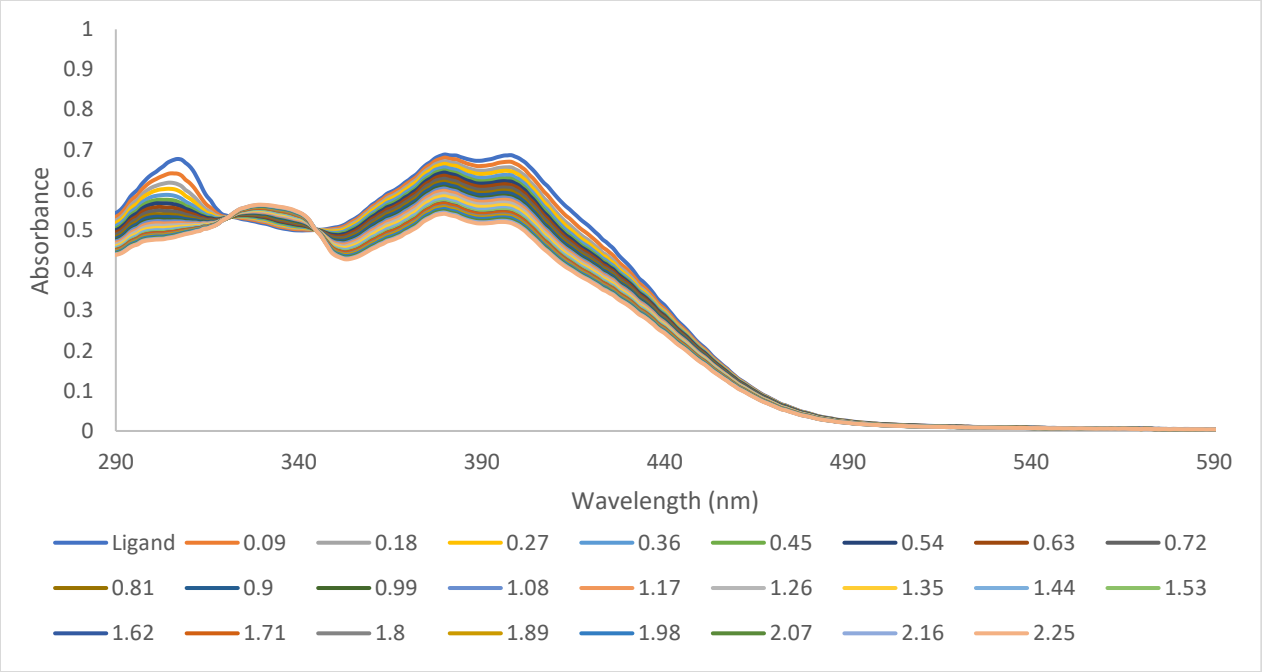

A.2.26 L3 (DMF) titration with Chromium (MeOH) (Shown at metal to ligand molar ratios of 0.09-2.25: 1)

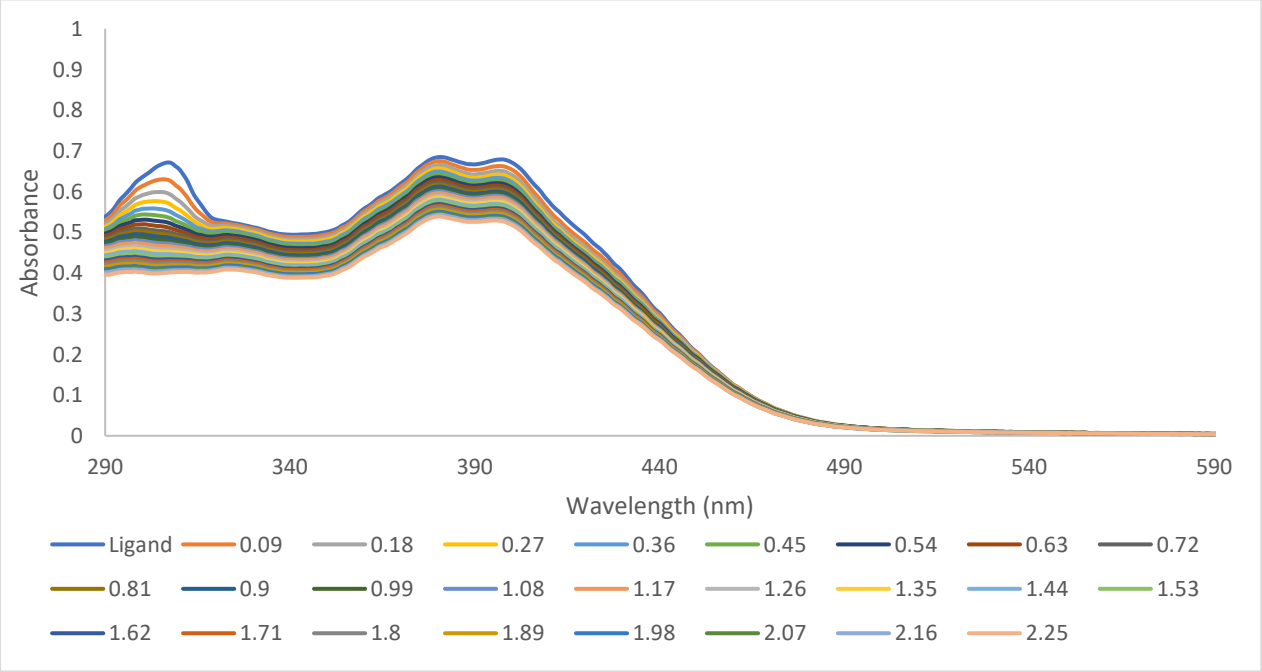

A.2.27 L3 (DMF) titration with Manganese (MeOH) (Shown at metal to ligand molar ratios of 0.09-2.25: 1)

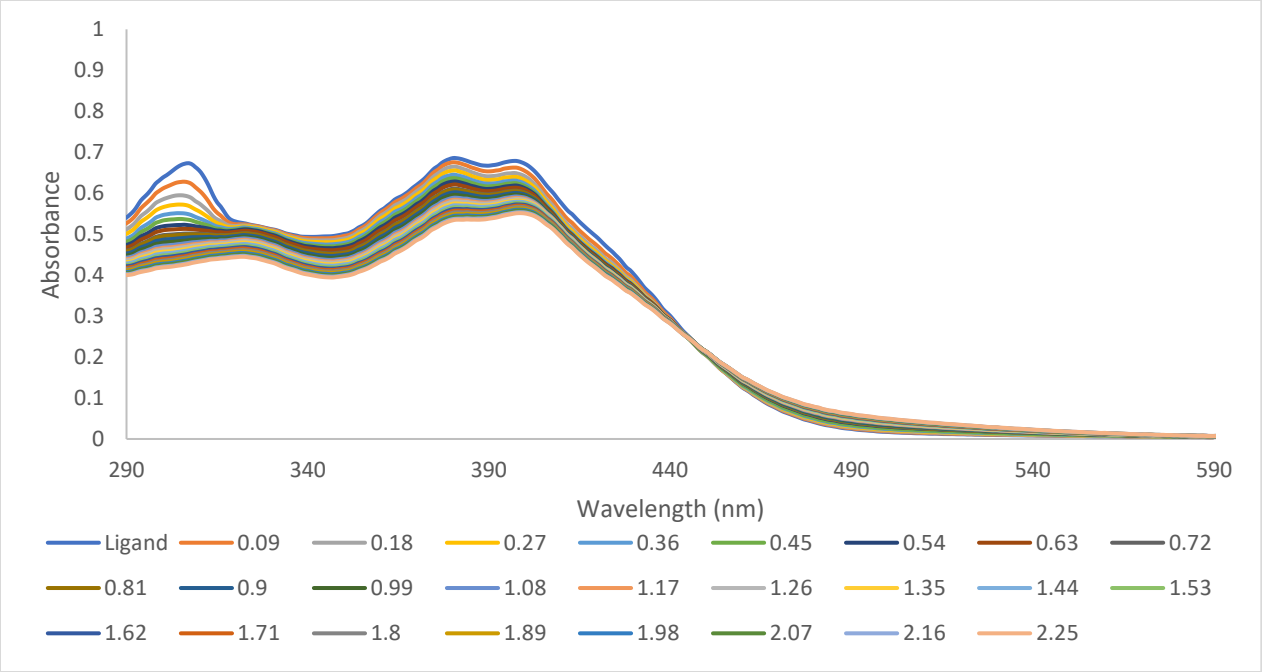

A.2.28 L3 (DMF) titration with Iron (MeOH) (Shown at metal to ligand molar ratios of 0.09-2.25: 1)

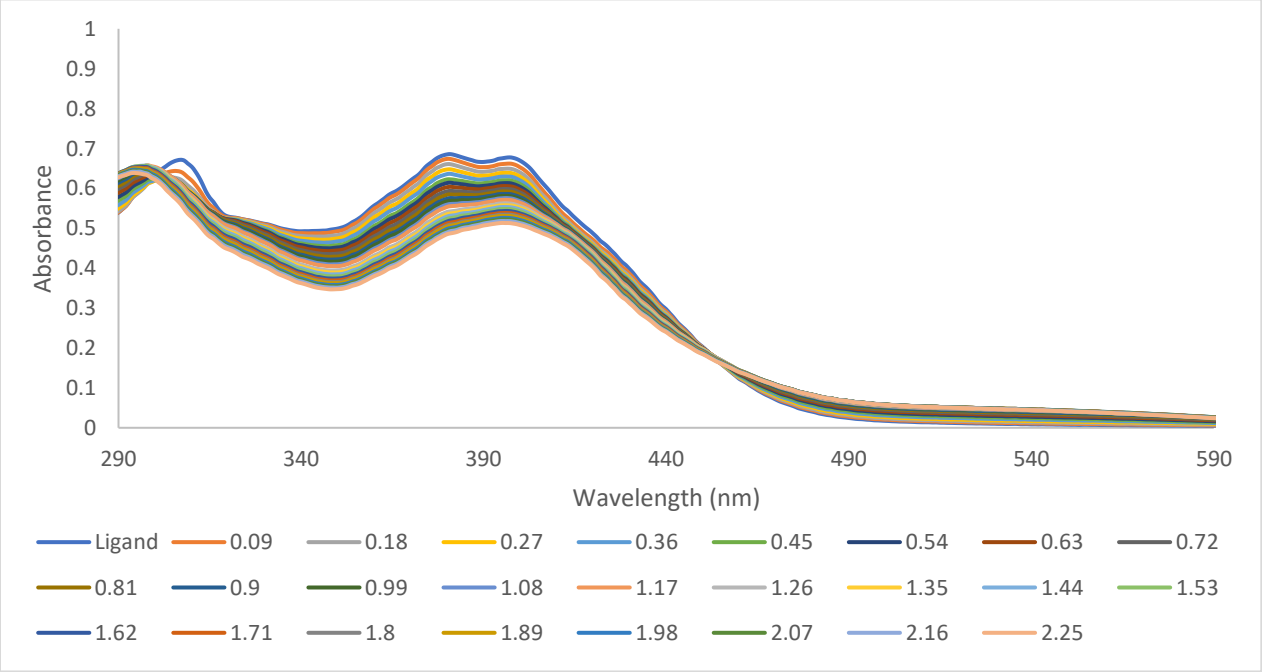

A.2.29 L3 (DMF) titration with Cobalt (MeOH) (Shown at metal to ligand molar ratios of 0.09-2.25: 1)

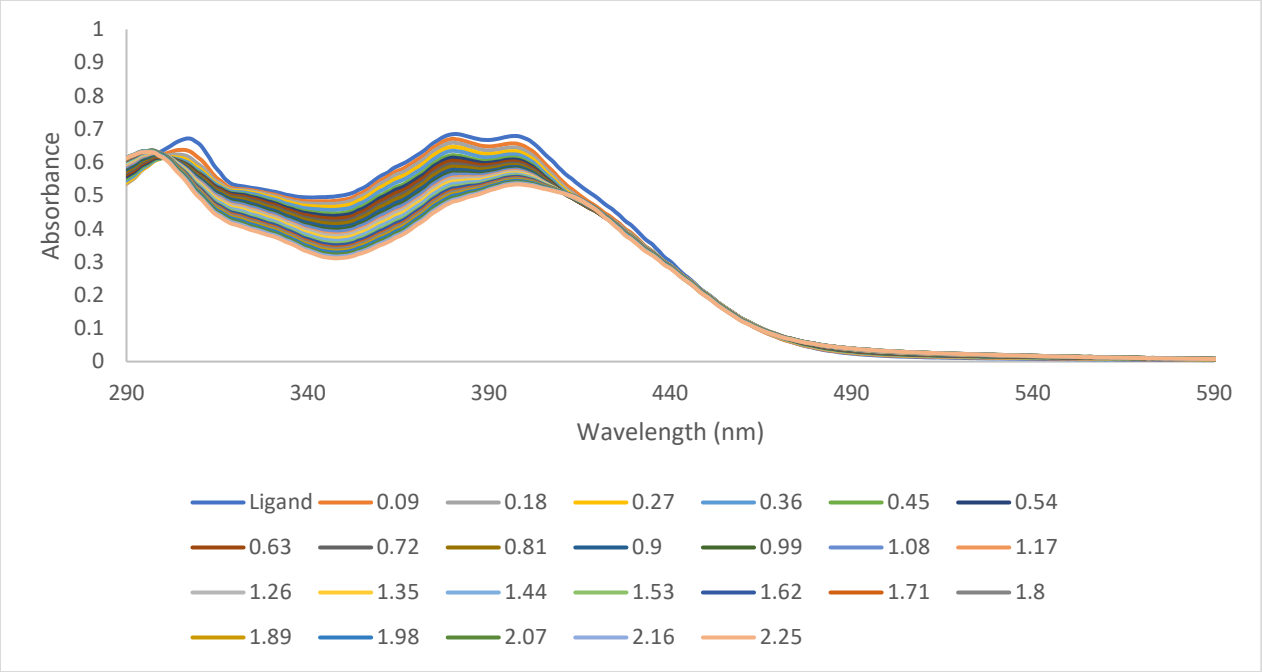

A.2.30 L3 (DMF) titration with Nickel (MeOH) (Shown at metal to ligand molar ratios of 0.09-2.25: 1)

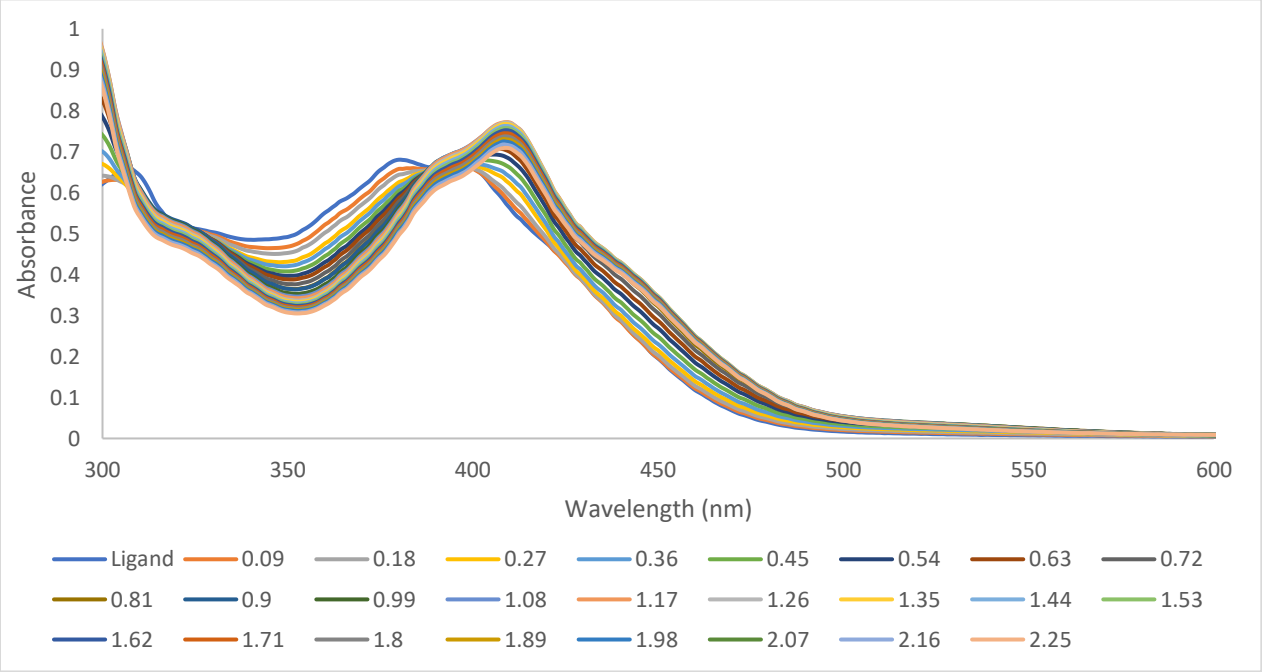

A.2.31 L3 (DMF) titration with Copper (MeOH) (Shown at metal to ligand molar ratios of 0.09-2.25: 1)

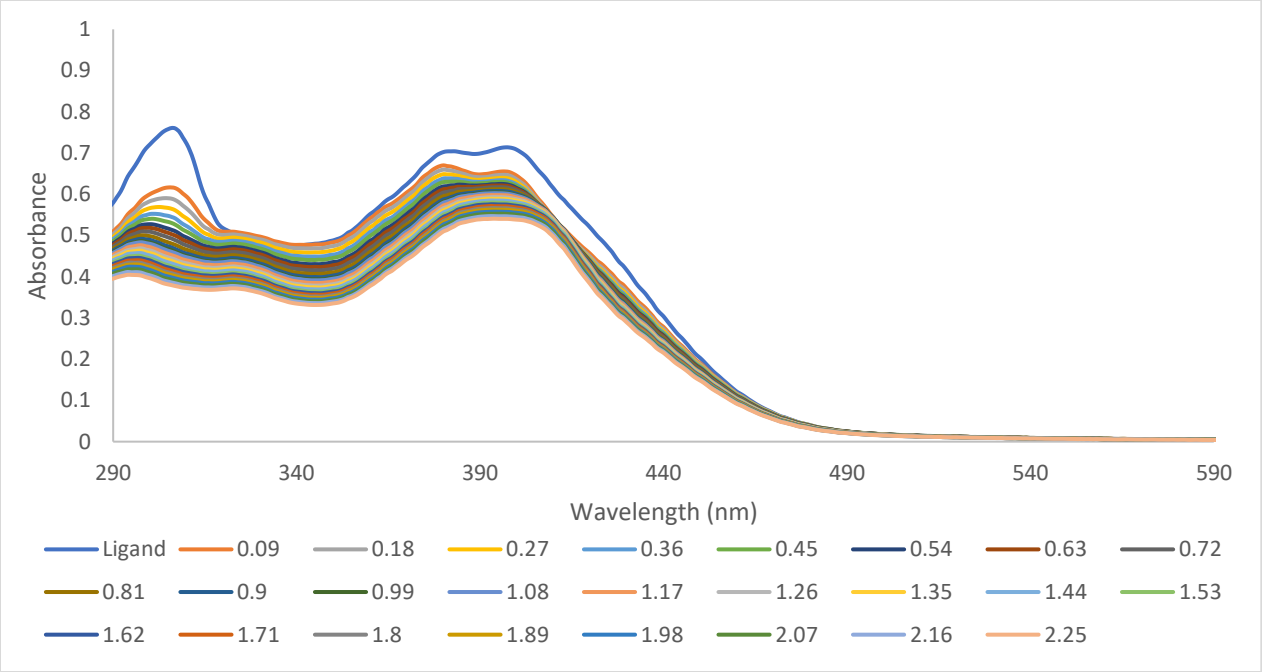

A.2.32 L3 (DMF) titration with Zinc (MeOH) (Shown at metal to ligand molar ratios of 0.09-2.25: 1)

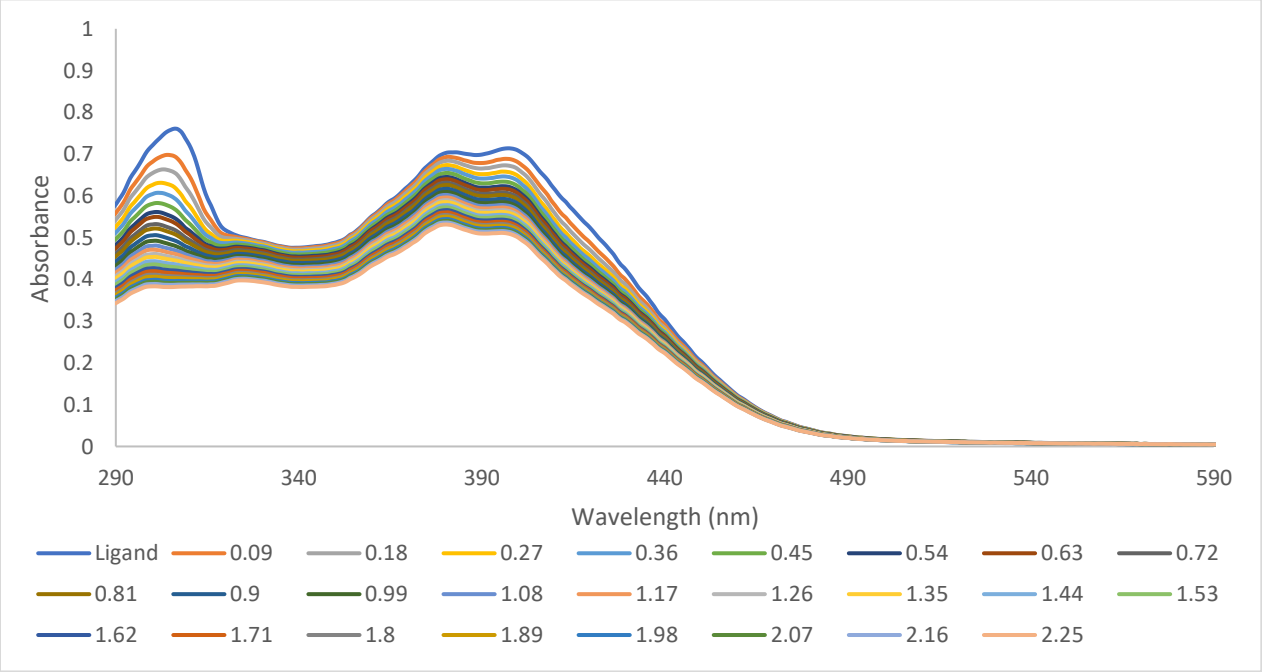

A.2.33 L3 (DMF) titration with Dysprosium (MeOH) (Shown at metal to ligand molar ratios of 0.09-2.25: 1)

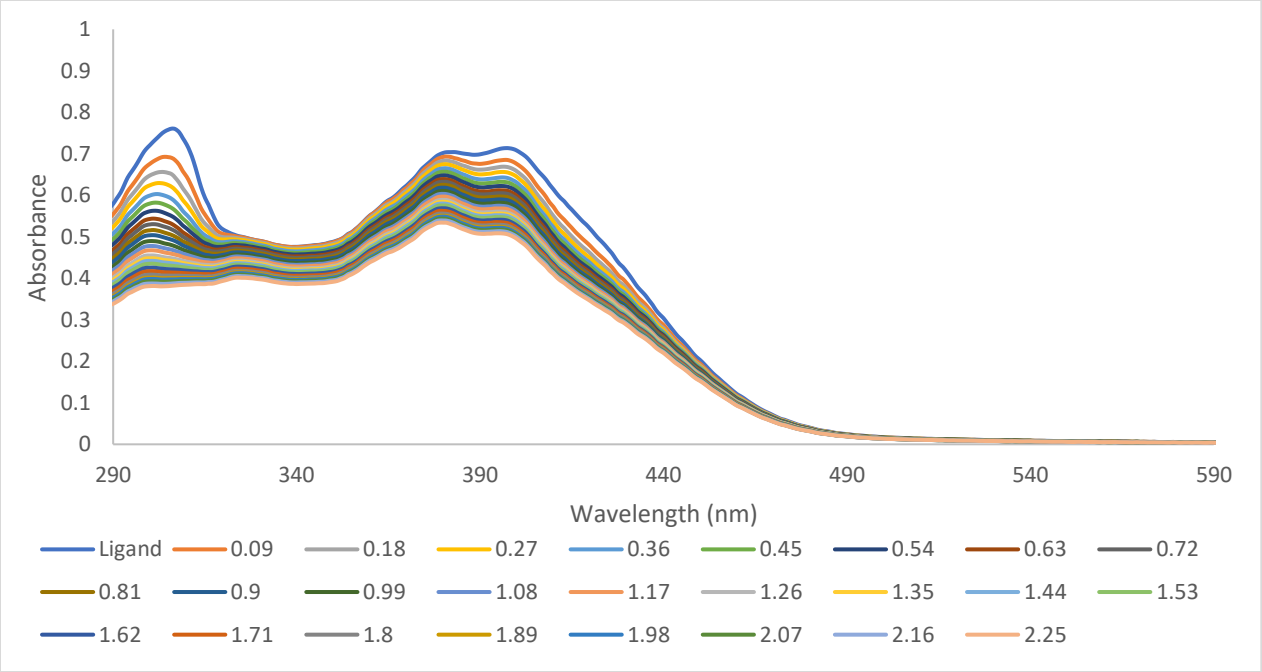

A.2.34 L3 (DMF) titration with Ytterbium (MeOH) (Shown at metal to ligand molar ratios of 0.09-2.25: 1)

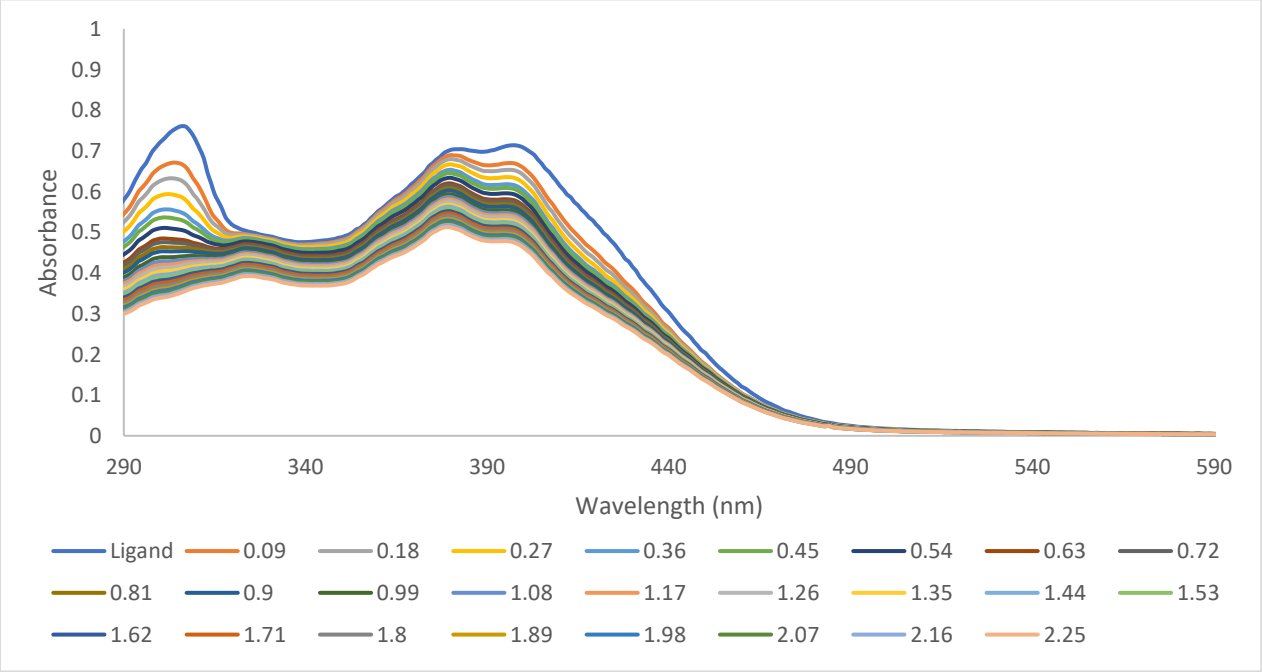

A.2.35 L3 (DMF) titration with Thorium (MeOH) (Shown at metal to ligand molar ratios of 0.09-2.25: 1)

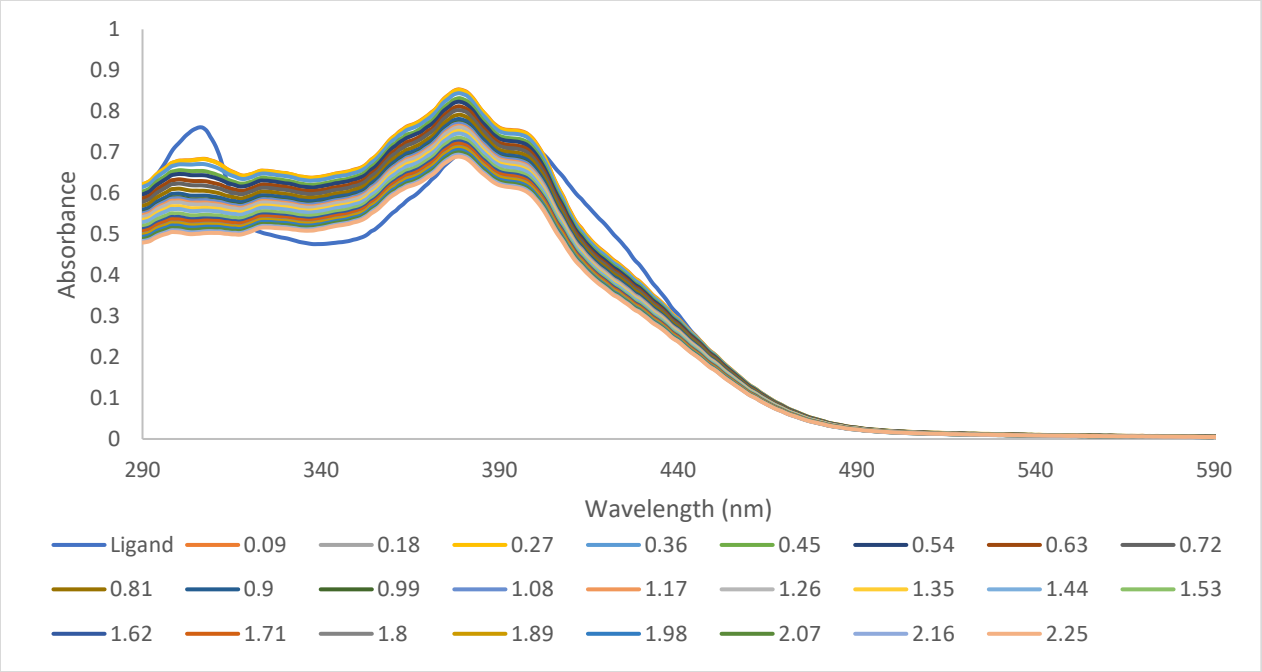

A.2.36 L3 (DMF) titration with Uranyl (MeOH) (Shown at metal to ligand molar ratios of 0.09-2.25: 1)

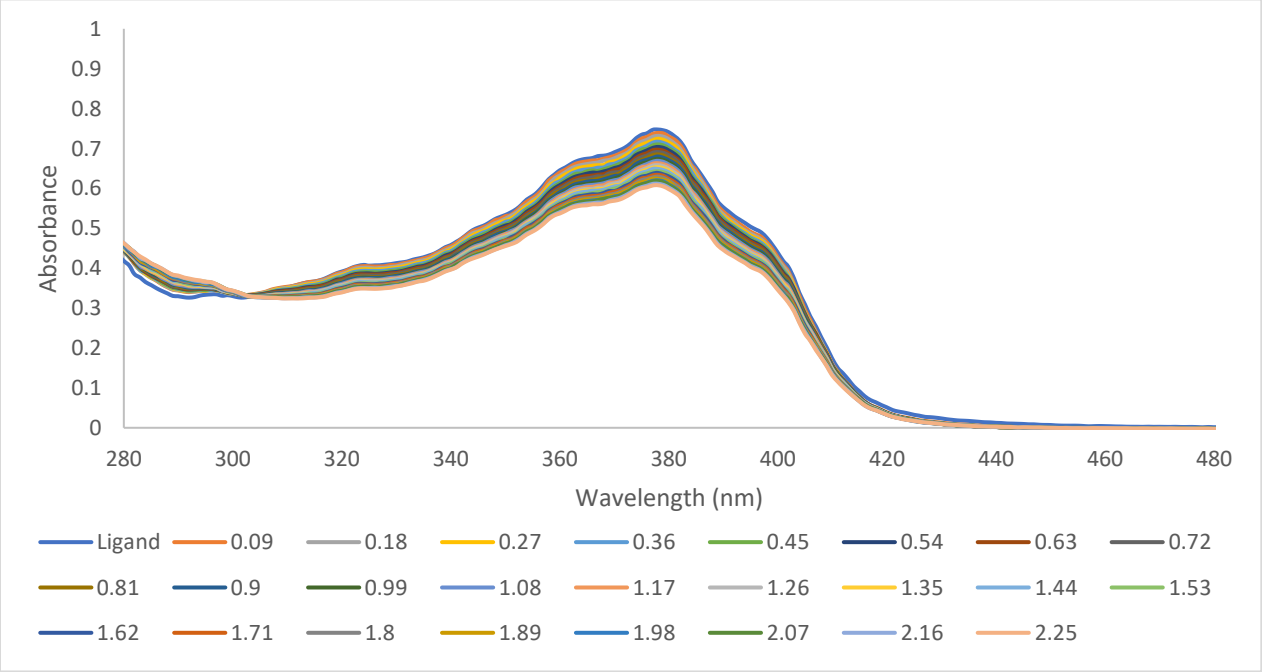

A.2.37 L4 (DMF) titration with Vanadyl (MeOH) (Shown at metal to ligand molar ratios of 0.09-2.25: 1)

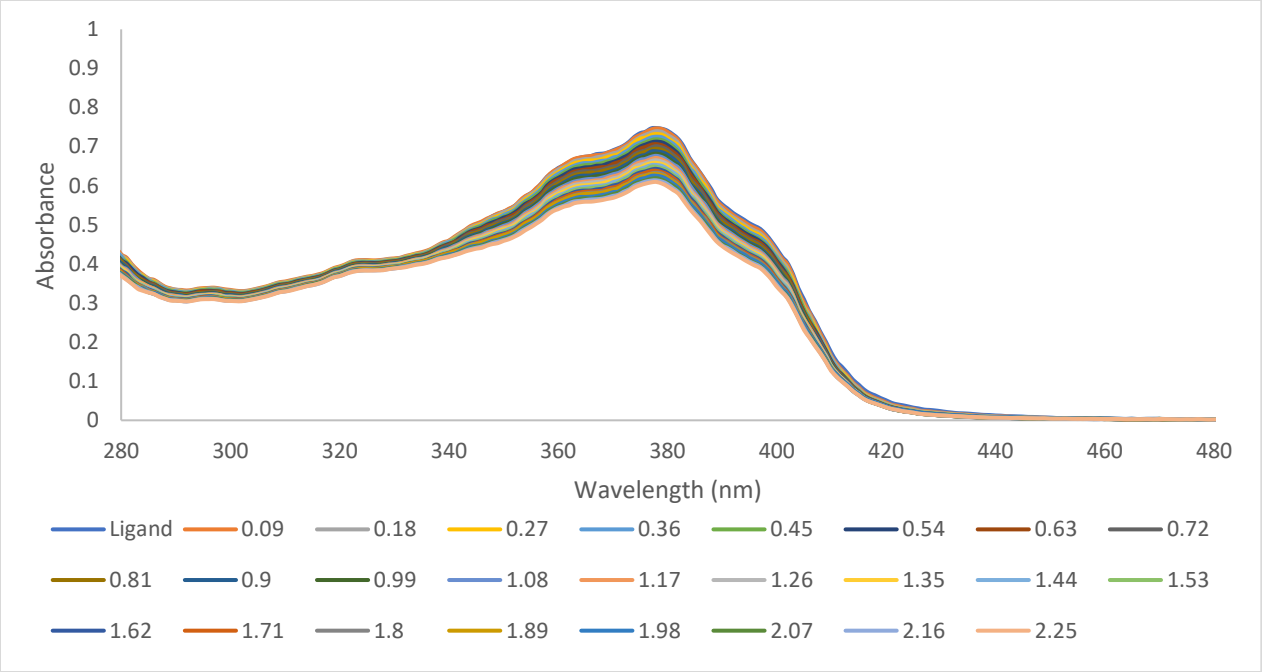

A.2.38 L4 (DMF) titration with Chromium (MeOH) (Shown at metal to ligand molar ratios of 0.09-2.25: 1)

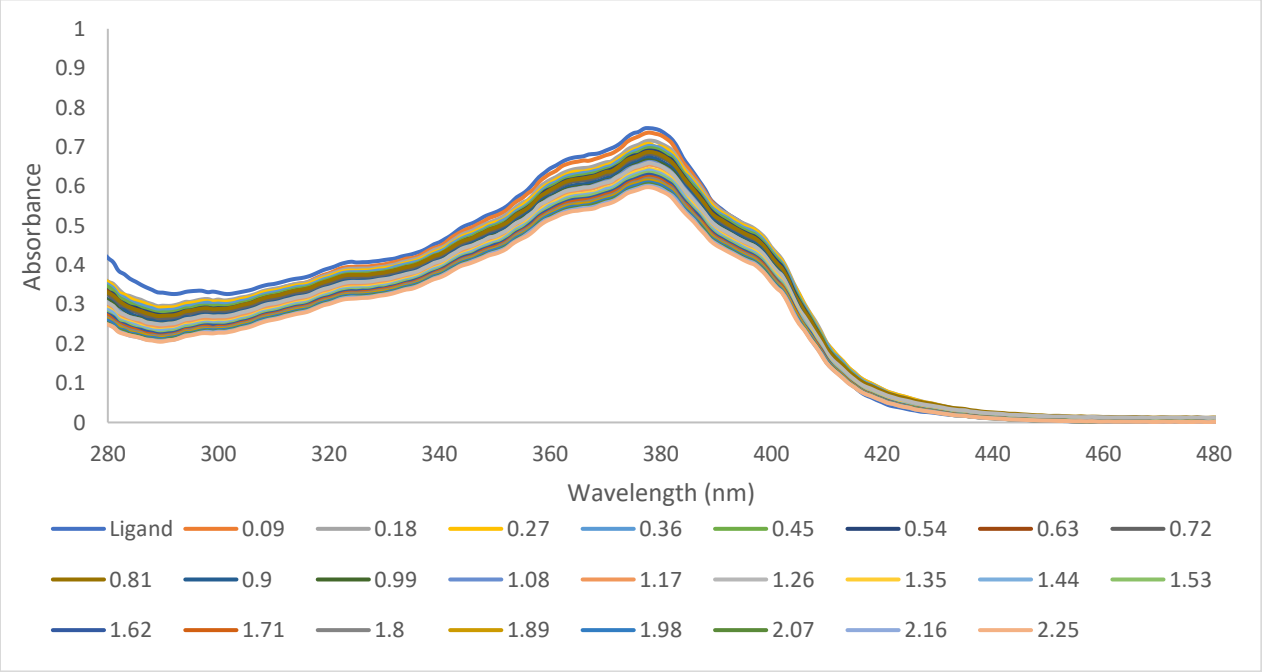

A.2.39 L4 (DMF) titration with Manganese (MeOH) (Shown at metal to ligand molar ratios of 0.09-2.25: 1)

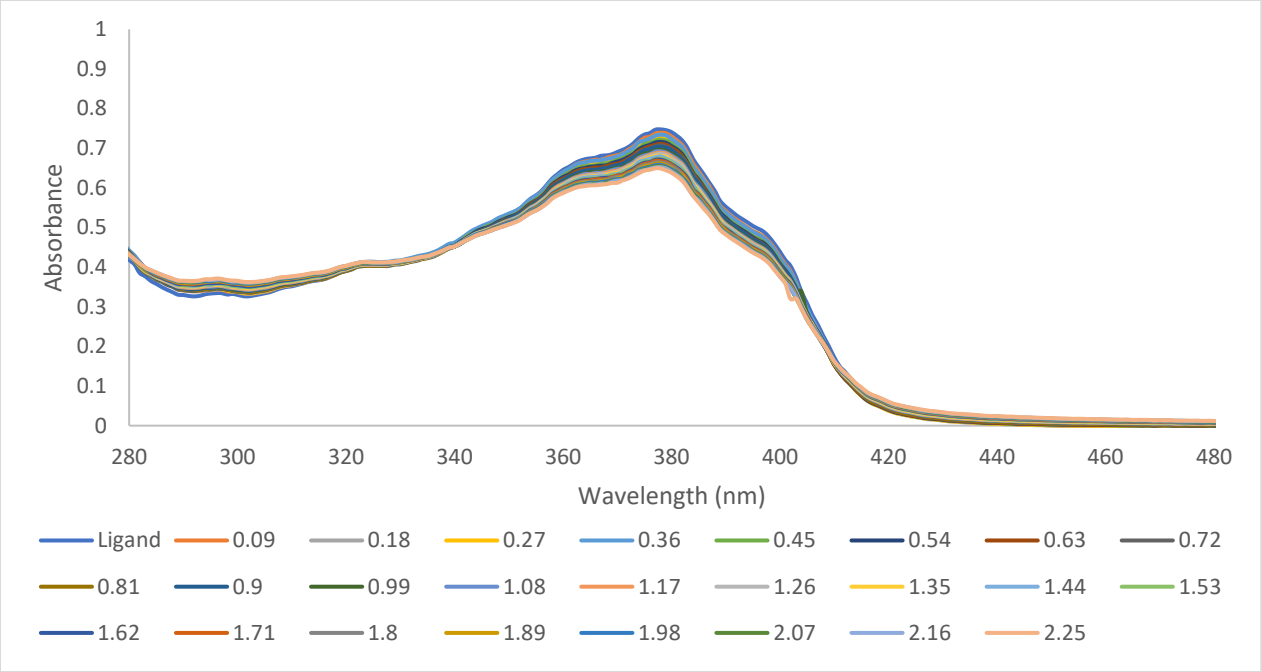

A.2.40 L4 (DMF) titration with Iron (MeOH) (Shown at metal to ligand molar ratios of 0.09-2.25: 1)

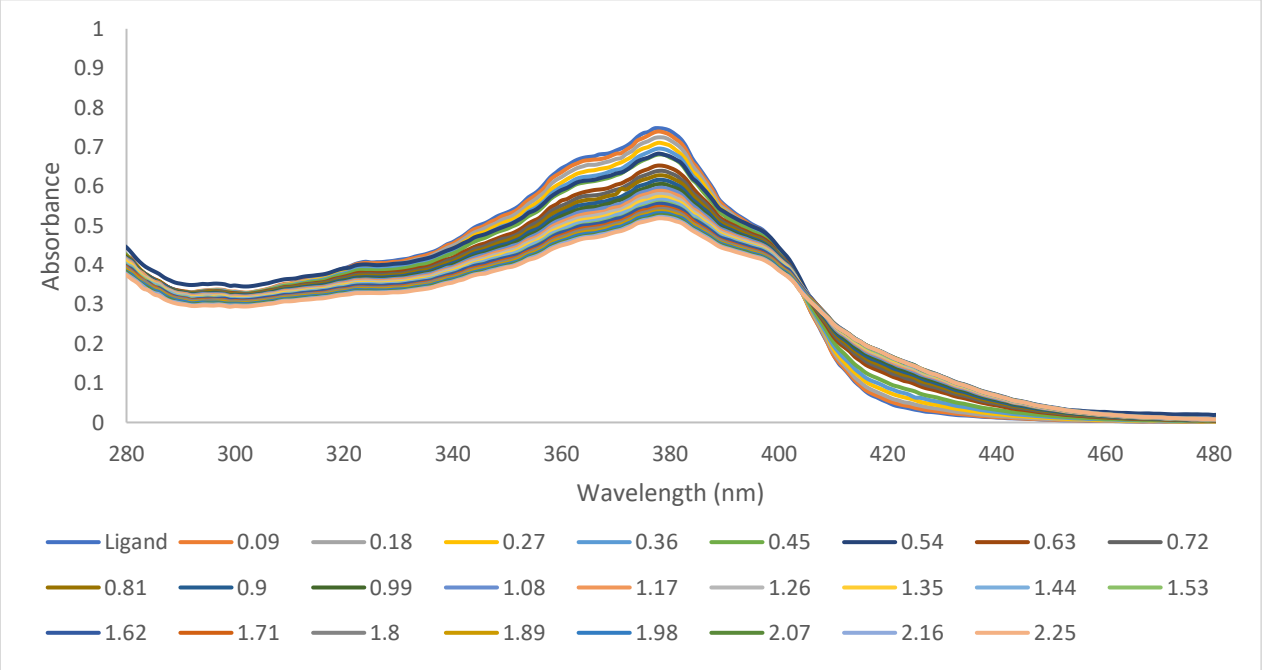

A.2.41 L4 (DMF) titration with Cobalt (MeOH) (Shown at metal to ligand molar ratios of 0.09-2.25: 1)

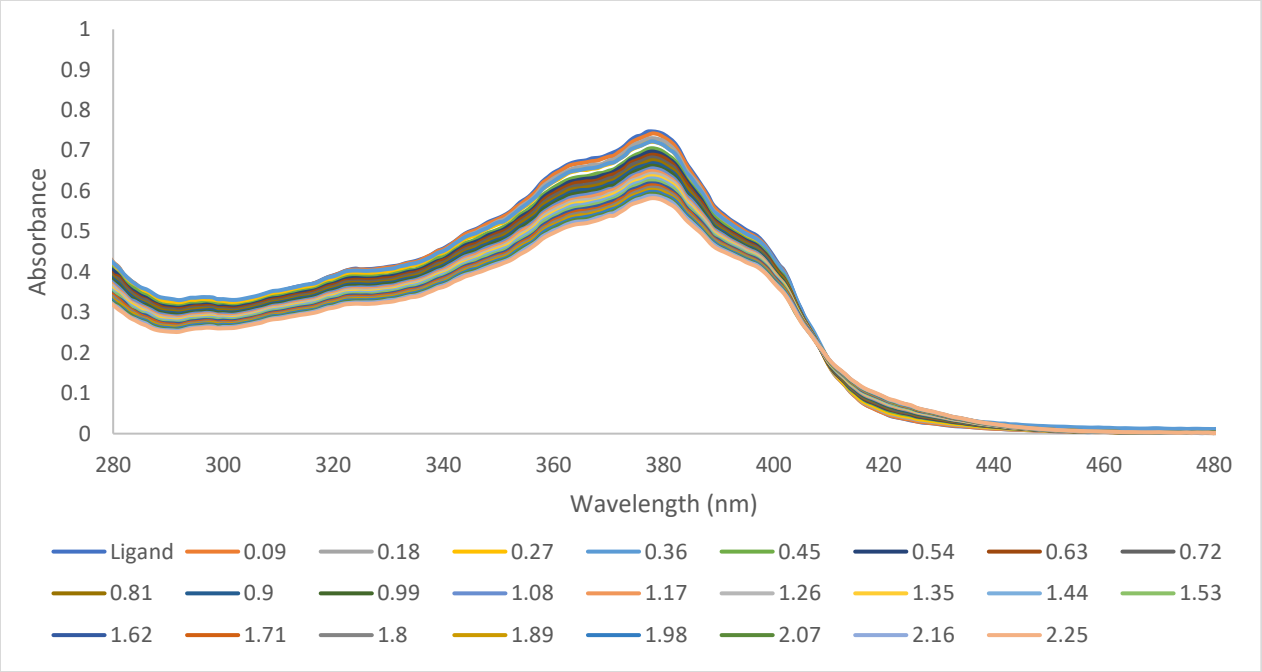

A.2.42 L4 (DMF) titration with Nickel (MeOH) (Shown at metal to ligand molar ratios of 0.09-2.25: 1)

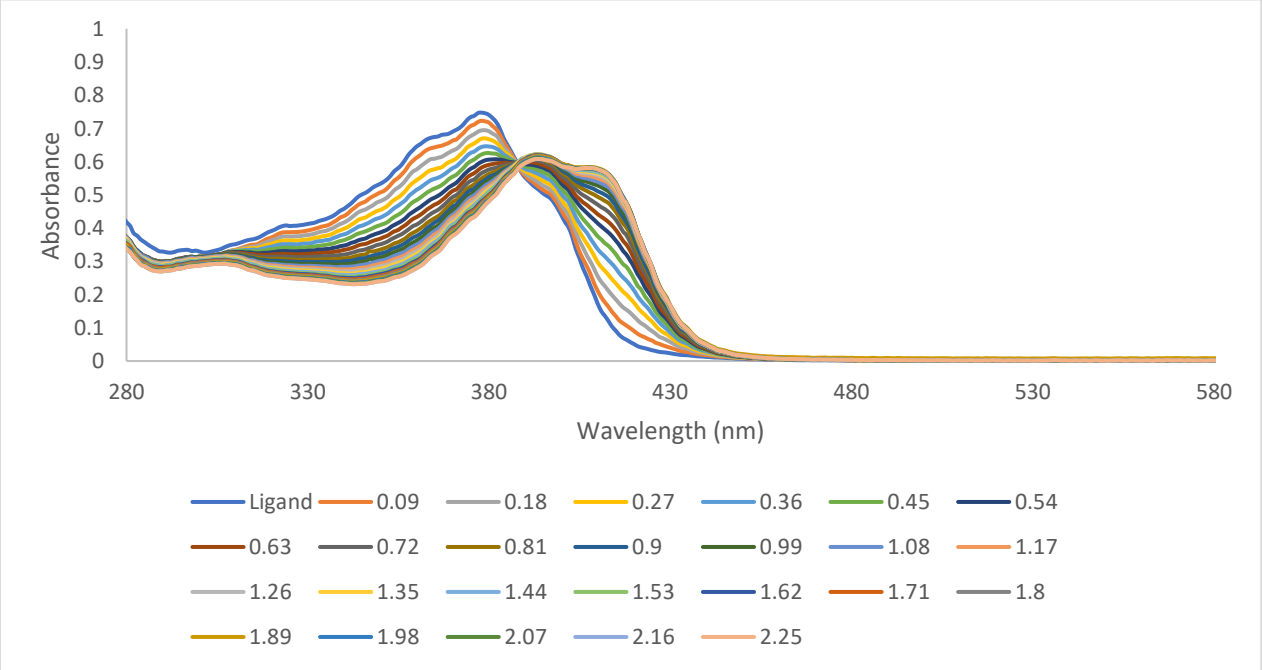

A.2.43 L4 (DMF) titration with Copper (MeOH) (Shown at metal to ligand molar ratios of 0.09-2.25: 1)

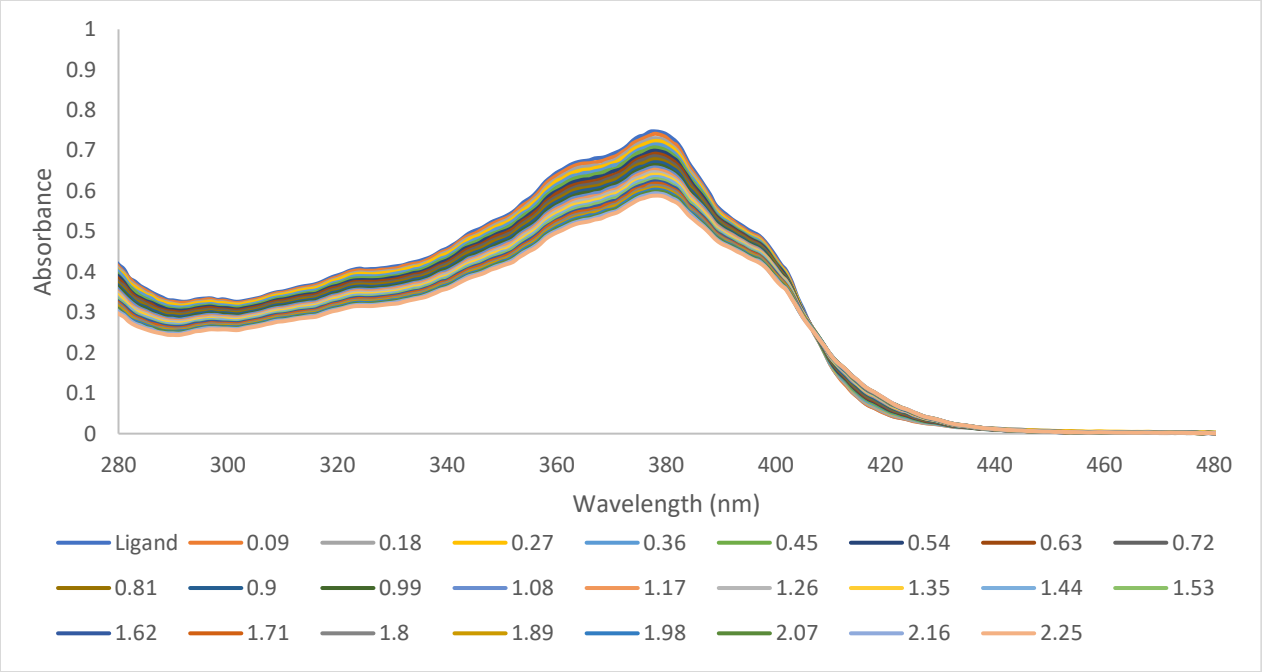

A.2.44 L4 (DMF) titration with Zinc (MeOH) (Shown at metal to ligand molar ratios of 0.09-2.25: 1)

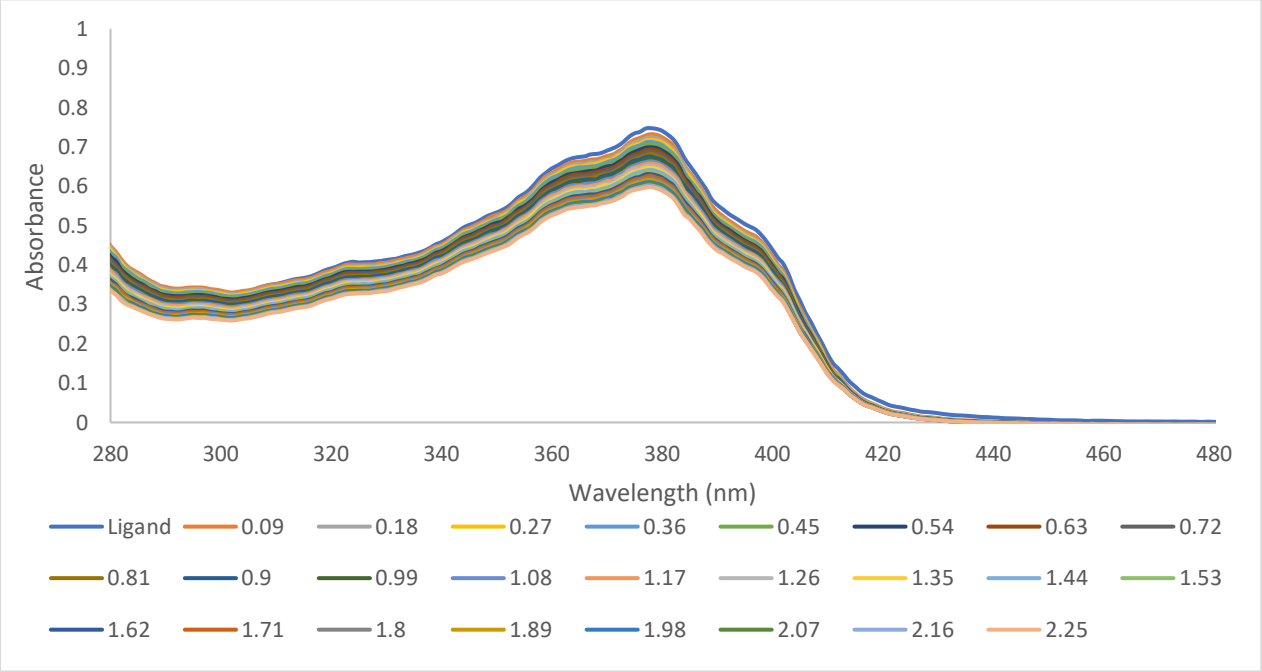

A.2.45 L4 (DMF) titration with Dysprosium (MeOH) (Shown at metal to ligand molar ratios of 0.09-2.25: 1)

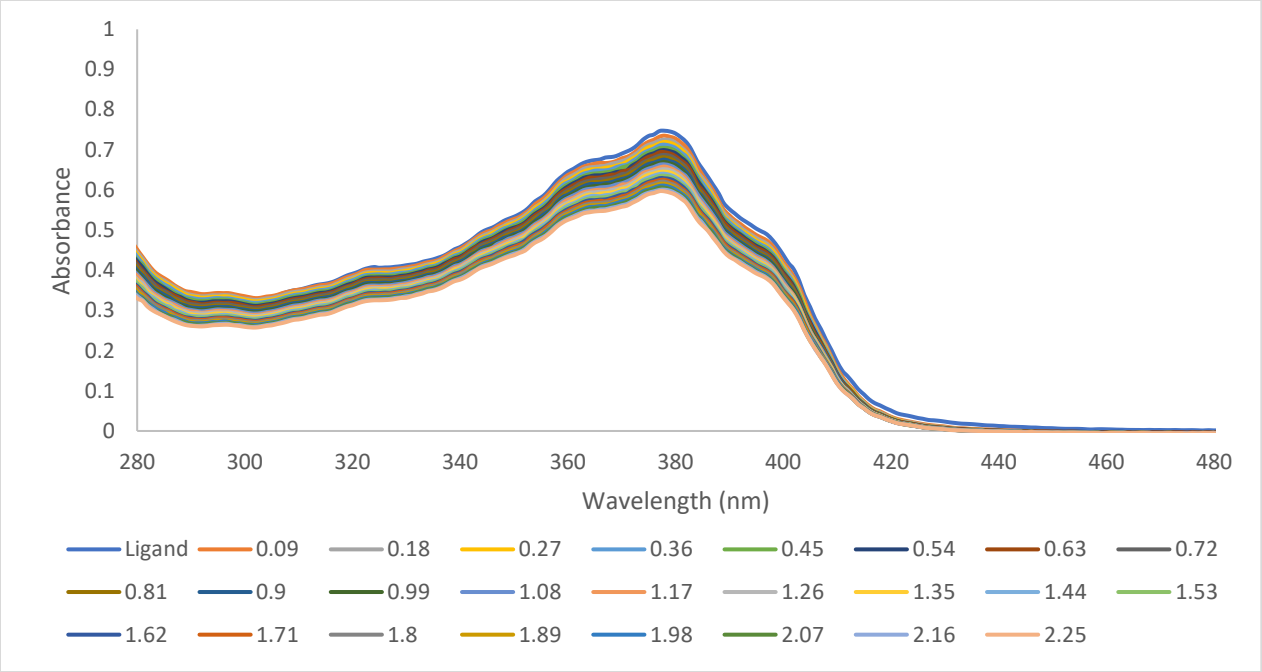

A.2.46 L4 (DMF) titration with Ytterbium (MeOH) (Shown at metal to ligand molar ratios of 0.09-2.25: 1)

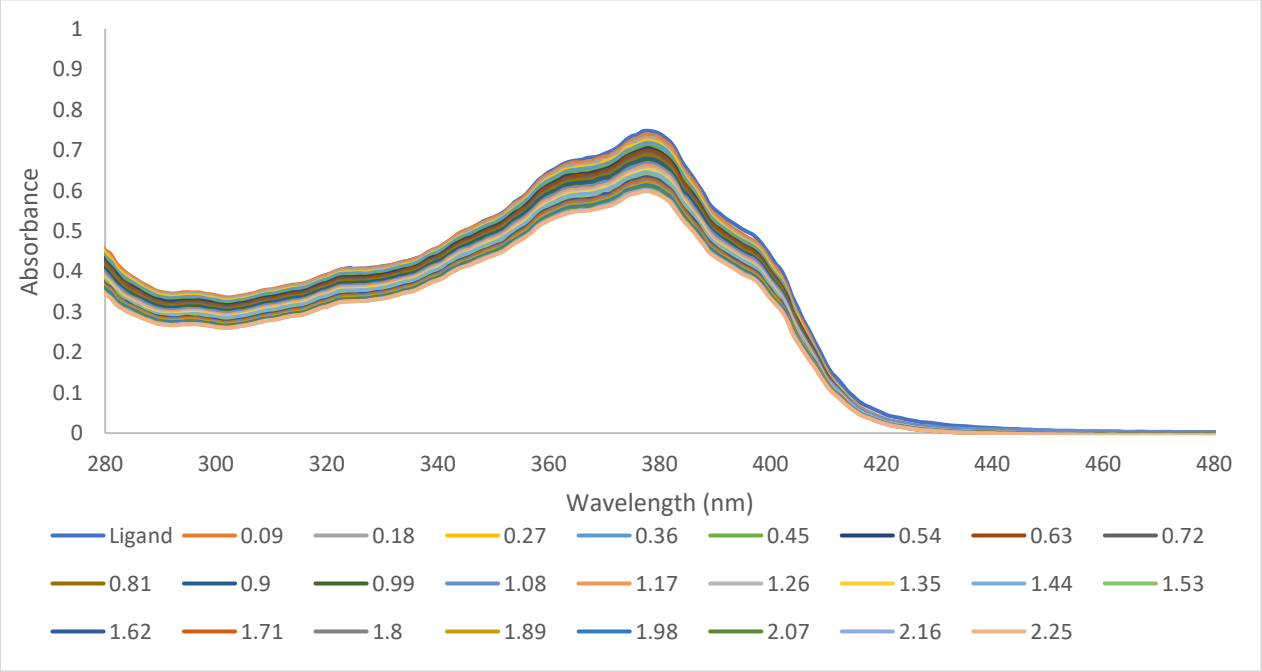

A.2.47 L4 (DMF) titration with Thorium (MeOH) (Shown at metal to ligand molar ratios of 0.09-2.25: 1)

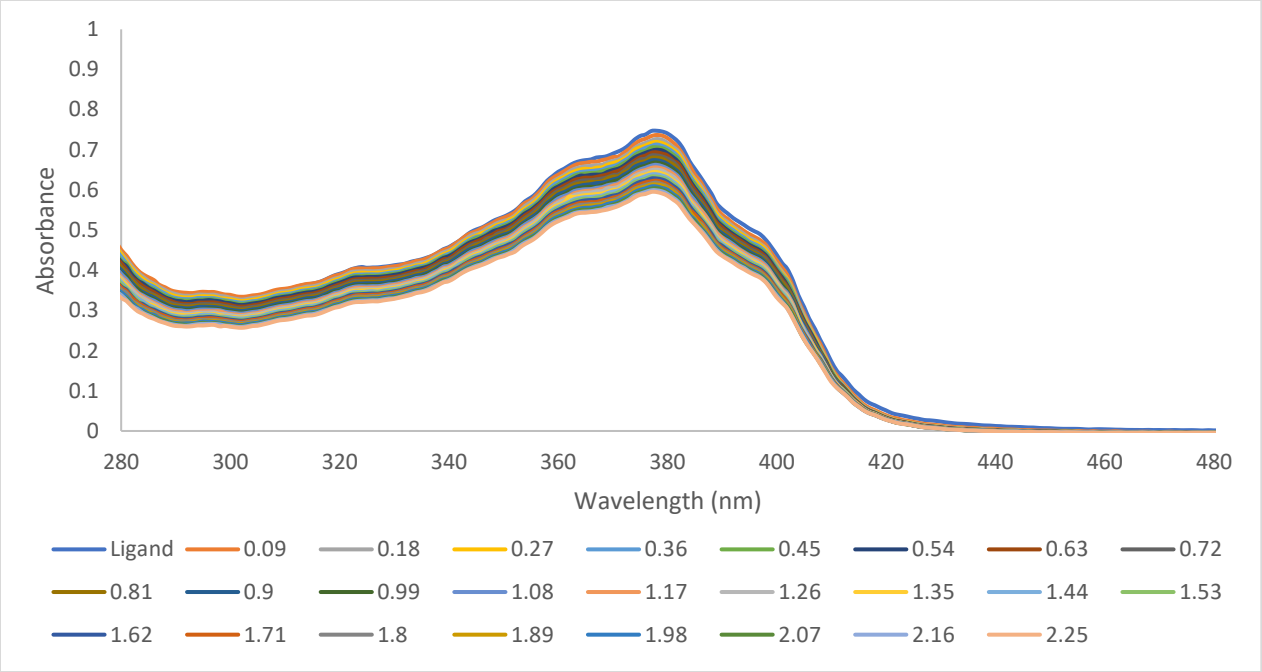

A.2.48 L4 (DMF) titration with Uranyl (MeOH) (Shown at metal to ligand molar ratios of 0.09-2.25: 1)

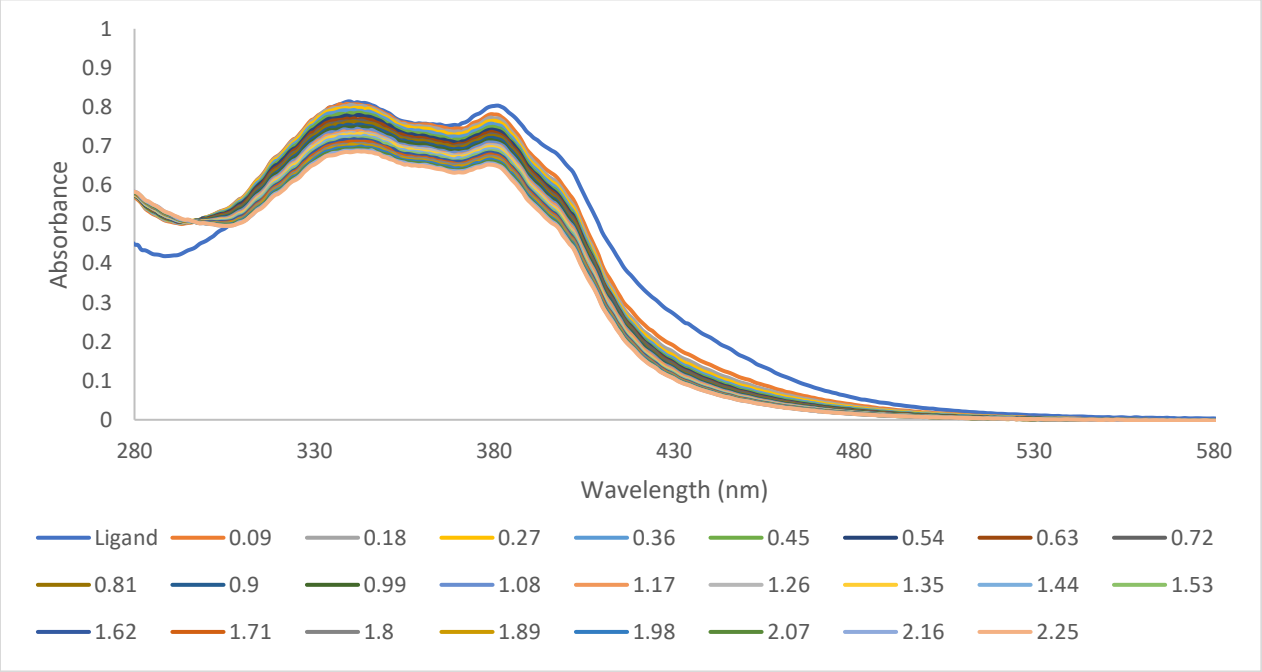

A.2.49 L5 (DMF) titration with Vanadyl (MeOH) (Shown at metal to ligand molar ratios of 0.09-2.25: 1)

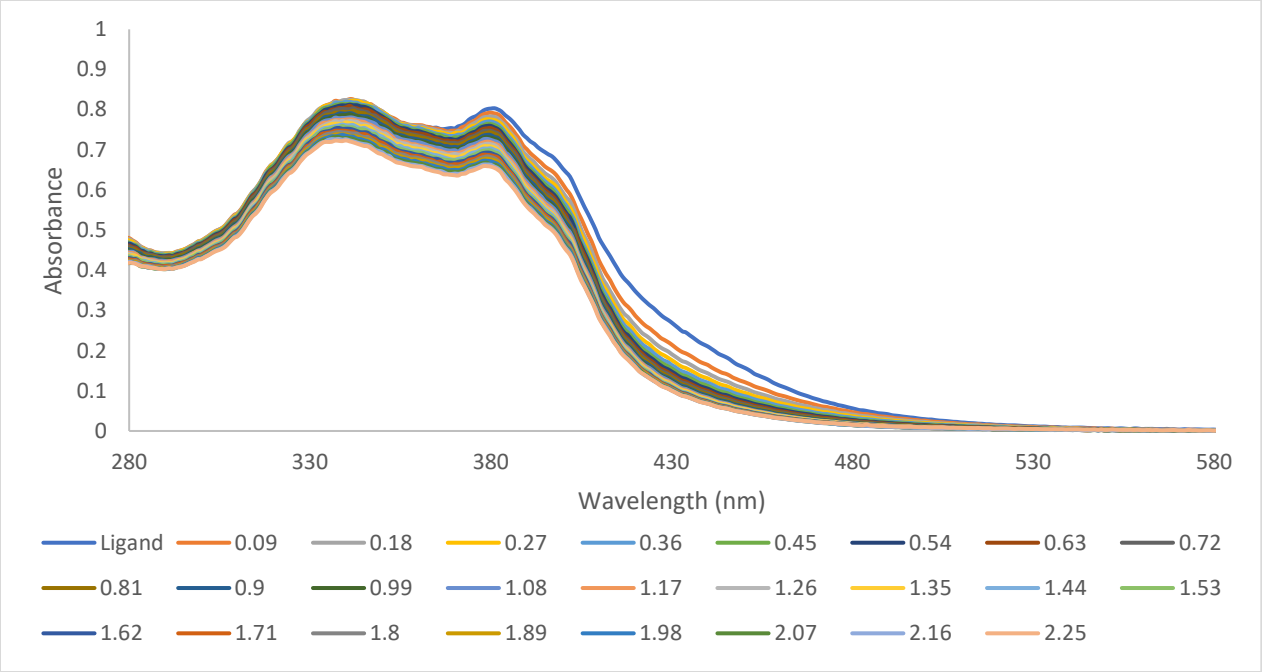

A.2.50 L5 (DMF) titration with Chromium (MeOH) (Shown at metal to ligand molar ratios of 0.09-2.25: 1)

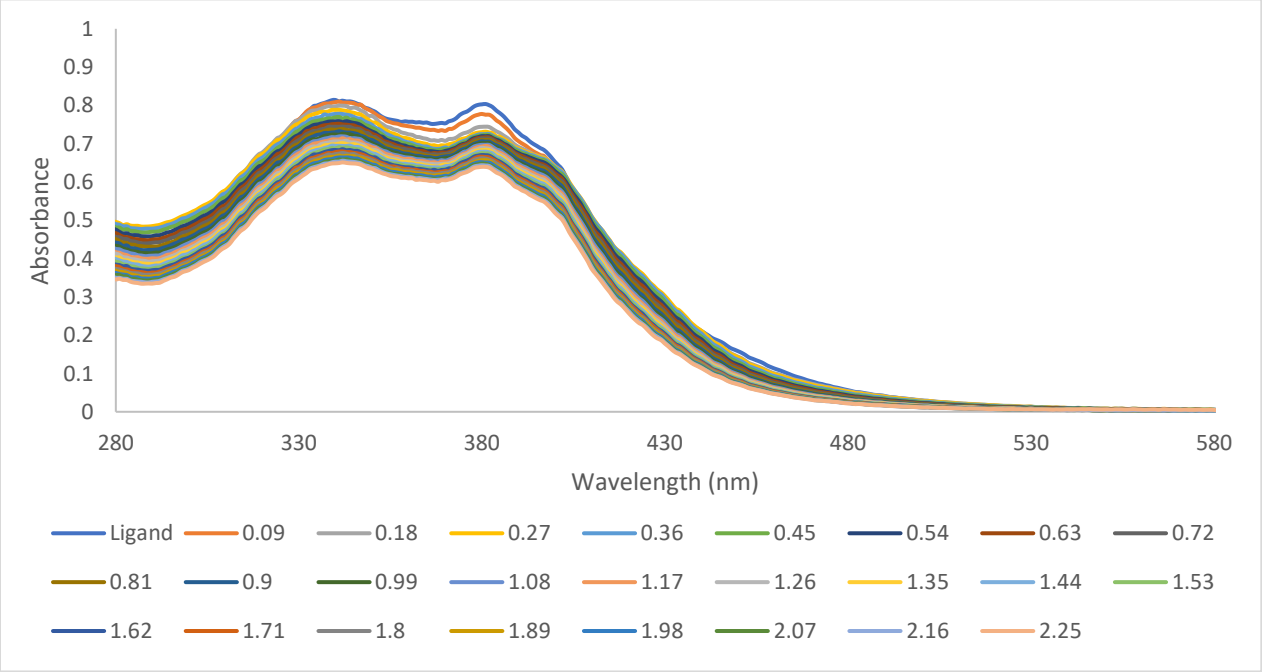

A.2.51 L5 (DMF) titration with Manganese (MeOH) (Shown at metal to ligand molar ratios of 0.09-2.25: 1)

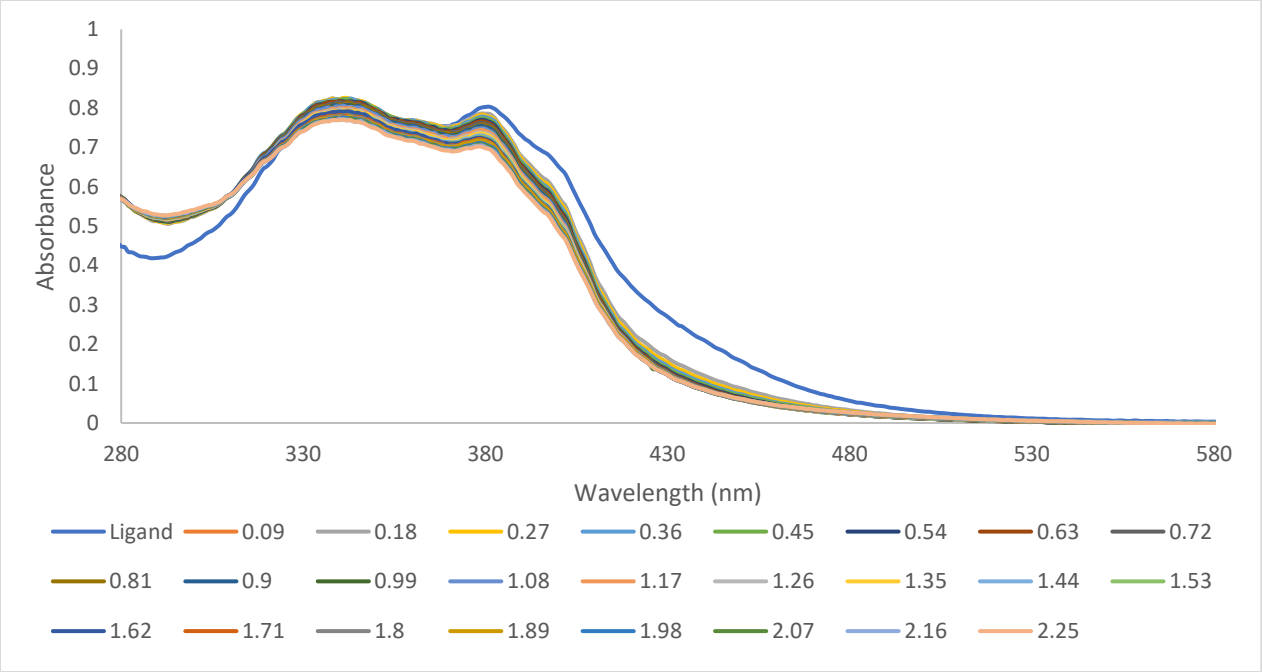

A.2.52 L5 (DMF) titration with Iron (MeOH) (Shown at metal to ligand molar ratios of 0.09-2.25: 1)

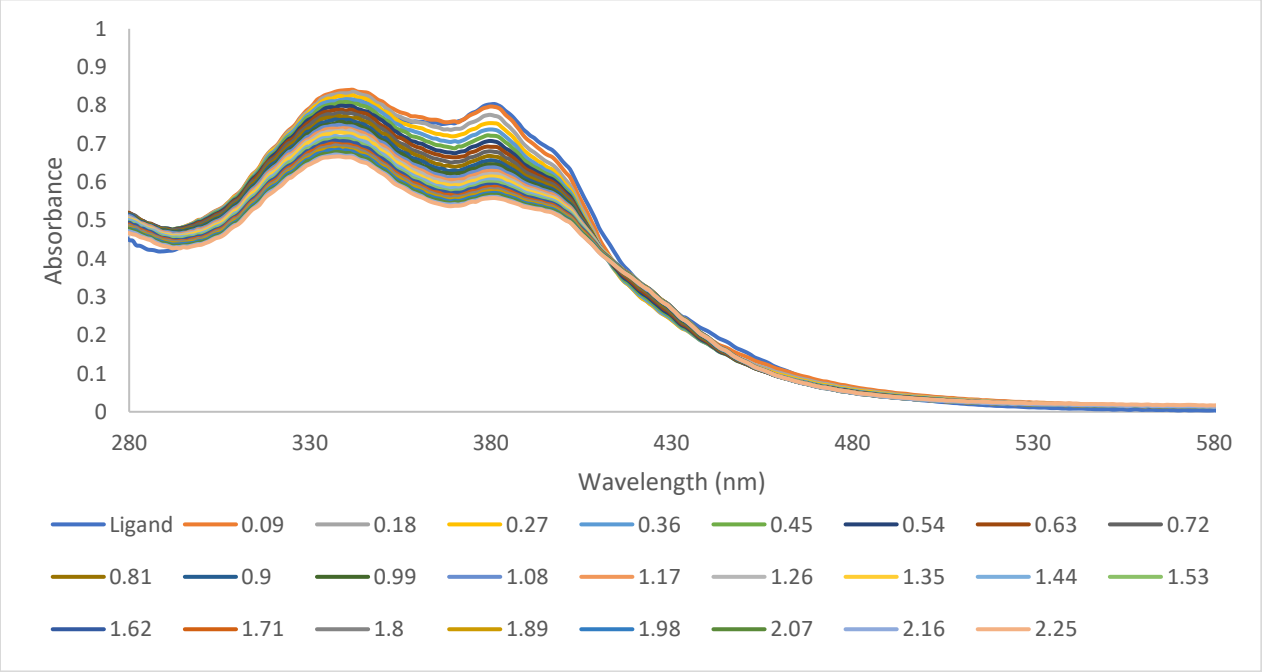

A.2.53 L5 (DMF) titration with Cobalt (MeOH) (Shown at metal to ligand molar ratios of 0.09-2.25: 1)

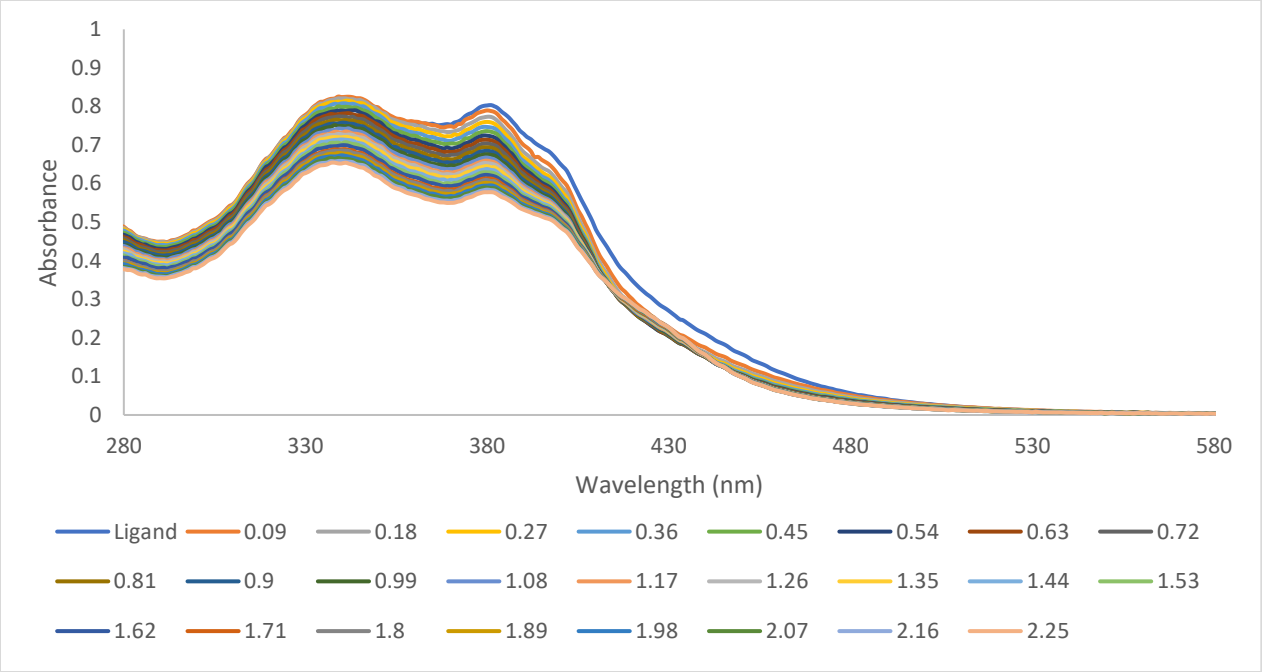

A.2.54 L5 (DMF) titration with Nickel (MeOH) (Shown at metal to ligand molar ratios of 0.09-2.25: 1)

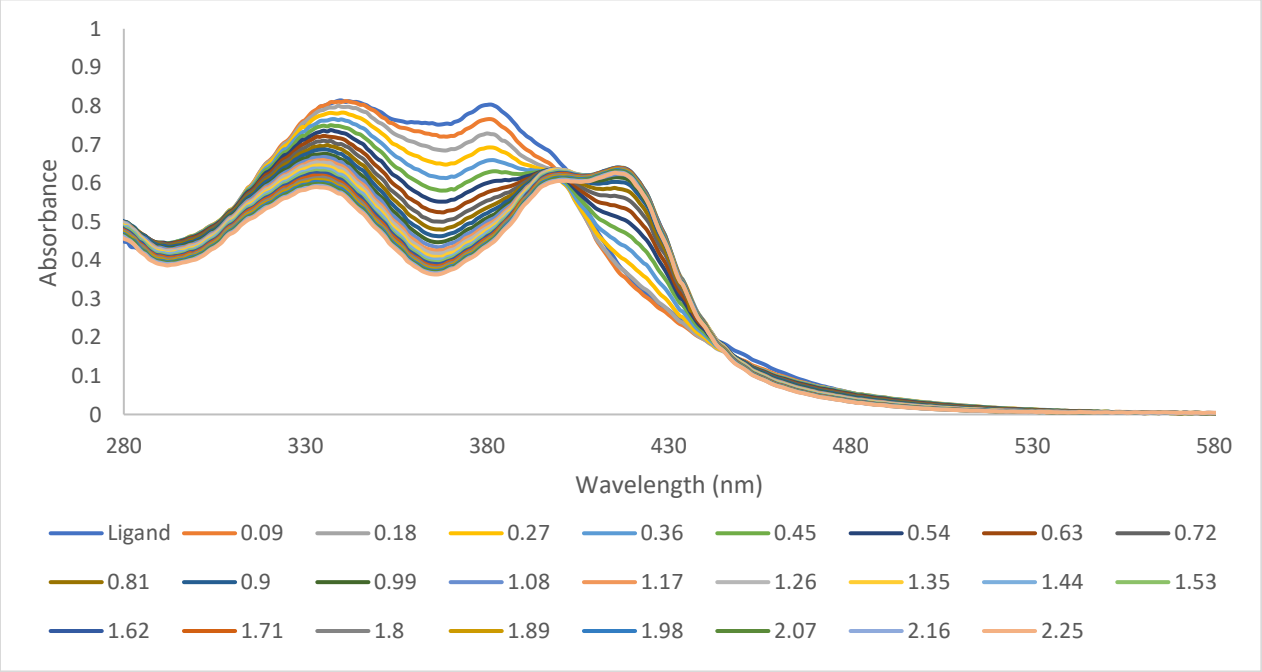

A.2.55 L5 (DMF) titration with Copper (MeOH) (Shown at metal to ligand molar ratios of 0.09-2.25: 1)

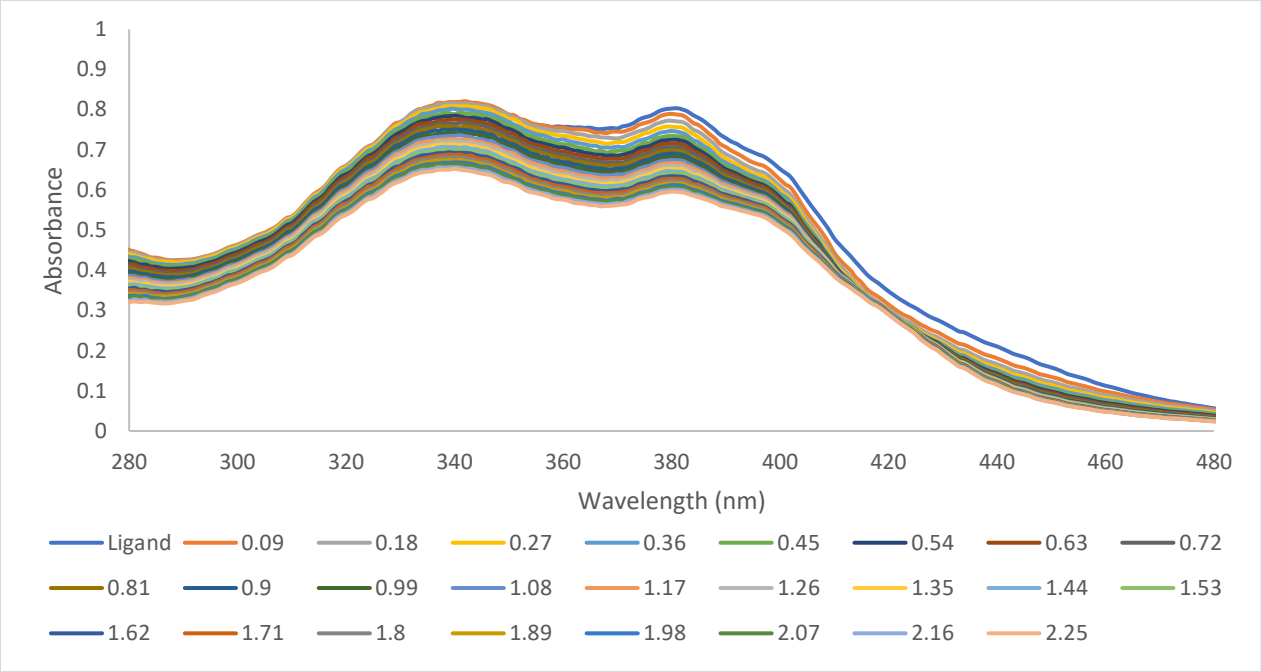

A.2.56 L5 (DMF) titration with Zinc (MeOH) (Shown at metal to ligand molar ratios of 0.09-2.25: 1)

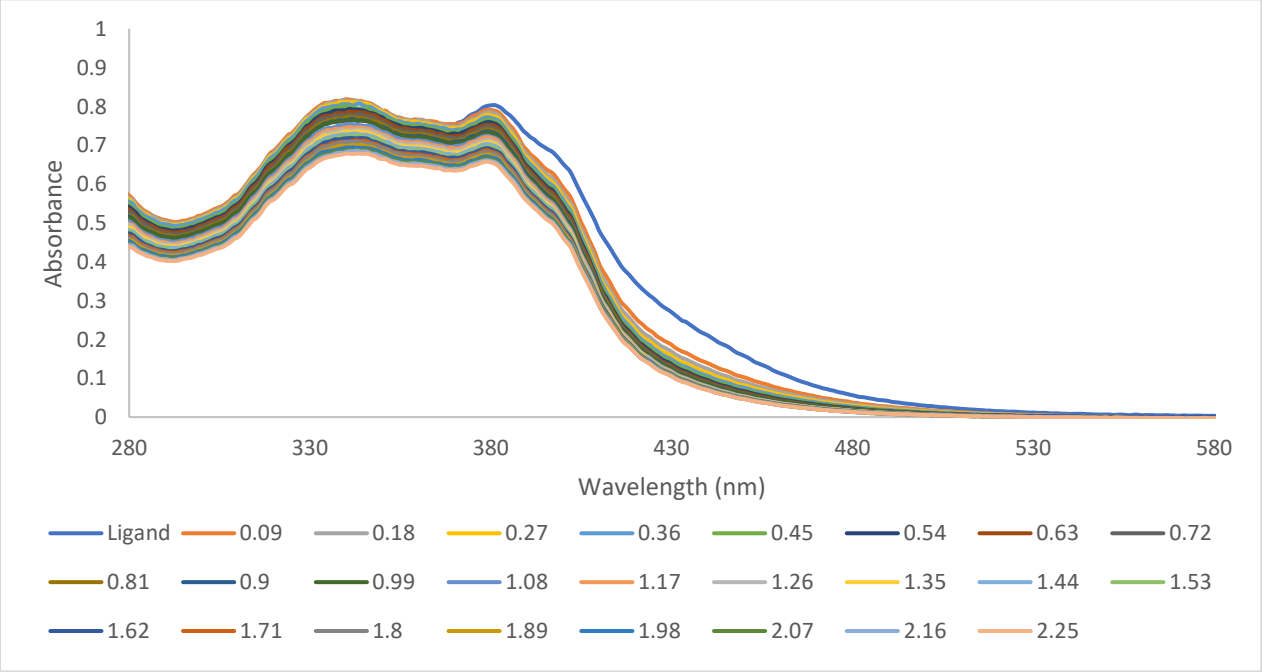

A.2.57 L5 (DMF) titration with Dysprosium (MeOH) (Shown at metal to ligand molar ratios of 0.09-2.25: 1)

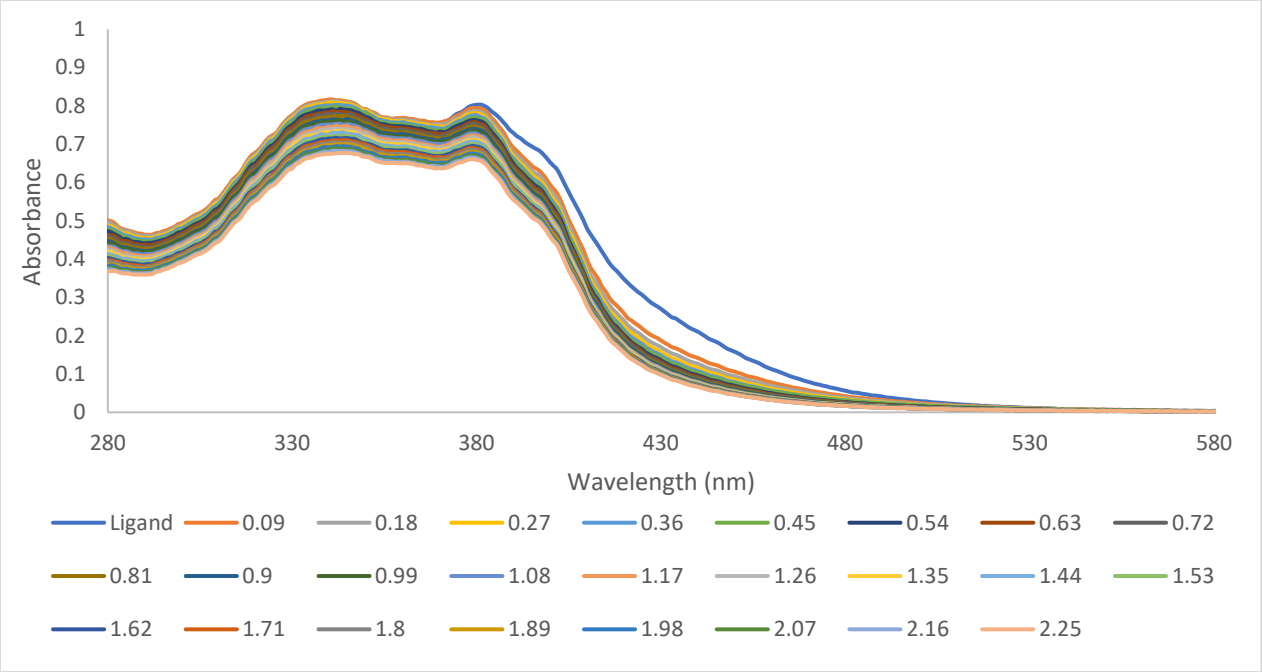

A.2.58 L5 (DMF) titration with Ytterbium (MeOH) (Shown at metal to ligand molar ratios of 0.09-2.25: 1)

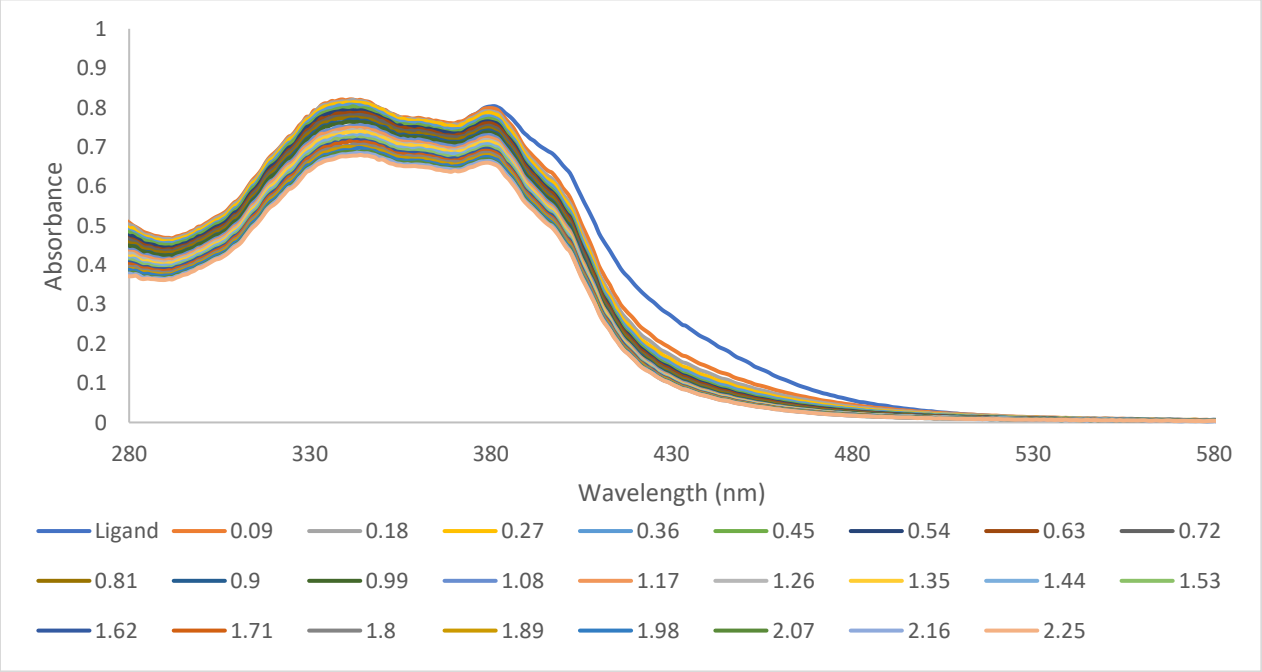

A.2.59 L5 (DMF) titration with Thorium (MeOH) (Shown at metal to ligand molar ratios of 0.09-2.25: 1)

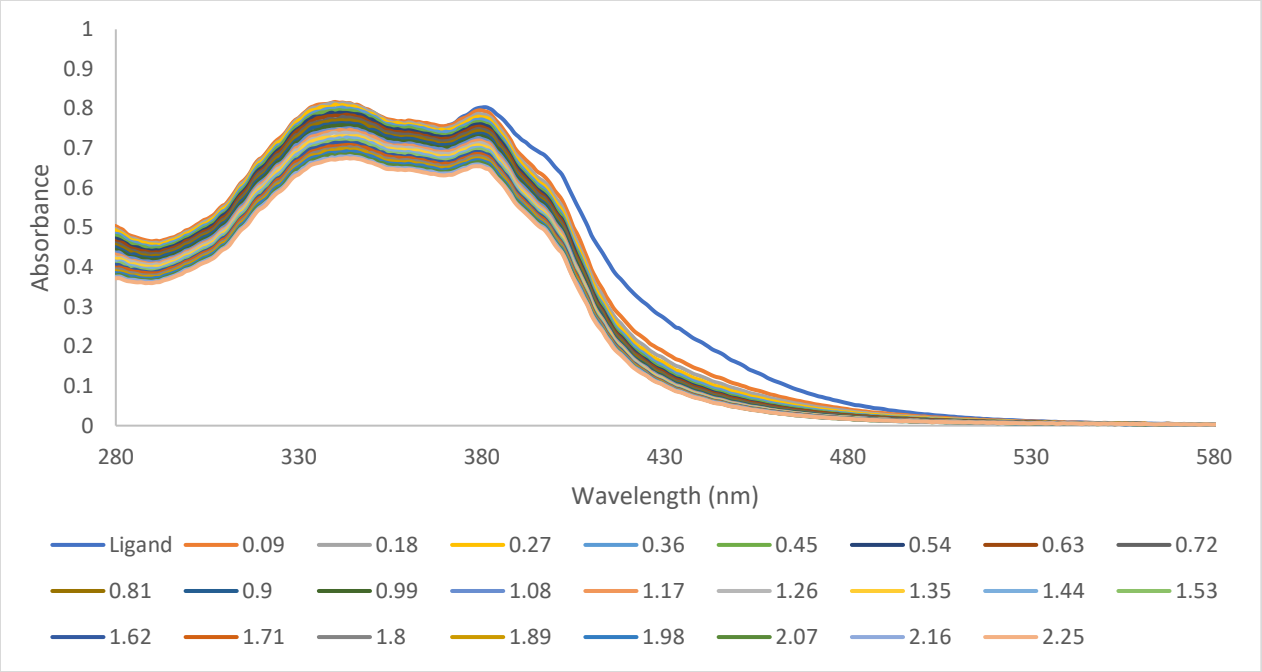

A.2.60 L5 (DMF) titration with Uranyl (MeOH) (Shown at metal to ligand molar ratios of 0.09-2.25: 1)

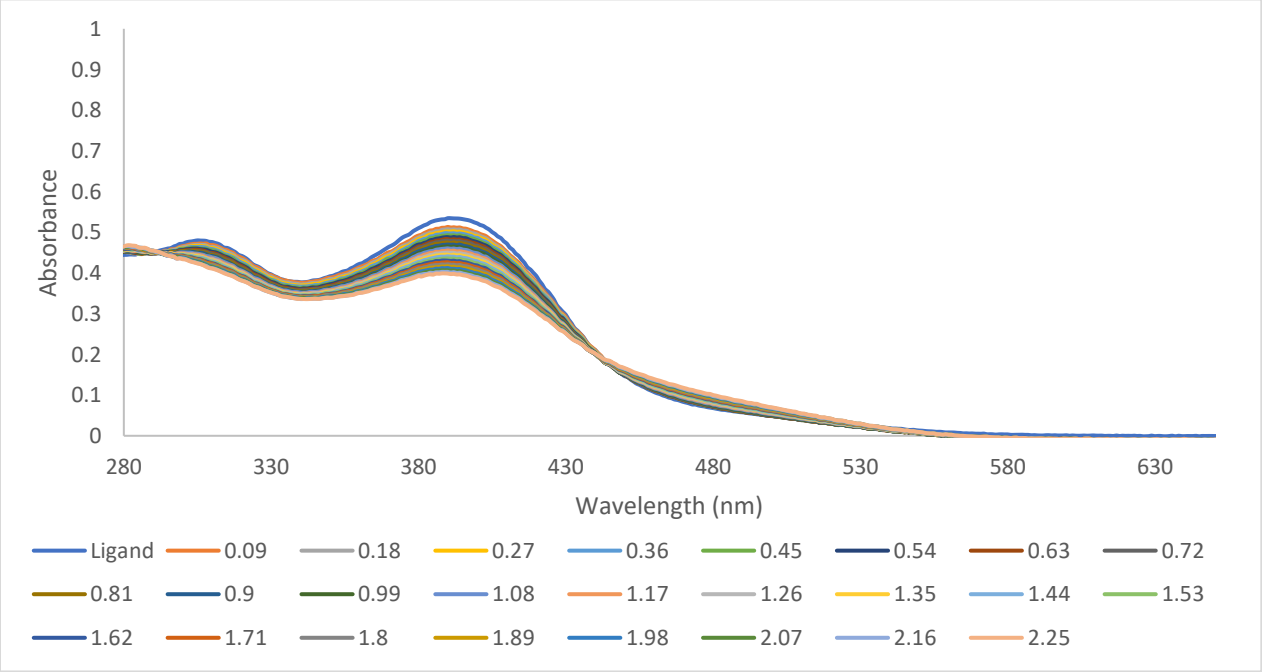

A.2.61 L6 (DMF) titration with Vanadyl (MeOH) (Shown at metal to ligand molar ratios of 0.09-2.25: 1)

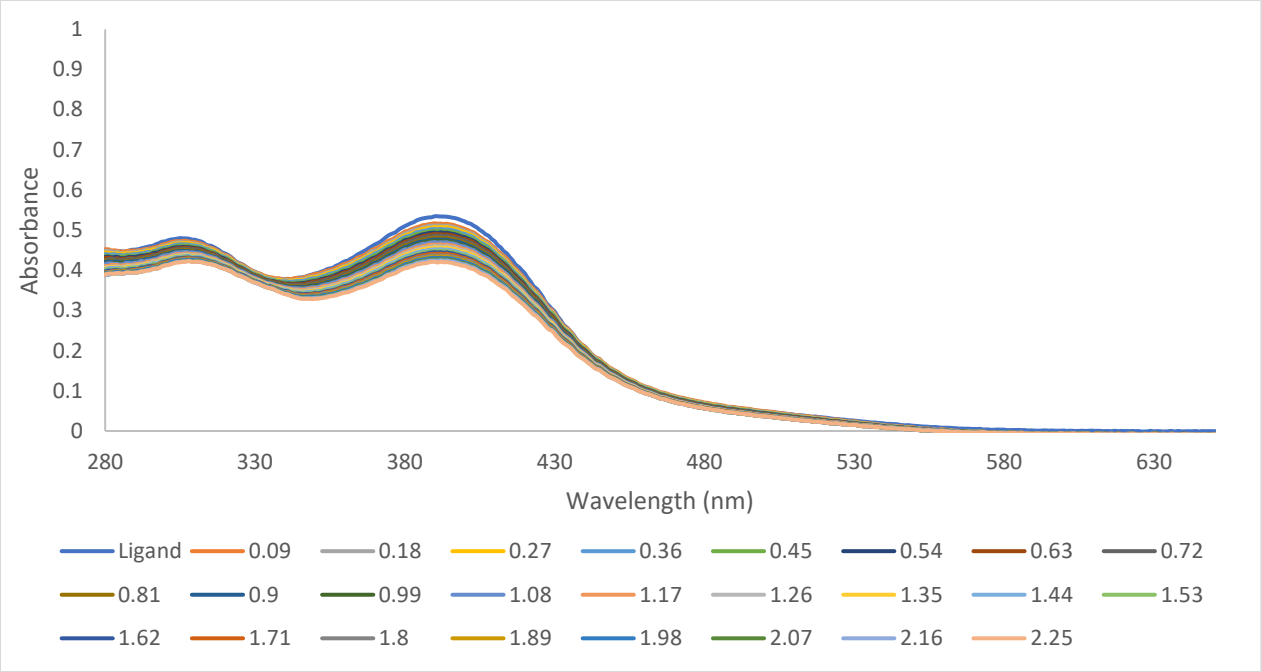

A.2.62 L6 (DMF) titration with Chromium (MeOH) (Shown at metal to ligand molar ratios of 0.09-2.25: 1)

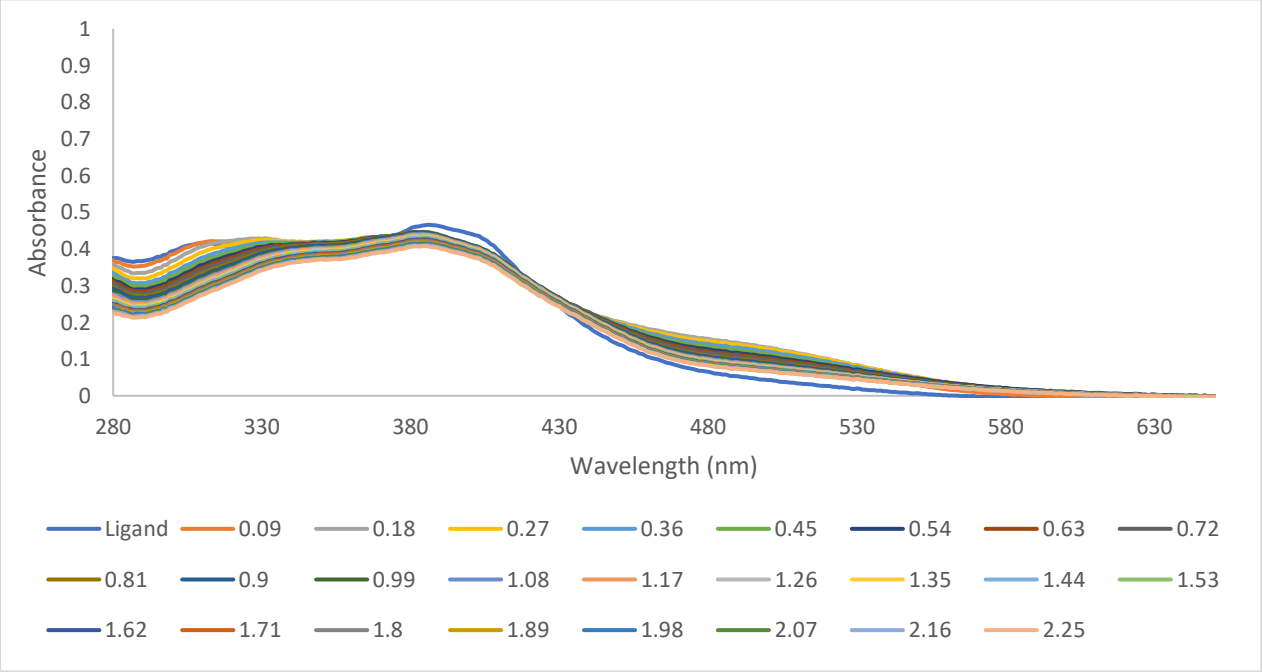

A.2.63 L6 (DMF) titration with Manganese (MeOH) (Shown at metal to ligand molar ratios of 0.09-2.25: 1)

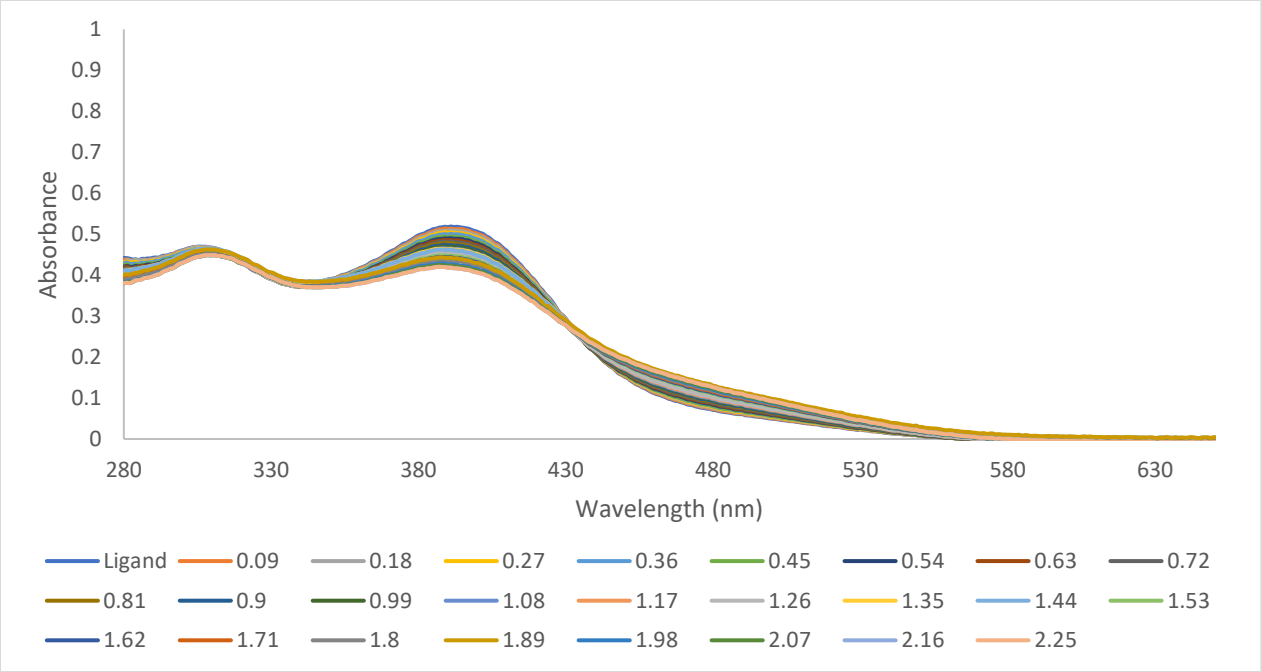

A.2.64 L6 (DMF) titration with Iron (MeOH) (Shown at metal to ligand molar ratios of 0.09-2.25: 1)

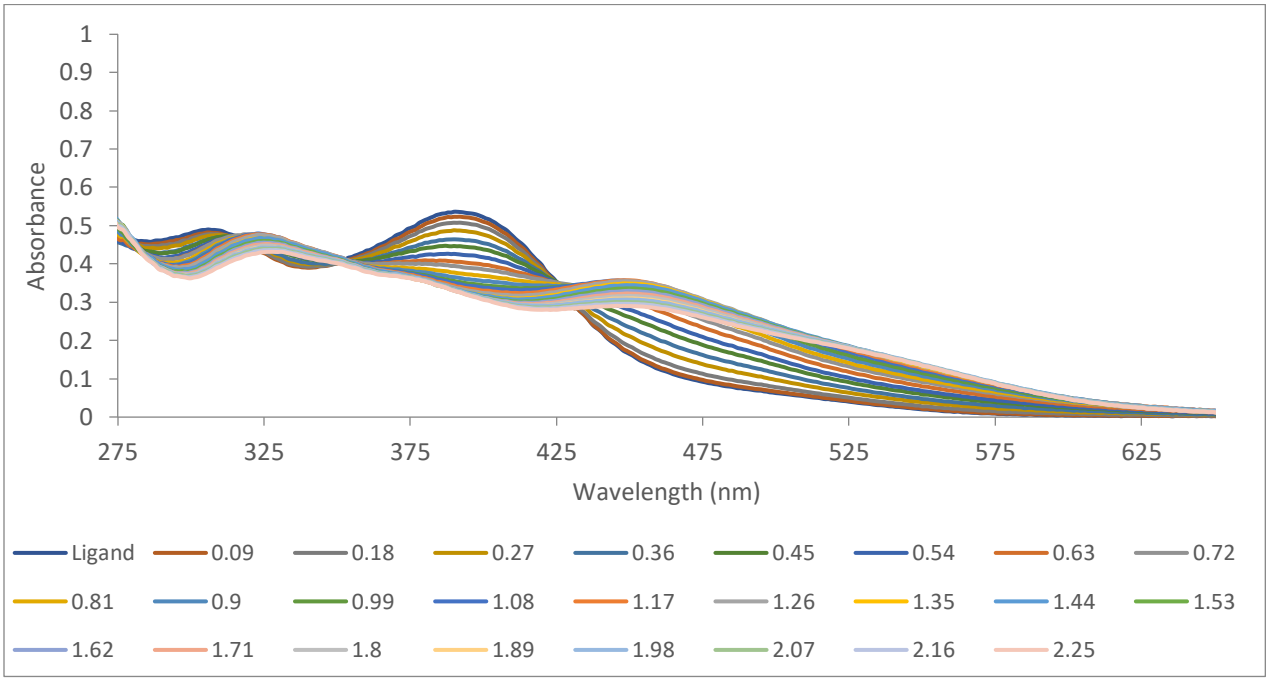

A.2.65 L6 (DMF) titration with Cobalt (MeOH) (Shown at metal to ligand molar ratios of 0.09-2.25: 1)

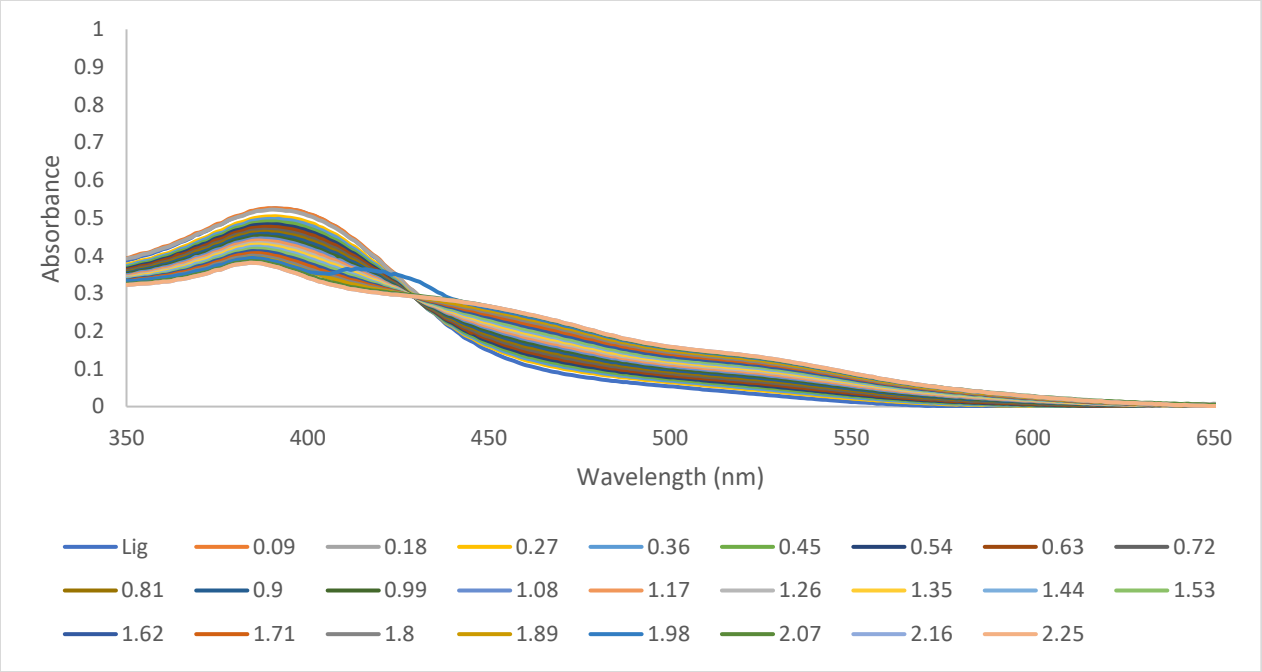

A.2.66 L6 (DMF) titration with Nickel (MeOH) (Shown at metal to ligand molar ratios of 0.09-2.25: 1)

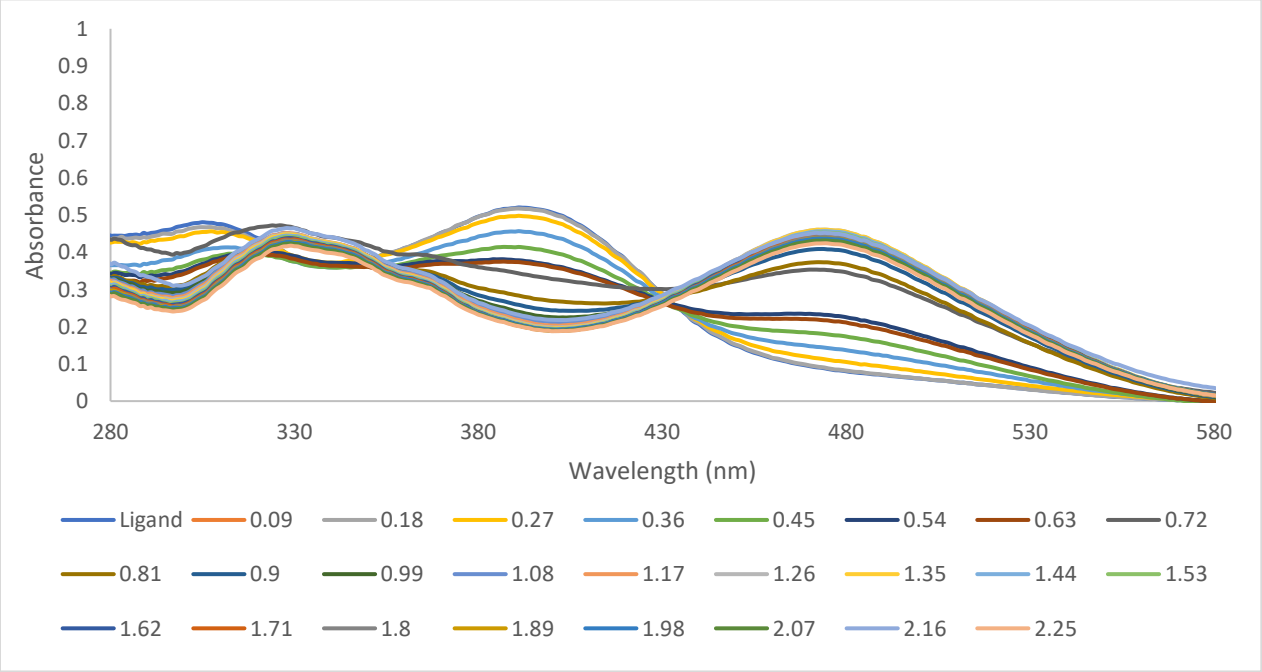

A.2.67 L6 (DMF) titration with Copper (MeOH) (Shown at metal to ligand molar ratios of 0.09-2.25: 1)

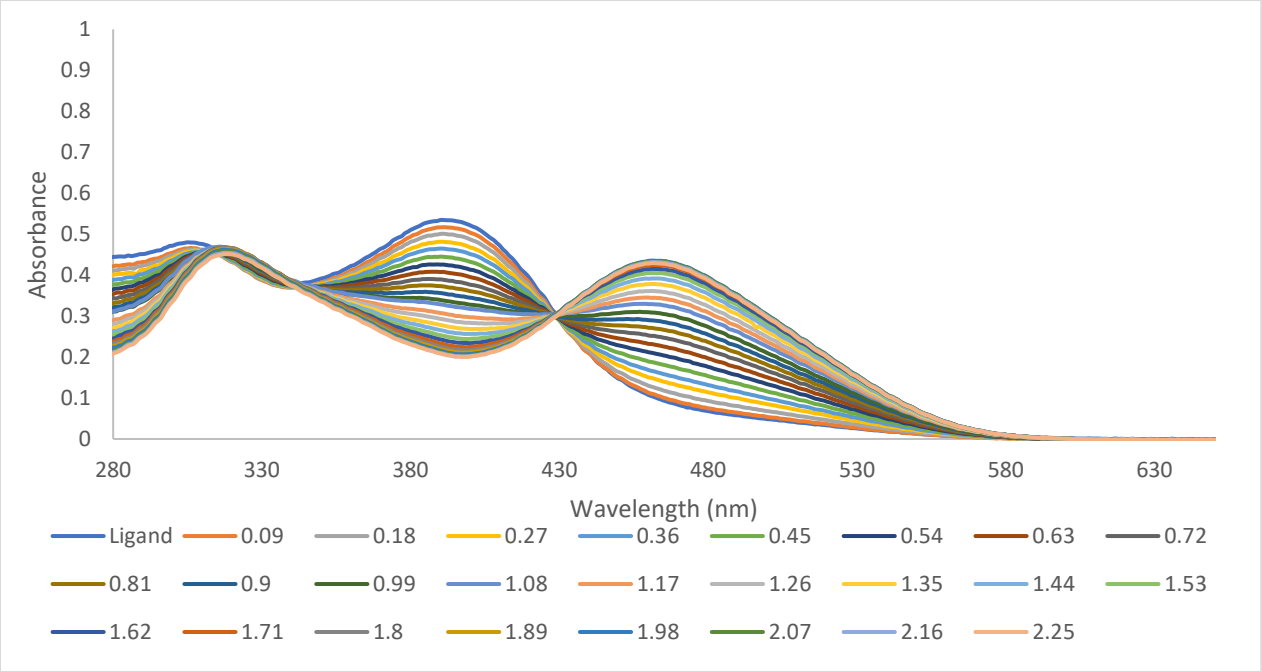

A.2.68 L6 (DMF) titration with Zinc (MeOH) (Shown at metal to ligand molar ratios of 0.09-2.25: 1)

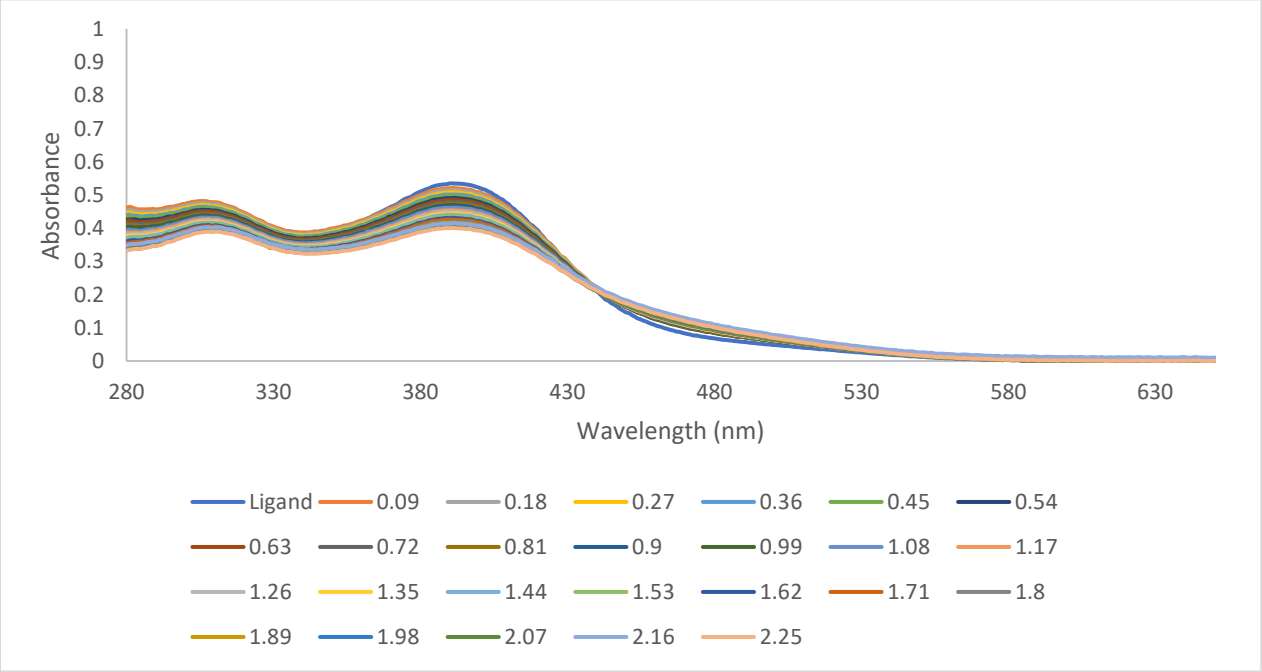

A.2.69 L6 (DMF) titration with Dysprosium (MeOH) (Shown at metal to molar ligand ratios of 0.09-2.25: 1)

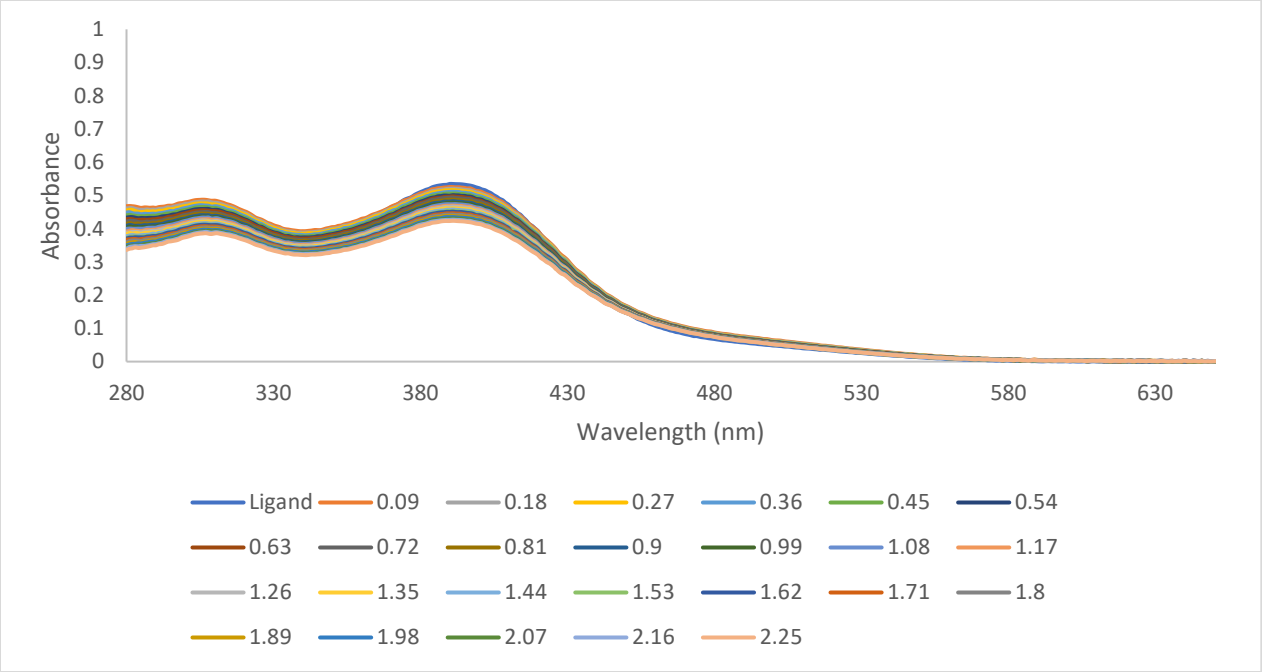

A.2.70 L6 (DMF) titration with Ytterbium (MeOH) (Shown at metal to molar ligand ratios of 0.09-2.25: 1)

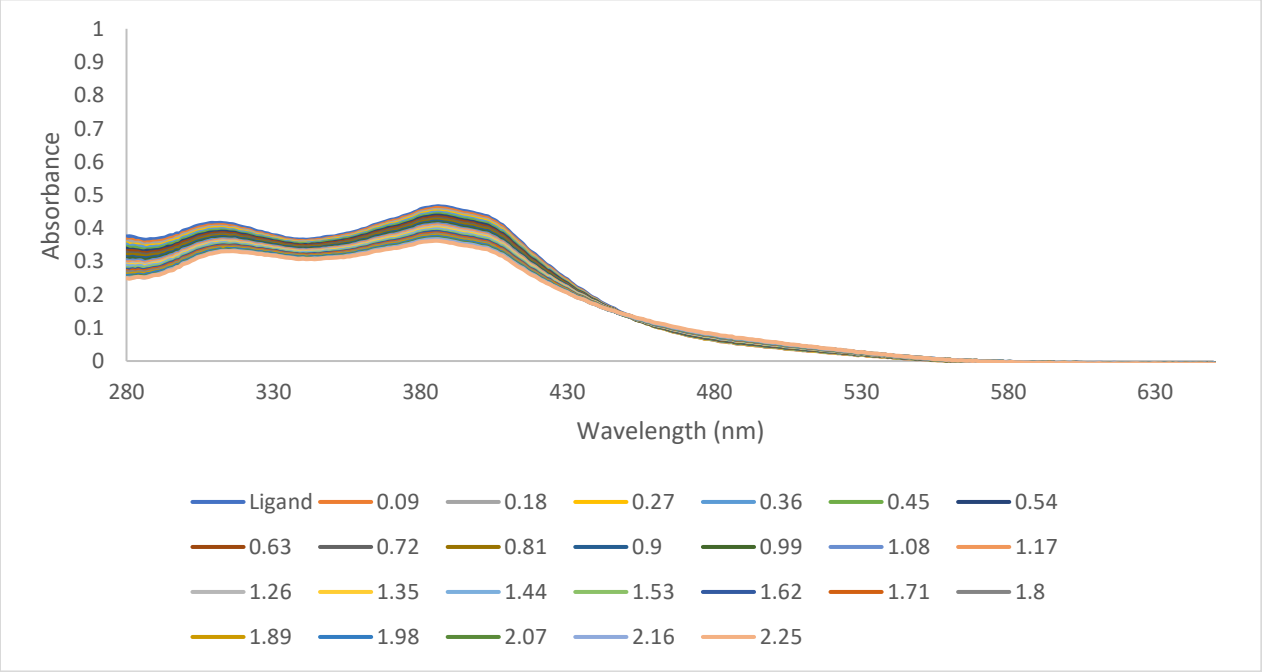

A.2.71 L6 (DMF) titration with Thorium (MeOH) (Shown at metal to ligand molar ratios of 0.09-2.25: 1)

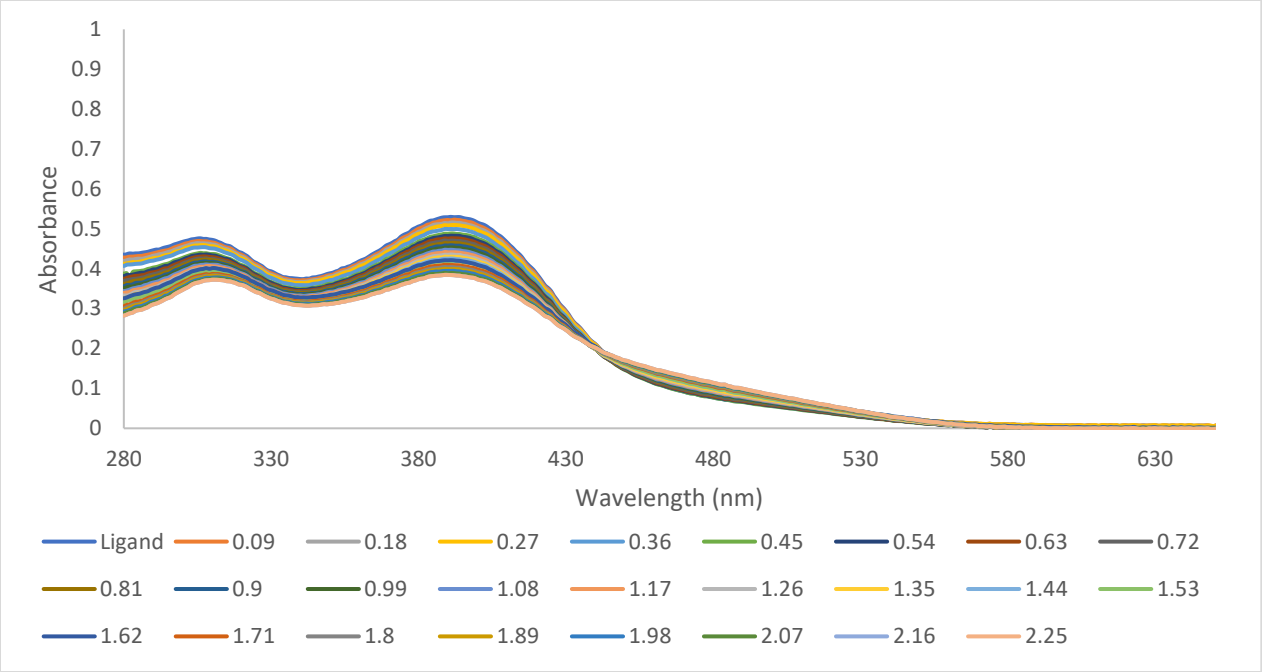

A.2.72 L6 (DMF) titration with Uranium (MeOH) (Shown at metal to ligand molar ratios of 0.09-2.25: 1)

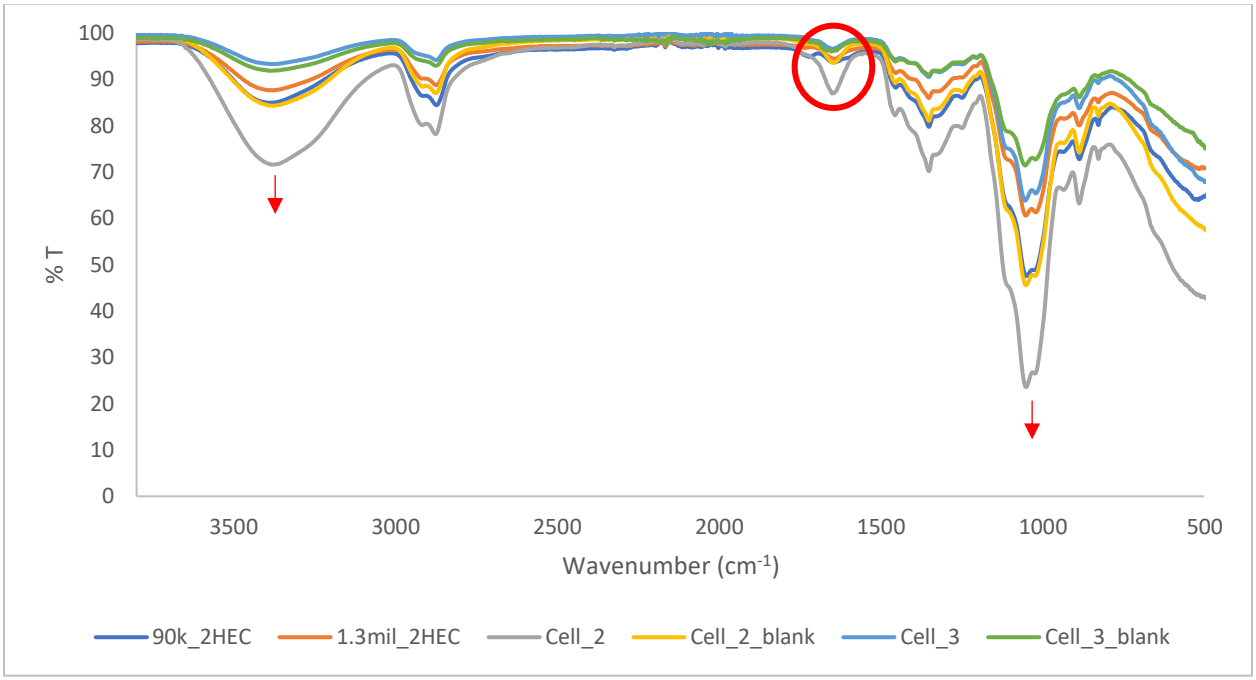

A.3.1 Glutaraldehyde cross-linked ligand-trapped films (Highlighting increase in OH character)

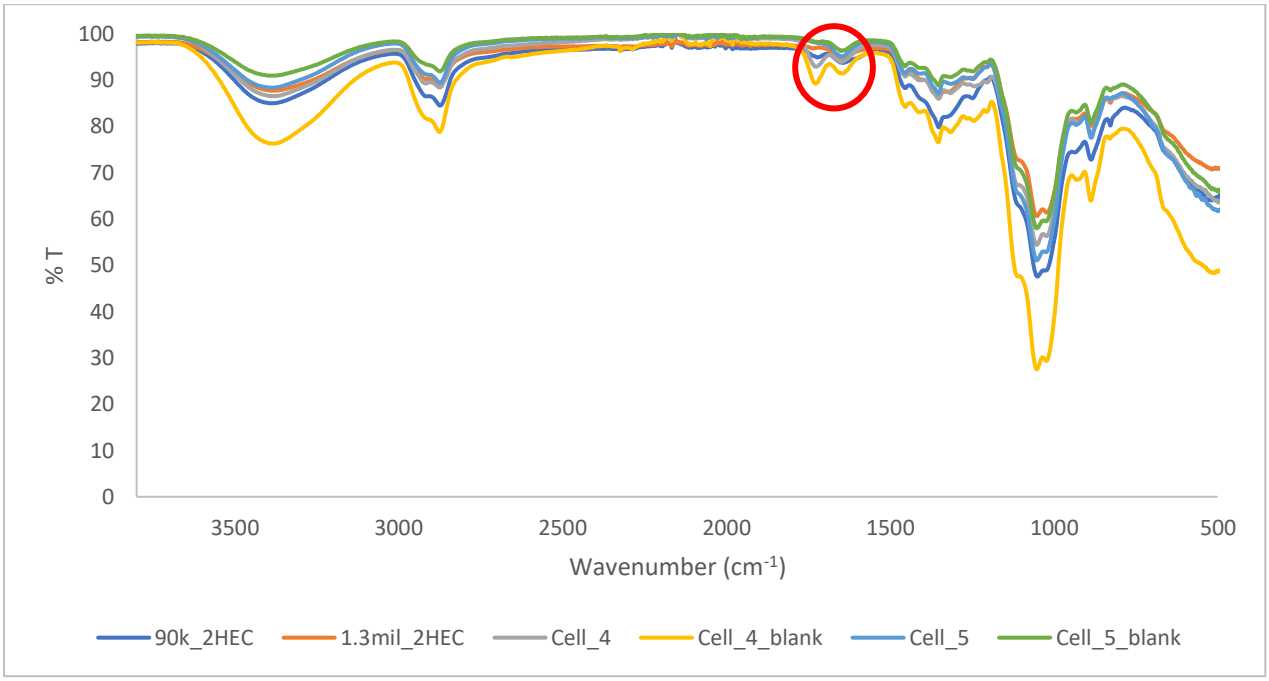

A.3.2 Citric acid cross-linked ligand-trapped films (Highlighting new ester peak)

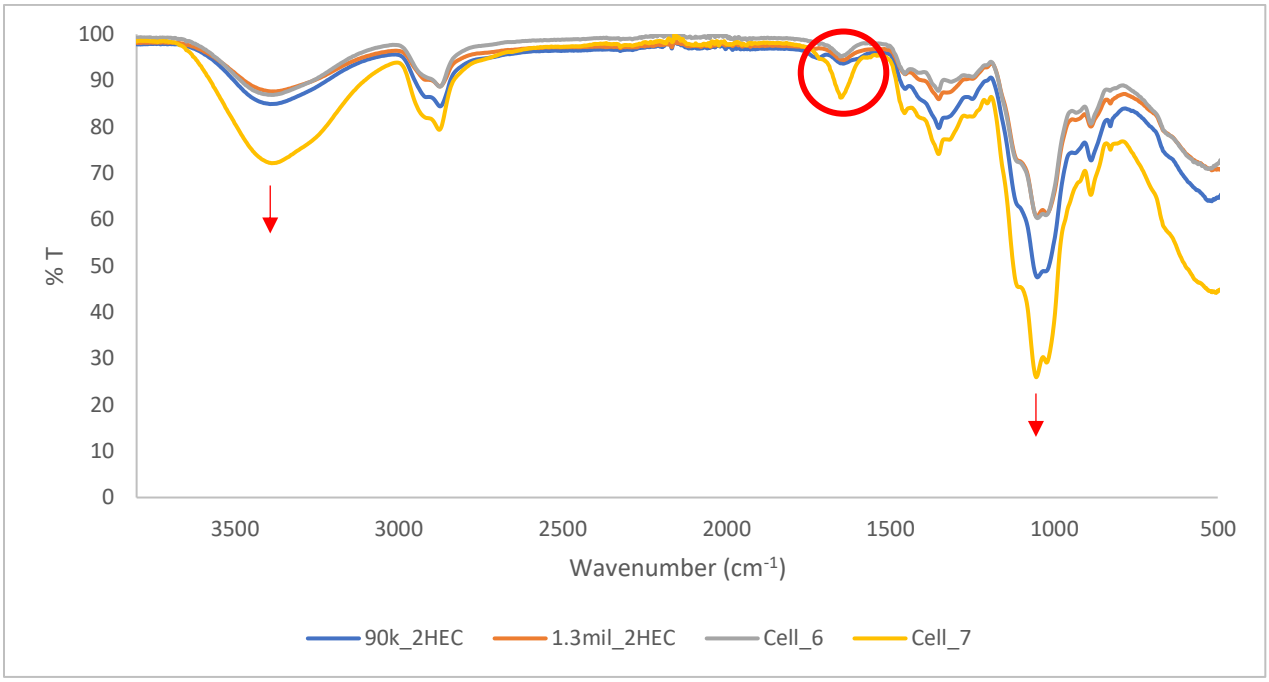

A.3.3 Glutaraldehyde cross-linked covalently bond ligand films (Highlighting increase in OH character)

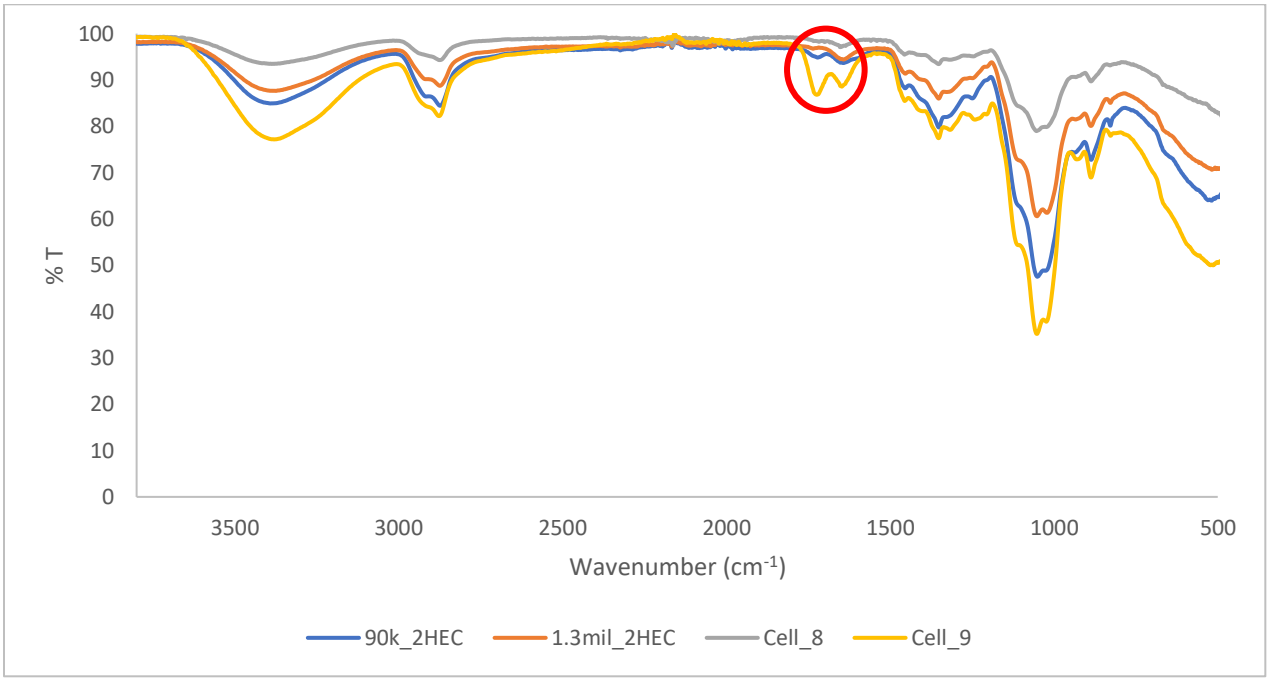

A.3.4 Citric acid cross-linked covalently bond ligand films. (Highlighting new ester peak)

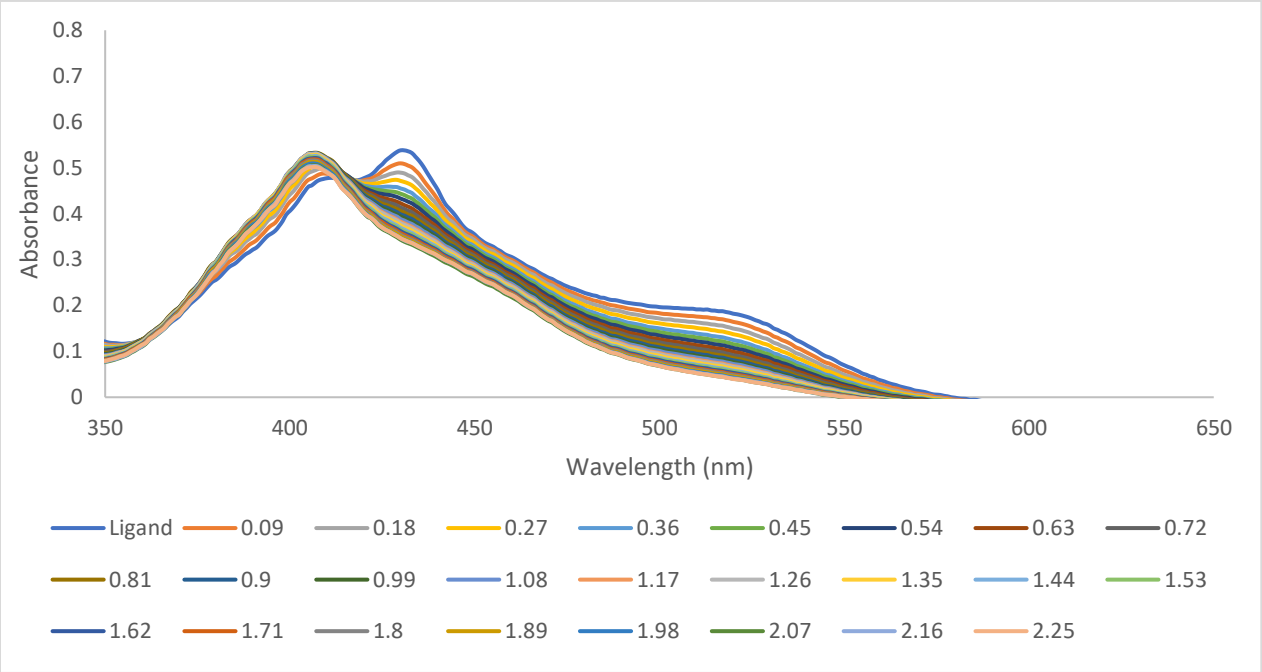

A.3.5 L7 (DMF) titration with Uranium (MeOH) (Shown at metal to ligand molar ratios of 0.09-2.25: 1)

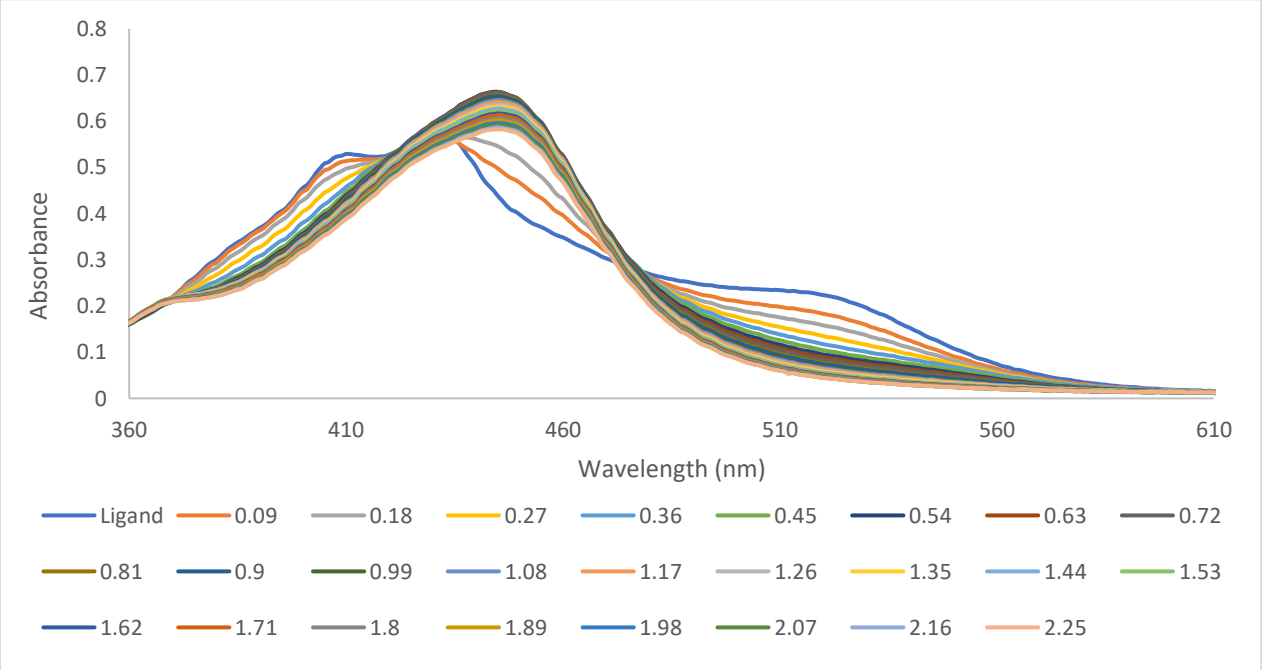

A.3.5 L7 (DMF) titration with Copper (MeOH) (Shown at metal to ligand molar ratios of 0.09-2.25: 1)

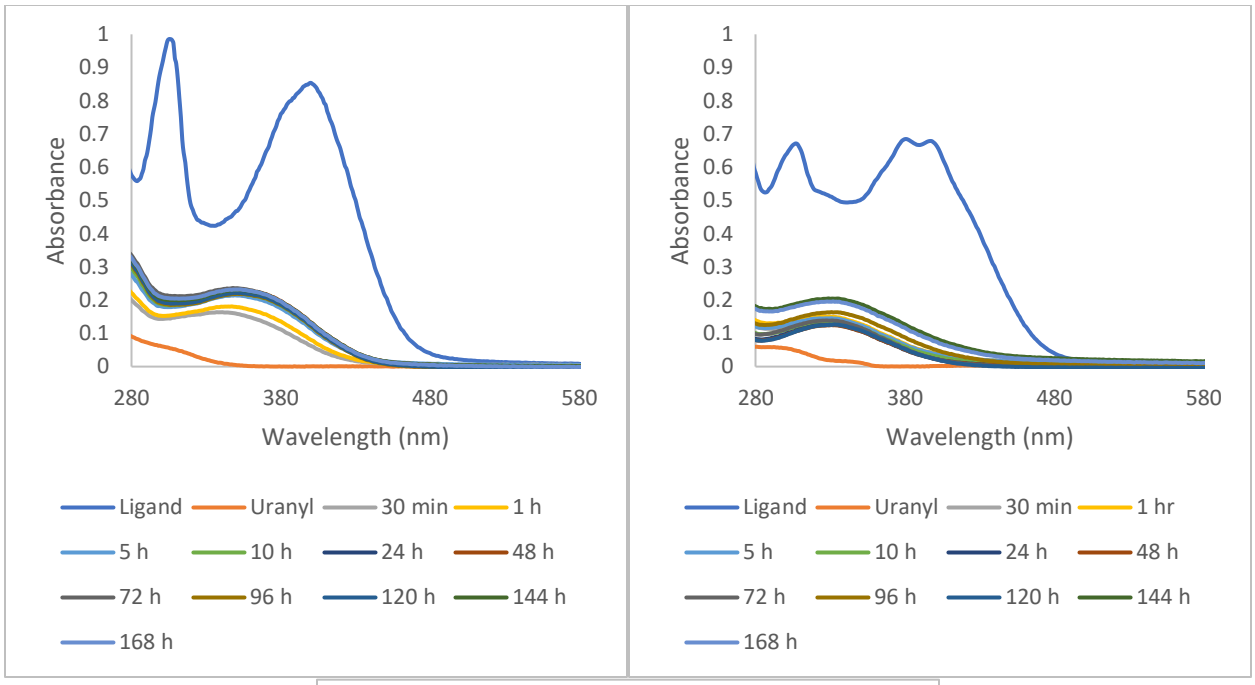

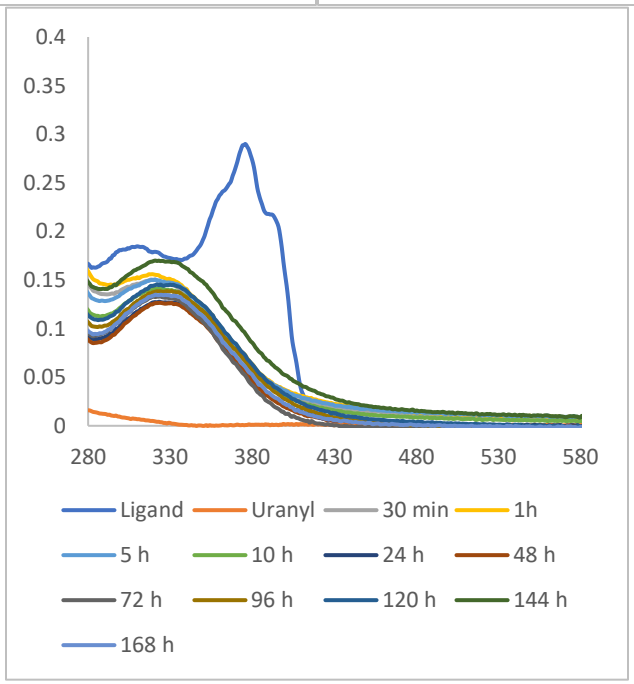

A.3.6 Leaching study of Cell-2 film: basic (top left) neutral (top right) acidic (bottom) media

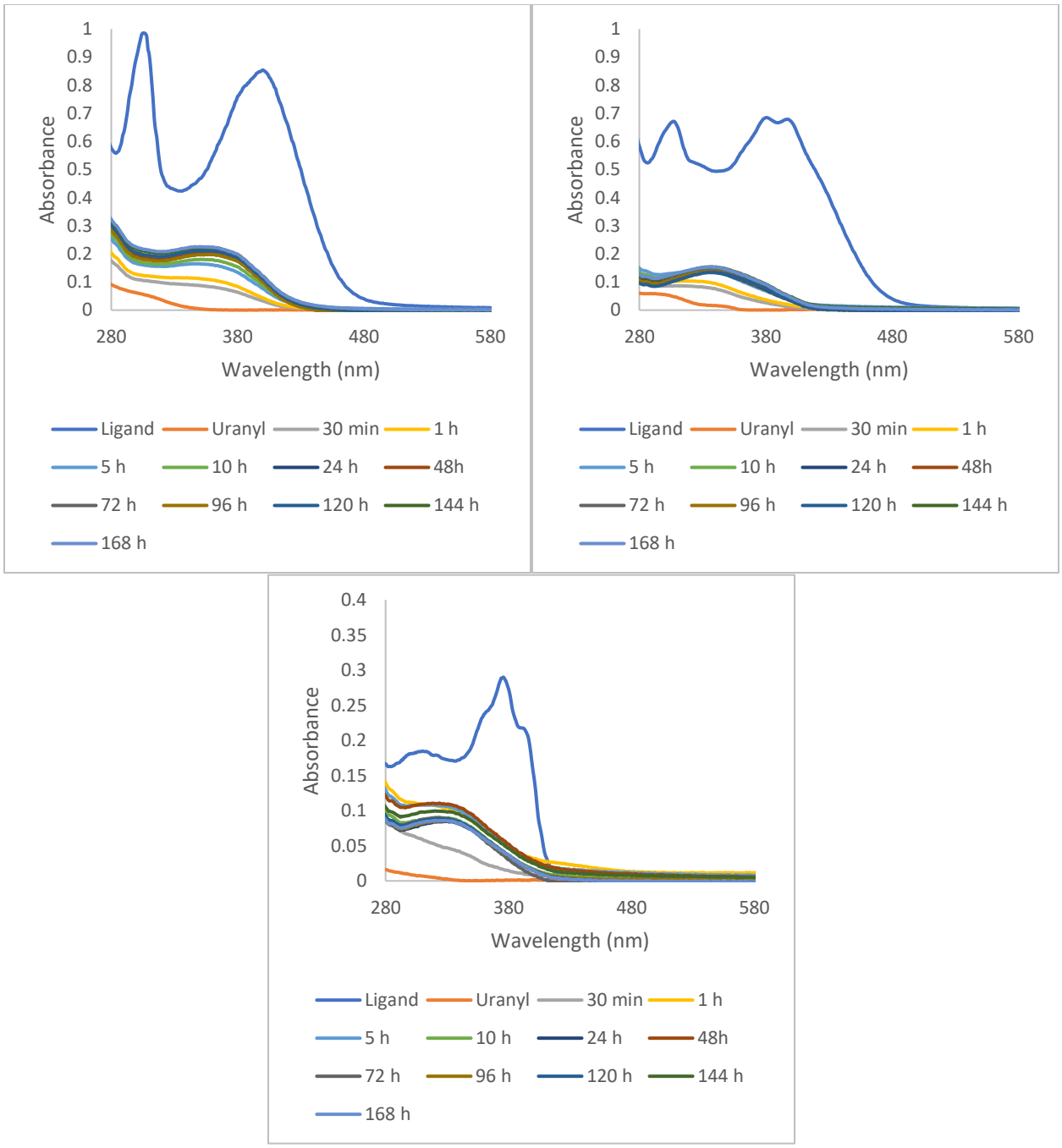

A.3.7 Leaching study of Cell-3 film: basic (top left) neutral (top right) acidic (bottom) media

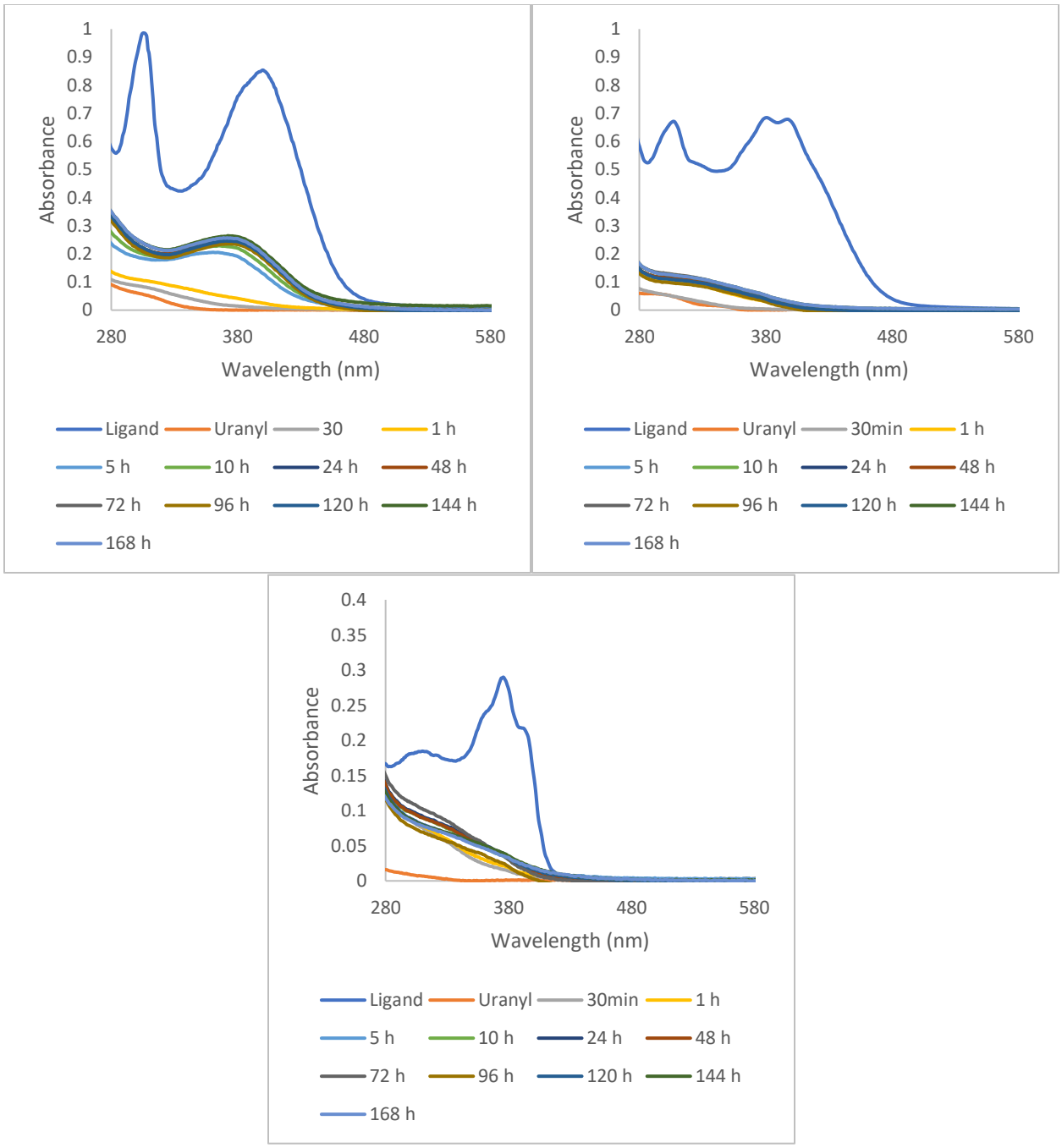

A.3.8 Leaching study of Cell-4 film: basic (top left) neutral (top right) acidic (bottom) media

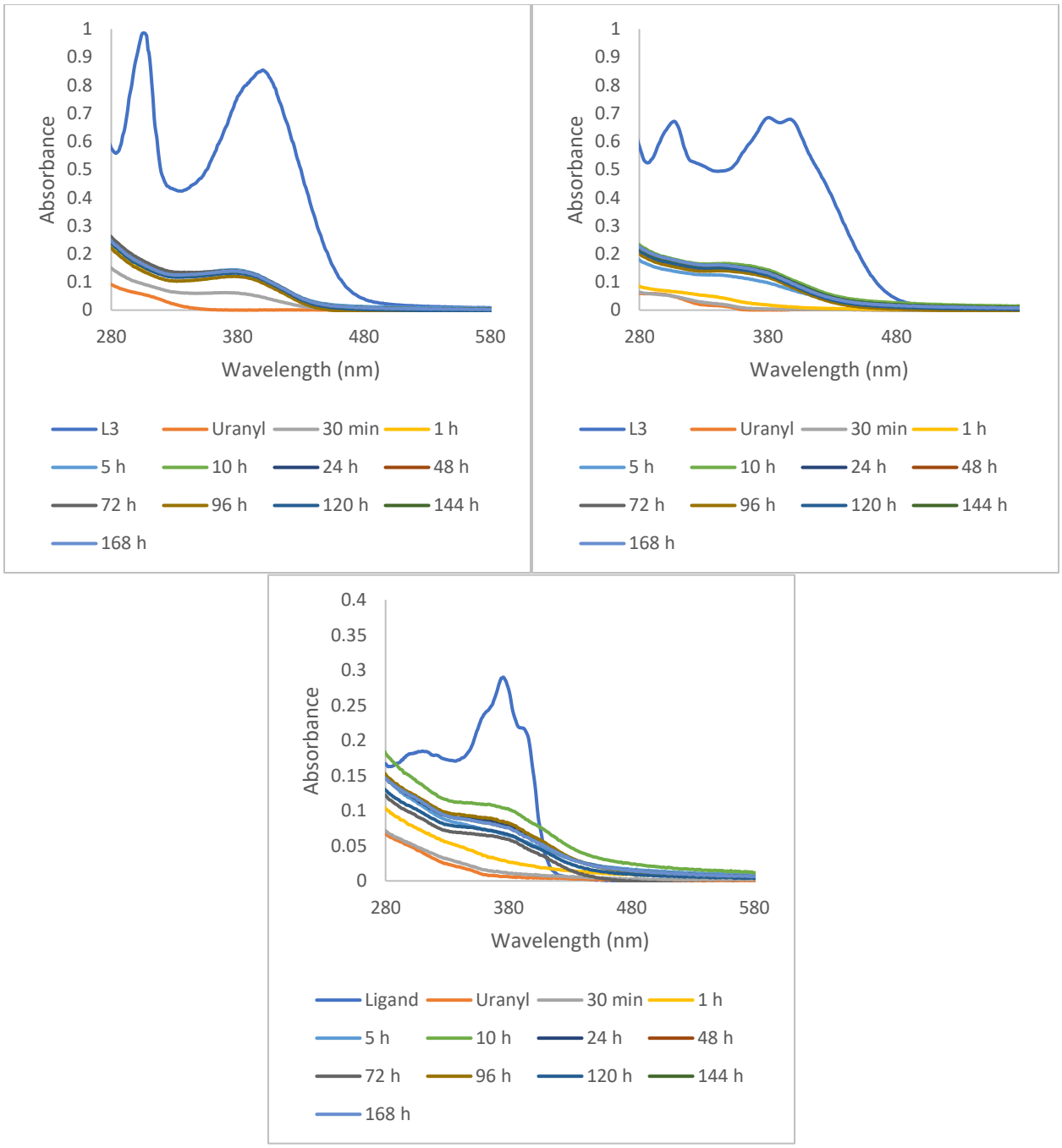

A.3.9 Leaching study of Cell-5 film: basic (top left) neutral (top right) acidic (bottom) media

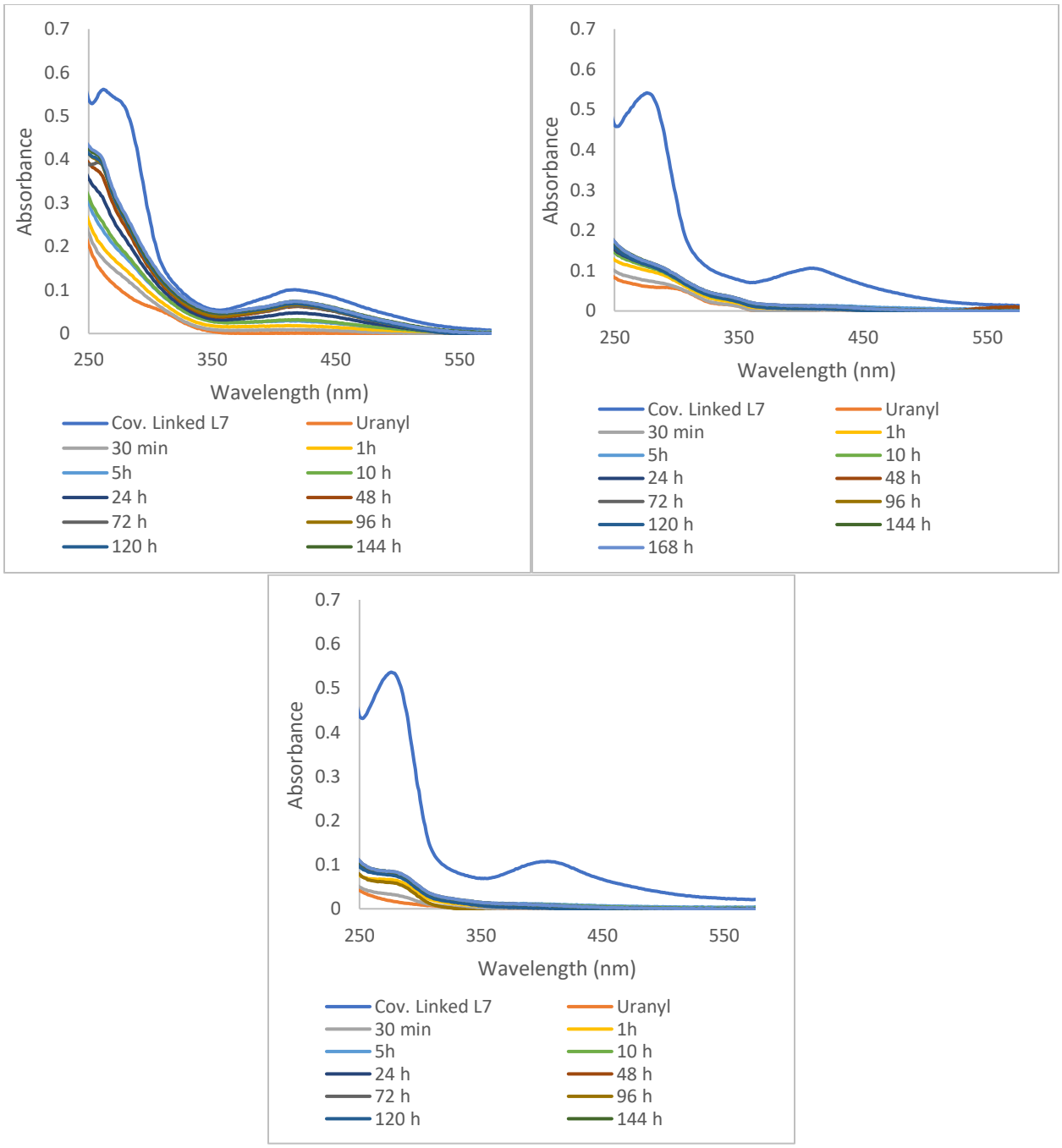

A.3.10 Leaching study of Cell-6 film: basic (top left) neutral (top right) acidic (bottom) media

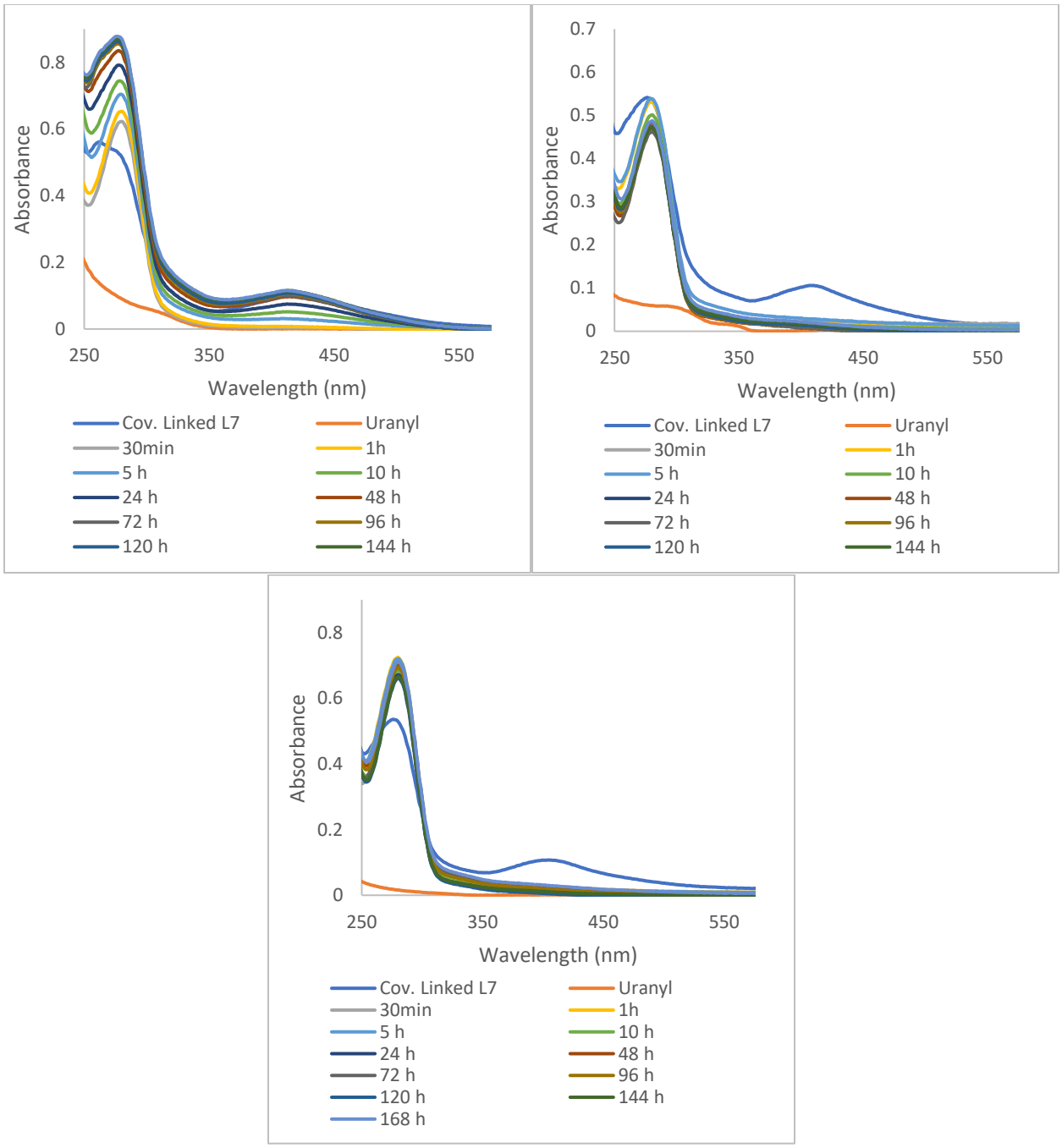

A.3.11 Leaching study of Cell-7 film: basic (top left) neutral (top right) acidic (bottom) media

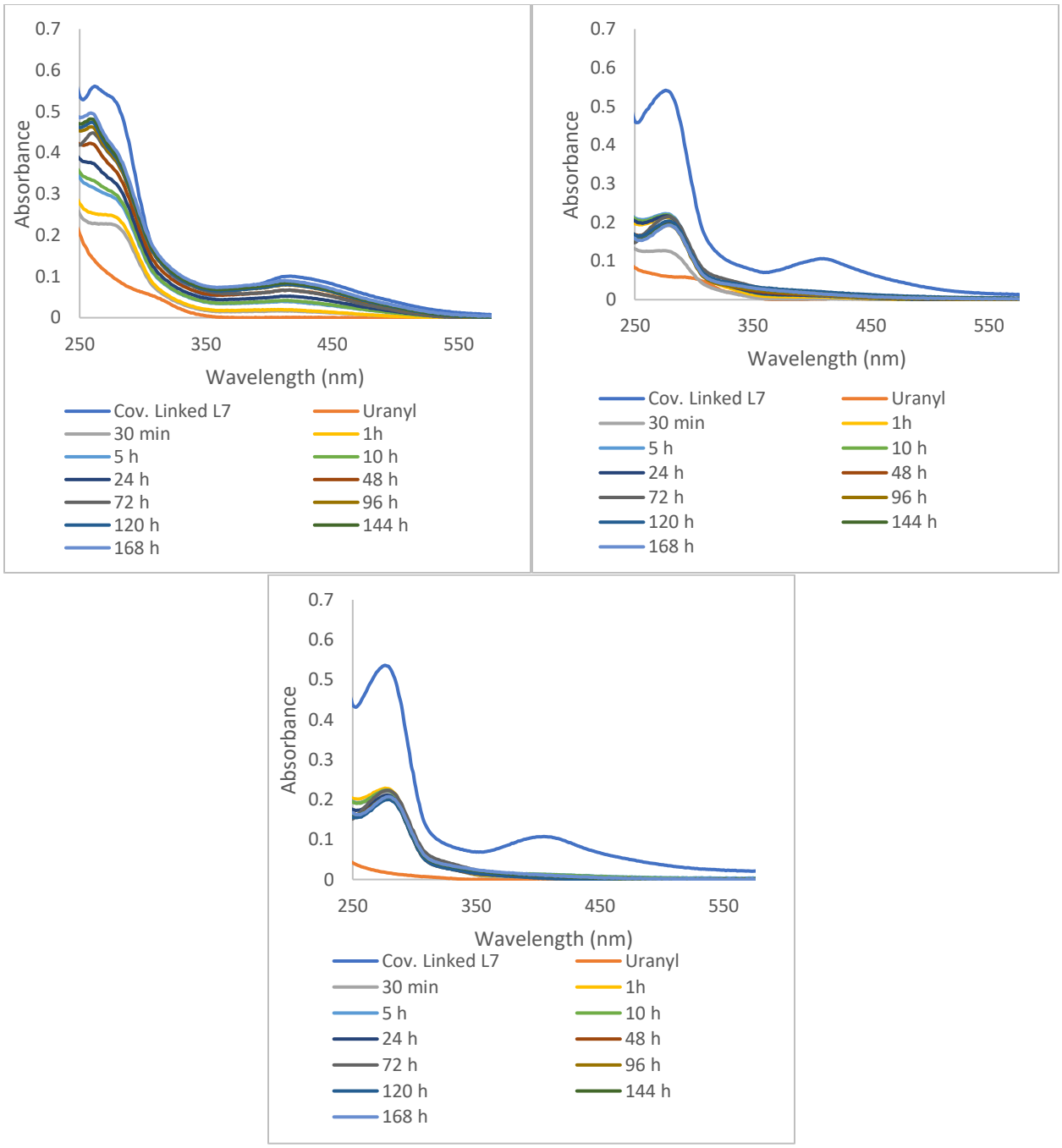

A.3.12 Leaching study of Cell-8 film: basic (top left) neutral (top right) acidic (bottom) media

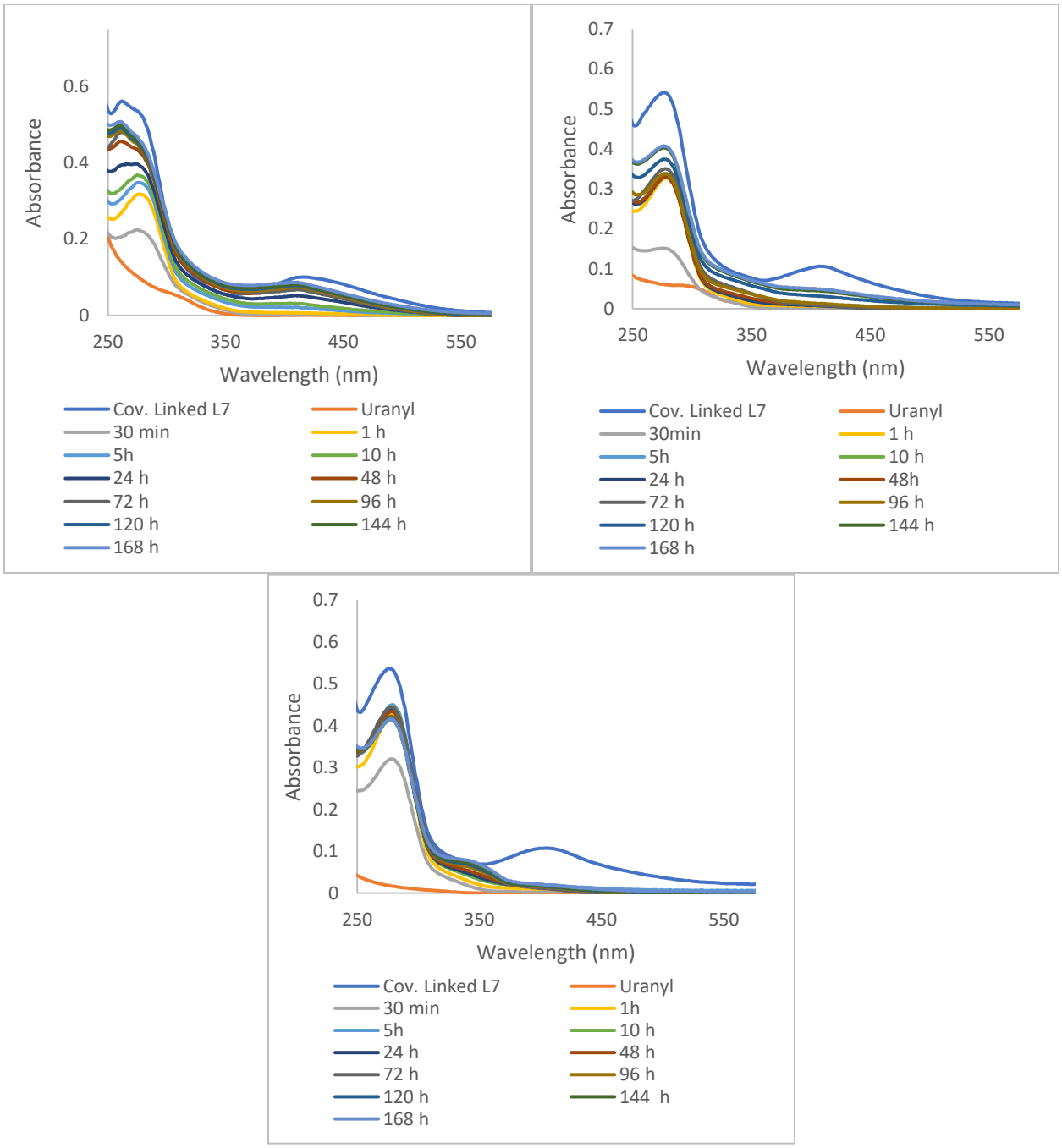

A.3.13 Leaching study of Cell-9 film: basic (top left) neutral (top right) acidic (bottom) media

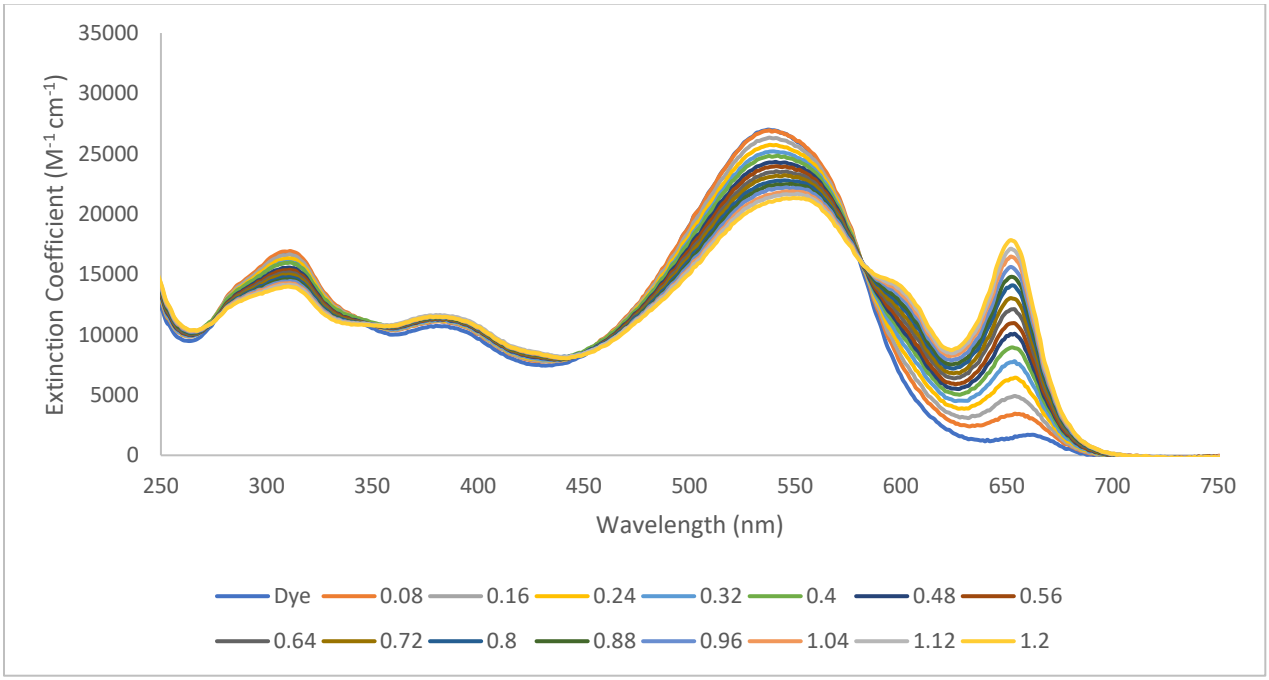

A.5.1 Uranyl titration with Arsenazo III dye (pH = 0) (Shown at metal to ligand ratios of 0.08-1.2: 1)

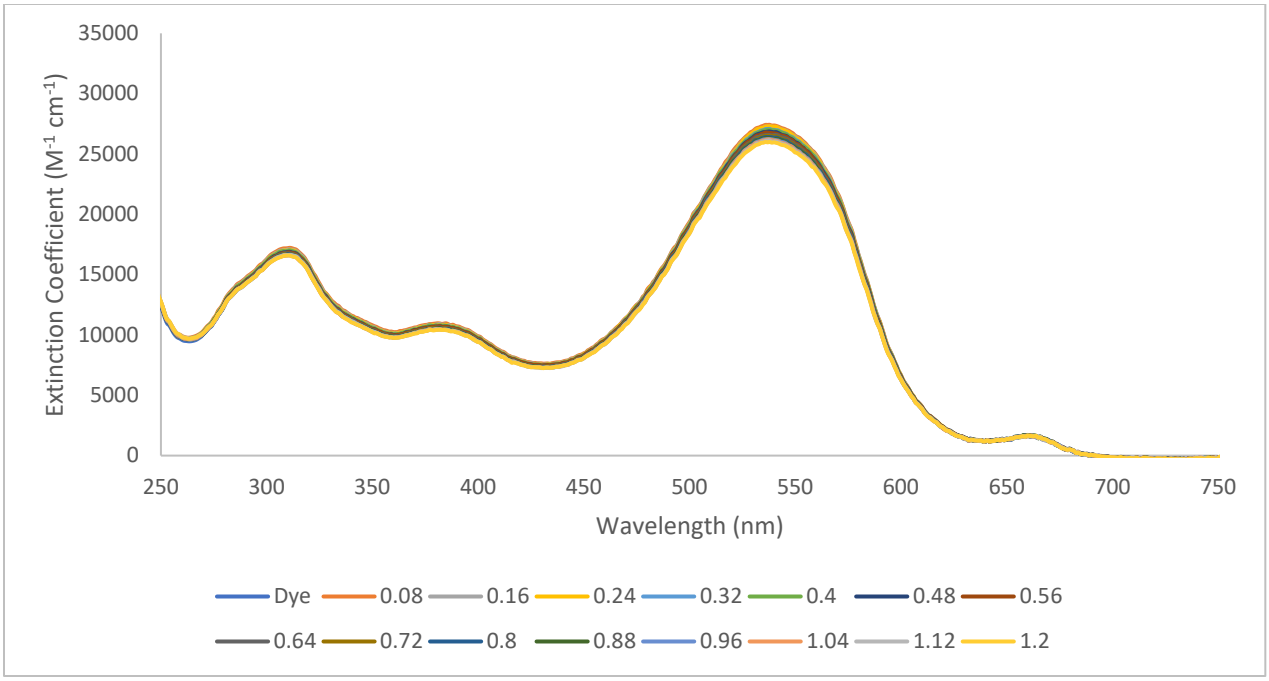

A.5.2 Ytterbium titration with Arsenazo III dye (pH = 0) (Shown at metal to ligand ratios of 0.08-1.2: 1)

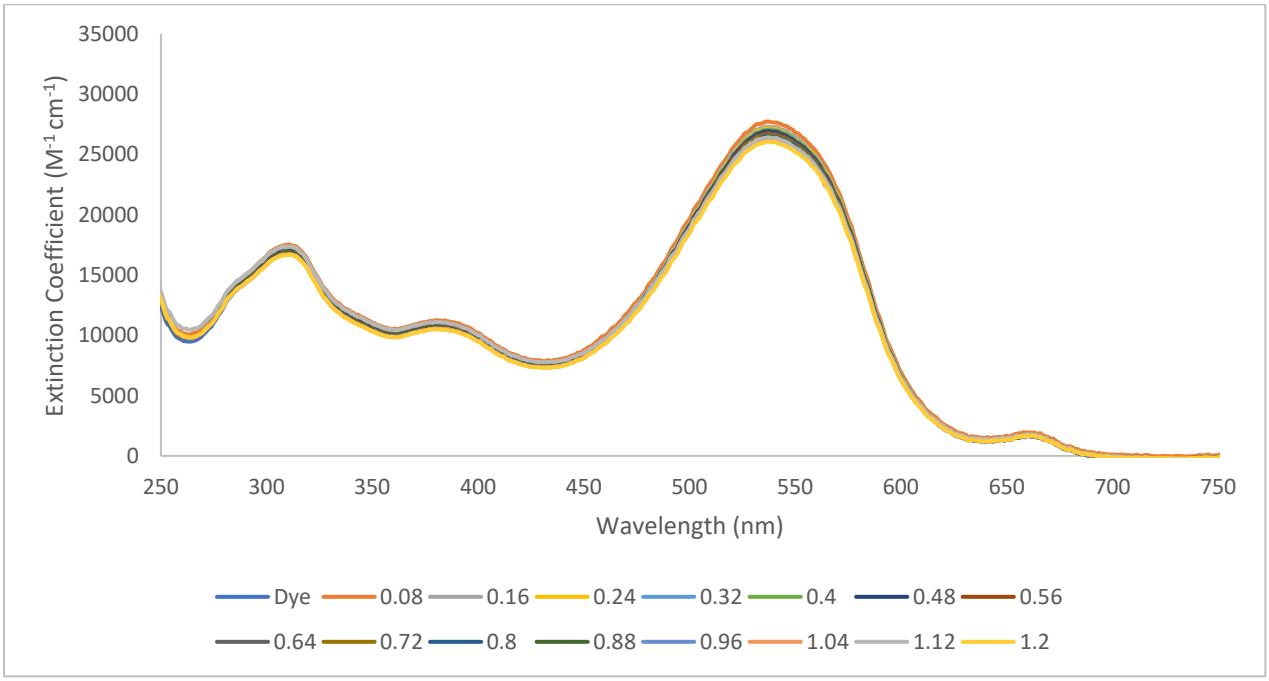

A.5.3 Copper titration with Arsenazo III dye (pH = 0) (Shown at metal to ligand ratios of 0.08-1.2: 1)

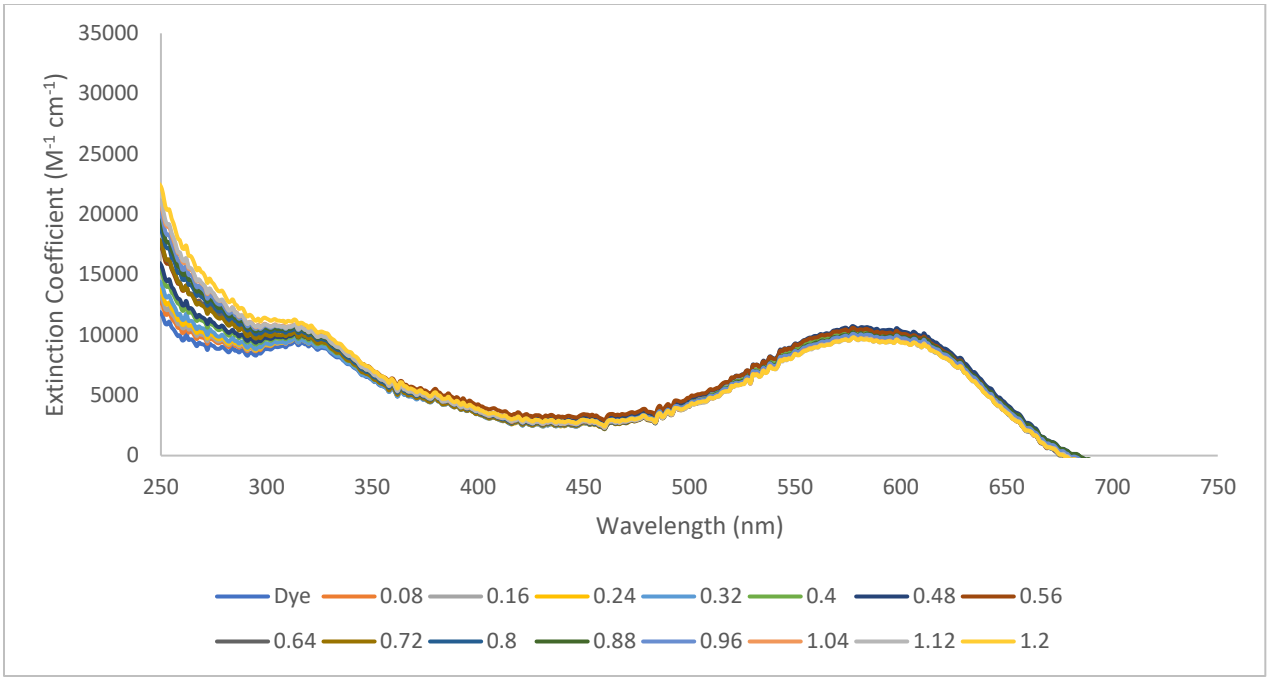

A.5.4 Uranyl titration with Arsenazo III dye (pH = 7) (Shown at metal to ligand ratios of 0.08-1.2: 1)

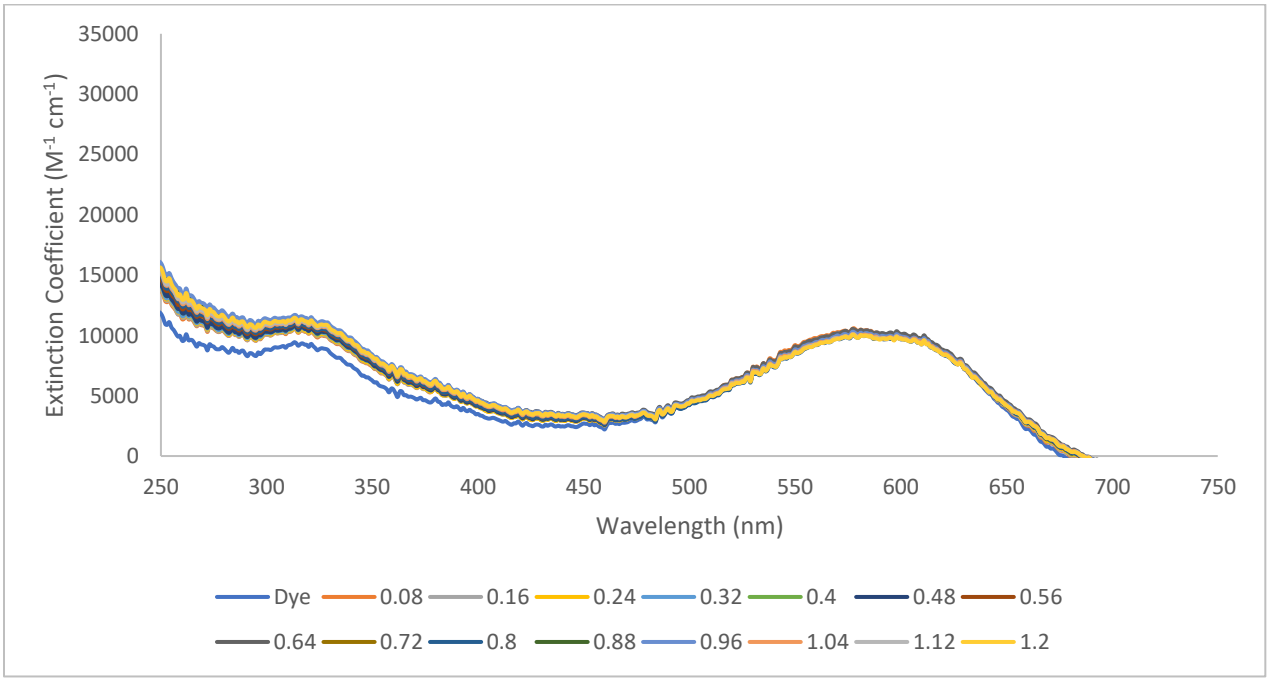

A.5.5 Ytteribum titration with Arsenazo III dye (pH = 7) (Shown at metal to ligand ratios of 0.08-1.2: 1)

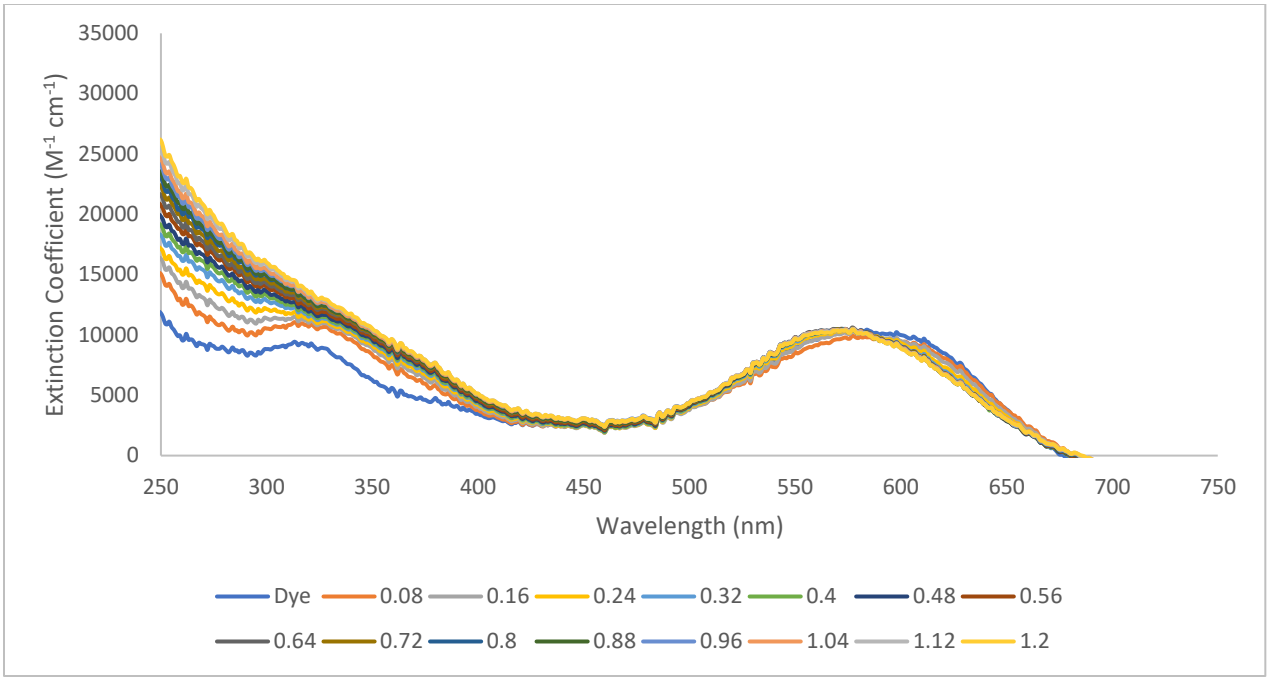

A.5.6 Copper titration with Arsenazo III dye (pH = 7) (Shown at metal to ligand ratios of 0.08-1.2: 1)

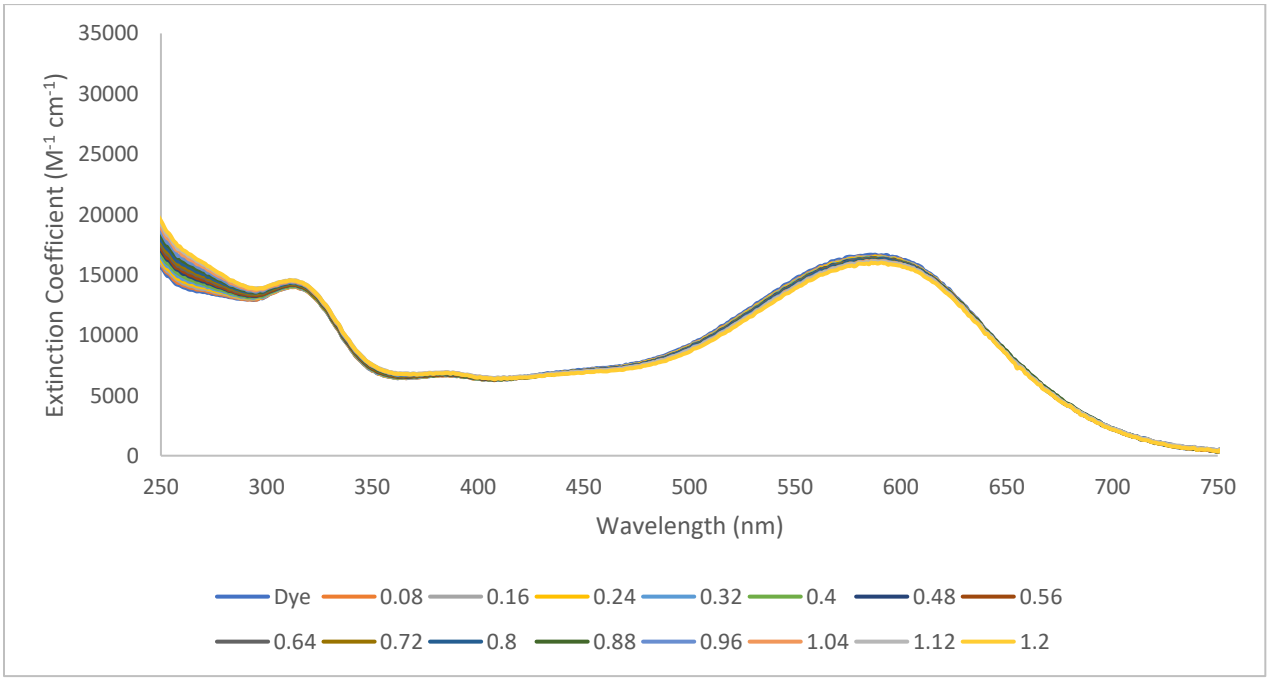

A.5.7 Uranyl titration with Arsenazo III dye (pH = 11) (Shown at metal to ligand ratios of 0.08-1.2: 1)

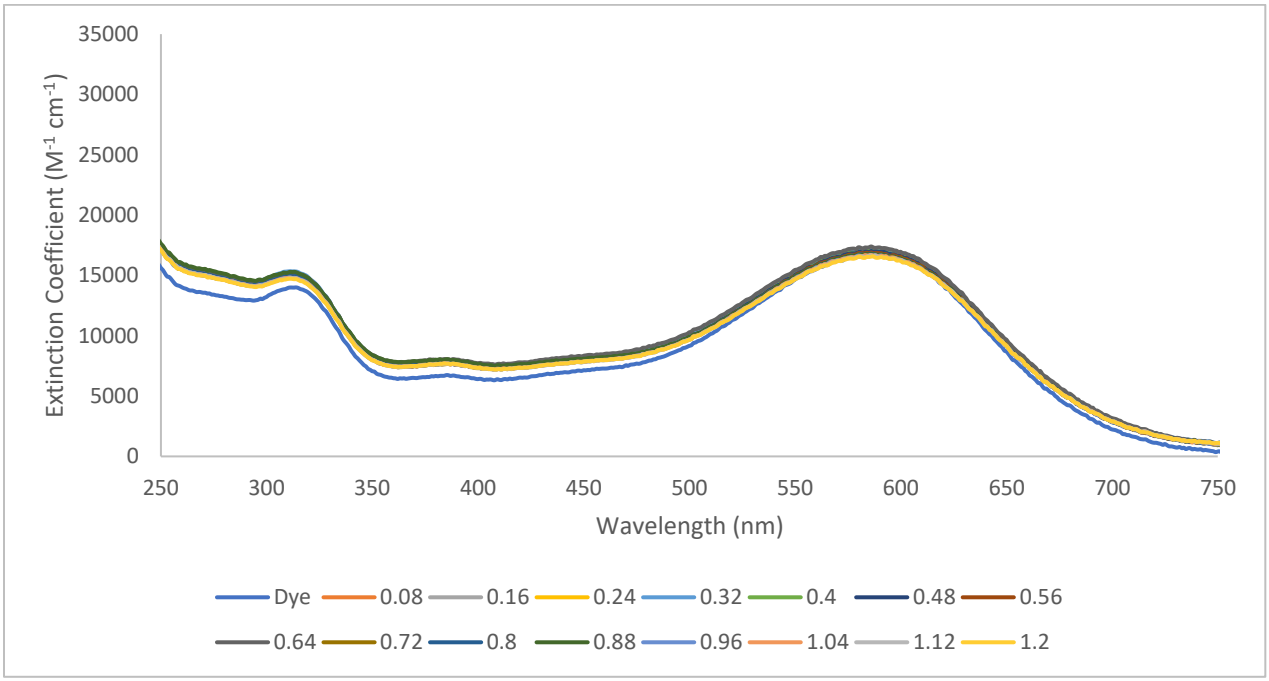

A.5.8 Ytterbium titration with Arsenazo III dye (pH = 11) (Shown at metal to ligand ratios of 0.08-1.2: 1)

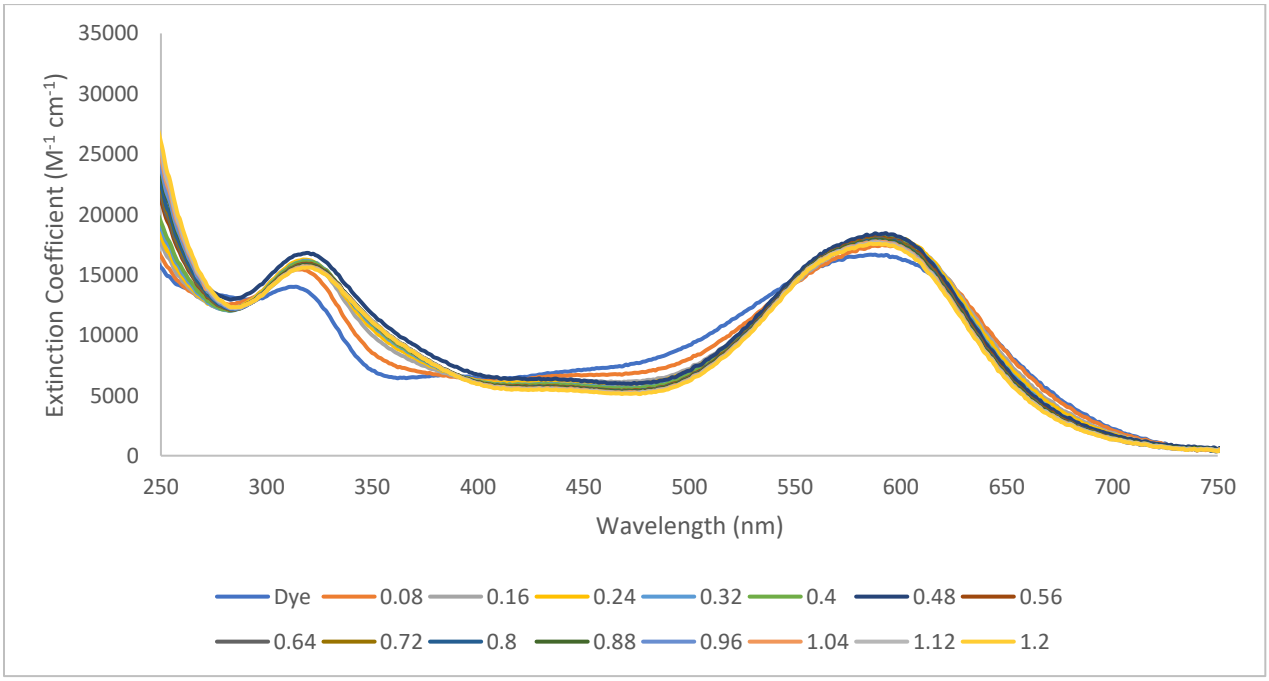

A.5.9 Copper titration with Arsenazo III dye (pH = 11) (Shown at metal to ligand ratios of 0.08-1.2: 1)